Development of an *In Vitro* Model of Contraction by Fibroblasts

by

Toby M. Freyman

B.S., Engineering Physics
Syracuse University, 1996

Submitted to the Department of Materials Science and Engineering in Partial Fulfillment of the Requirements for the Degree of

Doctor of Philosophy in Materials Engineering

at the
Massachusetts Institute of Technology
June 2001

Signature of Author_____
Department of Materials Science and Engineering
May 4, 2001

Certified by_____
Lorna J. Gibson
Matoulas S. Salapatas Professor of Materials Science and Engineering
Thesis Supervisor

Certified by_____
Ioannis V. Yannas
Professor of Polymer Science and Engineering
Thesis Supervisor

Accepted by_____
Harry L. Tuller
Professor of Ceramics and Electronic Materials
Chair, Departmental Committee on Graduate Students

Certain diagram pages have text that runs into the binding area. Very tight binding margins.

Development of an *In Vitro* Model of Contraction by Fibroblasts

by

Toby M. Freyman

Submitted to the Department of Materials Science and Engineering
on May 4, 2001 in Partial Fulfillment of the
Requirements for the Degree of
Doctor of Philosophy in Materials Engineering

Abstract

Dermal scars in adult humans are mechanically and functionally inferior to normal skin and can be physically disfiguring. The contraction of the wound by fibroblasts has been linked to the formation of scar. The mechanical and chemical signals, which control the contraction, are being investigated through the use of models of fibroblast contraction to understand the conditions which promote tissue regeneration. A cell force monitor (CFM) was designed and constructed to measure quantitatively the contraction of a highly-porous, collagen-GAG matrix by fibroblasts. Using this device, contractile force, displacement, and kinetics were compared for different values of cell density and total stiffness resisting fibroblast contraction. In addition, observation of live cells contracting individual matrix struts established the cellular mechanisms responsible for the matrix contraction measured in the CFM.

Observation of live cells revealed that macroscopic contraction of the collagen-GAG matrix was the result of forces generated during cell elongation. Contractile force normalized by the number of attached cells (~1 nN per cell) was independent of cell density (400 - 2,000 cells/mm^3) and total stiffness resisting contraction (0.7 - 10.7 N/m). Total contractile force was dependent on the cell density. These results indicated that the contractile force developed during fibroblast elongation was determined at the level of individual cells (not cooperatively) and was limited by force per cell (not displacement per cell).

The kinetics of macroscopic matrix contraction were also independent of cell density and system stiffness; contractile force reached an asymptotic value in ~15 h. Observation of live cells found the macroscopic time dependence likely resulted from the stochastic nature of cell elongation initiation and the time required for the fibroblasts to elongate completely (~2-4 h). Therefore, the time dependence of macroscopic matrix contraction did not reflect the time dependence of force generation by individual fibroblasts, but rather an average for the entire population.

Thesis Co-Supervisor: Lorna J. Gibson
Title: Matoulas S. Salapatas Professor of Materials Science and Engineering
Thesis Co-Supervisor: Ioannis V. Yannas
Title: Professor of Polymer Science and Engineering

Acknowledgements

Although I have been receiving the handshakes and congratulations for the successful completion of my thesis, my advisors Lorna (Prof. Gibson) and Prof. Yannas deserve a large part of the recognition. I thank you both for believing in me from the beginning and helping me to learn and grow as a doctoral student at MIT. You both will always have my respect and gratitude. In addition, I was extremely lucky to have had a "third advisor" in Prof. Spector. Your comments and enthusiasm about *contraction caused by cells* more than once helped put me on the right track and understand my thesis on a more fundamental level. Finally, I would like to thank Prof. Subra Suresh and Prof. Doug Lauffenburger for your help and guidance with my thesis.

I owe a special thanks to Dr. John Germaine and Sandra Taylor. Without Dr. Germaine's experience and advice on the design of the CFM I would still be trying to track down the source of the electronic drift! And, without Sandra's histology expertise my thesis would have be devoid of images of cells on matrix.

I would also like to thank the members of the Fibers and Polymers Lab at MIT, Prof. Spector's lab at the Brigham, and the Cellular Solids Group at MIT. Particularly, Lila, Donna, Mark, Bernie, Cyndi, Rayka, Shona, Courtney, Nick, Martha, and Tara for the friendly conversation and invaluable advice in the lab which surely helped and put things into perspective along the way.

Last but not least, I would like to thank my family and friends for their love and support. I give all of you most of the credit for where I am today. Thank you Mom, Dad and Todd for always pushing me to do my best and supporting me when I didn't quite make it. A special thanks to Todd and Amy for the amazing Sunday night dinners up in Andover.

Finally, to Krystyn who is by far the most important and treasured thing MIT introduced me to. Your love, caring, and, of course, understanding has made the last three years of my PhD work the best (did the last sentence have enough commas KJ?). Not only did you proof read my entire thesis more than once, just looking at you reminded me that work is not the most important thing in my life.

Table of Contents

List of Figures

List of Tables

Chapter 1. Introduction and Background

In adult humans, the healing of dermal wounds results in the formation of scar tissue. Compared to the tissue which it replaces, scar tissue is mechanically weaker [1], physically disfiguring, and can lead to the restricted motion of joints. The formation of scar tissue is accompanied by and has been linked to wound contraction [2, 3]. Contractile fibroblasts which migrate into the wound site are responsible for both the synthesis of the scar tissue and the associated contraction [2, 4]. In an attempt to understand the process of wound contraction and scar formation, these cells and their associated processes have received much attention in the past three decades.

Normal human dermis is composed of two layers, the epidermis and the dermis, separated by a basement membrane (**Fig. 1.1**). The epidermis is composed entirely of cells and regenerates spontaneously following injury, provided that a portion of the underlying dermis is still present. The dermis is composed of the following components: extra-cellular matrix (ECM) proteins (primarily type-I collagen), proteoglycans, fibroblasts, blood vessels, and nerve fibers. The ECM proteins provide a scaffold for the fibroblasts and, along with the proteoglycans, are responsible for the mechanical properties of the skin. In normal dermis, the collagen fibers are randomly oriented, forming an isotropic structure. In contrast, scar tissue is composed of highly planar collagen fibers that can exhibit a preferred alignment [5]. The direction of collagen fiber alignment is determined by the direction of highest tension in the healing wound. In addition, scar is less vascularized than normal dermis, resulting in a pale color.

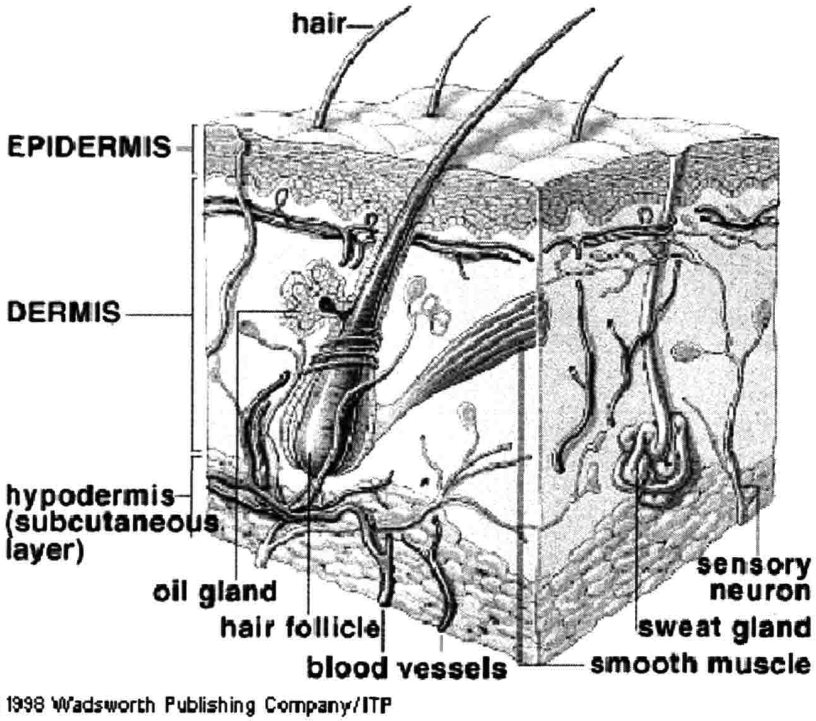

Figure 1.1 Schematic showing the structure of normal skin (http://www.as.wvu.edu/~rbrundage/) [Brundage, R. 2000].

In adult humans, dermal wounds close through the synthesis of scar tissue and contraction of the wound margins [2, 4]; regeneration of the dermis does not occur spontaneously [3]. Wound contraction occurs due to forces generated by fibroblasts which, through differentiation stimulated by factors in the wound environment, have acquired some characteristics of smooth muscle cells [4]. These differentiated, contractile fibroblasts have been termed myofibroblasts [4, 6].

Dermal wound healing occurs through several well-characterized steps starting with the formation of the blood clot immediately following injury [2]. The blood clot re-establishes hemostasis and provides a scaffold for the migration of cells into the wound. Monocytes from the blood then enter the wound and differentiate into macrophages. The macrophages attach to specific proteins of the extra-cellular matrix (ECM), degrade the damaged ECM, and release cytokines/growth factors which signal fibroblasts to migrate into

the wound site from the surrounding tissue. Fibroblasts then proliferate and synthesize new collagenous ECM. Simultaneously, new blood vessels form through the process of angiogenesis to supply the newly forming tissue with oxygen and nutrients. Due to the granular appearance of the new ECM and blood vessels, this composite structure has been termed 'granulation tissue'. After approximately the 2nd week following injury, fibroblasts in the wound site differentiate into myofibroblasts [2]. These cells are responsible for the contraction of the wound [4, 6, 7], a process which reduces the amount of new tissue which must be formed. The differentiation of fibroblasts into myofibroblasts has been shown to depend, in part, on the resistance of the wound to contraction. The resulting ECM in scar tissue is made mostly of collagen aligned along the direction of highest tension at the wound site. Thus, the mechanical forces present during wound healing regulate the function of the myofibroblasts and the architecture of the tissue which forms.

Inhibition of dermal wound contraction by myofibroblasts, using a highly specific collagen-GAG matrix, has been linked to the blockage of scar tissue formation and leads to the regeneration of the dermis [3]. The exact mechanisms through which this matrix facilitates the regeneration of skin have not been elucidated. Although wound contraction is not observed in wounds grafted with the collagen-GAG matrix, the myofibroblasts responsible for contraction are still present in the wound. Regeneration of the dermis *in situ* is a significant contribution in the effort to encourage tissues or organs to retain functionality following injury. A more detailed understanding of this process may lead to successful treatments for more complex tissues.

Myofibroblasts have been identified in many wounded/diseased tissues (*e.g.*, skin [4, 6, 7], peripheral nerves [8], anterior cruciate ligament [9], cirrhotic liver [10], asthma (bronchial mucosa) [11]). The control of new tissue formation through clinical treatments or

tissue engineered scaffolds would be greatly improved by a thorough knowledge of the processes by which these cells synthesize and remodel new tissue and the mechanical, chemical, and physical signals which control them.

1.1 Models for the Study of Contraction

The complex process of the development of contractile force by fibroblasts and the myriad factors which influence it motivate the development of experiments with which this phenomenon can be studied. The ideal experimental system will allow the investigator to monitor all mechanical and chemical signals which result from and affect the contractile force without disturbing the wound healing environment. This ideal system is approximated by both *in vivo* and *in vitro* models to study the development of contractile force by fibroblasts.

1.1.1 *In Vivo* Models of Contraction

The study of experimentally-created dermal wounds in human subjects is not ethically acceptable, so investigators have developed animal models. However, the healing of dermal wounds in animals is not identical to the healing process in humans, so an appropriate animal model must be selected and the results must be interpreted to account for anatomical and physiological differences. For example, the healing of dermal wounds in rodents occurs almost entirely through wound contraction; scar formation only accounts for a small fraction of total healing [3]. In contrast, skin wounds in humans close via approximately equal proportions of scar formation (47%) and wound contraction (53%). Dermal wounds in pigs close through similar proportions of scar formation and wound contraction to that in humans. Therefore, the pig is used as a model of human wound

healing, but there is an added cost of using larger animals and the disparities with human wound healing are unknown.

The use of an animal model has the benefit of providing an environment which currently cannot be replicated *in vitro*. These models have been used to identify materials and treatments which improve the healing of dermal wounds through histological analysis and non-invasive monitoring techniques (Integra [3], Apligraf [12]). However, techniques which could be used to monitor factors endogenous to the wound environment (*e.g.*, local contractile forces, chemical concentrations) would also make the wound environment more artificial. Thus, although an animal model can provide the proper environment for study, an increase in the number of factors which are monitored will likely decrease the relevance of the model.

1.1.2 *In Vitro* Models of Contraction

The large expense of development and employment of *in vivo* models, as well as the limitation of which and how many factors can be monitored and controlled with them, has led investigators to develop *in vitro* models of wound contraction. These *in vitro* models cannot duplicate the intricate network of chemical and mechanical signals present in a healing wound, but they do allow for experiments to be conducted in a highly controlled and controllable environment where many variables can be monitored simultaneously. The large numbers of degrees of freedom afforded by *in vitro* experimental work has led to the development of many different models.

Two general types of experimental models for measuring contraction *in vitro*, using cell-seeded gels or matrices, have emerged. The first model monitors contraction through the dimensional changes of a cell-seeded substrate over days or weeks [12-15]. The second

model quantitatively measures the contractile force and sometimes provides a resistance, in addition to the substrate, to the contraction developed by the seeded cells [16-20].

1.1.2.1 Measuring Contraction through Dimensional Changes of the Substrate

Monitoring the dimensional changes of a compliant, biocompatible material provides a simple, straight-forward technique with which to monitor contraction by cells (**Fig. 1.2**). This technique was developed more than 20 years ago by Bell *et al.* [12], and has since been used to define and understand the process of contraction of many different cell types [13-15, 21]. Use of this type of model has allowed researchers to determine that contraction depends on: cell attachment via the β_1 family of integrins [22, 23]; cytoskeletal elements [12, 13, 24]; and serum factors (TGF-β, PDGF) [13, 24-29].

Imposing an external restraint on the contraction of a collagen gel by cells has led to a variation of this type of model (**Fig. 1.2**). Physical restraint of the gel during the development of a contractile force by cells results in tension developing in the gel. The morphology and function of cells in a gel that is in tension vary markedly from those in an unrestrained gel [13, 30]. One investigator [13], reported that the cells in a restrained substrate resemble those in granulation tissue (healing dermis), while those in a freely contracting substrate resemble those in normal dermis. Subsequent experiments have shown that cells in restrained and unrestrained substrates respond differently to the growth factors relevant to wound healing. For example, a well known stimulant of fibroblast contraction, TGF-β, increased the production of the contractile protein α-smooth muscle actin in fibroblasts three-fold in restrained collagen gels; fibroblasts in freely floating gels do not show any significant increase [31]. Many investigators have found that the release of a restrained gel provided results on the contraction of collagen gels by elongated, tense cells.

This has been utilized to study the growth factor signaling pathways involved in contraction [32].

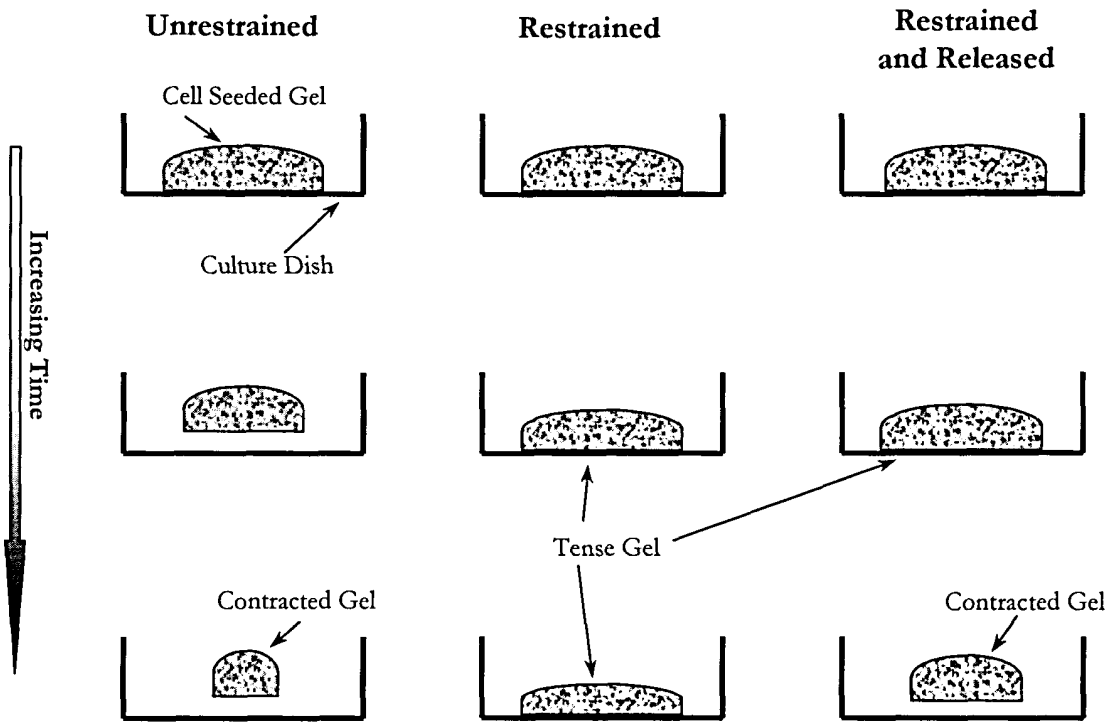

Figure 1.2 Schematic showing contraction of an unrestrained, fully restrained, and restrained-and-released cell-seeded, collagen gel. The gel adheres to the culture dish during casting. The left-most column shows a gel which was released from the substrate immediately following gelation. This gel contracts freely, so little internal tension can build up. The middle column shows a gel which adheres to the dish during the entire experiment. The restraint results in a tense gel. The right-most column shows an experiment where internal tension is allowed to build during a portion of the experiment, but the gel is then released from the dish and the cells contract it rapidly.

1.1.2.2 Measuring the Cellular Contractile Force

Contraction models which monitor dimensional changes provide a method to study contraction, but do not provide information on the parameter responsible for wound contraction: cell-generated forces. For this purpose, models which quantitatively measure the contractile force generated by cells have been developed. These models can be further

classified by whether the force is generated by one or many cells. In the former category classification, the cells are spatially and mechanically isolated from each other, and the forces generated by a single cell are measured. Originally, this mechanical isolation was achieved by seeding a very low density of fibroblasts onto a compliant silicone membrane, followed by analysis of the buckling pattern under active fibroblasts [33]. This method has subsequently been modified by replacing the silicone membrane with a substrate containing latex beads and observing the fibroblast-induced deflection of the beads over time [34]. This improvement simplified force calculations since the substrate deformed elastically (*i.e.*, not by buckling). The bead deflections were converted into force values via the substrate stiffness. Using this technique, investigators found that: force was transferred to the substrate during cell migration [33, 35, 36], pseudopod extension, and partial retraction [34, 37]; and cell movement and focal adhesions are guided by the substrate stiffness [38].

In the latter category of these quantitative models, a device equipped with a force transducer measured the macroscopic contraction of a three-dimensional substrate by fibroblasts [16, 18-20]. The contractile force developed by fibroblasts typically begins to increase within one hour of seeding, and approaches an asymptotic value within 36 h (details reported in Table 4.2). Both systems allow the cellular contractile response to be observed over time, but under different conditions. Using this model, investigators have reported the following: exogenously applied cyclical force dramatically affects the production of enzymes specific for ECM protein degradation [39, 40]; the force which develops appears to be a homeostatic level [16, 20, 41]; disruption of microfilaments results in a decrease in force [16, 42]; disruption of microtubules results in an increase in force [17, 42]; and contractile force is dependent on the tissue from which the fibroblasts were derived [43]. The model of contraction developed and employed in this work was similar to these previous models.

1.2 The Cell Force Monitor

In the present work, the model system developed to monitor contraction by cells measured the macroscopic contractile force generated by millions of fibroblasts attached to a highly-porous, three-dimensional, collagen-GAG matrix over time. This type of model was used because it allowed the force developed to be averaged over an entire population of cells, eliminating cell-to-cell variation and allowing cells to develop the force in a three-dimensional environment which was more relevant to the *in vivo* environment. In the following paragraphs, the choice of the three main components of this model are discussed: substrate, cell type, and force monitoring device.

1.2.1 Choice of Substrate

Unlike most previous models, this experimental system was designed to monitor the contraction of a highly-porous, type-I collagen and chondroitin-6-sulfate (a glycosaminoglycan, orGAG) matrix by cells. The collagen-GAG matrix provided several experimental advantages. The freeze-drying and subsequent crosslinking processes which were used to produce this matrix allowed the mechanical and microstructural properties (*e.g.*, stiffness, pore diameter) to be modified, independent of the chemical composition (*e.g.*, collagen-to-GAG ratio, GAG or collagen type). In addition, the open pore structure and size of the struts (~10 μm diameter) of the collagen-GAG matrix allowed for observation of the deformation of individual matrix struts by cells via a light microscope. This was beneficial because the macroscopic measurement of contraction by millions of cells yields a population average for contractile force, but does not reveal the mechanism by which individual cells develop these forces and matrix deformations. The study of how contractile fibroblasts interact with the collagen-GAG matrix has direct clinical relevance since it has

the capability to inhibit wound contraction. In fact, it has been shown to mediate the contraction and scarring resulting from severe burn wounds in humans.

1.2.2 Choice of Cell Type

For the purposes of this work, dermal fibroblasts (derived from rabbit dermis) were studied due to the major role they play in wound healing and contraction. The use of a dermal fibroblast cell-line would simplify the cell culture, but it has been reported that virally transfected cells do not exhibit decreased levels of the contractile protein α-smooth muscle actin as compared to primary cells [44, 45]. Ideally, human dermal fibroblasts would be used in these studies, but problems associated with obtaining human cells and the concern of infectious disease transmission made the use of fibroblasts obtained from an animal dermis more practical.

1.2.3 Design Parameters of the CFM

The cell force monitor (CFM) was designed to measure the uniaxial contractile force developed in a cell seeded sample of the collagen-GAG matrix over a period of time (usually > 20 h). The CFM allowed the stiffness of the resistance to contraction to be controlled. The resistance to contraction was an important variable in that it allowed the user to simulate different mechanical conditions *in vivo*. Thus, together with control of the chemical composition of the culture medium and the properties of the collagen-GAG matrix, the CFM allowed the user to define the mechanical, chemical, and physical environment under which the cellular contractile force developed.

1.3 Project Goals and Overview

This work was structured to accomplish the following three goals: 1) Development of an *in vitro* model to measure the contractile force developed by cells in a controlled environment; 2) Identification of the cellular mechanisms responsible for matrix contraction; and 3) Identification of the limiting mechanical factors in the development of matrix contraction by cells.

An *in vitro* model was developed to study the contraction over time of a three-dimensional collagen-GAG matrix by attached fibroblasts. To define the system, the mechanical and microstructural properties of the collagen-GAG matrix were determined (Chapter 2). A cell force monitor (CFM) was constructed, calibrated, and tested which allowed the contractile force developed by millions of cells attached to the matrix over time to be quantitatively measured (Chapter 3). The contraction of the collagen-GAG matrix over time by fibroblasts increased almost immediately following cell seeding and reached an asymptotic value after ~15 h in culture. In Chapter 4, a parameter fundamental to the use of this model, attached cell number, was found to relate linearly to the contractile force which developed. In addition, an exponential equation was established which described and allowed a quantitative comparison of the data from separate contraction experiments. Using this equation, it was established that a force of 1 nN was generated per cell with a time constant of ~ 5 h. Both of these values were independent of cell number. The two derived constants together with determination of attached cell number at the termination of each experiment enabled, a quantitative comparison of contractile data from different experiments (Chapter 4).

The mechanisms through which individual cells deformed the matrix were identified through the observation of live cells, the measurement of cell aspect ratio with time, and

immunohistochemical identification of the contractile protein α-smooth muscle actin. Using these techniques, it was established that the contraction of the collagen-GAG matrix occurred coincidentally with the elongation of fibroblasts along the matrix struts. In addition, the time dependence of the contractile force measured with the CFM was found to represent the actions of the population as a whole; not the time dependence of individual cells deforming the matrix (Chapter 5).

The contractile force which was developed in the collagen-GAG matrix by the fibroblasts was found to be limited by the force which developed, not the displacement. This was determined by varying the amount of resistance to contraction (stiffness) provided by the CFM (Chapter 6). The conclusions of each of these efforts are correlated in the final chapter (Chapter 7).

Chapter 2. Microstructure and Mechanical Properties of the Collagen-GAG Matrix

2.1 Introduction

As cells exert force on a porous material to which they are attached, the material provides a resistance to this force which is determined by its stiffness. If the porous material is sufficiently compliant, the cellular forces will result in macroscopic deformations of the material which can be measured. If the material is sufficiently stiff, however, the macroscopic deformations resulting from the cellular forces will not be measurable. Therefore, knowledge of the amount of resistance the material provides to cellular forces is crucial to measuring and understanding the forces exerted by cells.

The cellular forces which macroscopically deform porous materials are applied internally to individual pore walls (struts) which comprise the solid structure of the foam-like material. This internally initiated deformation is in contrast to the more common application of external forces to macroscopically deform materials, such as in simple compression. To draw conclusions about cellular forces from the measurement of macroscopic deformation, the link between the microscopic and macroscopic phenomena must be elucidated.

In this chapter, the macroscopic mechanical properties, the microstructure of the collagen-GAG matrix and the relationship between these features are discussed. An analysis of the matrix microstructure suggests that it is similar to other natural and man-made open cell foams (**Fig. 2.1**) [46]. However, comparison of the tension and compression stress-strain curves of the collagen-GAG matrix with those of other open cell foams reveals that it has a different mechanical response. This difference is linked to the local buckling of struts

prior to macroscopic deformation. Although this analysis was not detailed enough to allow for a complete understanding of the deformation mechanisms involved, it does provide a better understanding of the forces required to deform the collagen matrix macroscopically and of how the internal microstructure responds to applied forces.

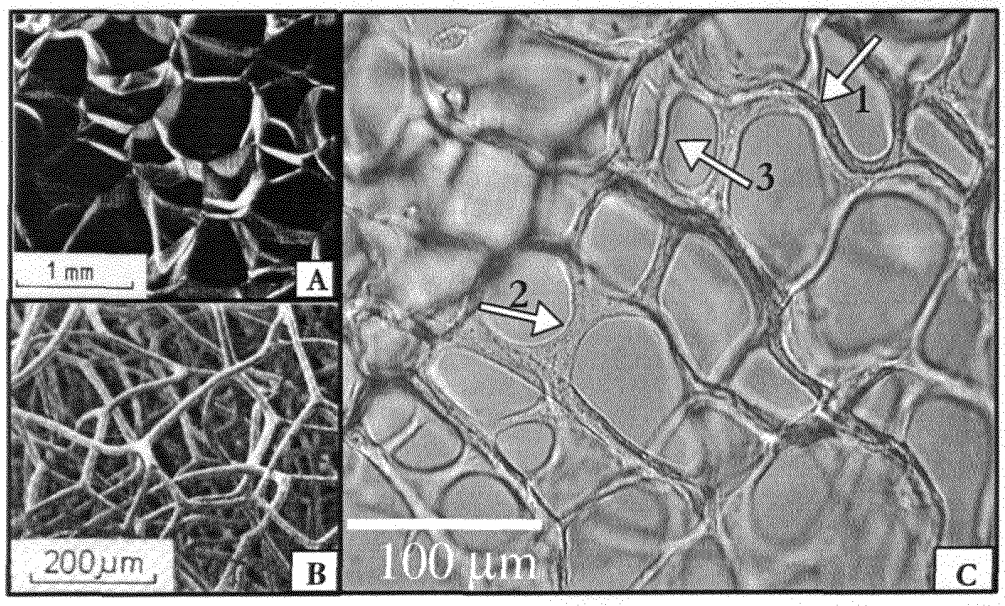

Figure 2.1 Micrographs showing the microstructure of a polyethylene foam (**A**), a sponge (**B**), and the collagen-GAG matrix (**C**). Some struts in the collagen-GAG matrix were curved prior to any imposed deformation by macroscopic or cellular forces (arrow 1). In addition, some local regions of the collagen-GAG matrix appeared to be more and less stiff, arrows 2 and 3, respectively.

2.2 Materials and Methods

2.2.1 Collagen Matrices

Micro-fibrillar type-I collagen (Integra Life Sciences, Plainsboro, NJ) was blended with 0.05M acetic acid at a concentration of 5 mg/ml for 90 minutes at 4°C (see Appendix A). A glycosaminoglycan(GAG), chondroitin-6-sulfate (0.44mg/ml) (Sigma Chemical Company, St. Louis, MO), was added to this mixture and blended for an additional 90 minutes at 4°C producing a white co-precipitate slurry. This slurry was degassed and then

freeze-dried (Genesis 25LE, Virtis, Gardiner, NY) at -43°C in stainless steel trays to produce a porous collagen-GAG matrix sheet (25 x 16 x ~0.3 cm). Sublimation of ice crystals during the freeze-drying process produced the pore structure. These sheets were then crosslinked by dehydrothermal (DHT) treatment at 105°C under a vacuum of < 50 torr for 24 hours [3]. This treatment leaves the collagen triple helix intact, if the moisture content of collagen prior to heat treatment is less than 1 wt. % [3, 47]. A second set of matrix sheets to be used in the free-floating experiments (Chapter 6) were crosslinked for only 1 hour, producing a less stiff matrix.

2.2.2 Matrix Pore Diameter

The microstructure of three-dimensional foams was determined quantitatively using standard stereological techniques from images of planar sections. Due to the fragile nature of the collagen-GAG matrix, it was difficult to obtain a cut surface that was not distorted or damaged in some way. Therefore, confocal fluorescence microscopy of stained matrix samples was used to observe two-dimensional sections of the matrix up to 1 mm below the surface, providing an undisturbed section for analysis. General observations about the three-dimensional microstructure were also made by viewing hydrated samples with a light microscope.

Collagen-GAG matrix samples were stained using a fluorescent conjugated type-I collagen antibody (see Appendix D.1). Images were gathered from stained samples hydrated in TRIS-buffer (Sigma Chemical, St. Louis, MO) using a confocal fluorescent microscope (MRC-600, Bio-Rad, Hercules, CA) (see Appendix D.2). To facilitate editing and analysis, they were then converted to binary images using NIH Image software (http://www.nih.gov). Once in binary format, the images were edited to erase marks caused

by poor image quality (**Fig. 2.2a**). This assured that the program was only counting cell walls. Examples of regions that needed correction for poor picture quality were dark regions in the middle of pores, or obviously speckled areas. Without this editing, the image analysis software would have interpreted a speckled area to be many small pores. These images were then analyzed with the help of a linear intercept macro written for NIH Image (see Appendix D.3). This macro finds the number of times that a series of parallel lines drawn across the image intercepts a white line (*e.g.*, a cell wall) at least 2 pixels wide (1.5 μm). Likewise, a pore was not considered a pore by the program unless the black region was at least two pixels wide. A circular region of the image was then selected using the circular selection tool and the macro executed. This processes was repeated for series of parallel lines rotated by 5° increments around the circular section and the mean intercept length, or average distance between cell walls was reported. The program then used these distances and angles to construct a best-fit-ellipse representing an average pore for the section analyzed (**Fig. 2.2b**). To account for measurement of pores which were not sectioned along their true cross-section, but rather at an arbitrary angle which would skew their calculated pore size, the ellipse major and minor axes were corrected by multiplying by 1.5 [46].

Matrix microstructure was described by both a pore diameter (the average of the best-fit ellipse major and minor axes) and an aspect ratio. The orientation of the best-fit ellipse for each image was determined, but since the orientation of pores throughout the matrix was random the value was not reported. The value of the reported average pore diameter was an average of values from 4 different matrix samples. At least 4 images were analyzed and averaged from each sample.

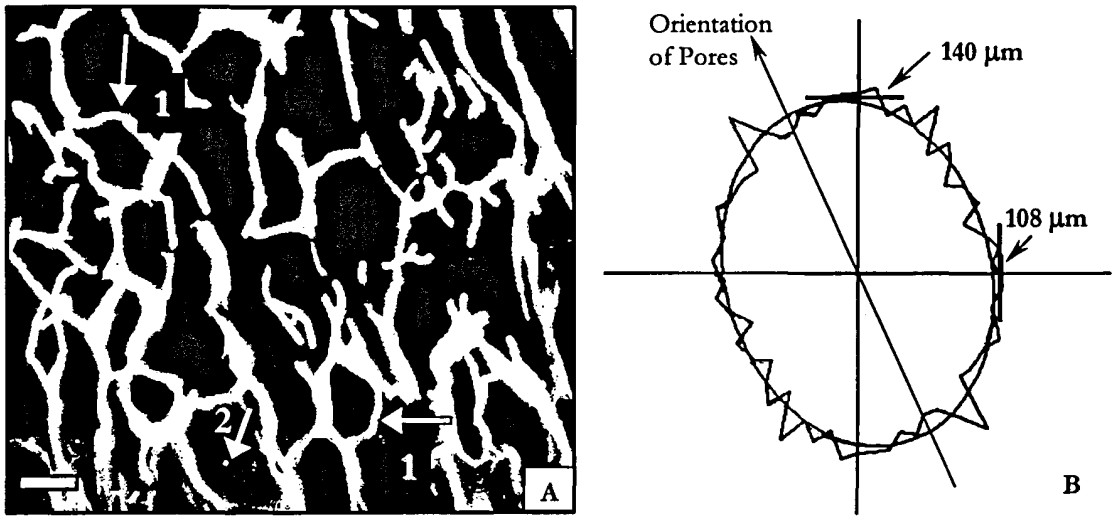

Figure 2.2. (A) A two-dimensional section of matrix from confocal fluorescent microscopy used in the pore diameter analysis (scale bar = 100 μm). Arrows **1** indicate pore walls that were curved prior to any deformation imposed by macroscopic compression or by cellular forces. Arrow **2** indicates an example of an artifact of poor picture quality that was edited out. (**B**) A representative polar coordinate plot of the linear intercept lengths (5° intervals) and the corresponding best-fit ellipse as reported by the Scion Image software. The average pore diameter for this sample was 124 μm and the aspect ratio was 1.3.

2.2.3 Mechanical Testing of the Collagen-GAG Matrix

2.2.3.1 Tension Testing

Fully processed collagen-GAG matrix sheets were cut into rectangular samples 85 mm x 25 mm x ~3 mm for tensile testing. The dry dimensions of each sample were determined using a micrometer (± 0.02mm). Due to the high compliance of the hydrated matrix samples, it was necessary to measure displacement optically via a video camera. For this purpose two parallel lines of black fabric paint were placed 15 mm apart, perpendicular to the axis of deformation (**Fig. 2.3c**), and allowed to dry overnight (see Appendix C.1). The marked samples were placed into 0.05M acetic acid for 1 hour to begin the re-hydration

process, then transferred to phosphate buffered saline (PBS), and stored at 4°C until testing began.

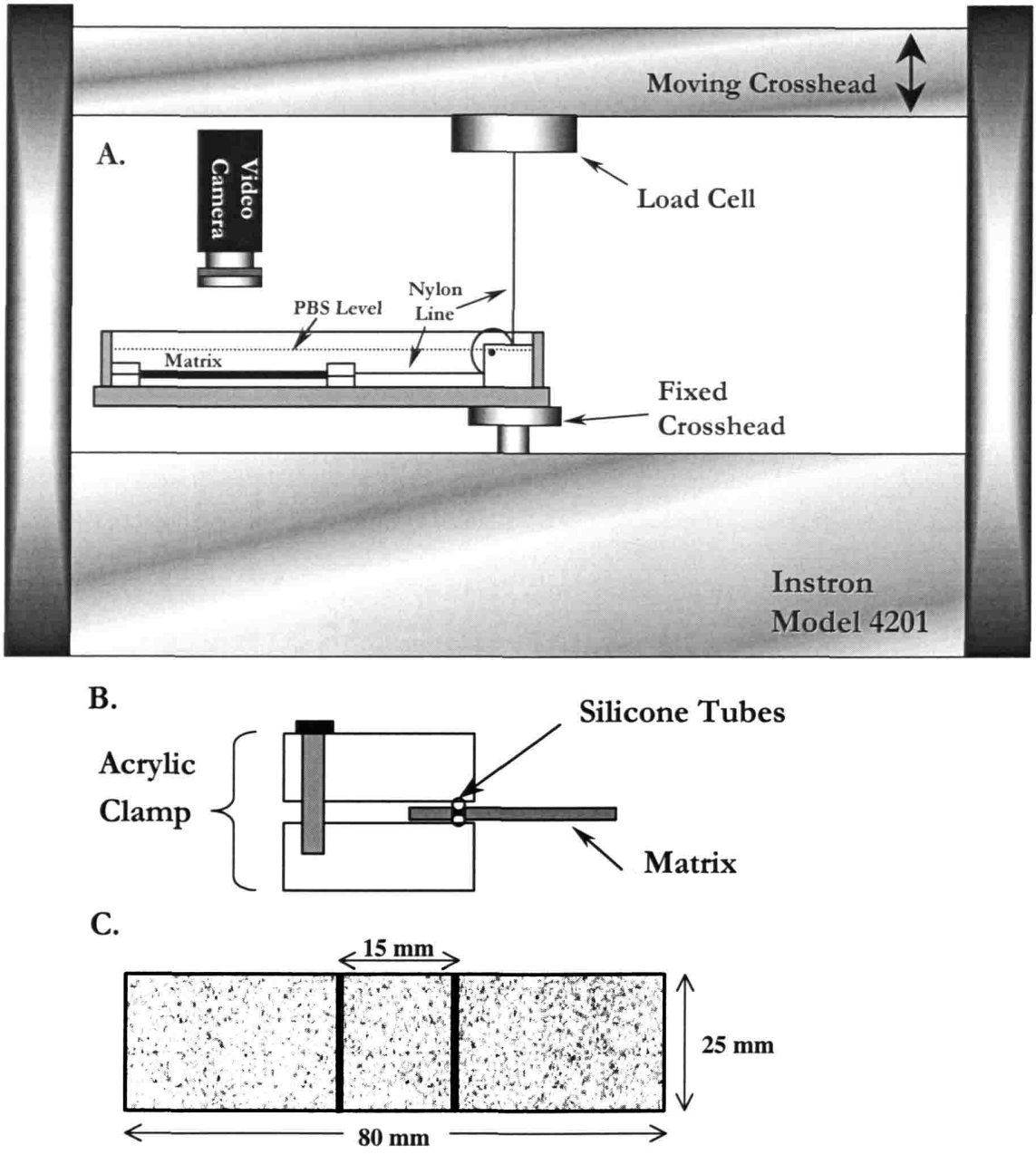

Figure 2.3. Side view tensile testing apparatus with video camera to measure strain optically (**A**). Magnified view of acrylic clamp used to grip matrix (**B**), and top view of a marked matrix sample (**C**).

Re-hydrated matrix samples were tested in phosphate buffered saline (pH = 7.4) at 37°C to simulate the conditions of subsequent experiments. The matrix sample was

oriented horizontally in an acrylic pan so that it could be submerged in the saline during testing (**Fig. 2.3a**). One end of the matrix was held in place by a fixed clamp, while the other end was held in a clamp that moved horizontally as the mobile crosshead of the universal testing machine (Model 4201, Instron, Canton, MA) displaced vertically. A nylon line and pulley were used to translate the vertical crosshead displacement into the horizontal matrix displacement. The stiffness of the nylon line was irrelevant since the displacement was measured optically and the matrix, nylon line and load cell were in series. To monitor the strain, a video camera (TM-1001-02, Pulnix America Inc., Sunnyvale, CA) connected to a VCR (AG-S555, Panasonic, Rockville, MD) was positioned so that the position of the two black lines on the matrix were recorded throughout the test (**Fig. 2.4**). The mobile crosshead was programmed to ascend at a speed of 1mm/minute. This displacement rate was chosen to minimize any effect of matrix viscoelasticity and of the release of fluid from the pores. Force data was gathered using a 50 N load cell (Model # 2512-305, Instron, Canton, MA) connected, through the Instron, to a data acquisition card (AT-MIO 16XE-50, National Instruments, Austin, TX) installed in a PC. A time stamp (**Fig. 2.4**) recorded with the images initiated simultaneously with the start of crosshead motion and load data acquisition (see Appendix C.1). This feature allowed video frames and load data points, both acquired at 30 Hz, to be synchronized.

Tensile engineering stress-strain curves were constructed from ~ 30 discrete points by correlating optical strain measurements with the load data, normalized by cross-sectional area. The video-recorded matrix displacement was replayed and images were acquireed, at 1 minute intervals, with a frame grabber card (HLImage++, Western Vision Software, Salt Lake City, UT) installed in a PC. Matrix displacement was determined using image analysis software (Scion Image) and a specialized macro (see Appendix C.1) that measured the

distance between the fabric paint lines in the images. The distance between lines was measured at a minimum of 5 locations and averaged to account for any inhomogeneities in the matrix deformation. Strain was calculated by normalizing average displacement measurements with the distance between the lines in the first frame acquired. Stress was calculated by normalizing the measured load by the cross-sectional area of the sample, calculated from the hydrated width and the unhydrated thickness of the matrix. The unhydrated thickness was used due to the high compliance of the hydrated matrix making measurement of this parameter after hydration difficult. A cursory analysis revealed the hydrated and unhydrated dimensions did not very significantly.

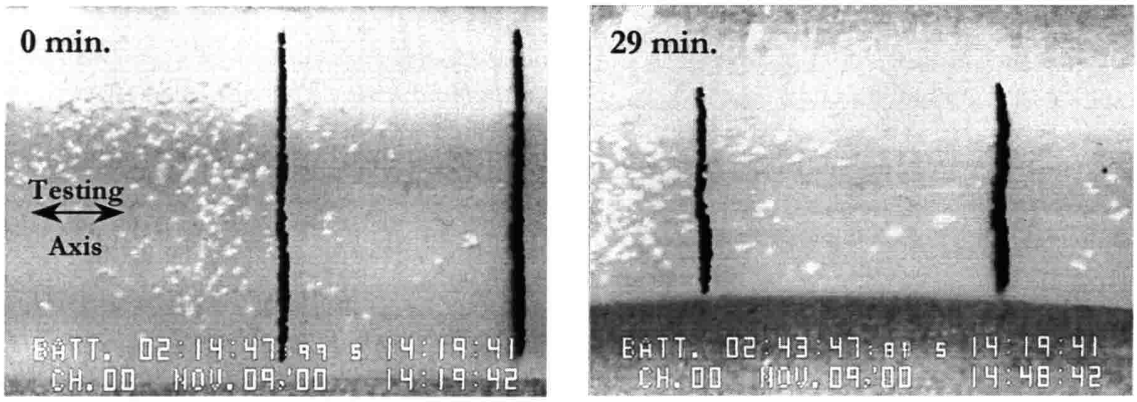

Figure 2.4. Images used for the optical strain measurement technique in the tensile tests, at the beginning of testing (0 min.) and at the end of testing (29 min.). The time stamp on the bottom of each image was used to correlate displacement and load. The distance between the black lines at the start of the test was 15 mm.

2.2.3.2 Compression Testing

The compressive response of the collagen-GAG matrix was determined using the device described in the following chapter (**Fig. 3.2**). Briefly, the cell force monitor (CFM) was designed to measure contraction of the collagen-GAG matrix by fibroblasts with time. Deflection of the cantilevered beam was monitored using an inductive transducer. The transducer converted the beam deflection into a voltage which was recorded using a PC.

The force applied to the beam end is linearly related to measured deflection by the beam's stiffness. Therefore, the CFM allowed simultaneous measurement of the force and displacement applied to the beam end.

Collagen-GAG matrix samples 5 mm x 13 mm x ~3 mm were rehydrated with PBS and placed between the horizontal translation stage and the cantilevered beam (**Fig. 2.5**). Prior to rehydration, the width and thickness of each sample were measured using a micrometer so that force could be converted into stress using the cross-sectional area. The dimensions of the matrix did not measurably change upon rehydration. Any sample which did not have parallel edges was discarded. In addition, the samples were pre-stressed by advancing the horizontal translation stage prior to the acquisition of the first data point in order to ensure that the entire surface was in contact with the beam and stage. The sample was then compressed, along the 5 mm long axis, by advancing the stage manually at discrete intervals (0.1, 0.2, 0.5, 0.8, 1.1 mm), causing both the beam and the matrix sample to deflect (see Appendix C.2). After a two minute delay following each compression interval, deflection of the beam was recorded as a change in voltage by a data acquisition card (AT-MIO 16XE-50, National Instruments, Austin, TX) installed in a PC. This delay allowed the matrix to reach a steady-state displacement following the increase in displacement. Force and displacement of the beam were then calculated from this voltage using calculated calibration factors (Chapter 3). The matrix and the beam were in series (**Fig. 2.5**), so the force in the beam was equal to the force in the matrix. Matrix stress was calculated by dividing the force by the cross-sectional area of each sample (13 x 3 mm). The deflection in the matrix was calculated by subtracting the beam end deflection from the stage displacement. Matrix strain was calculated by dividing the matrix deflection by the original length (5 mm).

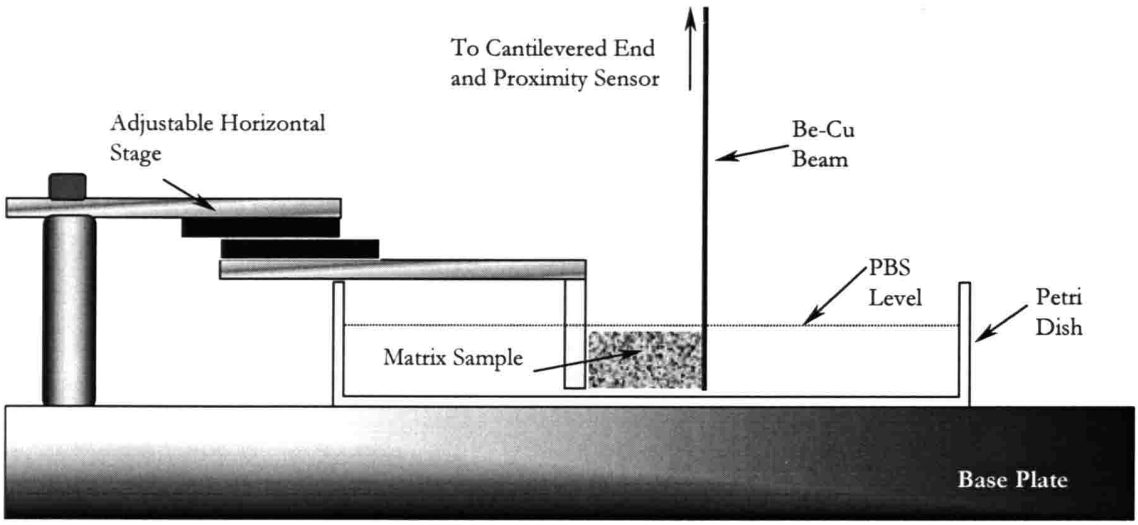

Figure 2.5. Schematic of compression testing setup utilizing the CFM. The sample is pushed with the horizontal stage causing both the beam and matrix to deflect. The beam deflection is measured using a proximity sensor (see Fig. 3.2).

An engineering stress-strain plot was constructed from individual samples. Samples were tested from two different matrix sheets each crosslinked for 24 h (n = 11and n = 5), to determine the variation between sheets. A matrix sheet crosslinked for only 1 h was also tested for the free-floating experiments described in Chapter 6 (n = 6).

2.3 Results

2.3.1 Matrix Pore Diameter

The analysis of two-dimensional sections yielded an average pore diameter of 138 ± 12 μm (n = 4) and an average aspect ratio of 1.2. This aspect ratio represented the preferred alignment of the pores in the image analyzed (*e.g.*, **Fig. 2.2**). Although not quantitatively analyzed, the pore alignment was only a localized phenomenon. In other words, for the small areas of the matrix analyzed the pores had a preferred alignment, but when the matrix was viewed macroscopically the pore orientation was essentially random, similar to a polycrystalline solid. In addition, a general observation of hydrated full-thickness matrix via

light microscopy was the presence of pore walls which were curved without any imposed deformation (**Fig. 2.1c** arrow **1**). This was also apparent in the planar sections (**Fig. 2.2** arrow **1**).

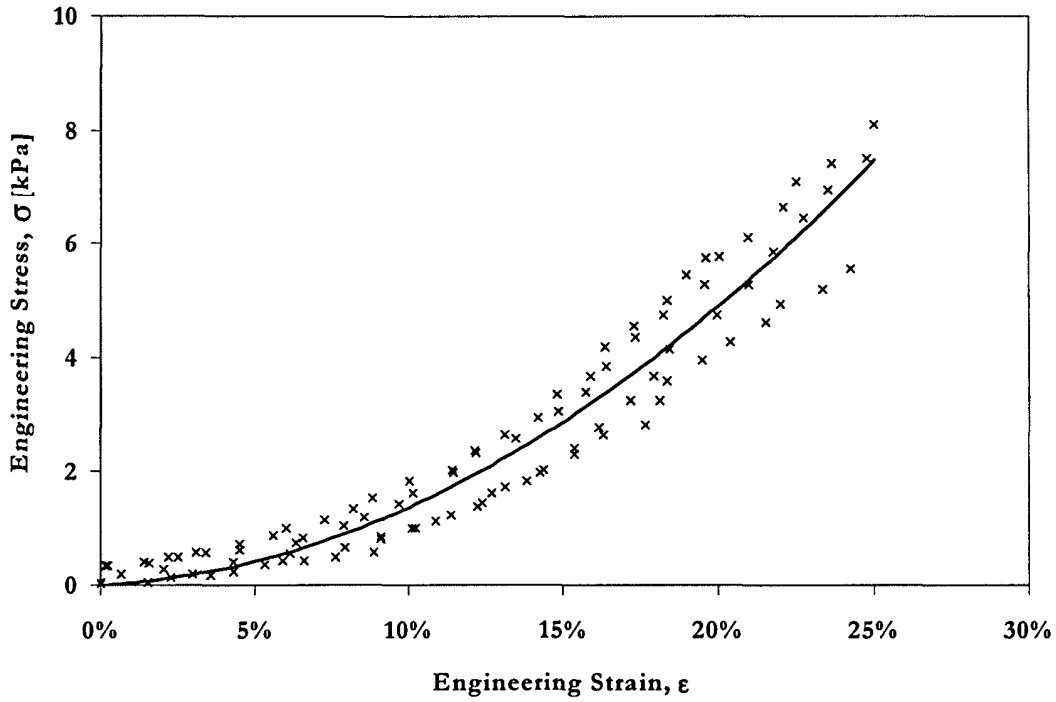

Figure 2.6. Tension stress-strain curve of hydrated collagen-GAG matrices at 37°C. Data points represent the results from 4 samples. Trendline is a best-fit second order polynomial.

2.3.2 Tension Testing

Tension testing of matrix samples resulted in a stress-strain curve for which the slope increased with increasing strain (**Fig. 2.6**). Matrices generally failed at a strain between 20-25%. In most samples, failure initiated at a small, localized tear which slowly propagated across the width of the sample. The initial tear did not occur near the clamps nor did it always occur at an edge of the sample. In addition, there was no correlation between the location of failure initiation and the fabric paint.

2.3.3 Compression Testing

A representative compressive engineering stress-strain curve is shown in **Figure 2.7.** All samples exhibited a linear ($R^2 \geq 0.96$) stress-strain behavior up to the highest strains tested (~20%). The average slope for all samples from a particular sheet of 24 h crosslinked matrix was determined to be 44 ± 5.9 Pa (n = 11). A second sheet of 24 h crosslinked matrix, tested to examine sheet-to-sheet variation, had an average slope of 54 ± 9 Pa (n = 5). The average slope for the matrices crosslinked for only 1 h, for use in the free-floating experiments (Chapter 6), was 19 ± 4.4 Pa (n = 6).

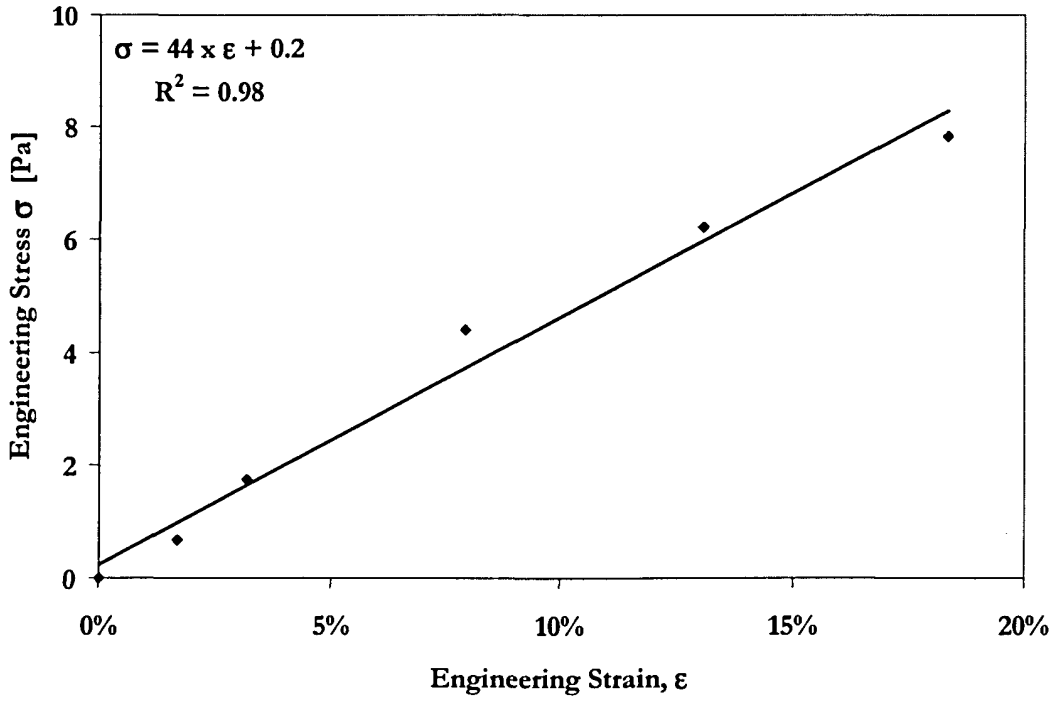

Figure 2.7. Representative compression stress-strain curve of hydrated collagen-GAG matrix. Other samples showed a similar linear response up to ~20% strain.

2.4 Discussion

2.4.1 Comparison of Collagen-GAG Matrix with Other Foamed Materials

The microstructure of the collagen-GAG matrix resembled that of other open cell foams (**Fig. 2.1**) [46]. The pore structure was not perfectly regular, resulting in local variations in matrix stiffness (**Fig. 2.1c** arrows **2** and **3**). This effect was compounded by the presence of struts which were curved prior to matrix deformation (**Fig. 2.1c** arrow **1**). The fibroblasts which were used in the experiments presented in the following chapters were ~10 to 20 μm in diameter when rounded and ~ 50 μm in length when elongated. Therefore, since the size of the fibroblasts was similar to that of the pores, localized variations in pore diameter, geometrical stiffness and irregularities in pore shape will most likely affect cell behavior.

2.4.2 Macroscopic Mechanical Properties of the Collagen-GAG Matrix

Neither the tension nor the compression stress-strain curve for the collagen-GAG matrix were qualitatively similar to those reported for more traditional foamed materials (**Figs. 2.6, 2.7, and 2.8**). Current theory predicts that the mechanical properties of a foam are determined by the properties of the pore wall material, the foam's pore volume fraction, and the pore geometry [46]. The production method and small size of the individual collagen-GAG matrix struts precluded determination of the pore wall material's mechanical properties under appropriate testing conditions. Therefore, a direct application of the current theory was not possible. An interpretation of the macroscopic mechanical testing results, based on a qualitative comparison with the stress-strain curves and the microstructure of other well-characterized foams, is presented.

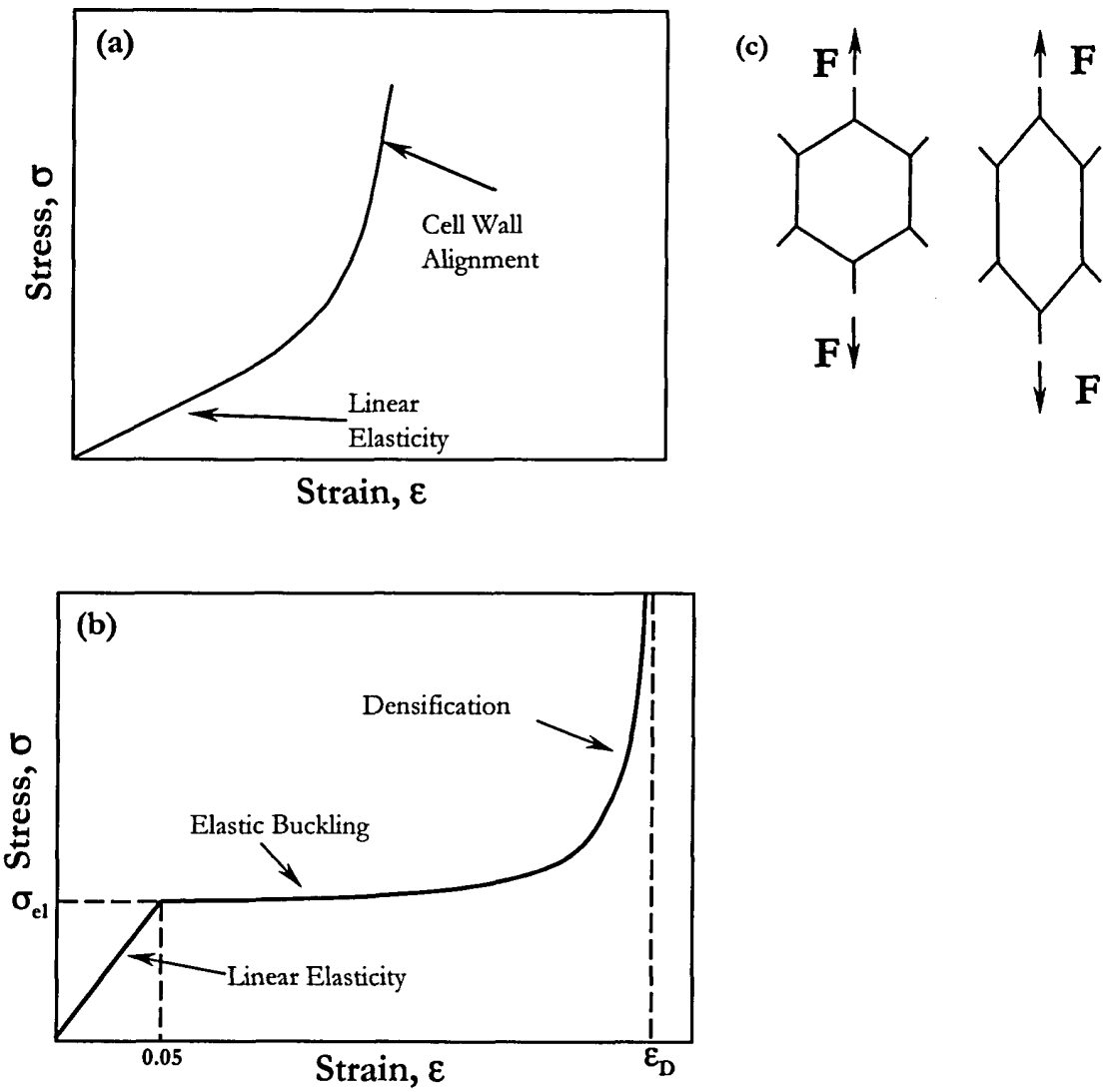

Figure 2.8. Tensile (a) and compressive (b) stress-strain curves representative of elastomeric foams. In (b), σ_{el} is the stress at which elastic buckling occurs ($\varepsilon \cong 0.05$ for open cell foams) and ε_D is the strain at which the foam's density is equivalent to that of the solid material. (c) Schematic illustrating the alignment of pore walls (struts) after tensile deformation. This phenomenon causes the increase in slope of the tension σ-ε curve at high strains.

The collagen-GAG matrix's tensile stress-strain curve did not exhibit the initially linear region reported for other foams (**Figs. 2.6 and 2.8**). In the literature [46], this small strain regime is linked to linear elastic bending of pore walls. Instead, there appeared to be a continuous increase in slope similar to the cell wall alignment region observed in traditional foams (**Fig. 2.8**). Due to the high compliance of the collagen-GAG matrix, it is likely that

the linear elastic deformation was not noticeable due to the resolution of the testing equipment. As the walls become aligned, they would be more resistant to deformation, resulting in an increasing slope in the tension stress-strain curve (**Fig. 2.8c**).

In contrast, the compression stress-strain curve was completely linear ($R^2 \geq 0.96$). The stress-strain curve for other foams in compression exhibits two linear or nearly linear regions: linear elasticity and elastic buckling (**Fig. 2.8**). Linear elastic deformation of most foams terminates beyond ~5% strain, followed by a sharp decrease in slope caused by the onset of elastic buckling of cell walls. The collagen-GAG matrix stress-strain curve had no such transition even to strains > 15%, suggesting that the linear elastic region was circumvented by another deformation mechanism(s). The observation of curved struts prior to any imposed deformation (**Fig. 2.1c** arrow **1**) would be consistent with immediate elastic buckling. Therefore, early deformation was likely the result of buckled struts preferentially deforming under the applied load, rather than linear elastic bending. The slope of this curve would then represent the slope of the elastic buckling region.

2.5 Conclusions

The pores of the collagen-GAG matrices were slightly elliptical (aspect ratio = 1.3). A representative pore diameter, determined by averaging the major and minor axes of the ellipse, was ~140 μm. The preferred alignment of elliptical pores was localized in regions < 1 cm on a side and these regions were randomly oriented throughout the matrix sheet. Therefore, the size of the matrix samples used in the contraction experiments preempted the need to account for the localized anisotropy. The shape and size of the pores and struts was not perfectly regular resulting in local variations in matrix stiffness. Since the size scale of fibroblasts was similar to that of the pore structure the local variations in stiffness likely

affected cell behavior. The macroscopic tension and compression stress-strain response of the matrix did not compare well with that reported for other porous materials. However, the linear nature of the compression response allowed for the calculation of a modulus (~44 Pa). This modulus was used to calculate the fibroblast contractile force due to the compressive nature of the matrix contraction by fibroblasts. The tensile properties reported in this chapter were not used to determine fibroblast contractile force.

Chapter 3. Design and Testing of the Cell Force Monitor (CFM)

3.1 Introduction

An important component of an *in vitro* model of cell-mediated contraction is the method through which contraction is monitored; the choice of this method will determine how the variables which affect the contraction will be controlled. Two experimental systems for measuring contraction *in vitro*, using cell-seeded substrates, have emerged from previous work. Non-instrumented systems measure the dimensional changes of a cell-seeded substrate over days or weeks [12-15]. Instrumented systems generally provide a resistance, in addition to the substrate, opposing contraction, and monitor changes in the contractile force developed by the seeded cells continuously, up to several days [16-20]. For this study, an instrumented system was designed and constructed which quantitatively monitors the contraction of a collagen-GAG matrix by fibroblasts immediately following cell attachment.

The goal of the design of the cell-force monitor (CFM) was to measure the contraction of the collagen-GAG matrix in the most direct and accurate manner possible. This goal was established so that measurement techniques would not complicate the interpretation of the contraction data. Our design was based on a similar device developed by Eastwood and his co-workers [18, 41]. In their device, one end of the substrate was held by a fixed clamp, while the other was connected to a wire A-frame which was attached to a cantilevered beam. The beam was instrumented with strain gages to measure its deflection as the substrate was contracted by the cells. The use of the wire A-frame introduced poorly

defined moments into the device, complicating the analysis of the contractile forces. In addition, the use of strain gages attached directly to the beam made it difficult to change the level of mechanical restraint, as well as the range and resolution of the forces measured. The design described in this study is a modification of Eastwood's device, in which the cantilever beam is attached directly to the clamp holding the matrix, providing a more accurate measurement of the matrix response. In addition, we introduced the use of an inductive transducer (proximity sensor), rather than strain gages, to measure the beam deflection, which allows the beam stiffness to be varied easily. A direct comparison between the CFM and Eastwood's device to determine the effect of these design changes has not been made, but our modifications do result in a more compact, mechanically simplified system.

The CFM allows the evaluation of the cellular contractile response under a variety of environmental conditions *in vitro*, including changes in matrix stiffness, changes in an externally opposed resistance to substrate contraction, and changes in the chemistry of the testing environment. The CFM has application in furthering understanding of the contraction associated with wound healing, and of the presence and role of contractile cells in diseased tissue. In addition, the CFM may prove useful in understanding the effect of forces on gene expression and cellular differentiation.

3.2 Device Design

The cell-force monitor (CFM) was designed to monitor the contraction of a compliant, biocompatible porous matrix by cells over time (**Fig. 3.1a**). Cell-seeded, rectangular matrix samples were clamped on either side along their long axis (**Fig. 3.1b**).

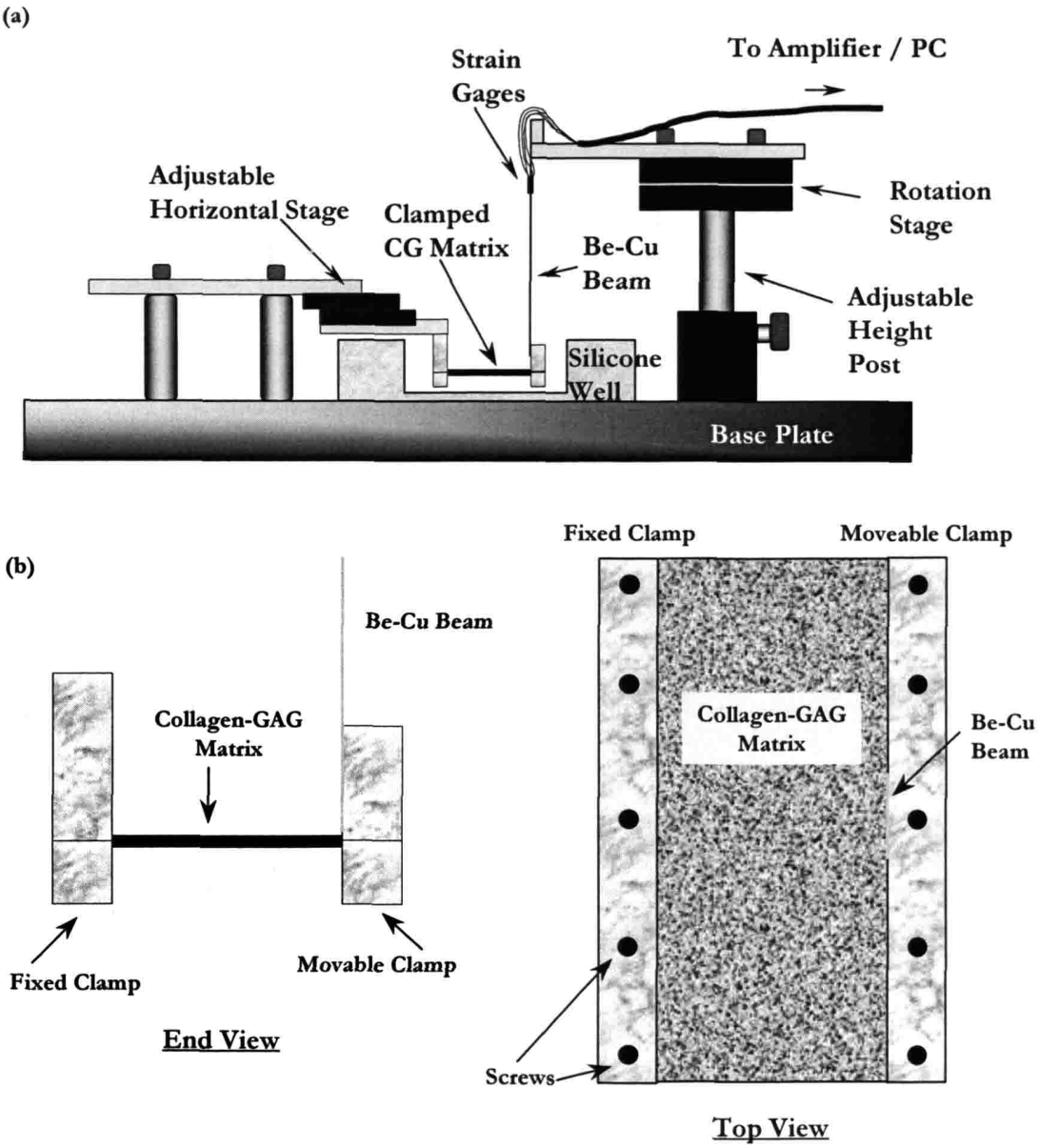

Figure 3.1. (**a**) Schematic of the strain gage cell force monitor (CFM). The matrix is held between a fixed clamp on the left and a second clamp, attached to an instrumented beam, on the right. Contraction of the matrix by the cells deflects the beam, allowing the cell force to be calculated. The beam deflection is measured by either strain gages or by a proximity sensor. (**b**) End and top view of a clamped collagen-GAG matrix attached to the CFM.

One clamp was fixed while the other was attached to an instrumented beryllium-copper beam (100mm x 10mm x 0.15mm; 2% Be - 98% Cu, Goodfellow Corp, Cambridge, UK). The end of the beam farthest away from the porous scaffold was rigidly clamped in the

vertical position. As the cells contracted the matrix, the beam deflected; measurement of this deflection, by either strain gages or a proximity sensor (**Fig. 3.2**), allowed the contractile force to be calculated.

The mechanical resistance of the system was controlled by changing the beam geometry (see Chapter 6). The scaffold and the clamps were submerged in cell culture medium in a silicone well. Adjustable stages were used to ensure that the clamps were parallel, the matrix was horizontal, and the beam was at its equilibrium position prior to the start of each test. The entire apparatus was mounted on an anodized steel optics plate (Edmund Scientific, Barrington, NJ).

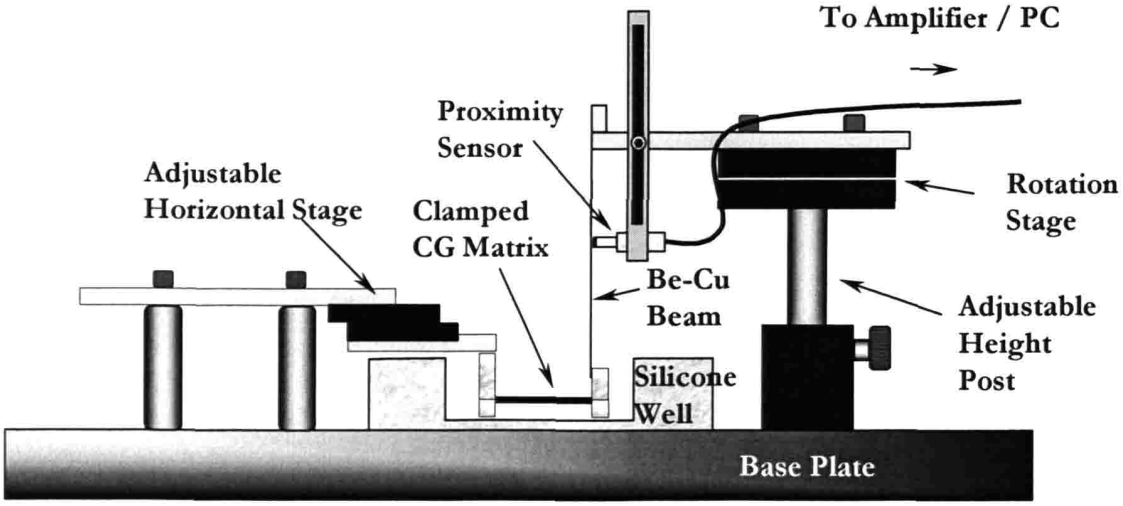

Figure 3.2. Schematic of the proximity sensor cell force monitor (CFM). See caption for **Fig. 3.1** for detailed description.

3.2.1 Strain Gage CFM

Four strain gages (N3K-06-S022H-50C Measurements Group, Inc., Raleigh, NC) were attached to the beam, two on each side, 15 mm from the clamped end. To ensure proper measurement, the gages needed to be well-bonded to the beam, while minimizing local stiffening of the beam. The gage manufacturer's recommendations for surface preparation (roughening, de-greasing, conditioning, and neutralizing pH) and for the

adhesive (M Bond 450, Measurements Group, Inc., Raleigh, NC) were followed (see Appendix E.1). The strain gages were then wired in a full-bridge configuration which compensates for temperature changes so that the voltage difference across the bridge, produced by bending, would be maximized. Signal voltage from the bridge, due to beam bending, was acquired by a data acquisition card (AT-MIO-16XE-50) installed in a PC using the strain gage accessory (SC-4083, National Instruments, Austin, TX). This accessory supplied a stable excitation of 5V to the bridge, and then amplified the output signal before transmission to the PC to reduce noise. When possible, shielded wires were used to reduce noise further. Data processing was performed by data acquisition software loaded on the PC (Labview, Austin TX); voltage values were acquired from the strain gage bridge at a rate of 1 per second, and were then averaged over 100 seconds to yield one data point (see Appendix E.6). The strain gage bridge and small diameter inter-gage connecting wires were coated with a 3:1 mixture of petroleum jelly and paraffin wax to protect the electronics from the high humidity in the incubator. This mixture minimized local beam stiffening without flowing at the elevated temperature (37°C) in the incubator. Commercially available coating materials including: silicone (3140-RTV), microcrystalline wax (M-Coat-W1), and solvent-thinned butyl rubber (M-Coat FBT) (Measurements Group, Raleigh, NC) were not as effective at protecting the gages from moisture.

3.2.2 Proximity Sensor CFM

A second CFM was built using an inductive transducer (proximity sensor) to detect beam deflections (**Fig. 3.2**). Without contacting the beam, the proximity sensor (KD-2300-1SU, Kaman Instruments, Colorado Springs, CO) measured beam movement by emitting an electromagnetic field and sensing impedance changes due to the conductive beam in the

field. The sensor measured deflections up to 1.3 mm from its front surface at a resolution of 0.1 μm. The voltage output for this sensor was 1 V/mm and varied linearly with distance to the beam. Voltage readings were acquired using the same method described above for the strain gage CFM. Modifications were made to firmly fix the sensor so that motion relative to the beam occurred only by bending of the beam. The modifications allowed the position of the sensor along the beam's length to be adjusted. The best sensor position maximized resolution while keeping the maximum expected deflection within the sensor's range. For these experiments, the sensor was placed 36 mm from the fixed end of the cantilever.

3.3 Methods

3.3.1 Measurement of Drift

To assess baseline function, the stability and signal-to-noise ratio of an undisturbed beam was recorded. To establish this baseline response, the CFM was prepared and placed in the incubator, as if for a matrix contraction experiment, but no clamp was attached to the beam. Voltages were then gathered for 20 hours in the manner described above. The drift in the average voltage with time and the peak-to-peak voltage change attributed to background noise were calculated. This measurement was repeated for both the CFM instrumented with strain gages and that instrumented with a proximity sensor.

3.3.2 Calibration of the CFM

The cell-force monitor recorded displacement data as voltage changes using either the strain gage bridge or the proximity sensor. In both systems, the voltage changes were proportional to the deflection of the beam, which, according to elementary beam theory, is proportional to the force opposing motion from the beam's equilibrium position. The

system was calibrated to convert voltage changes to displacements or forces (see Appendices E.2 & E.6). To calibrate for displacement, voltage changes were recorded after displacing the beam end by a known amount, from 0.2 to 2mm, with a micrometer (resolution 0.01mm). A minimum of 5 displacements were used to construct a plot of voltage vs. displacement. The resulting slopes from 3 such plots were averaged to yield a calibration factor. To calibrate for force, known masses, ranging from 3.2 mg to 2g, were placed on the end of the beam in the horizontal orientation. An initial deflection due to the beam's own weight was accounted for by using it as a zero point. The calibration range for displacement and force were selected to include the maximum values expected during cell-seeded matrix contraction experiments. Maximum values in actual experiments did not exceed these expectations.

The cellular contractile force was equal and opposite to the total force in the beam and the matrix. Since the beam and matrix displaced equal amounts, they acted in parallel, and the total force was the sum of each element. The opposing force in the beam, F_{beam}, was found directly from the voltage data using the calibration factors described above, while the opposing force in the matrix, F_{matrix}, was calculated using the compressive stiffness (measured in Chap. 2) of the matrix and the deflection of the beam end. Therefore, the total force exerted by the cells was:

$$F = F_{beam} + F_{matrix} = V \cdot C_{force} + V \cdot C_{displ.} \cdot K_{matrix} \qquad \textbf{(Eqn. 3.1)}$$

where V was the voltage measured, C_{force} and C_{displ} were calibration factors for force and displacement, respectively, and K_{matrix} was the compressive stiffness of the matrix. (Note: $K_{matrix} = (E_{matrix} \cdot A)/l$ where A and l are the cross-sectional area and length of the matrix, respectively.)

Due to the rigid attachment of the matrix to the beam, the deflection of the beam and the matrix were identical. Thus, the choice of beam or matrix stiffness can make one of the components of opposing force negligible (*e.g.*, if the beam is orders of magnitude stiffer than the matrix, then the matrix stiffness is negligible). It should be noted that the CFM, like most force transducers, directly measured displacement to infer force. Thus, if the combination of beam and matrix stiffness was sufficiently large, no noticeable deflection would be measured, even though the cells were generating a contractile force.

3.3.3 Cell Seeding and Force Measurement Assay

As a test of the CFM's functionality, a known number of fibroblasts in suspension were seeded onto a clamped, hydrated matrix sample (25 mm x 70 mm x ~3 mm; Length x Width x Thickness) attached to the CFM. The matrix sample was hydrated by submersion in 37°C culture medium for 30 minutes and blotted dried with filter paper (S&S #595, Dassel, Germany). The fibroblast suspension (830μl volume) was then evenly distributed over the top surface with a pipet. The matrix was held at 37°C for 10 minutes to encourage fibroblast attachment, and then the silicone well of the CFM was filled with culture medium. The entire apparatus was placed inside an incubator (Ultima 300T, Revco, Asheville, NC) at 37°C, 5% CO_2 and ~98% R.H., and data was acquired using the data acquisition program. The acquired voltage, representative of deflection of the beam, was translated into contractile force through application of **Eqn. 3.1**. Attached fibroblast number was determined at 22 hours by digesting the matrix in a buffered dispase (GIBCO, Grand Island, NY) solution (2.0 U/ml) at 37°C for 20 minutes and counting fibroblasts with a hemacytometer (Bright-Line, Hausser Scientific, Horsham, PA). Cell-free experiments were

performed to establish a baseline response of the matrix alone, which was subtracted from subsequent measurements with cells to yield the cell-mediated contractile response.

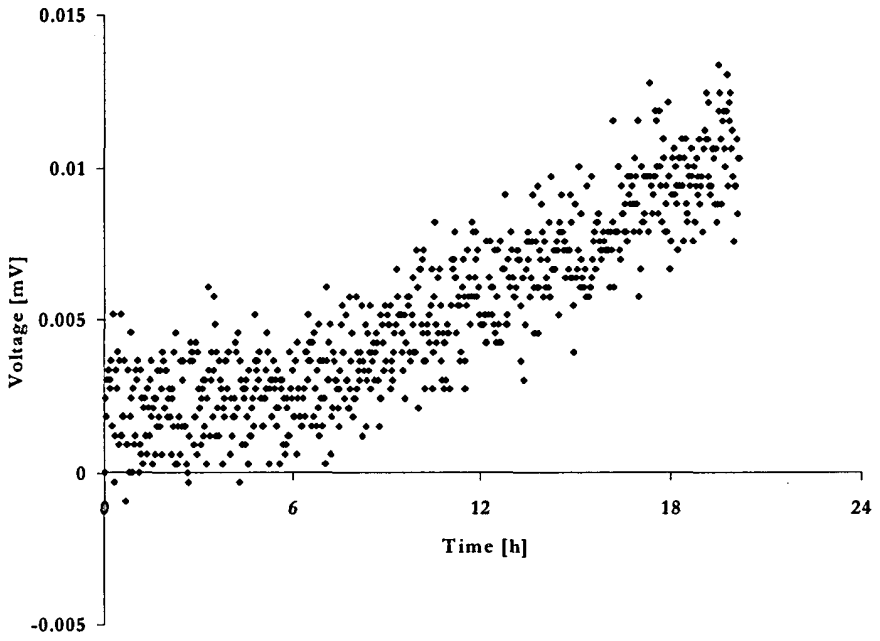

Figure 3.3 Plot of voltage over time for the strain gage CFM, in the incubator, to show the response with nothing attached to the beam. The drift was accounted for when analyzing cell contraction data by subtracting the cell-free control. The peak-to-peak noise, 5μV, was ~ 50x smaller than the signal produced from contraction by cells.

3.4 Results

3.4.1 Measurement of Drift

A baseline response for the CFM was established by placing it in the incubator with nothing attached to the beam. The signal recorded from the strain gage bridge drifted ~10 μV over 20 hours with a peak-to-peak noise of ~5 μV (equivalent to 200 μN) (**Fig. 3.3**). The signal from the proximity sensor had no noticeable drift over 20 hours with a peak-to-

peak noise of 1 mV (equivalent to 12 μN) (**Fig. 3.4**). An initial 1 mV decrease in the proximity sensor output signal occurred within the first hour of the test, most likely due to temperature change associated with opening and closing the incubator door. A typical force developed by cells seeded onto the collagen-GAG matrix was ~ 10 mN.

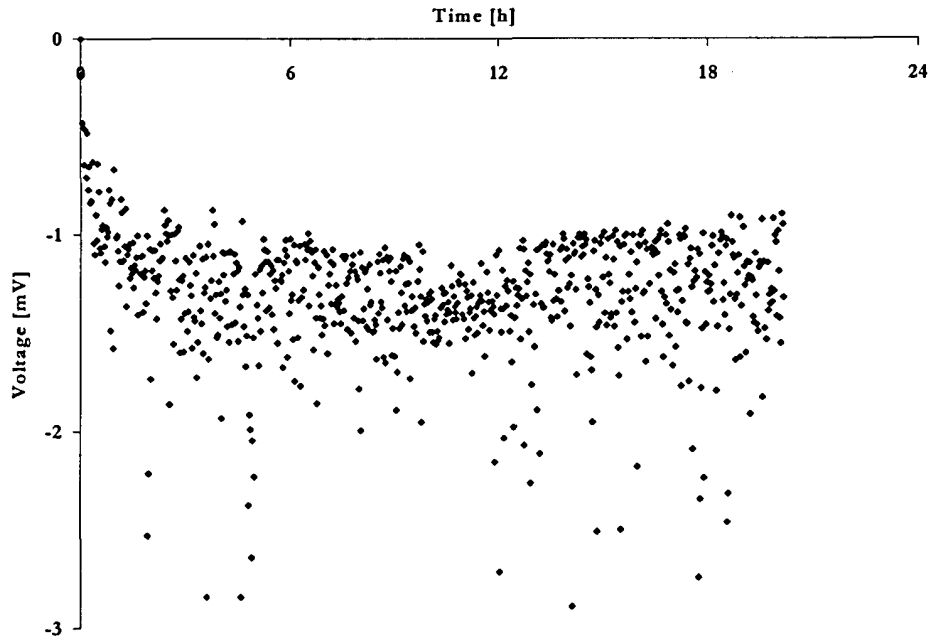

Figure 3.4 Plot of voltage over time for the proximity sensor CFM, in the incubator, to show the response with nothing attached to the beam. Following an initial decrease in voltage, no drift was noticeable. The peak-to-peak noise, 1mV, was ~ 800x smaller than the signal produced from contraction by cells.

3.4.2 Calibration of the CFM

The calibration curves for the strain gage CFM and for the proximity sensor CFM are shown in **Figs. 3.5** and **3.6**, respectively. The displacement-voltage and force-voltage data were linear, with $R^2 > 0.99$. The calibration factors are reported in **Table 3.1**. Beam stiffness was equivalent to the ratio of the two calibration factors (C_{force}/C_{displ}), and was measured as 2.0 and 1.7 N/m for the strain gage and proximity sensor CFMs, respectively.

This beam stiffness was ~ 6x higher than the stiffness of the matrix samples used in the experiments reported in this chapter $\left(K_{matrix} = 40Pa \cdot \frac{0.07m \cdot 0.003m}{0.025m} = 0.34 \frac{N}{m} \right)$.

When the proximity sensor was moved down the beam by an additional 32mm the sensitivity increased by a factor of 3 to 2.40 ± 0.018 mm/V. This new sensor position resulted in a slightly less linear response, with a correlation coefficient (R^2) of 0.9996.

Table 3.1. Calibration factors for the CFMs.

	Strain Gage CFM		Proximity Sensor CFM	
	Displacement (mm/V)	**Force (N/V)**	**Displacement (mm/V)**	**Force (N/V)**
Slope	2,780 ± 9	5.58 ± 0.18	7.21 ± 0.053	0.012 ± 0.0001
R^2	0.9999	0.9996	0.9999	0.9999

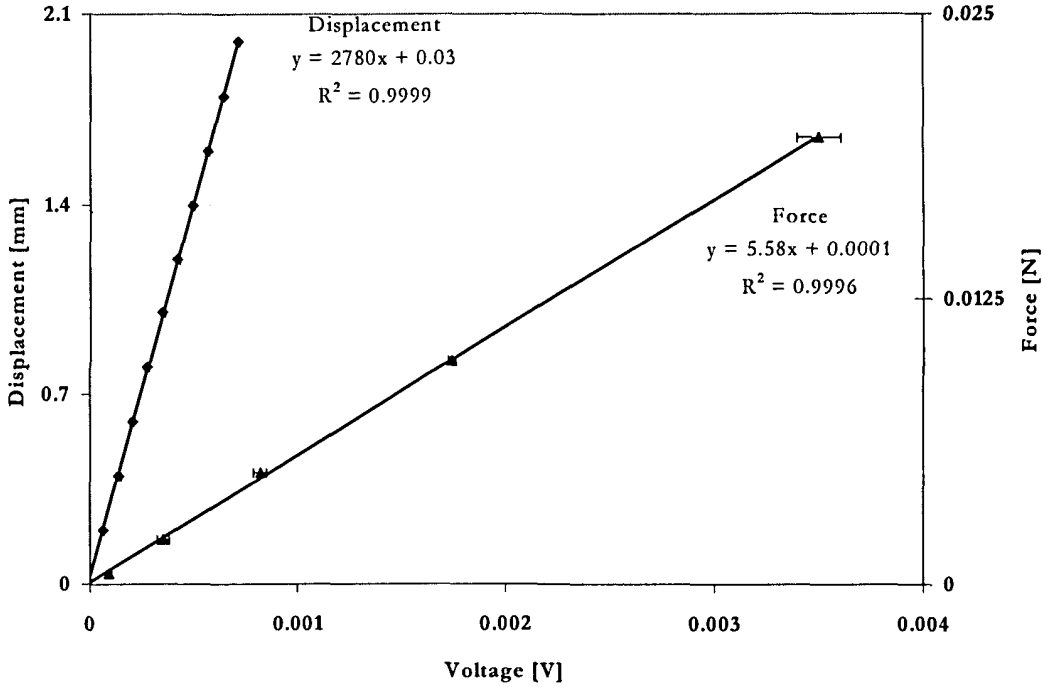

Figure 3.5. Strain gage CFM displacement and force calibration plots. The slope of these curves was used to convert voltage changes recorded during contraction experiments to force and displacement.

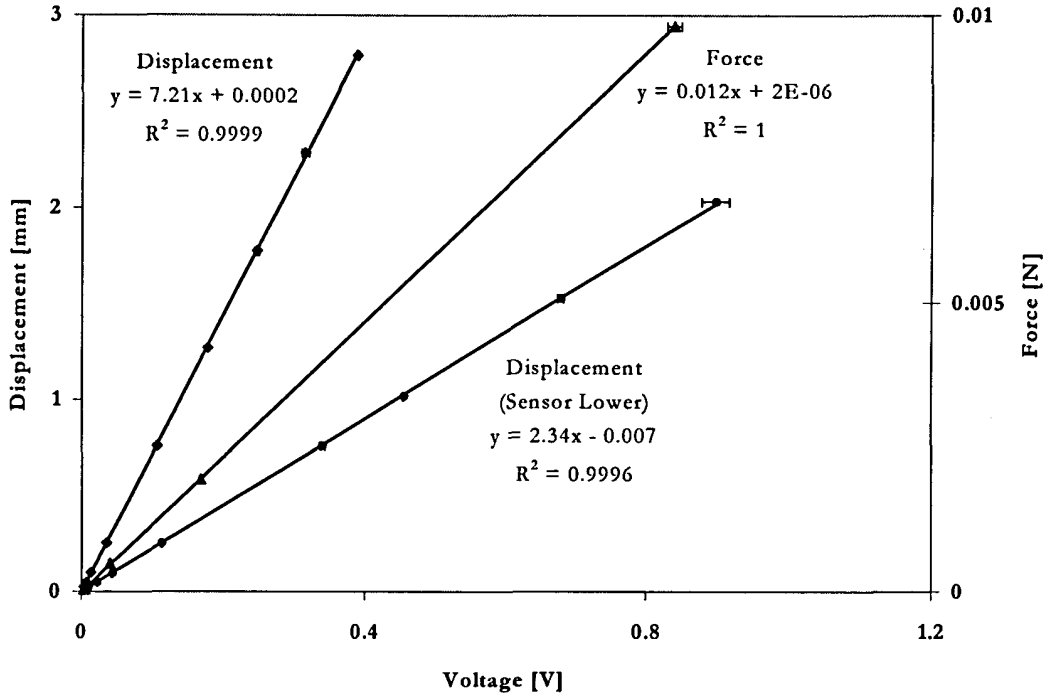

Figure 3.6. Proximity sensor CFM displacement and force calibration plots. The slope of these curves was used to convert voltage changes recorded during contraction experiments to force and displacement. The second displacement vs. voltage curve (marked sensor lower) shows that as the proximity sensor was moved closer to the beam end the measurements become more sensitive (larger voltage change for a smaller displacement or force change).

3.4.3 Measurement of Contractile Forces

A cell-free baseline response was established using the CFM (**Fig. 3.7**). The force increased rapidly initially and then, after approximately 3 hours, increased steadily at a rate of ~0.05mN/hour; this behavior was characteristic of all matrix samples.

The force developed in cell-seeded matrices was greater than that in cell-free matrices at times greater then 45 minutes (**Fig. 3.7**). For cell-mediated contraction, a steady-state force was reached after about 12 hours. This force level, 3 times that of the cell-free matrix, was stable up to termination of the experiment at 22 hours. Attached fibroblast

number at 22 hours was 7.2 million. Assuming that all of these cells participated in contraction, the average force of contraction was 1.25 nN per cell.

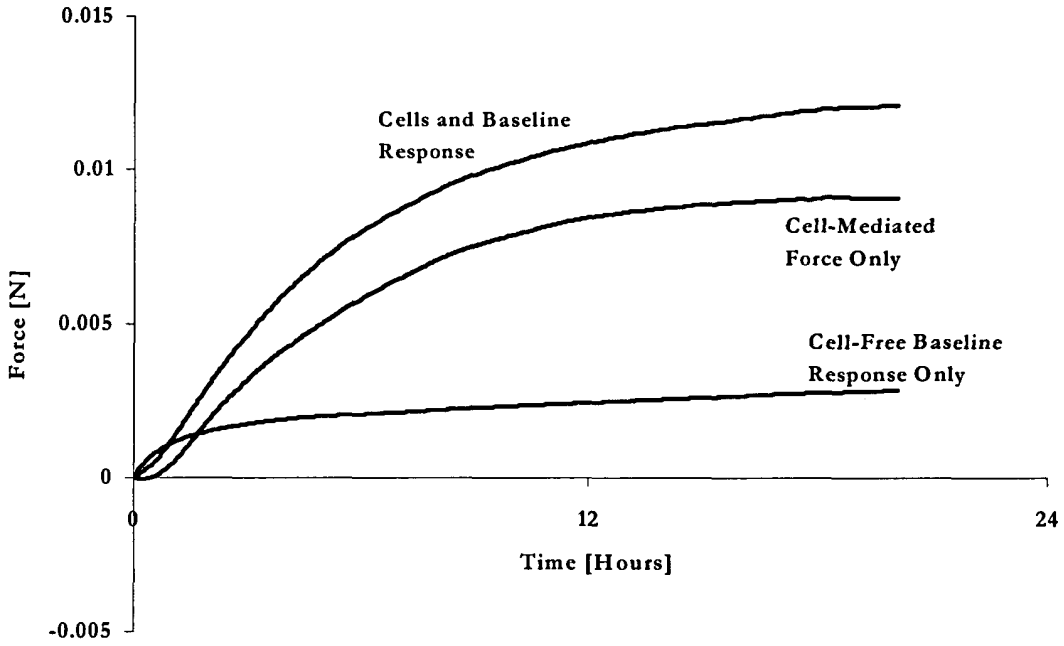

Figure 3.7. Force over time plot from the CFM for a cell-free matrix sample and a cell seeded matrix sample. The cell-mediated force was determined by subtracting the cell-free baseline from the cell-seeded matrix curve.

3.5 Discussion

3.5.1 Device Design

Substitution of the proximity sensor for the strain gage bridge further simplified the device and made it more versatile. Since the beam and sensor were not bonded together, replacing the beam or changing to a beam of a different stiffness required only an 1 hour. In addition, the beam stiffness was not affected by the instrumentation. The resolution and range of the proximity sensor CFM depended on the position of the sensor along the beam,

allowing the device to be tailored to obtain the highest resolution for different substrate/cell combinations, depending on the maximum expected force. The sensor was designed to detect motion of a surface of constant curvature, so beam bending may have limited the linearity of the proximity sensor CFM. This would be most noticeable when measuring large displacements with the sensor mounted near the moving beam end. However, the results presented here suggested this effect was likely negligible.

3.5.2 Functionality of Device

The ratio of force to displacement is a measure of the beam stiffness. From the range of elastic moduli supplied by the manufacturer, the calculated theoretical beam stiffness ranged from 1.53 – 2.05 N/m. The value obtained experimentally for the proximity sensor CFM, 1.7 N/m, was near the middle of this range. The higher value for the strain gage CFM, 2.0 N/m, was likely attributable to the strain gages, coating, wiring and adhesive adding stiffness to the upper portion of the beam.

Testing of the CFMs indicated that they were linear and able to measure the necessary range of contractile forces. The peak-to-peak noise of the strain gage and proximity sensor CFMs were 5% and 0.1% of the full-scale cell-mediated contractile force, respectively. These values indicated that both devices were able to resolve forces at the level required. However, the negligible amount of noise in the proximity sensor CFM suggested that it was a better instrument for measuring changes in contractile force.

3.5.3 Force Measurement

Contraction of the cell-free collagen-GAG matrix has been reported previously [15, 41]. The origin of this unseeded matrix response is not fully understood. Possible explanations include: relaxation of stresses established during freeze-drying or cross-linking,

an elution of GAG molecules with time, and/or a time dependent equilibration of the matrix with components of the culture medium. To obtain fibroblast-mediated force this baseline response was subtracted from the overall response.

Similarities in these data to those reported by others validated the use of this design [16, 18, 41]. Brown *et al.* [41] reported a steady-state value of 2.5 nN per cell established after ~20 hours in culture, compared to a steady-state value of 1.25 nN per cell after ~12 hours in culture with this new device. Explanations for this difference include: use of a different cell type (primary human dermal fibroblasts), seeding the fibroblast suspension onto a dry collagen-GAG matrix sample, differences in the force measurement device, and variation in culture medium or other experimental conditions.

Other investigators have generally neglected the substrate stiffness in calculating the contractile force from the deflection of a force transducer due to the relatively low value of substrate stiffness as compared to the stiffness of the transducer itself [16-18, 20]. However, there is a force associated with substrate deformation and, if it is comparable to or greater than that of the transducer, it must be included in the calculations. This is accomplished by multiplying the substrate stiffness by the measured substrate deflection and adding it to the force measured directly from the transducer. For the system described here, the scaffold stiffness was 17% of that of the beam and was included in the calculation of fibroblast-mediated contractile force.

Details describing the generation of fibroblast-mediated contractile forces are still scarce. The force development coincides with the spreading and migration of the contractile fibroblasts within the three-dimensional substrate material [43]. The value of the steady-state force that develops has been shown previously to be dependent on the chemical (*e.g.*, cytokines) and physical/mechanical (*e.g.*, collagen gel concentration) environment in which

the fibroblasts interact [16, 17]. The devices outlined in this chapter allow for specific control of these environmental conditions. Experiments using these CFMs to determine the effect of cell number, and beam stiffness on the contractile response of fibroblasts seeded onto the collagen-GAG matrix are described in Chapters 4 & 6, respectively.

Chapter 4. Effect of Attached Cell Number on Contraction of the Collagen-GAG Matrix

4.1 Introduction

The cell force monitor (CFM) was designed to measure the contractile force developed by many cells attached to a collagen-GAG matrix over time in a controlled environment. The CFM measurements from different experimental groups are compared to understand the cells' response to changes in experimental parameters. Due to the large number of cells which develop the contractile force, knowledge of how cell number affects the apparent force is imperative to proper interpretation of the response. The reasons for this are two-fold. First, if the cells act cooperatively to develop the contractile force, then they would also likely respond to environmental changes cooperatively. If this cooperation among cells can be unequivocally demonstrated, then the changes in contractile response measured with the CFM must be interpreted with this understanding. Second, the number of cells which attach to the collagen-GAG matrix can vary significantly from the number which were initially seeded. Therefore, knowledge of the relationship between attached cell number and the contractile force which develops will allow for comparison between experiments when attached cell number is not constant.

The force measured by the CFM could be developed cooperatively or individually by cells. This would result in a force which is insensitive or sensitive to the attached cell number, respectively. For example, it has been suggested by others [41] that the level of force which was developed by fibroblasts in a collagen gel was a homeostatic level. The issue of whether this homeostatic level was determined by each cell individually, or through

a coordinated effort by all of the cells, remains unanswered. If it was determined through a cooperative effort by the cells, the force should be relatively insensitive to changes in cell number; if the cells acted individually, then the force should be sensitive to changes in cell number. Discussion of other *in vitro* models of contraction by many cells does not address the role of cooperative cell behavior in the development of contractile force [16-18, 20, 41].

Other investigators have used various methods to account for cell number when interpreting contraction data from cell seeded collagen gels. When using collagen gels, the cells were embedded inside the gel during manufacture and the attached cell number was assumed to be equivalent to the seeded cell number [16, 18, 20]. Experiments were then performed with the same seeded cell number in each sample, or the force data were compared after normalization by the seeded cell number [18]. In order for normalization by seeded cell number to be appropriate, the dependence of force on cell number must be linear. In previous work [16], a linear relationship was established between the ratio of maximum force divided by time to reach this force and the fibroblast density in a collagen gel, but the direct relationship between cell density and force was not discussed. A more rigorous method of accounting for cell number utilized the cross-sectional area of cells in the plane perpendicular to the axis of force measurement [17]. This method assumed that the force of elements (cells) aligned parallel to the axis of measurement must be a constant, since these elements were in series. Therefore, a force developed per cross-sectional area of cells (stress) was reported. All of these methods may yield acceptable results, but no rigorous analysis of these procedures has been completed. In addition, the relationship between cell number in a collagen-GAG matrix and the force which is developed has not been established.

Another method of studying cell contractile force eliminates the problem of accounting for cell number entirely by directly measuring the force developed by individual cells [33, 36, 48, 49]. However, it is difficult to use this technique to establish a statistically significant average response for a population of cells. An average response must be compared when assessing the effect of a change in experimental parameters, since it is unlikely that all cells will exhibit an identical response. In addition, the environment in which cells develop forces *in vivo* cannot be mimicked using this system because the measurements take place on a two-dimensional substrate and no cell-cell interactions can occur.

The goal of this study was to determine the effect of fibroblast number (density) on the contractile force measured with the CFM, thereby providing a basis for comparing independent measurements made at arbitrarily selected levels of cell density. For all cell densities, the contractile force increased with time, eventually reaching an asymptote. An equation describing the contractile force as a function of time was utilized to interpret data. This equation described the data accurately and allowed for comparisons between data obtained under different conditions via the use of two empirical constants that described the asymptotic force level and the rate of force development. The level of the asymptotic force was observed to increase in direct proportion to the cell density. Normalization of the asymptotic force by the cell density resulted in a value of contractile force per cell, 1 nN, that was independent of cell density over the range 400 to 2,000 cells per mm^3. The time for development of the contractile force was also independent of cell density. The change in fibroblast density over the course of the experiment was statistically significant, but this change was not consistent with the time dependence of the force generation. These results

suggest that, in this system, individual cells develop contractile force independently (*i.e.,* not cooperatively) of the force generated by the surrounding cells.

4.2 Methods

4.2.1 Cell Culture

Dermal fibroblasts were isolated from New Zealand white rabbit skin explants (Appendix B). Briefly, immediately following sacrifice by pentobarbitol (Nembutal) overdose, a section of shaved skin was excised and placed in chilled, buffered saline (pH = 7.4). The epidermis was removed by placing the explanted tissues in a 37°C solution of dispase (GIBCO, Grand Island, NY) for 30 minutes, gently pulling the majority of the epidermis off with forceps and finally scraping the surface with a scalpel blade. The residual dermis was then cut into ~1 mm sized cubes with crossed scalpels, placed into tissue culture flasks, and incubated at 37°C, 5% CO_2 to allow the cells to migrate out of the explant. DMEM (GIBCO, Grand Island, NY) supplemented with 10% fetal bovine serum (FBS) (Hyclone Labs., Logan, UT), 2% penicillin/streptomycin, 1% fungizone and 1% L-glutamine (GIBCO, Grand Island, NY) was added to the flasks. The fibroblasts were then cultured and passaged for use in contraction experiments.

Cells cultured from explants are not stable with time *in vitro.* As they are cultured and passaged *in vitro* the cells de-differentiate, increase the content of α-smooth muscle actin in the cytoplasm and, after ~15 passages, will no longer divide or function normally. For this reason, it was necessary to work with cells within a narrow range of passages. To accomplish this, cells were cryopreserved (Appendix B) in 60 aliquots of ~1 million cells so they could be thawed as needed for experiments. Thawed aliquots were subsequently cultured for 1-2 passages to increase cell number, and seeded onto the collagen-GAG

matrices. Ideally, cryopreservation of cells would have occurred following the 1st passage to reduce cell de-differentiation, but 4 passages were required to attain a sufficient number of cells for all experiments. Therefore, the fibroblasts seeded onto the collagen-GAG matrices ranged from the 5th to 7th passage.

4.2.2 Cell Seeding and Force Measurement Assay

A known number of fibroblasts in suspension were seeded into a hydrated, rectangular matrix sample attached to the cell force monitor (CFM) (**Fig. 3.1a**). Matrix samples were cut to size (70 x 35 x ~3 mm) in a sterile hood using a razor blade and a Teflon® template. The samples were then clamped along each of the long edges with ultra-high molecular weight polyethylene clamps such that the exposed planar surface was 70 x 25 mm (see **Fig. 3.1b**). Matrix samples were hydrated by immersion in 37°C culture medium (10% FBS) for 30 minutes and then blotted dry with filter paper (S&S #595, Dassel, Germany) for ~ 30 s. The filter paper was used to dry the samples so that the cell suspension could penetrate the pores of the hydrated matrix. A cell suspension was produced by removing 5th - 7th passage cells from the culture flasks with trypsin-EDTA (Sigma, St. Louis, MO). Viable cell number was determined using Trypan Blue with a hemacytometer (Bright-Line, Hausser Scientific, Horsham, PA). Following centrifugation to remove the trypsin-containing medium, the cells were re-suspended in culture medium so that 830 μl of the suspension contained the total number of fibroblasts to be seeded on the matrix sample. Then, 830 μl of this suspension was pipetted onto the top surface of the matrix sample. Matrices were held at 37°C for 10 minutes to allow for fibroblast attachment before the silicone well was filled with culture medium (10% FBS). The entire apparatus was

placed inside an incubator (37°C, 5% CO_2 and ~98% R.H.) for the duration of the contraction experiment (22 h).

All contraction data were corrected for contraction not attributable to the fibroblasts by subtracting the average force over time curve for unseeded matrices (n = 3). Force over time data were grouped based on the number of cells attached at 22 hours (see next section). The average force over time curve was determined for each group ($n \geq 3$). Due to sharply increased difficulty in obtaining the highest cell density, this group contained only two samples (n = 2).

4.2.3 Cell Counting and Histology

Following each contraction experiment, the matrix sample was cut from the clamps and bisected. One half of the sample was rinsed by repeated immersion (10 times) in 37°C Dulbecco's phosphate buffered saline(DPBS) (Gibco, Grand Island, NY) to remove unattached cells. Samples were then placed in a 2.0 U/ml solution of dispase (Gibco) at 37°C for ~20 minutes to digest the collagen matrix. Attached cell number was then determined from the dispase solution with a hemacytometer. The other half of the sample was chemically fixed for 24 h with 10% neutral buffered formalin. The fixed samples were embedded in glycomethacrylate (GMA), sectioned (5 μm), and stained with hematoxylin and eosin (see Appendix G). Hematoxylin stains the nucleus of the cells a dark red-brown color and eosin stains the cell cytoplasm and the collagen-GAG matrix a salmon pink color. The cell's cytoplasm always stained slightly darker than the matrix making identification of the cell-matrix border possible. A digital camera (DEI-750, Optronics Engineering) attached to a light microscope (Labophot, Nikon) was used to gather images for a qualitative analysis of cell morphology and the manner in which cells interact with other cells and the matrix.

The number of attached fibroblasts was determined at 0 and 22 hours for 8 and 14 million seeded cells (n = 7). These samples were cut from the clamps at either 10 minutes post-seeding (0 h) or 22 hours post-seeding, rinsed with DPBS, digested with 2.0 U/ml dispase and the attached cell number determined with a hemacytometer. These experiments mimicked those performed in the CFM, but were reduced in physical dimensions by one-third to conserve materials. Statistical analysis showed that this scaling had no significant effect ($p > 0.8$) on the attached cell number at 22 h when compared to the full-size samples cultured in the CFM (**Fig. 4.1**).

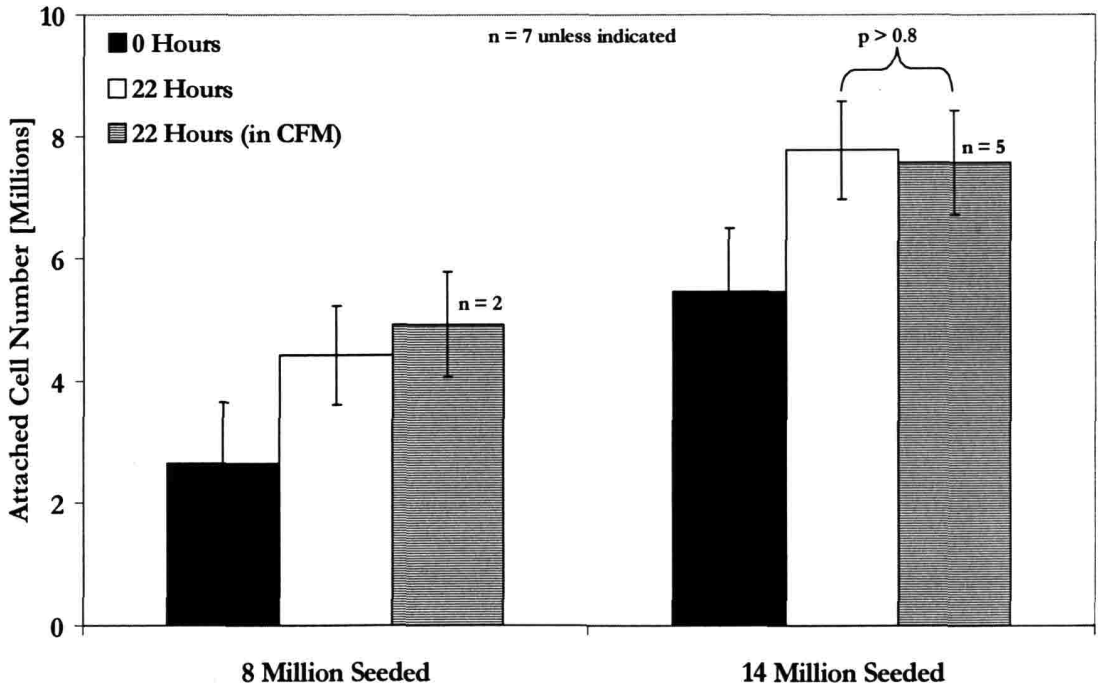

Figure 4.1. Attached cell number variation with time for two different values of cell number seeded. Cell number increased significantly (two-way ANOVA, $p = 0.03$) during the 22 h in culture.

4.2.4 Statistical Methods

Two-way ANOVA was used to determine the significance of the effect of time in culture on attached cell number. The statistical similarity between the slope of the force over time curve at the end of each experiment and zero slope was determined using the two-tailed, heteroscedastic Student's t-Test.

4.3 Results

4.3.1 Contractile Response

Fibroblasts seeded onto collagen-GAG matrices produced a characteristic contractile response curve. The contractile force developed within 1 hour of starting the test and persisted until the end of the test, about 22 hours later. The contractile force generated by the fibroblasts was both a function of time and the number or density of attached fibroblasts (**Fig. 4.2**). Within the first hour post-seeding, most samples showed a slight temporary decrease in force, compared to the cell-free matrix samples. At all fibroblast densities, contractile force increased after the initial lag, and approached an asymptote after approximately 12 hours. After 12 hours, the average slope of the force-time data for all cell densities was 3×10^{-5} N/h, statistically not different from zero ($p > 0.1$). This asymptotic level was maintained until the experiment ended 10 hours later. Higher fibroblast densities resulted in a contractile force which both increased at a higher rate and eventually reached a higher asymptote.

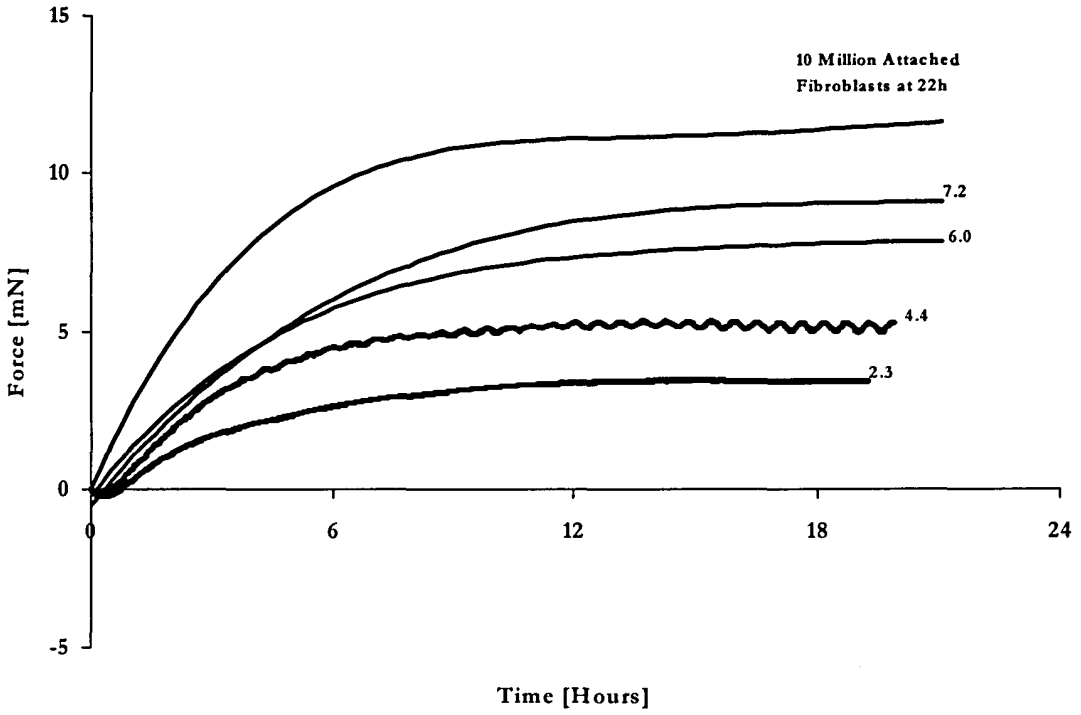

Figure 4.2. Contractile force plotted against time, for several densities of attached fibroblasts at 22 hours (cell number in millions). Raw data is plotted for 2.3 and 4.4 million attached cells to show data scatter. Higher densities are shown by trend lines for clarity.

The asymptotic force was linearly proportional to the density of attached fibroblasts ($R^2 = 0.97$) through a range of 2.3 to 10 million fibroblasts per sample or 400 to 2,000 fibroblasts/mm^3 (**Fig. 4.3**). Since the slope was constant, the contractile force per cell was observed to be independent of cell density. The value of the slope, 1 nN/fibroblast, represented the contractile force per cell and is expressed mathematically by:

$$F_a = N_{cells} \cdot F_{cell} \qquad (4.1)$$

where F_a is the asymptotic force value, N_{cells} is the number of cells, and F_{cell} is the force per cell. In addition to the asymptotic force, the force at a given time was linearly related ($R^2 > 0.89$) to the attached cell density at 22 hours (**Fig. 4.4**). The 95% confidence level for the intercept (-0.8 to 3.2 mN) included the origin. Due to this inclusion of the origin and the

uncertainty associated with extrapolated data, the non-zero value of the intercept will not be addressed further.

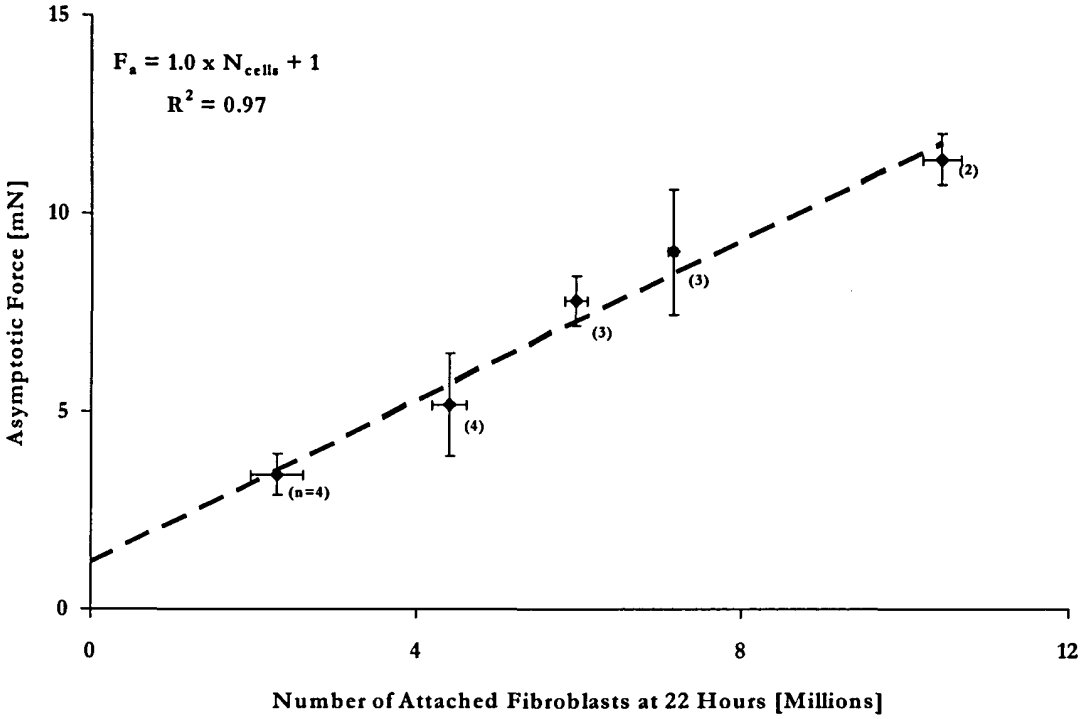

Figure 4.3 Asymptotic force plotted against number of attached cells per sample at 22 hours, showing a linear relationship.

4.3.2 Attached Fibroblast Number with Time

The number of attached fibroblasts was determined at 0 and 22 hours post-seeding. This was performed for 8 and 14 million fibroblasts seeded per CFM sample (n = 7). For both values of seeded cell number, a minimum of 20% of the seeded fibroblasts were attached at 0 hours (10 minutes post-seeding), and the fraction increased to 50% at 22 hours (**Fig. 4.1**). Specifically for 8 million seeded cells, an initial attached cell number of 2.7 million increased by 48% to 4.0 million after 22 hours. Similarly for 14 million seeded cells, an initial number of 5.8 million increased by 34% to 7.8 million. Therefore, the number of cells which were attached at 22 h was ~50% of the number which were seeded, with a

standard error of ± 12% (*e.g.*, for 8 million cells seeded 4 ± 1 million cells are attached at 22 h). Two-way ANOVA revealed a significant effect ($p = 0.03$) of time in 3-dimensional matrix culture on attached fibroblast number. Since the rinsing step may have removed loosely attached fibroblasts, this assay may report lower attached fibroblast densities at early times, lowering this significance.

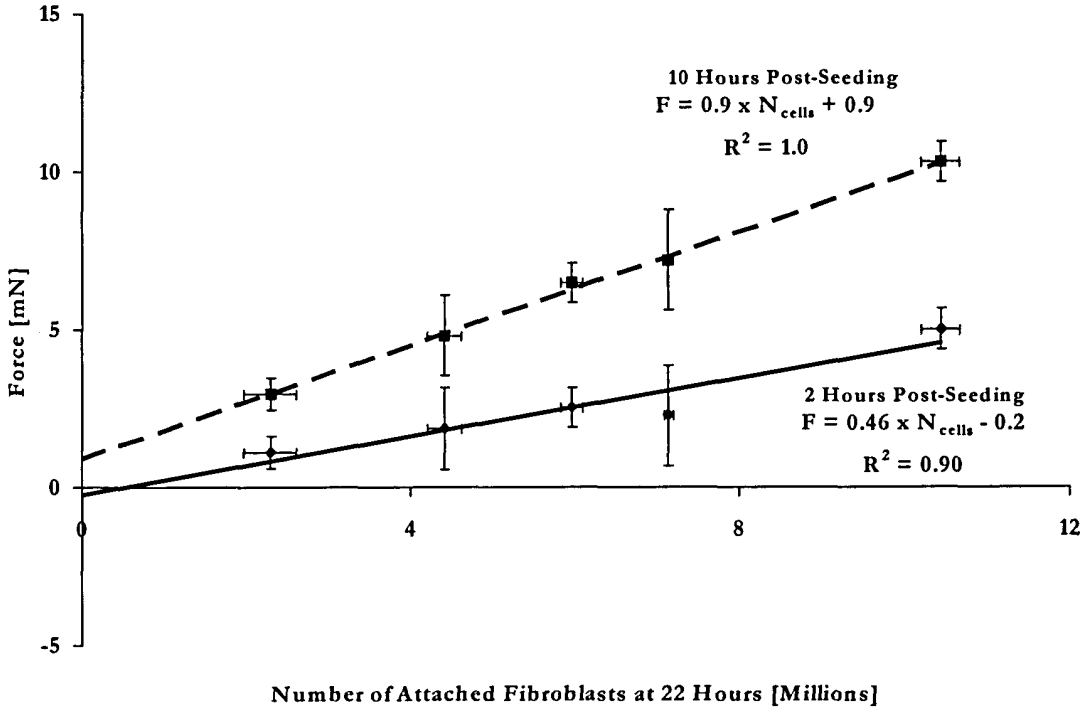

Figure 4.4 Force plotted against attached cell number per sample at 22 hours, showing a linear relationship at 2 hours (*solid line*) and 10 hours (*dashed line*) post-seeding.

4.4 Discussion

Normalization of contractile force by attached cell number resulted in superposition of force-time curves for all levels of cell density onto one curve which approached an asymptotic force of 1 nN within 12 hours. This behavior is described well by the equation

$$F = F_a \cdot \left(1 - e^{-(t/\tau)}\right) \qquad (4.2)$$

where F_a is the asymptotic force value, F is the force at post-seeding time t, and τ is the time constant. Lines of best fit for each force-time curve, grouped and averaged based on attached cell number in **Fig. 4.2**, were generated using a MATLAB algorithm (Appendix E.5) which returned the constants F_a and τ. The correlation coefficient for each curve was > 0.98. The data were grouped by attached cell number at 22 h, and values of F_a and τ (average ± standard error) were determined for each group (**Table 4.1**). The value of the time constant for all fibroblast densities was not statistically different ($p > 0.2$) from the average 5.2 ± 0.5 h, suggesting that the kinetics of force generation were independent of fibroblast density.

The use of the exponential relationship in Equation 4.2 was established for data comparison purposes. The physical significance, if any, of the parameters F_a and τ and the functional relationship posed has not yet been established. The linear relationship between force and cell density at all times supported the use of this functional relationship. By combining Equations 4.1 and 4.2, a more general equation relating τ, force per attached cell (F_{cell}), time (t), and the number of attached fibroblasts at 22 hours (N_{cells}) was established. Note that F_{cell} and τ are constants which were experimentally determined for this system.

$$F(t, N_{cells}) = F_{cell} \cdot N_{cells} \cdot \left[1 - e^{-t/\tau}\right] \qquad (4.3)$$

Results presented in this paper support the use of this equation within the range of cell densities tested (400 – 2,000 cells/mm^3). Other groups [16-20, 41, 42], using similar devices to measure fibroblast contraction of collagen gels, reported force versus time data whose shape is consistent with the use of this equation. In fact, Delvoye *et al.* [16] used a

ratio of asymptotic force over time-to-asymptotic force to compare experimental groups. A linear relationship between this ratio and fibroblast density was reported; however, the data [16] were not presented in a form that allowed comparison with the predictions of Equation 4.3.

Table 4.1. Exponential Curve Fit Parameters (τ, F_a)

Total # of Attached Cells in Matrix (x 10^6)	Time Constant, τ [h]	Asymptotic Value, F_a [mN]
2.3 ± 0.31	5 ± 1.3	3.7 ± 0.6
4.4 ± 0.21	4 ± 0.5	5.4 ± 1.4
6.0 ± 0.13	5 ± 0.4	8.1 ± 0.5
7.2 ± 0.05	7 ± 1.5	10 ± 1.9
10 ± 0.23	4 ± 0.5	12 ± 0.7

The above discussion assumes that the attached cell number determined at 22 h did not change prior to that time. We have shown that the attached cell number does increase by the same percentage, ~ 40%, over the 22 h of testing for two different values of initial seeded cell number. The linearity of force at 2 and 10 h with attached cell number (determined post-test at 22 h) suggests that the fraction of cells attached increases with the same time dependence for all cell densities **(Fig. 4.4)**. The increase in attached cell number could be the result of either more cells attaching to the matrix or cell proliferation over time in culture. The doubling time for the fibroblasts when grown on tissue culture plastic was ~12 h. Therefore, cell proliferation could potentially cause this increase in cell number. In addition, attachment of a fibroblast to the matrix does not ensure its participation in the

generation of force. For these reasons, the values of force per cell reported in this paper are likely smaller than the actual values, particularly at earlier times. However, the results are representative of the average response for the entire fibroblast population.

The contractile response and asymptotic force per cell, F_{cell}, described here are consistent with results reported by others for several cell types tested under similar conditions using collagen substrates [16-18, 20, 41, 42]. With one exception [19], the range of values of force per cell reported by these groups (0.1 – 9.8 nN/cell) is comparable to the value of 1nN reported here (**Table 4.2**). Since different testing conditions, cell, substrate and media types were used, the similarity among these values is striking.

Table 4.2. Force per cell from data reported by other investigators.

Force per Cell (nN)	Time to Plateau [h]	Type of fibroblast (passage)	Substrate	Ref.
.98 – 9.8	6-12	Human & calf skin	collagen gel [0.45mg/ml]	[16]
6	36	Chick embryo (2^{nd})	collagen gel [0.87 mg/ml]	[17]
0.1	~ 24	Human skin	collagen gel [1mg/ml]	[18]
3	~ 9	Human skin	collagen gel [1mg/ml]	[43]
5.5	~8	Human skin	collagen gel [1mg/ml]	[42]
200	5	Embryonic human lung (MCR5 line)	collagen gel	[19]
2.5	~20	Human skin	collagen-GAG Matrix	[41]
2	~ 7	Human skin	collagen gel [1mg/ml]	[41]
4	~4	Human skin (6^{th} – 9^{th})	collagen gel [1.5mg/ml]	[20]
1	~ 8	Rabbit skin (3^{rd} – 6^{th})	collagen-GAG matrix	[50]

Despite substantial differences between the collagen-GAG matrices used for these experiments and the more commonly used collagen gels, the contraction results are remarkably similar for these two types of substrates. In a collagen gel, fibroblasts are embedded in a hydrated network of 50-500 nm thick collagen fibrils with a nominal pore diameter of 1-10 μm [15]. Fibroblasts in the collagen-GAG matrix are attached to struts of ~10 μm diameter which form irregular, roughly spherical pores of ~140 μm diameter, and are often seen isolated from other fibroblasts and attached to only one matrix strut (**Fig. 4.5**). Noting that the diameter of a rounded fibroblast is ~ 20 μm, it is apparent that fibroblasts embedded in a collagen gel are in contact with the gel along most of its membrane surface, while fibroblasts attached to the collagen-GAG matrices are attached only along a portion of the cell membrane. This phenomenon may result in contact guided migration, elongation, and/or contraction in the collagen-GAG matrix. In contrast, the collagen gel provides an environment that is much more spatially homogeneous, in which contraction likely occurs via collection of collagen fibrils around the fibroblast by filipodia retraction [16]. In addition to the pore microstructure, the structure of collagen and the stiffness of the collagen-GAG matrix differ from those of collagen gels. In the collagen-GAG matrix, the triple-helical collagen molecules are not assembled into a fiber with a regular period, whereas, they are in the collagen gel [51]. Although the identity of binding regions was not observed in this study, the presence of a glycosaminoglycan (GAG) component in the former matrix suggests the presence of binding regions that are absent in collagen gels. In spite of all these differences, the fibroblasts seem to develop a similar force per cell in both environments.

Evidence from other investigators suggests that the asymptotic force is a homeostatic cellular response [16, 20, 41] which is probably the manifestation of a feedback

loop that acts to minimize a major deviation from this force level. The value of the asymptote is also known to be dependent on the chemical composition of the culture medium [16, 17]. Of particular interest is the linear dependence of the asymptotic value on the number of cells attached to the matrix. This directly proportional relation suggests the fibroblasts act independently of one another to develop the asymptotic level of force throughout the matrix. If, for example, the cells were cooperatively attempting to establish a particular level of force in the matrix, the level should be independent of fibroblast density; this is not observed.

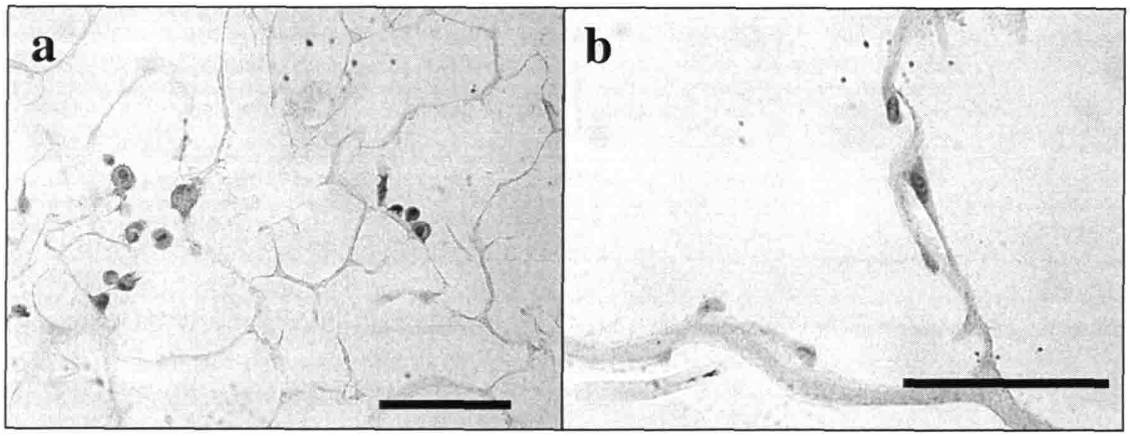

Figure. 4.5. Hematoxylin and eosin stained sections to show differences in fibroblast morphology at 0 and 22 hours post seeding. At 0 hours (**a**) most fibroblasts exhibit a rounded morphology, while at 22 hours (**b**) a majority of cells appear to be elongated. (scale bars = 100 mm)

4.5 Conclusions

The density of attached fibroblasts in a collagen-GAG matrix is related linearly to the asymptotic contractile force generated by the fibroblasts. The development of contractile force with time followed a residual decaying exponential relationship which was fully described by two experimentally determined constants, the asymptotic force per cell and a time constant. Although collagen gels and the collagen-GAG matrices used here differ chemically, mechanically, and microstructurally, the values of contractile force per cell

developed in both were observed to be similar in magnitude. It has been suggested [16, 41] that a population of fibroblasts minimizes externally imposed changes from the asymptotic level of force established prior to such disturbances. The dependence of contractile force on the number of attached fibroblasts suggests that this equilibrium level is determined by individual cells and is not a cooperative effect.

Chapter 5. The Micromechanics and Cellular Mechanisms of Fibroblast Contraction of Collagen-GAG Matrices

5.1 Introduction

Contractile fibroblasts are thought to play a major role in the organization of extracellular matrix during wound healing. In healing skin wounds, inhibition of wound contraction by these cells, using a specific analog of the extracellular matrix, has been linked to blocking of scar tissue formation [3]. In contrast to normal dermis, scar tissue is undesirable because of its inferior mechanical properties, potential to restrict the range of motion at joints, and physical disfigurement. In addition to healing skin, contractile cells have been identified in many wounded or diseased tissues (*e.g.,* transected peripheral nerve, injured anterior cruciate ligament, and cirrhotic liver) [4, 8, 9]. In these cases, the contractile cells have been identified as myofibroblasts. A marker which distinguishes myofibroblasts from fibroblasts is the presence of the protein α-smooth muscle actin in the cytoplasm. For these reasons, investigators have been studying the contractile forces developed by cells using *in vivo* and *in vitro* models.

In vivo, contractile cell behavior is difficult to monitor and the environment in which contraction occurs is not well-defined or controllable. This has led the development of *in vitro* models of contraction, either for individual cells or for populations of cells. Typically, in studies of individual cells, the cells are seeded onto a planar substrate and the deformation of the substrate by the cell is measured [33, 35, 36, 48, 49, 52]. The value of the contractile force is then determined using the stiffness of the substrate [34, 35, 37]. This technique

allows correlation of the development of the deformation (and force) with cell processes such as pseudopod extension and cell migration [34, 37, 53]. Studies of populations of cells have generally involved seeding of the cells onto a porous three-dimensional lattice such as a collagen gel [12, 13, 16-18, 31, 32]. The macroscopic deformation of the lattice is then measured, yielding an average response for the cell population. Again, forces are calculated based on the stiffness of the resistance to contraction [16-18]. This method does not allow for a direct correlation of force with individual cell processes. The benefits of measuring the macroscopic contraction and force of a population of cells are that the three-dimensional lattice better mimics the *in vivo* environment and, furthermore, population-averaged responses are measured, masking cell-to-cell variation.

In vitro models of contraction by a population of cells have established the force which developed over time subsequent to cell attachment. Typically, the contractile force increased from zero within 1 hour of attachment and reached a plateau within 8 to 24 hours, which was stable for up to several days [16-18, 20, 41, 43]. The fibroblasts reacted to minimize perturbations from this level, a phenomenon termed tensional homeostasis [16, 20, 41]. The force developed by individual cells has been estimated by normalizing the macroscopic value of force by cell number yielding an average force per cell of 0.1 to 9.8 nN/cell [16-18, 20, 41, 43]. The efficacy of this normalization in determining force per cell has not been conclusively determined, but the values are similar to those reported for the measurement of force developed by individual cells on two-dimensional substrates (~20 nN) [34, 37]. However, the measurement of force macroscopically does not allow elucidation of the cellular processes responsible for developing this force. Post-experimental, histological analysis suggested that the forces measured for fibroblasts in a collagen gel resulted from traction forces during migration, but this has not been conclusively proven [43].

Previously, it was found that fibroblasts attached to a porous, collagen-based matrix develop a force of 1 nN per cell during the 15 hours following seeding (Chap. 4). In this chapter, the cellular processes which produced these contractile forces were identified by observing cell behavior, morphology, and expression of α-smooth muscle actin (SMA) under conditions similar to the contraction experiments. Specifically, the average change in cell morphology with time, the percentage of cells expressing α-SMA with time, and the actions of individual, live cells which led to matrix deformation were observed. From these data it was established that matrix deformation at the microscopic level occurred coincidentally with cell elongation; not with cell migration or cell contraction. Individual matrix struts were buckled or bent by the elongating cells. A high percentage of fibroblasts attached to the collagen-GAG matrix expressed α-SMA and this percentage did not change significantly over time. Comparison of the time for the individual deformation events to occur (2-4 h) with the time over which the average change in cell morphology and force (~15 h) progressed suggested the time-dependence of the force development was the result of the sequential activation of cells and the time for one cell to induce deformation of the matrix. The force plateau is related to the limiting deformation that the cells impose on the matrix, due to either geometric constraints (for instance, in collapsed, buckled struts) or due to the maximum force that the cytoskeletal elements can withstand. This work improved upon the model of contraction described previously (Chap. 4) by allowing correlation of contractile force with the cell processes that were responsible for its development.

5.2 Methods

5.2.1 Measurement of Cell Aspect Ratio with Time

To determine the change in the aspect ratio of fibroblasts with time, fibroblasts were seeded onto mechanically clamped matrix samples which were sacrificed at various time points post-seeding. Dry matrix samples, 33 mm x 26 mm, were fixed into polyethylene clamps separated by an aluminum brace (**Fig. 5.1**). Fibroblasts were pipetted onto the surface of dry, clamped matrices at a density of ~1,500 cells/mm^3. The seeded matrices were then placed into individual wells of a tissue culture plate (8-well rectangular, Nalge Nunc International, Naperville, IL). Following a 10 minute delay to allow for cell attachment, the wells were filled with DMEM and placed into a cell culture incubator. These matrix samples were sacrificed by replacing the DMEM with a solution of 10% neutral buffered formalin at 0, 4, 8, 15, 22, or 48 hours post-seeding. Three samples were tested at each time point in order to quantify sample-to-sample variation. Chemically fixed samples were then embedded in glycomethacrylate (GMA) (see Appendix G.2), and then cut along the plane of the matrix as 5 μm sections. The sections were then stained with hematoxylin and eosin to reveal cell morphology (see Appendix G.3).

Using a light microscope (Labophot, Nikon) fitted with a digital camera (DEI-750, Optronics Engineering), images were gathered from multiple sections of each sample. The aspect ratio of each cell was determined using the Particle Analysis Tool included with Scion Image software (http://www.scioncorp.com/) (see Appendix G.5). The outline of each cell was identified by tracing it using the pen tool. This Particle Analysis Tool then determined the best fit ellipse for each cell and returned the major and minor axis of the ellipse. The aspect ratio was calculated by taking the ratio of the major and minor axes. Only cells which

appeared to be in contact with the matrix and had a visible nucleus were included in the analysis. Approximately 200 cells were analyzed from each sample. The average aspect ratio was determined for each sample and these values were then averaged to yield an average aspect ratio and standard error for each time point (n = 3). In addition, a histogram of aspect ratios was constructed to identify the change in distribution of aspect ratios with time. For this purpose, all cells from each time point were grouped together (~600 cells per time point).

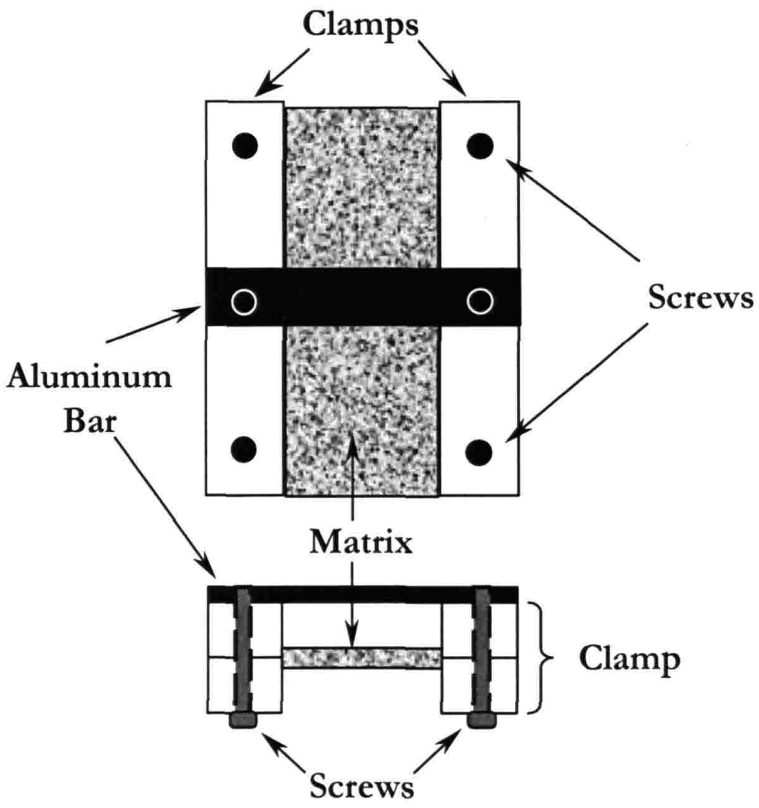

Figure 5.1. Schematic of clamping system used to hold cell-seeded matrices for average cell aspect ratio determination.

5.2.2 Immunohistochemical Identification of Myofibroblasts

A portion of each fixed sample was processed to reveal the presence of the protein α-smooth muscle actin (SMA) in the cytoplasm of attached fibroblasts. Matrix pieces (5 mm

x 5 mm x ~ 3 mm) fixed in 10% neutral buffered formalin were embedded in paraffin (see Appendix G.1), sectioned at 10 μm, and immunohistochemically stained with a primary antibody to α-smooth muscle actin (SMA) (Sigma Chemical Co., St. Louis, MO) (see Appendix G.4). After clearing with xylenes and blocking with animal serum and hydrogen peroxide, the sections were incubated with the primary antibody. A negative control was prepared by substitution of animal serum for the primary antibody. The sections were then incubated in a biotin conjugated secondary antibody (Sigma), rinsed with PBS and then incubated with ExtrAvidin peroxidase (Sigma). Finally, an AEC-kit (Zymed, San Francisco, CA) was used to stain α-SMA by formation of red-brown colored deposits upon reaction with peroxidase. Sections were then counterstained with Mayer's hematoxylin to reveal cell nuclei. In addition to staining the nuclei, hematoxylin stained the collagen-GAG matrix struts so they were visible in the light microscope.

Images from immunohistochemically stained paraffin sections were gathered using a digital camera (DEI-750, Optronics Engineering) attached to a light microscope (Labophot, Nikon) to determine the percentage of fibroblasts expressing α-SMA. Cells positive for expression of this protein were identified by a red-brown color in the cytoplasm. The shape of each cell was noted by assigning it to one of the following groups: elongate (aspect ratio > 2.0), round (1.0 ~ 1.3), indeterminate (1.3 ~ 2.0). In addition, it was noted if the fibroblast appeared to be bending or buckling a strut. Bent or buckled struts were identified by an obvious, qualitative difference in curvature between points of cell attachment as compared to the rest of the strut. Samples from 0 and 22 hours post-seeding were processed (n = 2) and at least 41 cells were analyzed from each sample. All cells from samples at the same time point were pooled together for analysis.

5.2.3 Live Cell Imaging

To determine the process by which the fibroblasts elongate and contract the matrix, live cells attached to the matrix were videotaped continuously with time (see Appendix H). A section of collagen-GAG matrix (~300 μm thick)was shaved from the full-thickness (~3 mm) matrix using a razor blade. This sample was then seeded with cells by submersion in a suspension of fibroblasts for 10 minutes. The actions of a single cell were then recorded using the setup shown in **Fig. 5.2**. The cell-seeded matrix sample was placed in the well of a microscope slide filled with DMEM supplemented with 25mM HEPES buffer. A glass cover slip was placed on top of the well, securing the matrix sample on at least one side. Mechanically clamping the sample in this way prevents movement during imaging. A heated stage (Biostage 600SM, 20/20 Technologies, Wilmington, NC) held the slide and maintained its contents at ~ 37°C during the imaging experiment. A light microscope with a digital camera connected to a VCR (AG-DS555 Panasonic, Rockville, MD) was used to record the actions of an individual cell continuously, at 30 images per second, for up to 6 h. Due to the time required for the setup of the experiment video recording was begun approximately 30 minutes after cell seeding. The time shown on these images indicated the time following the start of recording. In some cases, isopropyl alcohol was added to the culture medium near the end of the experiment in order to show the relaxation of the matrix after cell death. Following each experiment, the video was replayed and discrete images were gathered via a frame grabber card (Snappy Video Snapshot, Play Inc., Rancho Cordova, CA) in order to show the mechanical interactions of the cell with the matrix.

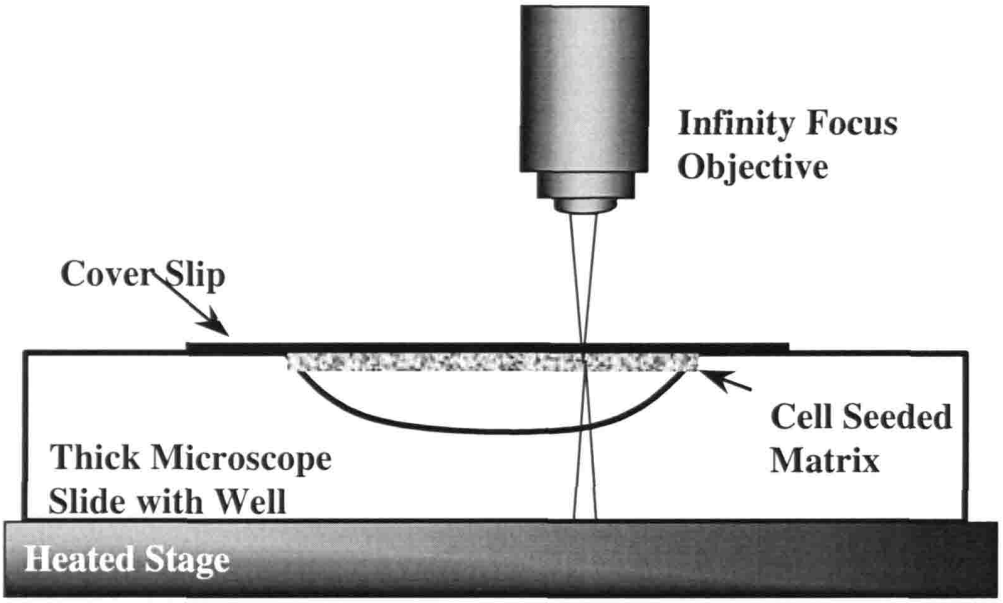

Figure 5.2. Schematic of live cell imaging setup. The objective is directly attached to a light microscope fitted with a digital video camera.

5.3 Results

5.3.1 Aspect Ratio Measurement

Initially rounded fibroblasts (diameter ~ 20 μm), attached to the collagen-GAG matrix, elongated over time (**Fig. 5.3**). Note that in many cases, the elongated cells were attached to the matrix only at their end points, with a visible gap between the cell and the matrix along most of the length of the cell (**Fig. 5.3c, d**). The average aspect ratio increased from 1.4 to 2.8 during the first 15 h in culture (**Fig. 5.4**). Although a slight increase in average aspect ratio was observed between 15 and 48 h, this increase was not statistically significant (ANOVA, $p = 0.17$).

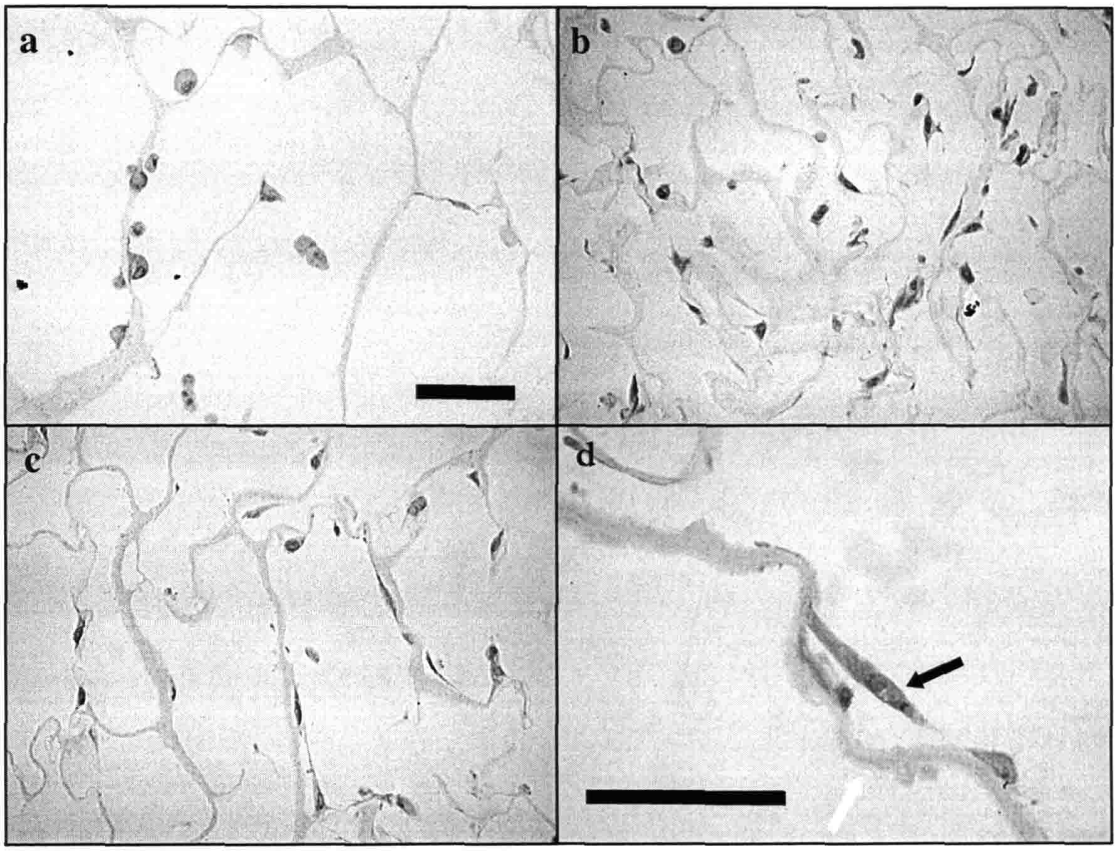

Figure 5.3. Light micrographs of H&E stained sections of cells attached to the collagen-GAG matrix fixed at 0, 8, and 22 hours post-seeding, images **a**, **b**, and **c** respectively. These images are representative of those analyzed to determine average aspect ratio. Cells are darker than the matrix struts and in some a darker, ovoid nucleus is visible. Image **d** (22 h) at higher magnification shows an elongated cell (black arrow) which appears to have shortened the matrix strut (white arrow) to which it was attached by ~40 μm. Scalebar = 100 μm

A histogram of the aspect ratio of all cells at each time point showed an initially narrow distribution which became wider and shifted to the right with time (**Fig. 5.5**). The percentage of cells with an aspect ratio < 2 (rounded) decreased with increasing time, from ~95% at 0 h to about 25% after 22 h. Aspect ratios > 5 (highly elongated) became more prevalent after 4 h in culture, but fibroblasts with these high aspect ratios were never a substantial percentage of the population. A value of the average aspect ratio of ~2.5 appeared to be a critical point in the distribution: observation of aspect ratios > 2.5

increased infrequency with time, while observation of aspect ratios < 2.5 decreased in frequency with time.

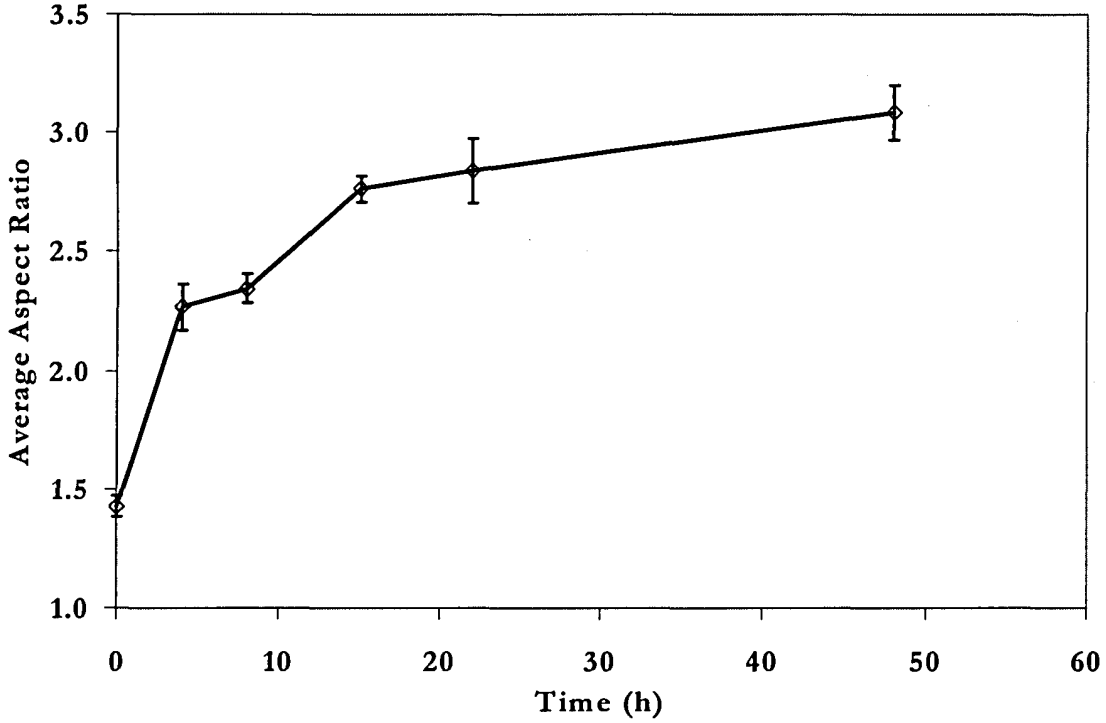

Figure 5.4. Plot of average aspect ratio of fibroblasts with time seeded on the collagen-GAG matrix. The average aspect ratio increased up to 15 h post-seeding. The increase in average aspect ratio after 15 h is not statistically significant.

5.3.2 Myofibroblast Identification

The absence of the red-brown color in adjacent negative control sections (i.e. not exposed to the primary antibody) established that the stain used was specific for the α-SMA protein. The percentage of fibroblasts positive for α-SMA was not significantly different ($p > 0.33$) between 0 and 22 hours: 88 ± 1 and 75 ± 7 %, respectively. Of the cells that appeared to deform the pore walls at the 22 hour time point, 74 ± 4 % were positive and only 16 ± 6 % negative. In addition, 90 ± 1 % of these fibroblasts were assigned to the elongate morphology group.

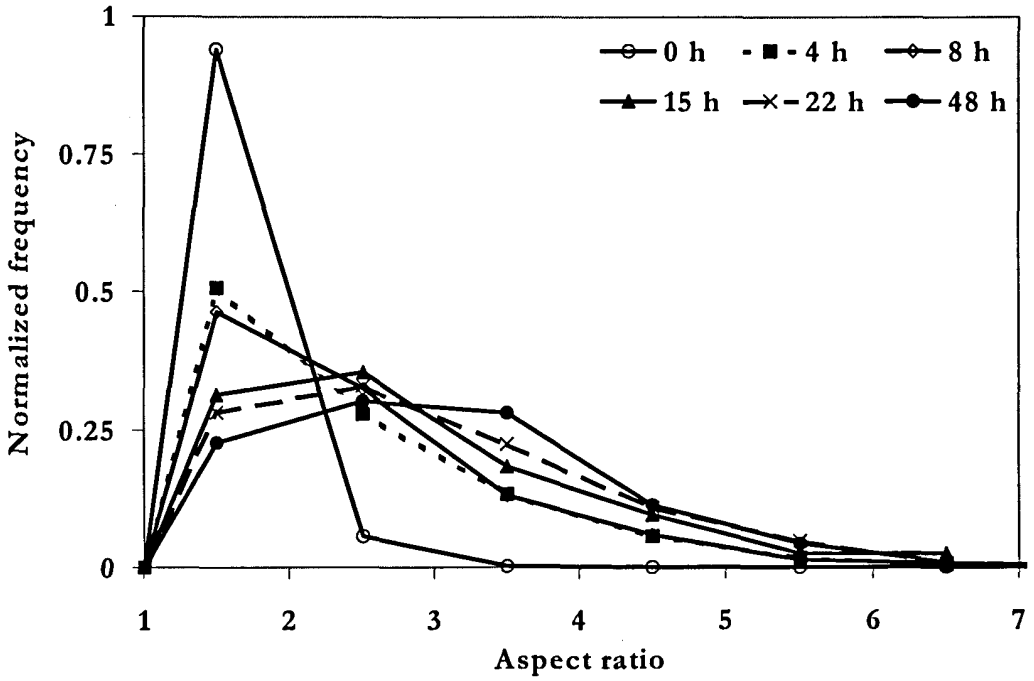

Figure 5.5. Histogram showing the frequency of fibroblast aspect ratios at different times post-seeding. The distribution shifts toward higher aspect ratios and becomes wider with increasing time.

5.3.3 Live Cell Imaging

Imaging of live cells allowed the continuous observation of the interaction of individual cells with the collagen-GAG matrix over time. Representative images from observations of 20 pieces of cell-seeded, collagen-GAG matrix from different experiments are described here. We first summarize some overall observations and then give a more detailed description of the process of cell elongation and matrix strut deformation.

In some cases, cell elongation along the entire length of a strut produced extensive matrix deformation, leading to complete collapse of individual struts (**Fig. 5.6 and 5.7**). One cell attached to two neighboring struts, extended two pseudopods in different

directions along one of them and contracted the portion of the strut between the extened pseudopods (**Fig. 5.8**). In one case, strut collapse was associated with the extension of a pseudopod only partially along the length of a strut (**Fig. 5.9**). In all four cases (**Figs. 5.6-9**), matrix deformation was initiated within about 60 minutes of seeding the cells onto the matrix. Finally, one cell elongated along a matrix strut, released or ruptured the attachment at one end, retracted to a rounded configuration, and then repeated the process of elongation, release, retraction and rounding (**Fig. 5.10**); throughout this process there was little matrix deformation.

Membrane ruffling and pseudopod and filopod extension over the entire surface of cells were apparent from the beginning of the videotaping. These events were most persistent at the cell-matrix interface of elongating cells (**Fig. 5.9, arrows C and E and Fig. 5.10 arrow E**). The extensions were transient, each lasting for only a few minutes. They did not always directly lead to permanent spreading of the cell in the direction of extension (**Fig. 5.9, arrow E**). The membrane extension events were also observed in cells which did not elongate at all during our observations (**Fig. 5.9 cell D**).

The cell elongation initially occurred through the thinning and extension of the cytoplasm near the periphery of the cell. In some cells, this process resulted in a prominent region around the nucleus near the center of the cell at early times (**Figs. 5.6, 5.7, 5.10**). Cell elongation appeared to be affected by the local configuration of matrix struts (cells elongated preferentially along the matrix strut axis) (**Figs. 5.6, 5.7, 5.8, 5.10**). In several instances, a gap could be seen between the matrix strut and the mid-region of the cell and the adhesion points were towards the periphery of the cell (**Fig. 5.6 arrow D; Fig. 5.7 ; Fig. 5.10 arrow C),** suggesting that as the cell elongates, new adhesion sites form with the extending cytoplasm, so that the attachment points are always near the furthest extension of the cell.

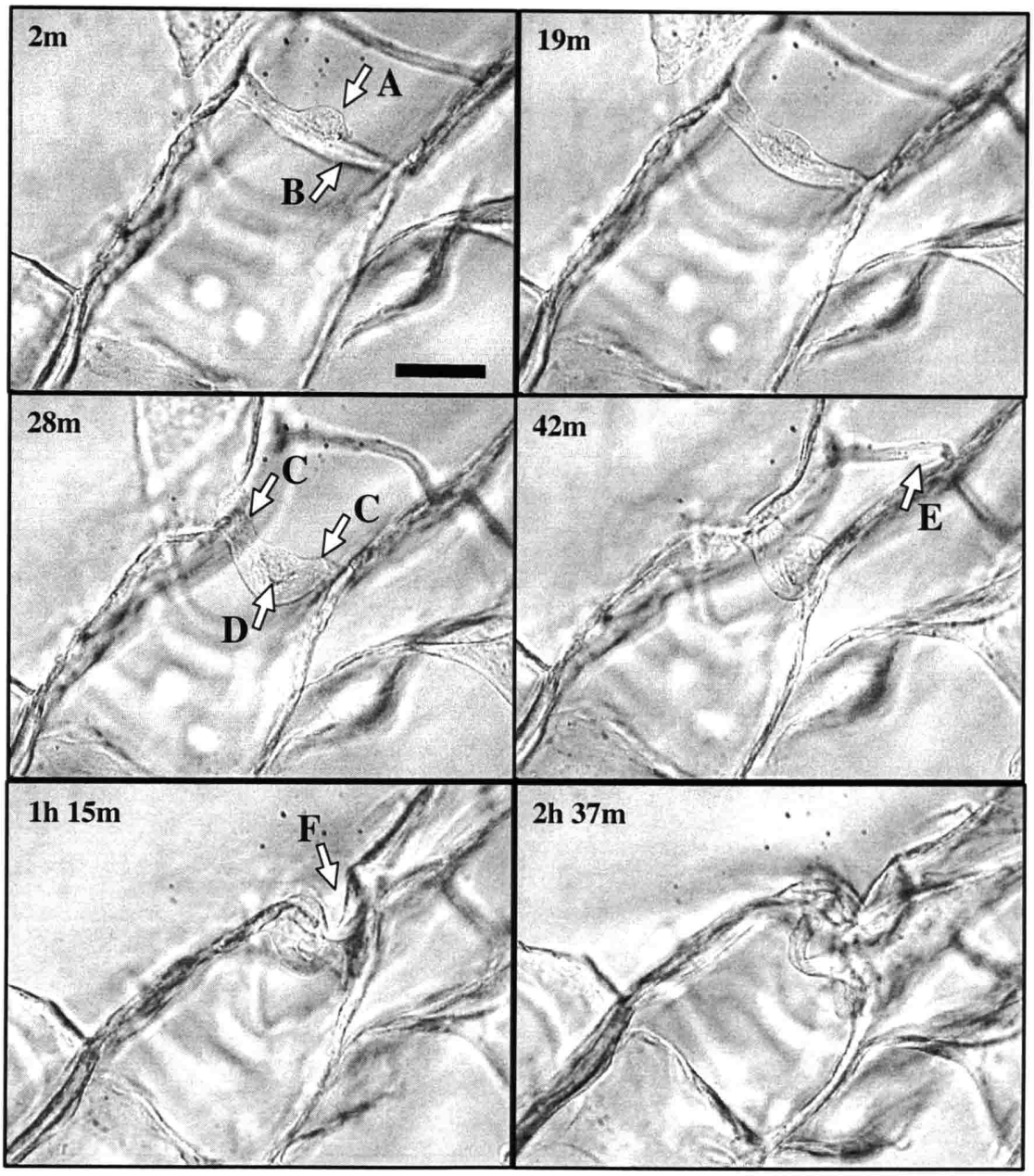

Figure 5.6. Sequence of images depicting a cell (arrow **A**) simultaneously elongating and deforming a matrix strut (arrow **B**). As the ends of the strut were drawn closer (2 - 28 minutes), the cell extended towards the ends of the strut (arrows **C**); it did not contract along with the strut. The buckling of the strut under the cell resulted in the release of adhesions sites near the cell center (arrow **D**). Neighboring struts were observed to buckle to accommodate the overall geometric changes in the matrix due to the imposed deformation (arrow **E**). Following complete buckling of the strut to which it was initially attached, the cell deformed another strut (arrow **F**). Most of the deformation occured within the first hour. The number in the upper left corner of each image indicates the time, in hours and minutes, after the start of video recording which was ~ 30 minutes after seeding. (Scalebar = 50 μm)

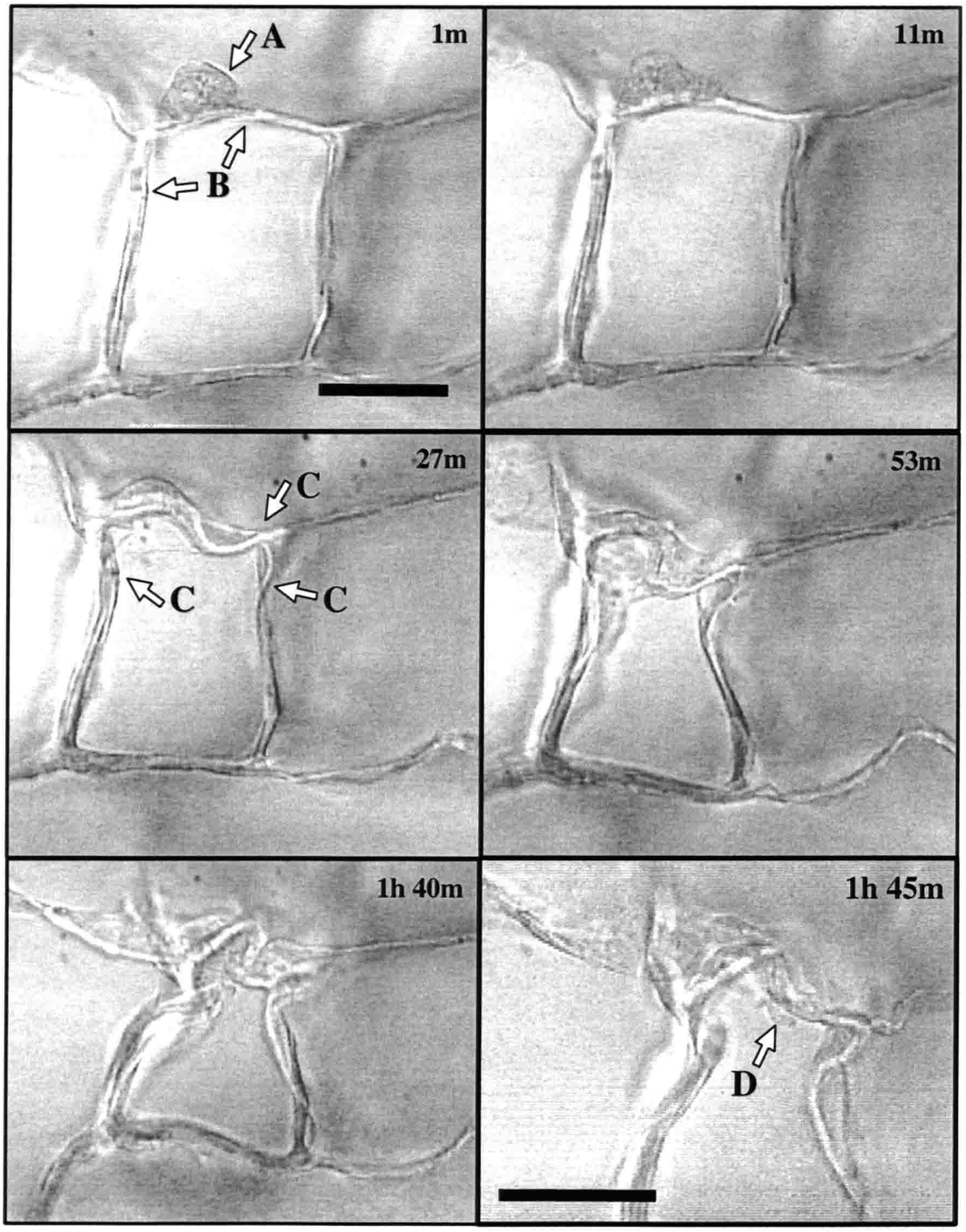

Figure 5.7. Sequence of images showing a cell (arrow **A**) elongating and deforming matrix struts (arrows **B**). Several struts deformed as the cell spread (arrows **C**). Deformation appeared to have slowed significantly or stopped by 1h 40m. Retraction of an individual pseudopod (arrow **D**) following the addition of isopropyl alcohol to induce cell death, is pictured in the final image. The number in the upper right corner of each image indicates the time, in hours and minutes, after the start of video recording which was ~30 minutes after cell seeding. (Scalebar = 50 mm)

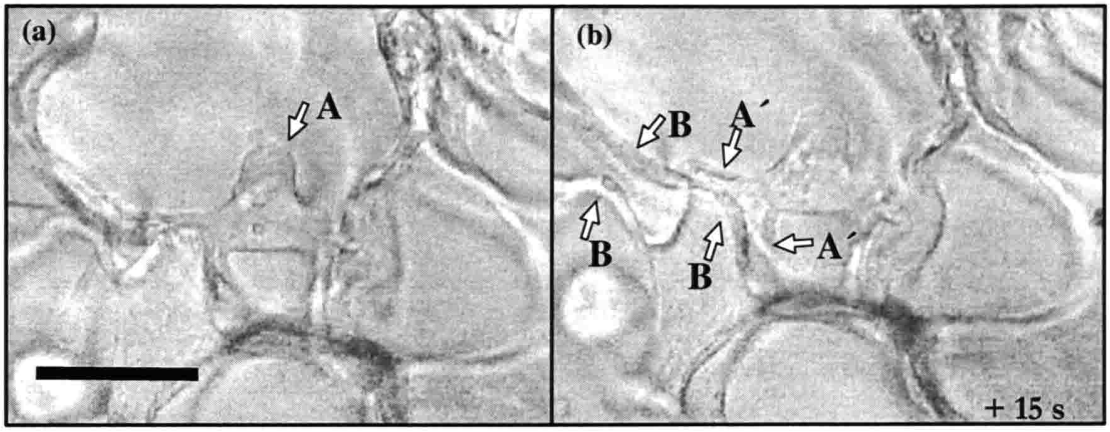

Figure 5.8. (**a**) Cell (arrow **A**), 2 h and 25 m after seeding, which had attached to the matrix and elongated. (**b**) Fifteen seconds after isopropyl alcohol was added to induce cell death, following capture of image **(a)**. Arrows **A´** indicate pseudopods which had extended along two different directions and released due to the addition of alcohol. The struts which relax following cell death are indicated by the arrows **B**. (Scalebar = 50 μm)

Typically, cells appeared to reach a final, elongated morphology within 2 to 4 h of the start of elongation (**Figs. 5.7, 5.10 cell A**), but this process was not always initiated immediately (**Fig. 5.10 cell A**). The delay in the start of elongation was observed to be as long as 1 h 45 m after video recording began (~2 h 15 m after cell seeding) (**Fig. 5.10**). However, some cells showed no evidence of elongation through the end of video recording (2 h) despite the active extension and retraction of filopods and pseudopods (**Fig. 5.9 cell D**).

Generally, matrix deformation occurred simultaneously with cell elongation (**Fig. 5.6, 5.7**). For instance, in **Fig. 5.6**, the two images at 19 and 28 minutes indicate that the cell elongated to the ends of the strut while bringing the strut ends together. A similar pattern is observed in **Fig. 5.7**, images at 11 and 27 minutes. The largest deformations occurred by buckling and/or bending of struts by attached cells (**Fig. 5.6, 5.7**): buckling can result in complete collapse of the strut, leading to large deformations and local strains in the matrix. We note that buckling or bending of the strut by the cell also requires deformation of the

neighboring struts to accommodate overall geometrical changes in the matrix (**Fig. 5.6, arrow E**).

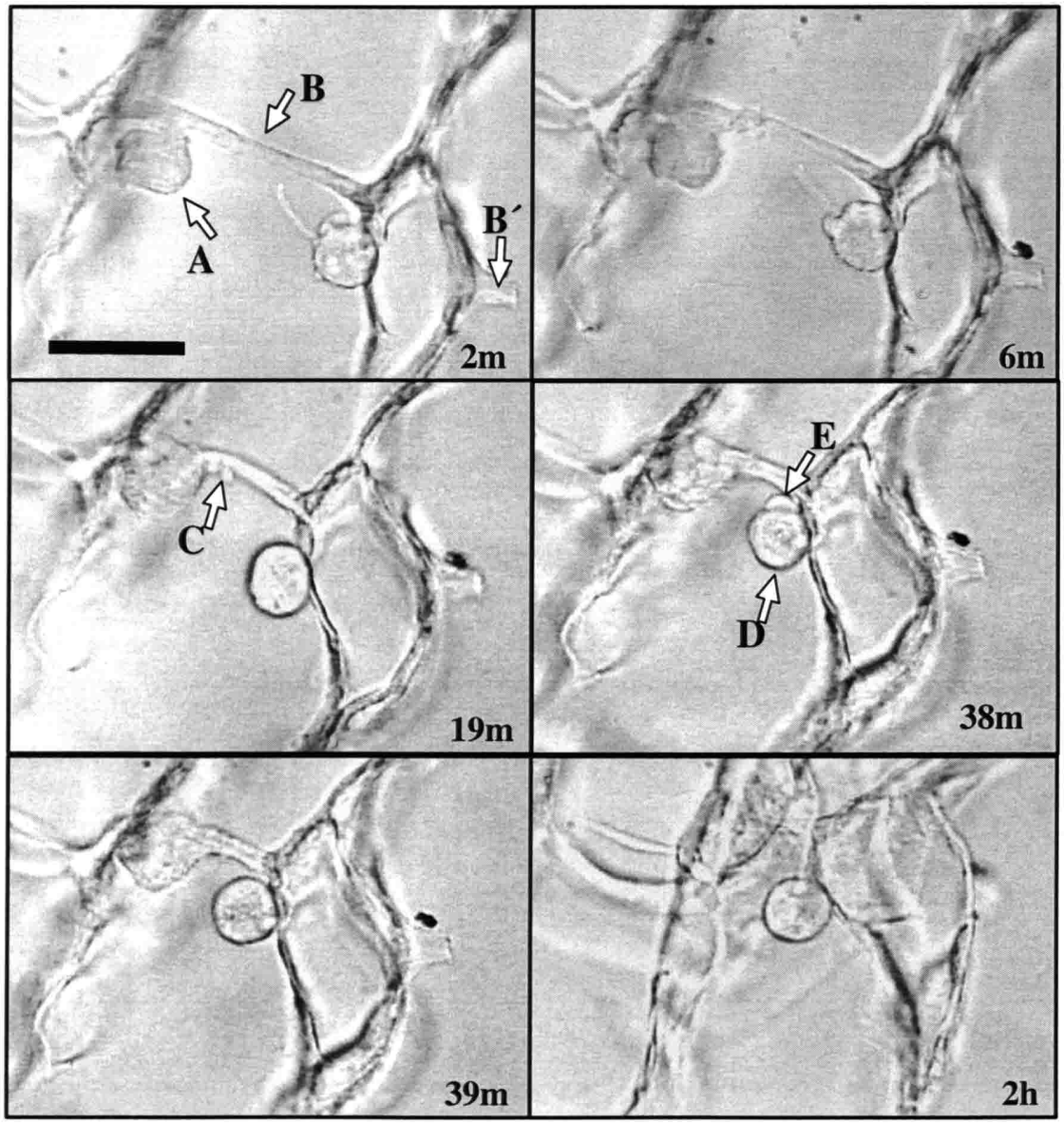

Figure 5.9. Sequence of images depicting a cell (arrow **A**) deforming a matrix strut (arrow **B**). The cell did not elongate significantly as the strut deformed, but pseudopod extension at the cell-strut interface was apparent (arrow **C**). Cell elongation was likely frustrated by the low stiffness in this region of the matrix due to a lack of connectivity with other matrix struts on the right side. A second cell (arrow **D**) actively extended pseudopods (arrow **E**) and retracted them, but did not elongate or deform the matrix. The number in the lower right corner of each image indicates the time, in hours and minutes, after the start of video recording which was ~30 minutes after cell seeding. (Scalebar = 50 μm)

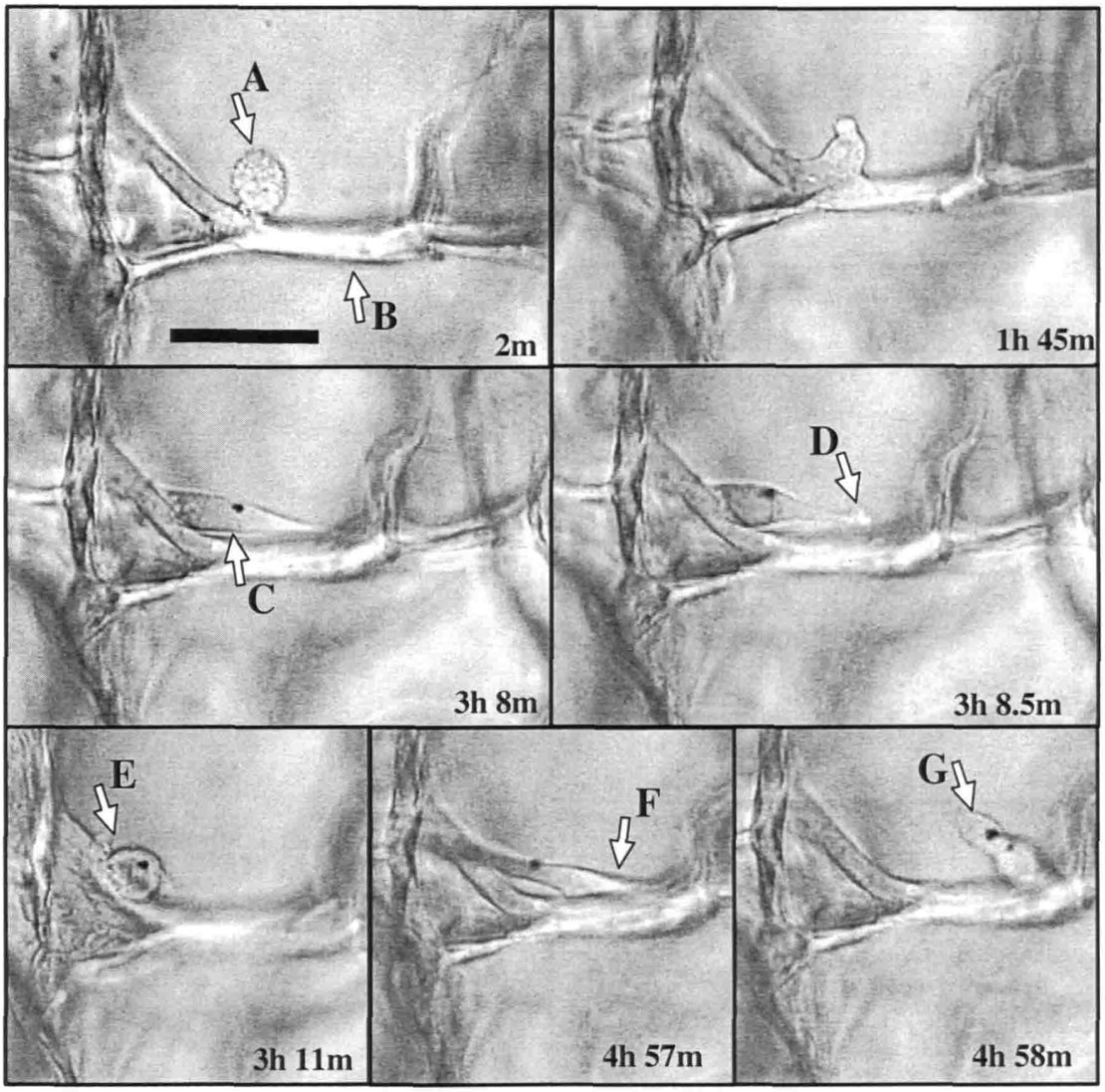

Figure 5.10. Sequence of images showing a cell (arrow **A**) which elongated on a matrix strut (arrow **B**) almost 2 hours after attachment. After significant elongation, adhesion sites near the cell center began to release (arrow **C**) and eventually catastrophic failure of attachment at one end of the cell resulted in rapid retraction of the cell (arrow **D**) and a slight matrix relaxation. Within several minutes, the cell became round, pseudopod extension was observed (arrow **E**) and the process of elongation, release of adhesion sites near the cell center, and catastrophic failure at one end was repeated. The number in the lower right corner of each image indicates the time, in hours and minutes, after the start of video recording which was ~ 30 minutes after seeding. (Scalebar = 50 μm)

Some cells extended pseudopods in multiple directions, attaching to, and deforming, the matrix. Following complete collapse of the strut to which it was initially attached, the cell labeled A in **Fig. 5.6** extended a second pseudopod and attached to another,

neighboring strut, bending it downwards (**arrow F**). Similarly, the cell in Fig. 7 extended a second pseudopod to the vertical strut on the left of the image after the extension of the first pseudopod along the length of the top horizontal strut; the attachment points of both pseudopods are labeled (**arrow C**) on the figure. Bending deformation of the vertical strut is apparent on the image at 27 minutes and is larger on the image at time of 1 hour 40 minutes. The cell in **Fig. 5.8** also extended two pseudopods in different directions which attached to the same strut, buckling it (**Fig. 5.8, arrow A'**). Partial recovery of the strut deformation after cell death (induced by the addition of isopropyl alcohol to the culture medium) can be seen in **Figs. 5.7 (final image, arrow D) and Fig. 5.8 (arrows B-B).**

The local stiffness of the matrix in the region of a cell appears to affect the ability of the cell to deform an individual strut. In **Fig. 5.9**, there appears to be an unusually large pore in the region of the deforming strut, on the right side of the images; this pore may have been created by cutting the disconnected strut (B'), during the matrix preparation. Both the large pore and the disconnected strut suggest that this region may be relatively compliant. The cell on the nearby strut only partially elongates along the strut, yet it produces large deformations in the strut. In contrast, the local stiffness of the matrix in **Fig. 5.10** is significantly higher than that of the deforming matrix struts in **Fig. 5.6 and 5.7**, as a result of the larger thickness of the strut (arrow B) as well as the triangulated geometry of the struts on the left hand side of the images. In this case, the cell initially elongates along the matrix; at time 3 hours 8.5 minutes, the attachment on the right hand side of the cell fails catastrophically (arrow D), resulting in fast retraction of that end of the cell and subsequent rounding less than 3 minutes later (arrow E). The cell then elongates to the right once more over a period of slightly less than 2 hours (arrow F). Catastrophic failure of the attachment point on the left hand side of the cell (arrow G) is apparent in the final image of the

sequence. The catastrophic failure and subsequent retraction of the cell produces a net motion of the cell, first to the left, and then to the right of its initial position.

Deformation of the matrix through cell contraction, following elongation, was not observed. Cell migration did not appear to be a requirement for matrix deformation. The only observed migration was due to the release of adhesion at one end of a cell (**Fig. 5.10**) and was associated with a relaxation of force applied to the matrix by the cell.

5.4 Discussion

5.4.1 Cell Processes Linked to Microscopic Matrix Deformations

Matrix deformation was associated with cell elongation. The extension of pseudopods and filopods at the cell-matrix interface generally preceded cell elongation, but this action did not directly result in deformation of the matrix. It has been reported by other investigators [38, 54-56] that the substrate to which cells are attached must have sufficient stiffness to resist cellular forces in order for cells to elongate properly. From these observations, a potential explanation for collagen-GAG matrix deformation observed is as follows: Matrix deformation provides the extracellular resistance necessary for cell elongation and the matrix stiffness determines the extent of matrix deformation.

None of the observations of live cells suggested that matrix deformation occurred simultaneously with cell migration. Fibroblast migratory rates reported by others range from 5 to 100 μm/h [52, 57], and would have resulted in noticeable movement (> 10 μm) during the observations summarized in this manuscript. However, the process of cell elongation during the time of observation made an unambiguous determination of cell migration difficult. Therefore, it cannot be conclusively stated that cell migration did not occur or

commence coincidentally with matrix deformation, rather, it appears that large deformations occurred without observable net fibroblast migration.

The absence of observable fibroblast migration during matrix deformation is supported by the presence of α-smooth muscle actin in more than 85% of the cells, which has been linked to low motility of fibroblasts [58]. In addition, it has been reported that *in vitro* traction forces are weakest in the most mobile cells (leukocytes and nerve growth cones)[52]; fibroblasts are considered one of the least mobile cell types [57, 59]. Observations by other researchers of individual fibroblasts in two-dimensional culture on a collagen gel suggested that nonmotile cells possessed the most favorable mechanism of generating and maintaining force on the substrate [34, 37]. In these collagen gel studies, cellular events leading to migration via rapid pseudopod retraction were accompanied by a dramatic loss of force (deformation) applied to the collagen gel by the cells. Extension or slow partial retraction of pseudopods were accompanied by similar increases in the force (20 nN per event) [34]. Little or no net cell translocation was observed as a result of these two events. The observations of fibroblast interaction with the collagen-GAG matrix reported in this manuscript, were consistent with the conclusion that force was applied to the matrix during cell elongation, not via rapid retraction of pseudopods resulting in cell migration.

The presence of α-smooth muscle actin (SMA) in the cytoplasm is a marker for myofibroblasts. After having been cultured on plastic in the presence of serum, fibroblasts differentiate into myofibroblasts [58, 60, 61]. Since the fibroblasts which were seeded onto the collagen-GAG matrix had been cultured it is not surprising that such a high fraction stained for positive α-SMA. Interestingly, not all of the fibroblasts observed to be deforming the matrix expressed α-SMA and/or were elongated. Although fibroblasts staining for α-SMA are considered contractile fibroblasts, fibroblasts not staining for α-

SMA have been reported to contract collagen gels in a similar manner [43]. A fibroblast which is rounded and also deforms the matrix suggests that the local matrix stiffness was not high enough to support cell elongation.

5.4.2 Microscopic Deformations Leading to Macroscopic Matrix Contraction

Interaction of fibroblasts with the matrix struts resulted in local deformations as large as 50 - 60 μm. Local deformations of this magnitude were also observed in full-thickness matrix samples restrained by clamps (**Fig. 5.3d**), confirming that the observations in the live cell experiments were not uncharacteristic of those in the cell force monitor (CFM). The macroscopic, uniaxial matrix deformation measured by the CFM for 2 million cells attached to a specimen of matrix 25 mm long, 70 mm wide and 3 mm thick was ~ 1 mm [50]. The pore size of the matrix was 140 μm, so that there are about 180 pores along the length of the specimen. The average deformation of a single row of pores across the width of the matrix specimen in the CFM is, then, about 6μm, or approximately one-tenth of the observed maximum strut deformations in the live cell imaging specimens (50-60 μm). The difference is due to several factors: many struts do not have cells attached to them; some cells do not elongate or produce strut deformations; and the cells do not all contract along the axis of measurement.

The magnitude of the deformation developed by a particular cell depended strongly on the local configuration and size of the struts, as well as the orientation of the cell to the struts; these conditions determined the local stiffness experienced by the cell. For example, the deformed struts associated with the elongated cells in **Figs. 5.6 and 5.7** are much longer and thinner than the undeformed strut associated with the elongated cells in **Fig. 5.10**. Consider in more detail the cell elongation and matrix deformation shown in **Fig. 5.6**. Cell

spreading could occur only along the axis of the matrix strut. All forces developed by this cell during the process of elongation were directly applied to that strut. As the cell elongated, and the adhesion sites became further apart, the force applied to the strut by the cell approached that for buckling of the strut (see eqn (1), below). In a single, isolated strut, buckling produces large deformation at constant load. In the matrix strut loaded by the cell, large deformations are also possible if the cell can apply sufficient force to produce compatible deformations in the surrounding matrix struts (by bending or buckling). In contrast, the combination of the triangulated struts and a shorter, stubbier strut seen in **Fig. 5.10** is a very stiff configuration, allowing little deformation, even following significant elongation of the cell. The lack of stiffness in a particular matrix region may also impede cell elongation. In **Fig. 5.9**, the cell rapidly deformed the strut without significant elongation. The region of the matrix to which this cell was attached likely had a low stiffness, due to the lack of connectivity with other struts on the right-hand side of the image. Thus, the matrix deformed significantly at cell-generated forces below those required to mediate cell elongation.

5.4.3 Time Dependence of Contraction

The plot of average aspect ratio with time represents how the entire population of cells elongated over the period of observation (**Fig. 5.4**). Noting that the average aspect ratio did not increase after 15 to 22 hours, the time constant for cell elongation was estimated to be in the range of 5-7 hours, similar to that for the development of contractile force by the entire population of cells [50]. This suggests a link between the average elongation of the cell population and the macroscopic contraction of the population.

Time dependence of the macroscopic contraction and the elongation of the cell population can be compared with the time dependence for the elongation of individual cells. The time required for the population to reach an asymptotic value for contraction and elongation (between 15 and 22 h) was significantly longer than the time it took an individual cell to elongate and deform the matrix (2 to 4 h). In addition, the elongation of some cells was delayed for several hours. This delay was likely due to fibroblasts being at different stages of the cell cycle at the time of seeding or response to local variations in stimuli. These two observations suggest that the time dependence of the population-averaged measurements was due both to the time dependence of individual elongation and deformation processes, as well as to the stochastic nature of the initiation of these processes throughout the matrix. The broadening of the aspect ratio histogram peaks with time (**Fig. 5.5**) is consistent with the conclusion that cells do not elongate uniformly. If cells elongated uniformly, the histogram peak would shift to larger aspect ratios without broadening. Therefore, the time constant of population-averaged measurements does not reflect the behavior of individual cells.

5.4.4 Micromechanical Model of Contraction on Collagen-GAG Matrix

In our previous study of contraction of the same collagen-GAG matrix by fibroblasts using the cell force monitor (CFM) we found that the development of the contraction, Δ, or force, F, with time, t, can be described by an equation of the form:

$$\Delta \text{ or } F \propto \left[1 - e^{(-t/\tau)}\right]$$

where τ, the time constant, was measured to be about 5 hours. The contraction and corresponding force reach plateau values which depend linearly on the number of attached cells. In this study, we found that the deformation of the matrix struts was associated with

cell elongation. The time constant for population averaged cell elongation was 5-7 hours (**Fig. 5.4**), similar to that for the contraction or force found previously from the CFM study.

Observations from live cell imaging relevant to the mechanics of strut deformation are as follows. The points of attachment are near the furthest extension of the cell. As cells elongate, a gap is often visible between the matrix strut and the mid-region of an elongating cell (**Figs. 5.6, 5.10**) suggesting that adhesion sites at the mid-region of the cell detach while new adhesion sites form with the extending cytoplasm. Other investigators have reported that a majority of adhesion sites are near the cell periphery of elongated fibroblasts [59, 62]. Matrix struts deform by buckling (when the cell elongates along one strut and is attached towards the ends of the strut *e.g.,* **Fig. 5.6, 5.7**), or bending (when the cell is attached to two or more struts *e.g.,* **Fig. 5.7, 5.8**) depending on the geometrical arrangement of the cell and its attachment sites to the matrix. Buckling can lead to large strut deformations, stopping only when adjacent struts at either end of the buckling strut come into contact with each other, completely collapsing that end of the pore. Bending appears to produce smaller deformations than buckling and, in some cases (**Figs 5.6, 5.7**), occurs after buckling of an adjacent strut.

The mechanics of matrix contraction by strut buckling are as follows. Tension in the actin fibers within the cytoskeleton induces a compressive force in the matrix strut via the adhesion sites (**Fig. 5.11a, d**). As the cell elongates, and attachment points are concentrated at the cell extensions, the length of the strut between the loading points increases (**Fig. 5.11b, c**), decreasing the load necessary to produce buckling. We note that the load at which a column buckles is given by the Euler buckling load,

$$P_{cr} = \frac{n^2 \pi^2 EI}{l^2} \qquad (1)$$

where n is a constant which depends on the stiffness of the adjacent struts, E is the Young's modulus of the strut material, I is the moment of inertia of the strut (for solid circular cross sections, for instance, $I \propto r^4$), and l is the length of the column or strut between the loading points. Once the buckling load is reached, large deformations are possible with only small increases in load (**Fig. 5.11g**), leading to significant collapse of the strut.

The mechanics of matrix contraction by strut bending are as follows. If the cell is attached to more than one strut, tension in the actin fibers can produce strut bending (**Fig. 5.11e, f**). The bending deformation, δ, of a linear elastic, isotropic beam of span l, under a load F, is given by:

$$\delta = \frac{Fl^3}{CEI} \qquad (2)$$

where E and I are again the Young's modulus of the strut material and the moment of inertia of the strut cross section, respectively, and C is a constant which depends on the stiffness of the adjacent struts. Bending deformations are linearly related to the applied force. For a matrix strut deformed by a cell, the maximum deflection is limited by the maximum force the actin fibers can apply. This is in contrast to strut buckling where the resistive force does not increase significantly for increases in deformation after the buckling load is reached (**Fig. 5.11g**).

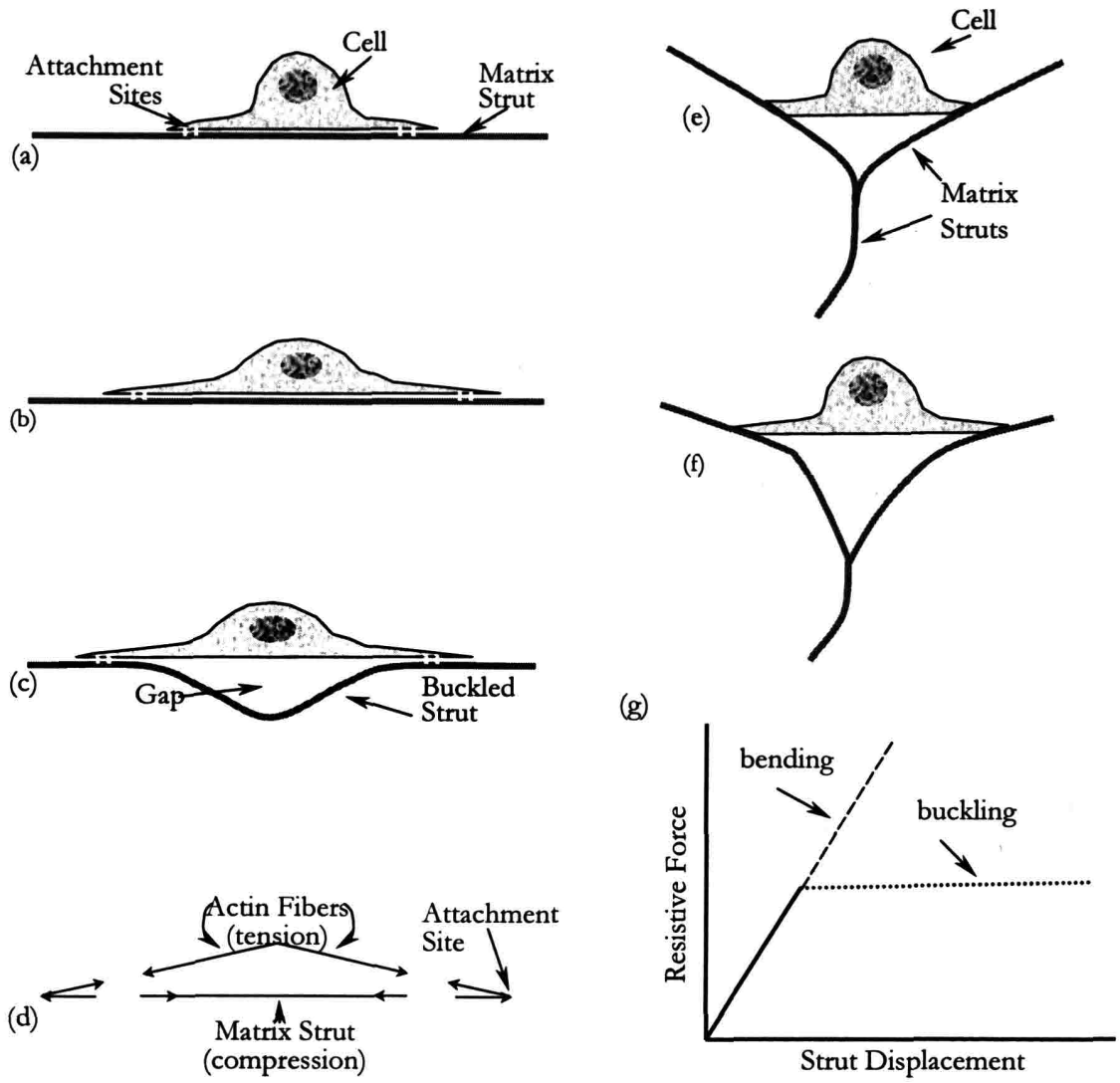

Figure 5.11. (**a,b**) Sketches of cell elongation, showing attachment sites forming at cell extension. (**c**) Sketch of matrix strut buckling due to force developed by the actin fibers in the cell, showing gap between cell and strut. (**d**) Free body diagram of forces, showing tension in the actin fibers, compression in the matrix strut and the resulting balance at the attachment site. (**e,f**) Sketches showing cell attached at a strut junction resulting in bending of the struts due to the force developed by the cell. (**g**) Schematic plot of the resistive force provided by the matrix struts for a given displacement imposed by the cell. Note that following the onset of buckling, resistive force does not increase significantly for increases in deformation.

This first order mechanical analysis of the matrix deformation is consistent with the observation of a deformation or force plateau in the CFM tests: strut deformation by buckling and bending is limited by either the constraints of the strut geometry or by the

maximum force that the actin fibers can apply, respectively. Increasing the number of cells attached to the matrix increases the number of struts deforming, increasing the force plateau. More detailed finite element calculations can be used to determine if the overall deformation and force plateau are linearly dependent on the number of struts deforming by bending and buckling. The time dependence of macroscopic matrix contraction is determined by the actions of individual cells, but a functional relationship between them has not yet been established. A mechanical model which connects the actions of individual cells with the overall macroscopic deformation may aid in understanding the time dependence.

5.5 Conclusions

The macroscopic contraction of collagen-GAG matrices observed previously [50] was the result of millions of fibroblasts individually bending or buckling matrix struts. Immunohistochemical analysis showed that a majority of these fibroblasts (> 75%) were contractile fibroblasts or myofibroblasts typically found in healing wounds. The individual deformation events produced a broad range of local matrix deformations (barely observable to > 50 μm per cell) which appeared to depend on the local matrix stiffness. Macroscopic contraction within the 15 h following cell attachment was due to force generated during myofibroblast elongation. The time dependence of macroscopic contraction was found to be the result of the stochastic nature of the initiation of cell elongation combined with the time required for each cell to reach its final morphology (2 - 4 h). The micromechanics associated with the buckling or bending of individual struts by cells may, in part, explain the observation of a force plateau in the macroscopic contraction experiments. A more detailed understanding of how many individual deformation events led to a macroscopically measurable force or displacement will aid in the interpretation of these macroscopic results

to determine cell behavior. The macroscopic measurement of matrix contraction by cells has led to a better understanding of the role of the cytoskeleton, chemical signaling, extracellular matrix properties, and integrin binding play in the development of force by cells.

Chapter 6. Effect of Stiffness on Fibroblast Contraction

6.1 Introduction

During one of the final stages of dermal wound repair, contraction, which is associated with the differentiation of fibroblasts into myofibroblasts, occurs [13]. The presence of myofibroblasts has been linked to wound contraction and scar formation [3, 7, 13, 63]. Closure of a wound by scar formation results from a combination of contraction and ECM production. Concurrent with the differentiation of fibroblasts is an increase in the stiffness of the wound due to extra-cellular matrix production and general remodeling. Along with chemical signals, it has been suggested that the higher ECM stiffness is a cue for the differentiation. After the wound has closed the prevalence of myofibroblasts decreases, presumably through apoptosis [4], and the scar tissue becomes sparsely populated by normal dermal fibroblasts as ECM remodeling slows [13].

The use of a collagen-GAG extra-cellular matrix (ECM) analog, grafted onto the debrided wound bed, has resulted in the formation of a partially-regenerated dermis, instead of scar tissue, through the reduction of wound contraction [3]. As part of the wound healing response, fibroblasts and other cells migrate into the ECM analog within the first few days and remodel it by producing new collagen and enzymes specific for ECM proteins. The formation of partially regenerated dermis and corresponding elimination of scar tissue has been linked to the ECM analog's ability to reduce wound contraction. Interestingly, myofibroblasts thought to be responsible for wound contraction are present in ECM analog grafted wounds. In contrast, culture of a fibroblast seeded collagen-GAG matrix sample *in vitro*, results in the contraction of the sample.

The link between the presence of myofibroblasts and wound contraction is under investigation *in vitro* using various methods to monitor the contraction of a fibroblast-populated gel or matrix [19, 20, 37, 64]. Several devices have been built which allow the contractile force to be measured as a function of time [16-18, 20, 41]. Results from some of these experiments suggest the force generated by the fibroblasts is a homeostatic response such that any externally effected change in this force elicits a cellular response to minimize the change [16, 20, 41]. Many cellular processes, including α-smooth muscle actin production, are affected by altering the stiffness of the substrate on which the cells are cultured *in vitro* [31, 38, 65]. An understanding of the link between substrate stiffness and fibroblast differentiation *in vitro* may lead to an explanation for the appearance and disappearance of myofibroblasts *in vivo*.

We have previously described a cell force monitor (CFM), designed to measure the contractile force generated by cells seeded onto a porous matrix (Chapters 3 & 4). In this study, we report results of three sets of experiments designed to measure the effect of the total system stiffness on the contractile response of fibroblasts. First, three cell force monitors with differing beam stiffnesses were used to measure the short term (22 h) contractile response. Second, the elongation of the fibroblasts during the contraction in the cell force monitor was compared for two different beam stiffnesses. Finally, unrestrained, free-floating matrices with different degrees of crosslinking (and hence, stiffness) were used to measure the long term (15 day) contractile response. If the level of force generated by the fibroblasts is truly a homeostatic, or force-limited, response, the force generated per cell should be independent of the total stiffness. However, if the displacement produced per cell is independent of the total stiffness, the contractile response is displacement-limited. The

experiments described in this study are designed to indicate if fibroblast contraction is force-limited or displacement-limited.

6.2 Methods

6.2.1 Collagen Matrices

Collagen-GAG matrix sheets were produced as described previously (Chapter 2) Matrix samples to be used in the cell force monitor experiments and the free-floating experiments were crosslinked by treatment at 105°C under a vacuum of < 50 torr for 24 hours [3]. A second set of matrix samples, to be used in the free-floating experiments, were crosslinked for only 1 hour, producing a less stiff matrix. Compressive modulus was determined for the matrix samples used in each set of experiments as described previously (Chapter 2) (CFM experiments 47 Pa; free-floating 24 h crosslink 54 Pa, and 1 h crosslink 19 Pa). Rectangular samples, 50mm x 28mm x 3 mm, for cell force monitor experiments, and disks, 9mm in diameter x 3mm thick, for free-floating experiments, were cut from the fully processed matrix sheets.

6.2.2 Quantitative Measurement of Contraction Using the Cell Force Monitor

The cell force monitor (CFM) described previously (Chap. 3 and 4) was used to monitor the force developed by fibroblasts seeded into collagen-GAG matrices under three different total stiffness conditions. A clamped, fibroblast-seeded collagen-GAG scaffold was held fixed at one end and attached to a compliant beam on the other in the proximity sensor model CFM (**Fig. 3.2**). The proximity sensor monitored the beam deflections resulting from contraction of the scaffold by the fibroblasts without contacting the beam. This modification allowed beam stiffness to be varied, through changes in beam geometry,

with little effort. The design of the proximity sensor/beam configuration resulted in a voltage response which was linear with beam displacement and force applied to the beam. This voltage was recorded for 22 hours post-seeding by a data acquisition card (AT-MIO-16XE-50, National Instruments, Austin, TX) installed in a PC (Compaq, Pentium II). Force and displacement of the beam were calculated by multiplying the recorded voltage by the appropriate calibration factor (Chapter 3). Opposing force in the matrix was calculated using the compressive stiffness of the matrix and the deflection of the beam end. The beam and matrix were in parallel so that the deflection of the beam end and matrix were identical and the total force was the sum of the force in each element:

$$F_{total} = F_{beam} + F_{matrix} = V \cdot C_{force} + V \cdot C_{displ.} \cdot K_{matrix} \qquad (6.1)$$

where V was the voltage measured, C_{force} and $C_{displ.}$ were calibration factors for force and displacement, respectively, and K_{matrix} was the stiffness of the matrix.

In this study, the stiffness of the CFM was controlled by varying the beam geometry. Three CFMs, identical except for their beam stiffnesses, were used to measure the contractile response of the fibroblasts. The matrix stiffness was constant at 0.7 N/m $\left(K_{matrix} = 47\ Pa \cdot \frac{0.05\ m \cdot 0.0045\ m}{0.015\ m} = 0.7\ \pm\ 0.09\ N/m \right)$. The three beam geometries were chosen such that the beam stiffness was either: negligible compared to the matrix stiffness (dimensions 150 mm x 10 mm x 0.005 mm), similar to the matrix stiffness (dimensions 90 mm x 10 mm x 0.15 mm), or much higher than the matrix stiffness (dimensions 50 mm x 10 mm x 0.15 mm). Total CFM stiffness was equal to the sum of the beam and matrix stiffness (**Table 6.1**). Five tests were done in each CFM with a given beam stiffness.

After the freeze drying and crosslinking processes, specimens of the matrix material were cut to the appropriate size and rehydrated by immersion in 10ml DMEM with 10% FBS in a tube for 10 minutes (see Appendix E.3). A suspension of 4 million fibroblasts was then added and attachment of the fibroblasts to the matrix was facilitated by placing the tube on a rocking platform in a cell culture incubator for 10 minutes. Cell seeded matrices were then carefully attached to the cell force monitors, and data acquisition begun.

Table 6.1. Total stiffnesses for CFM experiments.

	Beam Stiffness [N/m]	**Matrix Stiffness [N/m]**	**Total Stiffness [N/m]**
Stiffest CFM	10	0.7	10.7
Intermediate CFM	0.7	0.7	1.4
Least Stiff CFM	3.3×10^{-6}	0.7	0.7

Voltage data for contraction as a function of time were corrected for any voltage changes not attributable to the interaction of the fibroblasts with the matrix by testing unseeded matrix samples and subtracting the average (n = 3) response from the cell seeded response for each stiffness group. The corrected voltage data and the calibration factor C_{displ} was used to calculate the displacement; the calibration factor C_{force} and the matrix stiffness were also used to obtain data for force against time (equation 6.1). The resulting displacement vs. time and force vs. time curves for each experiment were normalized by attached cell number at 22 h and averaged (n = 5).

In addition to a qualitative comparison of the curves for the average force and displacement per attached cell vs. time, individual curves were characterized by fitting the data to the exponential relationship:

$$F_c = F_{cell} \cdot \left(1 - e^{-(t/\tau)}\right) \quad \text{or} \quad d_c = d_{cell} \cdot \left(1 - e^{-(t/\tau)}\right) \tag{6.2}$$

where F_c and d_c are the force and displacement per cell at time t, F_{cell} and d_{cell} are the asymptotic force and displacement per cell, and τ is the time constant. This relationship was fit to the data using non-linear regression analysis giving two fitting parameters which describe each data set, F_{cell} or d_{cell} and τ. These parameters were then grouped by total stiffness and averaged. Only one time constant was determined for each experiment since force and displacement are linearly related through stiffness. The different stiffness groups were also compared by the characteristic rate of contraction per cell (d_{cell}/τ).

Following the experiment, the sample was cut from the clamps and bisected. Half of the sample was fixed in 10% neutral buffered formalin for histological analysis. The remaining half was rinsed in 37°C phosphate buffered saline(PBS) to remove unattached cells and then digested in a 2.0U/ml solution of dispase (GIBCO, Grand Island, NY) at 37°C. The attached cell number at 22 hours post-seeding was determined by counting cells in the dispase digest using a hemacytometer.

6.2.3 Fibroblast Morphology Determination

The effect of CFM stiffness on fibroblast morphology at 22 h post-seeding was determined by measuring fibroblast aspect ratio in images of stained histological sections as previously described (Chap. 5.2.1). Two groups of fibroblast-seeded matrix samples were cultured in CFMs of different stiffness for 22 hours (n = 4). One group had a stiffness equal to that of the matrix (0.7 N/m), while the other was roughly 4 times greater (2.7 N/m). The aspect ratios of at least 65 cells from each sample, for a total of 280 cells per stiffness group, were measured using the particle analysis tool provided with Scion Image

(http://www.scioncorp.com/) (see Appendix G.5). Only fibroblasts which appeared to be attached to the matrix and in which a dark, ovoid nucleus could be identified were included. The average aspect ratio for each sample was determined and then averaged with all samples in that stiffness group (n = 4). In addition, aspect ratio measurements from all samples of the same stiffness were plotted on a histogram to determine if total stiffness had an effect on the distribution of aspect ratios.

6.2.4 Free-Floating Experiments

The long-term effects of collagen-GAG matrix stiffness on fibroblast-mediated matrix contraction were determined by monitoring the dimensional changes of free-floating disks of matrix crosslinked for either 1 h or 24 h. Disks of collagen-GAG matrix, 9 mm in diameter, were rehydrated and seeded using the same method as in the CFM experiments. Unseeded controls and fibroblast-seeded matrix disks were then floated on DMEM with 10% FBS in agarose-coated 12-well tissue culture plates (see Appendix F). The diameter of the matrix disks was recorded on days 1, 3, 6, 7, 9, 12, 13 and 15 by comparing them to printed circles of a known diameter (± 0.5 mm).

Reduction in diameter against time for each sample was calculated by subtracting the diameter at that time point from the diameter at day 1 and deducting the average diameter change measured in the cell-free matrices over the same time period. Percent reduction in diameter, for each sample, was determined by dividing this value by the diameter at day 1 for that sample. The average and standard error were then determined for each time point from the individual values of percent reduction in diameter (n = 8 for days 3 and 6; n = 4 for days 7, 11, 13, and 15). In addition, attached cell number was determined for both matrix stiffnesses at days 1, 6, and 15 (n = 3) by the dispase digestion method described above. On

each of these days, one sample from each matrix stiffness group was fixed in 10% neutral buffered formalin and subsequently embedded in GMA. Light micrographs, from hematoxylin and eosin (H&E) stained GMA sections, were gathered to compare qualitatively changes in fibroblast distribution and matrix microstructure with time.

6.2.5 Statistical Methods

A two-tailed, heteroscedastic Student's t-test was used to determine the significance of the effect of stiffness on: cell number at 22 hours post-seeding; fibroblast aspect ratio in CFM experiments; and matrix diameter at various days post-seeding in free-floating experiments. Two-way ANOVA was used to determine the significance of the effects of time and crosslink treatment on cell number in free-floating samples.

6.3 Results

6.3.1 Quantitative Contraction Measurement Using the CFM

Contraction experiments using the CFM provided a time continuous measurement of matrix displacement from which average displacement and force per cell were calculated for three different levels of total stiffness. Displacement and force per cell increased with time, approaching an asymptotic level by ~ 10 h post-seeding for all total stiffnesses (**Fig. 6.1, 6.2**). A plot of displacement per cell against time showed that the asymptotic level was lower for higher values of total stiffness (**Fig. 6.1**). In contrast, a plot of force per cell against time showed similar asymptotic levels for all total stiffnesses (**Fig. 6.2**). There was no significant effect ($p > 0.4$) of total stiffness on attached cell number at 22 h, approximately 900,000 cells per CFM sample.

The curve fit parameters, d_{cell}, F_{cell}, *and* τ, resulting from fitting equation 2 to the data in the plots of displacement and force per cell against time are reported in **Table 6.2.** All curve fits resulted in a high correlation with the data, $R^2 > 0.98$. The total stiffness had a significant effect ($p = 0.0006$) on the asymptotic value of displacement per cell and had no significant effect ($p = 0.6$) on F_{cell} ~3 nN. The time constant, τ, is a measure of how quickly the displacement or force develops. The average time constant for the stiffest system (7.9 h) was not statistically different ($p > 0.1$) from those for the two lower stiffness systems (5.2 and 5.1 h) (**Table 6.2**). The characteristic rate at which each cell contracted, d_{cell}/τ, (**Table 6.2**) was also affected by the total stiffness; the fibroblasts contracted the less stiff systems more rapidly.

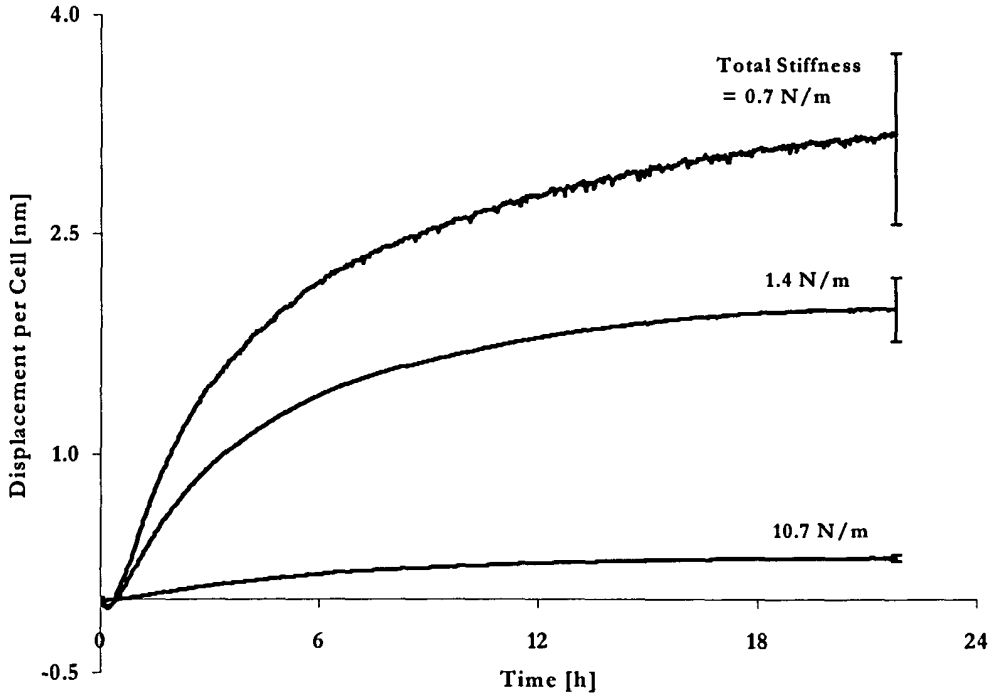

Figure 6.1 Plot of displacement per cell over time for different total stiffnesses. The displacement developed per cell increased as the total stiffness decreased.

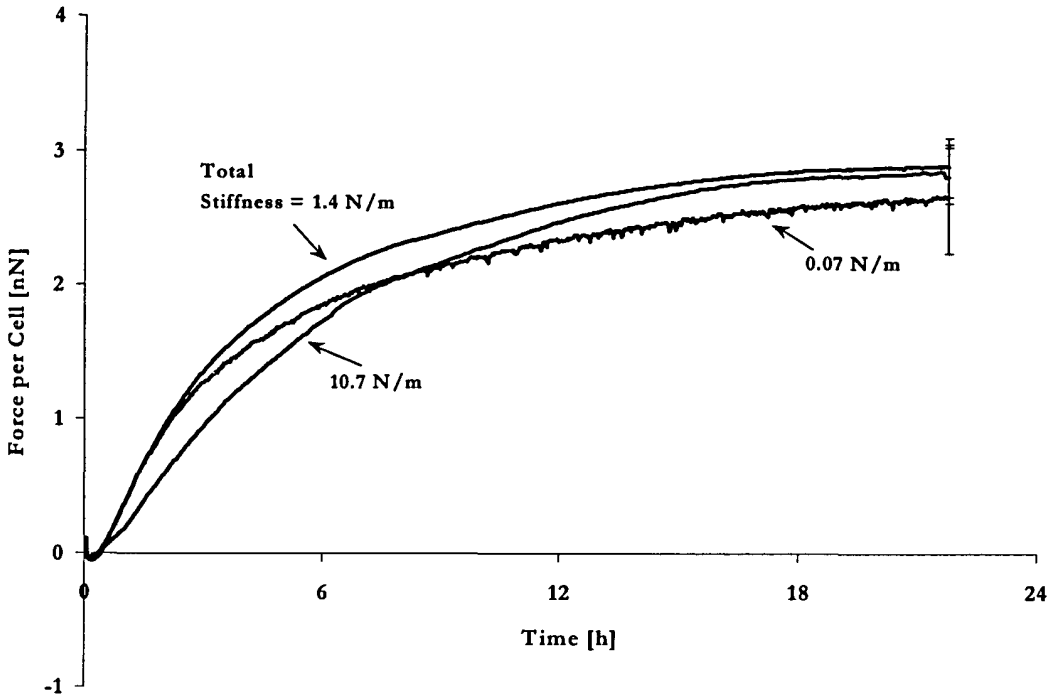

Figure 6.2 Plot of force per cell over time for different total stiffnesses. The force developed per cell was independent of the total stiffness.

Table 6.2. Exponential Curve Fit Parameters

Curve Fit Parameters	Total Stiffness [N/m]		
	10	**1.4**	**0.7**
Mean Asymptotic Force per Cell, F_{cell} [nN]	3.2 ± 0.3	2.9 ± 0.2	2.7 ± 0.4
Mean Asymptotic Displacement per Cell, d_{cell} [nm]	0.32 ± 0.03	2.0 ± 0.2	3.2 ± 0.6
Mean Time Constant, τ [h]	7.9 ± 1.3	5.2 ± 0.85	5.1 ± 0.60
Rate of Contraction per Cell [nm/(h·cell)]	0.04 ± 0.004	0.38 ± 0.04	0.63 ± 0.06

6.3.2 Aspect Ratio Comparison

To determine if fibroblasts altered their morphology in order to increase the amount of displacement per cell, the average and frequency distribution of fibroblast aspect ratios at 22 h post-seeding for the two total stiffnesses were determined. The average aspect ratio of fibroblasts in the compliant and stiff systems, 2.3 and 2.1 ± 0.15, respectively, was not statistically different ($p = 0.39$). The distribution of aspect ratios was also similar for both stiffnesses (**Fig. 6.3**). Half of the fibroblasts were only slightly elongated (aspect ratio < 2) after 22 h. The remaining fibroblasts appeared to have elongated (aspect ratio > 2), with some aspect ratios as high as 7.

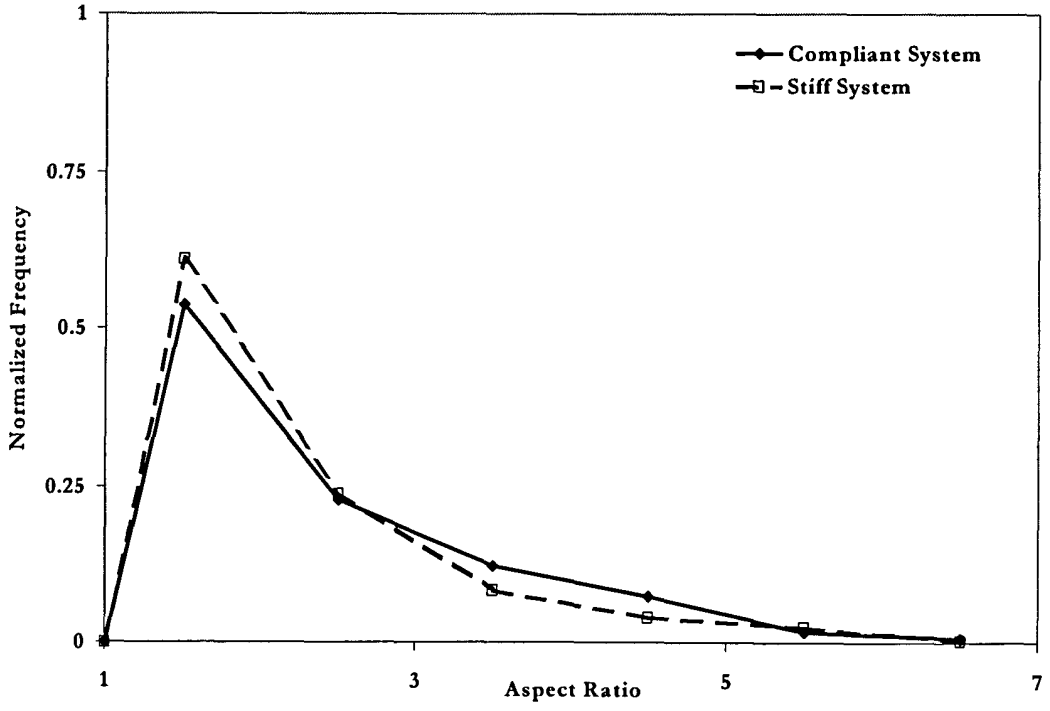

Figure 6.3 *Histogram showing the distribution of aspect ratios at 22 h post-seeding for cells cultured under two different total stiffnesses.*

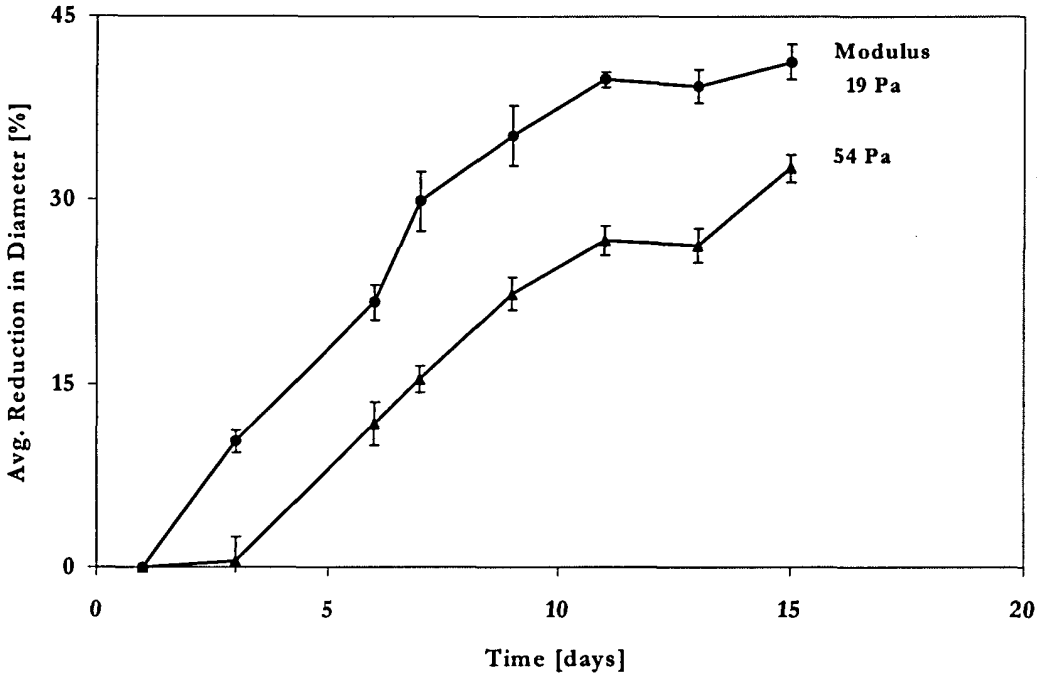

Figure 6.4 Plot showing the effect of initial matrix stiffness on the average reduction in diameter of free-floating matrix disks over two weeks in culture. The attached cell number does not vary significantly with time or between initial stiffness groups.

6.3.3 Free-Floating Matrix Contraction

Fibroblast-mediated contraction of free-floating collagen-GAG matrix disks was greater in the more compliant matrix (**Fig. 6.4**). At all time points, the difference in percent diameter reduction was significantly greater for the lower stiffness matrix samples ($p < 0.007$). During the first 3 days, the diameter of the stiffer matrix did not change significantly from day 1 ($p = 0.1$) while that of the lower-stiffness matrix decreased by 10%. For the lower-stiffness matrix, the percent reduction in diameter per day, ~4%, was approximately constant until the day 6. Between days 6 and 7, the percent reduction in diameter per day increased to 8%. Beyond this point diameter reduction slowed such that after the 11^{th} day there was no statistically significant change ($p > 0.2$) in the diameter. After the initial lag and up to day 11, the stiffer matrices' diameter reduced at about the same rate

(~3%/day) as that observed in the less-stiff matrices. Between days 11 and 13, no noticeable diameter reduction was recorded; however, after day 13, contraction resumed at a rate of 3% per day. The average rate of contraction, defined by the slope a straight line fit to the data after day 3, was similar for both groups (2% per day). The attached cell number, 139,000 fibroblasts per disk, was not significantly affected by time in culture or cross-linking treatment ($p > 0.3$).

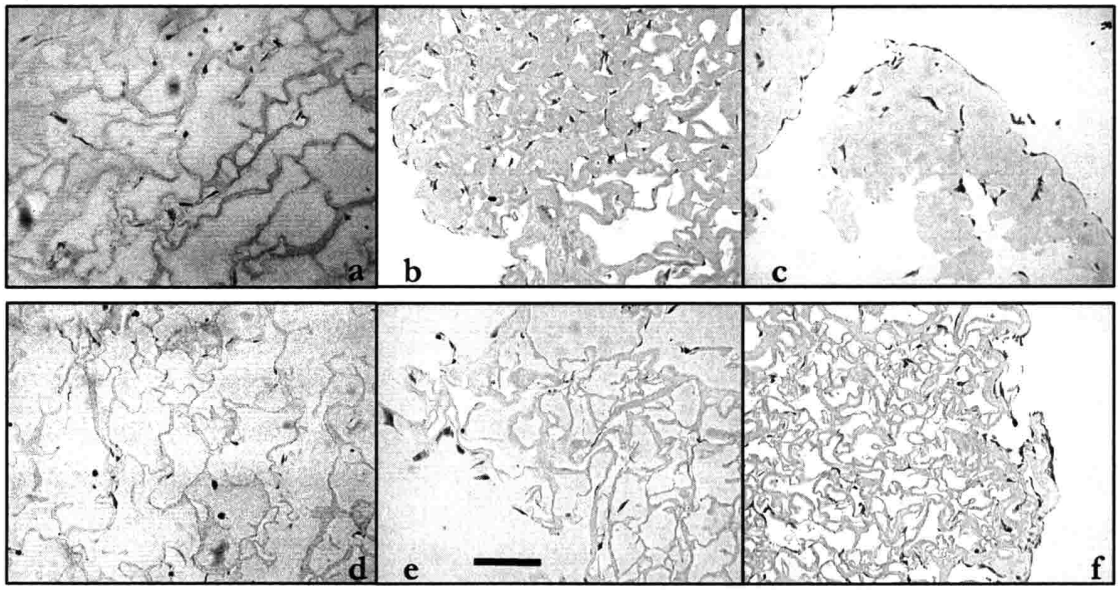

Figure 6.5. Light micrographs of H&E stained GMA sections of free-floating matrix samples showing cell distribution and matrix microstructure changes with time. Less stiff matrix disks shown in a, b, and c for time-points 1, 6, and 15 days, respectively. More stiff matrix disks shown in d, e, and f for time points 1, 6, and 15 days respectively. Scalebar = 200 μm

Qualitative image analysis of H&E stained GMA sections showed a similar distribution of fibroblasts and matrix microstructure for both matrix stiffnesses at 1 day post-seeding (**Fig. 6.5**). By the 6th day, the pore diameter and fraction of void space had decreased noticeably in the less stiff matrices. By day 15, fibroblasts in the interior of the less stiff disks appeared to be completely surrounded by matrix, with no discernible pore structure and a one-cell thick layer of fibroblasts was present on the outside edge. In

contrast, after 6 days the stiffer matrices showed no obvious pore diameter reduction. By day 15 there was a noticeable change in the pore diameter and fraction of void space. The collagen-GAG fibers appeared to have swelled more for the less stiff matrix samples by the 6^{th} day, contributing to reduction in void space. No further analysis of this phenomenon was completed.

6.4 Discussion

6.4.1 Asymptotic contractile force is independent of total stiffness

Quantitative contraction results show that fibroblasts contract the substrate to attain a particular value of force per attached cell; not a particular value of displacement per attached cell. Contraction proceeded until an asymptotic force of ~3 nN per cell was reached, regardless of displacement per cell (0.3 - 3 nm). The value of asymptotic force per cell, F_{cell}, and the time constant, τ, were comparable to the values of 1 nN and 5.2 h, respectively, reported in Chapter 4. These previous experiments showed the total force developed in the collagen-GAG matrix sample was dependent on the number of cells, but F_{cell} and τ remained constant. The discrepancy in the value of F_{cell} may have been due to the use of a different fibroblast seeding technique, serum lot, and matrix sample size. We can now conclude for this system, the force per attached cell and the time constant for the development of the force were independent of the total number of cells and the total stiffness of the system.

Other investigators have reported the substrate stiffness does affect cell behavior. Fibroblasts cultured on collagen-coated, polymer sheets of low stiffness showed reduced spreading, increased rates of motility, and had irregularly shaped and highly dynamic focal adhesions as compared to stiffer sheets [38]. Other investigators [31] reported, the degree of

restraint of a fibroblast populated collagen gel greatly reduced the production of α-SMA in response to TGF-β_1 stimulation over several days; increased gel restraint resulted in a 3-fold higher increase in α-SMA. In addition to effects on cell processes, the linkage between integrins and the cytoskeleton was found to strengthen in response to an increase in the extra-cellular matrix's ability to resist cellular forces [65, 66]. Quantitative measurement of the contractile force, using a device similar to the one described in this paper, of an anchored fibroblast populated collagen gel following cell seeding showed an increase in force for an increase in the concentration of the collagen gel [16]. Although it is likely the collagen gel's stiffness increased with increasing concentration, other parameters of the gel may also have changed (*e.g.* microstructure, efficiency of force transfer) making a comparison between contractile force and stiffness difficult. In fact, Bell *et al.* [12] reported a decrease in overall contraction for an increase in collagen concentration in free-floating, fibroblast populated collagen gels. This dichotomy highlights the difficulty of comparing results from free-floating and anchored collagen gels. The independence of contractile force with stiffness reported in this paper does not contradict any of the stiffness dependent cell behavior cited above.

6.4.2 Force Generation is a Homeostatic Level

Fibroblasts acted to minimize externally imposed changes from the asymptotic level of force [16, 20, 41]. This behavior, termed tensional homeostasis [41], was interpreted to be a negative feedback loop through which the cell actively tried to maintain a particular level of force in the substrate. Data, presented in this paper, showed that the level of force which satisfied the homeostatic criteria was likely to be independent of the stiffness of the substrate. The fibroblasts maintained a very similar force in the matrix at all times regardless

of the amount or rate of deformation required (**Table 6.2**). Other investigators [38] reported that cell spreading was adversely affected when cells were seeded onto a very compliant substrate. If our hypothesis linking cell elongation with matrix contraction is correct, this would have resulted from the substrate not providing enough mechanical resistance to allow for proper cell spreading. The homeostatic response to external factors would then have been a reaction by the cell to reestablish its morphology.

6.4.3 The Cellular Mechanism of Matrix Contraction

It was previously shown (Chapter 5.4.1) that the force measured in the CFM was linked to cell elongation. Specifically, the level of force was related to the amount of extra-cellular support necessary for proper cell elongation. Changing the total system stiffness did not affect the level of force developed by fibroblasts; therefore, displacements increased with decreasing system stiffness. This suggests that the development of force through cell elongation was a force limited process, or individual cells generated larger displacements to attain the level of force.

Elongation was observed to occur through a spreading and thinning of the fibroblast's cytoplasm (Chapter 5). The deformation observed in struts suggested that as cells elongate, adhesion sites form at the leading edge, and likely release near the cell center (**Figs. 5.6 & 5.10**). The compression of a strut under an elongating cell is counterintuitive. A possible explanation for this phenomenon is the simultaneous centripetal movement of adhesion sites and centrifugal movement of cytoplasm (**Fig. 6.6**). The centripetal movement of adhesion sites in stationary cells has been described previously [67]. Therefore, the increase in deformation which was observed suggested that the centripetal motion of adhesion sites occurred until a particular level of extra-cellular force was reached.

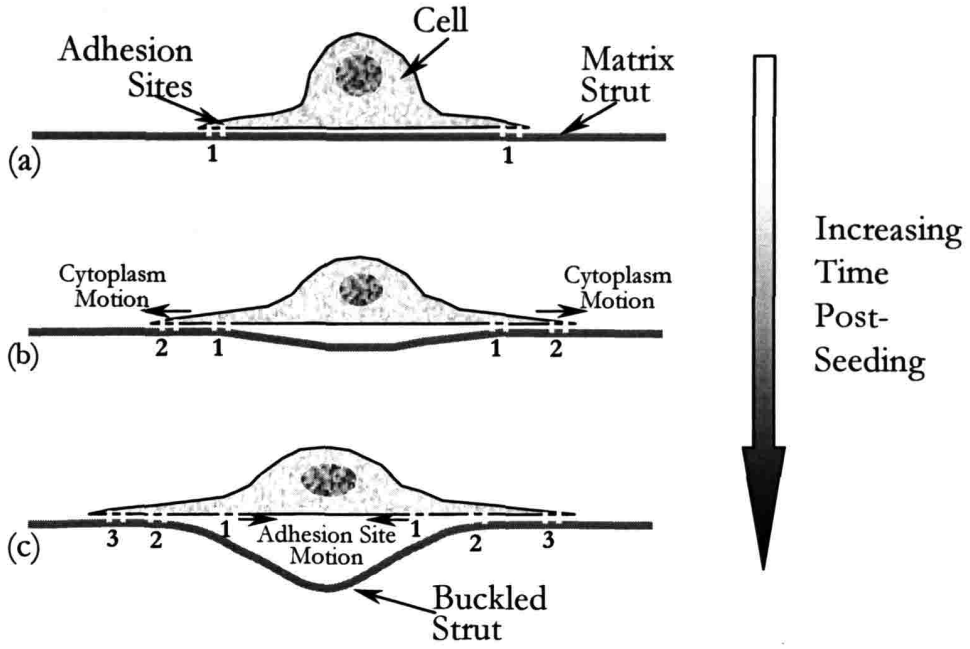

Figure 6.7. Schematic showing the centripetal motion of adhesion sites and the centrifugal motion of cytoplasm. This attempts to explain the phenomenon of simultaneous cell elongation and matrix contraction. (**a**) As the cell elongates, due to cytoplasm motion, new adhesion sites form near the leading edge. (**b**) Adhesion sites 1 move centripetally, new adhesion sites form (2) at the leading edge of the elongating cell. The matrix strut buckles due to the force generated by the cell. (**c**) The adhesion sites (1) have detached from the matrix strut as they near the cell center and the matrix strut moves away as it deforms. Adhesion sites (3) continue to form at the leading edge of the elongating cell and established adhesion sites moving centripetally further deform the strut.

The time constant defining the development of matrix contraction in the CFM was not dependent on the total stiffness, but the rate at which displacements were generated per cell were dependent on the total stiffness (see **Table 6.2**). Previously, the time dependence of matrix contraction in the CFM was explained by the stochastic nature of cell elongation initiation and the time required to reach a final elongated state (Chapter 5.4.3). Individual cells were observed to reach a final deformation state within ~2-4 h, while the population-averaged elongation and contraction in the CFM took ~15 h. The independence of the time constant for CFM experiments with varying system stiffness suggested that the process just described was not sensitive to the external resistance (stiffness) provided. However, the

similarity in time constants and large differences in value of displacement per cell indicated that individual cells deformed the matrix more rapidly when cultured in the less stiff system. Therefore, not only was the mechanism of matrix deformation associated with cell elongation limited by the force, it was also capable of developing larger displacements at faster rates to maintain the time dependence.

6.4.4 Fraction of fibroblasts participating in contraction

The above arguments assume that the fraction of cells which participate in the contraction of the collagen-GAG matrices does not vary with changes in total stiffness. Force and displacement numbers were normalized by the number of fibroblasts at the termination of the contraction experiments. It is possible that only a fraction of the attached fibroblasts actively participated in the contraction. This can be explained by differences in the cell cycle, localized variations in stimuli, and cell-cell proximity. The aspect ratio or amount of cell elongation is an indication of a fibroblast's activity *in vitro*. The observation of fibroblasts which have not elongated significantly, aspect ratios less than 1.2 after 22 h in culture (**Fig. 6.3**), are evidence for the presence of inactive fibroblasts. However, the similarity in the average aspect ratio and in the distribution of aspect ratios (**Fig. 6.3**) for a four-fold difference in total stiffness suggests the fraction of active cells is not dependent on the total stiffness.

6.4.5 Matrix stiffness affects contraction occurring over several days

The contraction of free-floating fibroblast-seeded collagen-GAG matrices was greater for less-stiff matrices after 15 days in culture (**Fig. 6.4**). This contraction can be divided into three phases: lag, steady contraction, and slowing contraction. The presence of the lag phase for the stiffer matrices is consistent with previously reported results [15]. The

majority of contraction occurs in the steady contraction phase, prior to the 11th day in culture. After this phase, the less-stiff matrices had contracted 50% more than the stiffer matrices. Compared to the 300% increase in stiffness, there does not seem to be a simple linear relationship between initial stiffness and long term, unrestrained contraction. This result is not entirely unexpected since changes in crosslink density affect matrix properties other than stiffness (*e.g.* degradation rate, degree of collagen swelling).

A similar decrease in contraction of tenocyte-seeded collagen-GAG matrices for an increase in crosslinking was observed previously [15]. In this case, a linear relationship ($R^2 > 0.7$) was established between contraction, normalized by DNA content, at 21 days and the tensile modulus of the collagen-GAG matrices over a much larger range of stiffness using several different crosslinking treatments. Although experimental setups of this type do not provide a clear link between contraction and matrix stiffness, it does provide insight into the long-term contractile behavior of fibroblasts in matrices with different initial stiffness.

The increase in contraction with decreased initial matrix stiffness in the free-floating contraction experiments is consistent with the independence of the force generated per cell and total stiffness from the CFM experiments. However, the force with time curves from the CFM experiments shows a trend towards an asymptotic value of force per cell. This conclusion seems to contradict the continued contraction of the free-floating matrices over several weeks. If the asymptotic level of force is actually a value which the cells attempt to attain, the continued contraction could be explained by the free-floating matrices inability to provide sufficient resistance to contraction coupled with the continued decrease in resistance due to degradation. In addition, the difference in the mechanical stress state due to the attachment to the CFM also make direct comparisons difficult.

6.5 Conclusions

The level of contractile force generated by fibroblasts, while they are elongating on collagen-GAG substrates, is not dependent on the amount of resistance to contraction (*i.e.* total stiffness). This demonstrates that fibroblast contraction is a force limited behavior; not displacement limited. Cell elongation occurs simultaneously with the development of this force and has the same independence of total stiffness. Therefore, the cytoskeletal mechanism of force generation, occurring coincidentally with cell elongation, is capable of increasing the displacement of adhesion sites in order to develop the asymptotic level of force. Although, a detailed understanding of how the passive mechanical signals provided by substrate materials affect cell processes is still unavailable, *in vitro* modeling of cell-mediated contraction continues to provide useful information.

Chapter 7. Conclusions

The goals of this study were to establish a new model in which to study matrix contraction by fibroblasts, to identify the cellular mechanisms responsible for and the mechanical factors which limit matrix contraction by fibroblasts.

A new model based on the contraction of a collagen-GAG matrix by dermal fibroblasts was developed and tested. Specifically, a device named the Cell Force Monitor (CFM) allowed the macroscopic contractile force and displacement of the matrix to be continuously monitored over time. The model permitted independent control over the microstructural (collagen-GAG matrix), chemical (growth medium), and mechanical (CFM and matrix stiffness) environments. In addition, the open microstructure of the collagen-GAG matrix allowed for the observation of deformation of matrix struts by fibroblasts.

It was established that macroscopic contraction of the collagen-GAG matrix was the result of forces generated during cell elongation. The force per cell was found to be independent of cell density (400 - 2,000 cells/mm^3) and total system stiffness (0.7 - 10.7 N/m). However, the total contractile force was dependent on the cell density, which indicates that the cells did not act cooperatively to establish a particular level of force in the matrix. These results indicated that the contractile force developed during fibroblast elongation was determined at the level of individual cells (not cooperatively) and was limited by force per cell (not displacement per cell). Force per cell was calculated simply by normalizing by the number of cells present in the matrix. In future work, mechanical and/or computer modeling may be used obtain a more detailed analysis of how the macroscopic measurement of force in a matrix can be related to the force developed by

individual cells. For this purpose, the relationship between the tensile and compressive mechanical properties and the properties of the pore wall material will need to be elucidated.

The kinetics of macroscopic matrix contraction were independent of cell density and system stiffness. Microscopic analysis found that the macroscopic time dependence likely resulted from the stochastic nature of cell elongation initiation and the time required for the fibroblasts to elongate completely. Therefore, the time dependence of macroscopic matrix contraction did not reflect the time dependence of force generation by individual fibroblasts, but rather an average for the entire population.

References

1. Levenson SM, Geever EF, Crowley LV, Oates JFI, Berard CW, Rosen H. The healing of rat skin wounds. *Annals of Surgery* 1965; **161**:293-308.
2. Singer AJ, Clark RAF. Cutaneous Wound Healing. *NE J. of Med.* 1999; **341**:738-746.
3. Yannas IV, Lee E, Orgill DP, Skrabut EM, Murphy GF. Synthesis and characterization of a model extracellular matrix that induces partial regeneration of adult mammalian skin. *Proc Nat Acad Sci USA* 1989; **86**:933-937.
4. Desmouliere A, Gabbiani G. The role of the myofibroblast in wound healing and fibrocontractive diseases. In: Clark RAF, ed. *The Molecular and Cellular Biology of Wound Repair.* New York: Plenum Press, 1996. p. 391-423.
5. Ferdman AG, Yannas IV. Scattering of light from histologic sections-A new method for the analysis of connective-tissue. *J Invest Dermatol* 1993; **100**:710-716.
6. Gabbiani G, Ryan GB, Majno G. Presence of modified fibroblasts in granulation tissue and their possible role in wound contraction. *Experientia* 1971; **27**:549-550.
7. Gabbiani G, Hirschel BJ, Ryan GB, Statkov PR, Majno G. Granulation tissue as a contractile organ. A study on structure and function. *J Exp Med* 1972; **135**:719-734.
8. Chamberlain L, Yannas I, Hsu H, Spector M. Connective tissue response to tubular implants for peripheral nerve regeneration: The role of myofibroblasts. *J Comp Neurol* 2000; **417**:415-430.
9. Murray M, Martin S, Martin T, Spector M. Histological changes in the human anterior cruciate ligament after rupture. *J Bone Joint Surg Am* 2000; **82A**:1387-1397.
10. Rockey DC, Friedman SL. Cytoskeleton of liver perisinusoidal cells (lipocytes) in normal and pathological conditions. *Cell Motility and the Cytoskeleton* 1992; **22**:227-234.
11. Roche WR. Fibroblasts and asthma. *Clin Exp Allergy* 1991; **21**:545-548.
12. Bell E, Ivarsson B, Merrill C. Production of a tissue-like structure by contraction of collagen lattices by human fibroblasts of different proliferative potential *in vitro. Proc Nat Acad Sci USA* 1979; **76**:1274-1278.
13. Grinnell F. Fibroblasts, myofibroblasts, and wound contraction. *J Cell Biol* 1994; **124**:401-404.
14. Mueller SM, Shortkroff S, Schneider TO, Breinan HA, Spector M. Meniscus cells seeded in type I and type II collagen matrices *in vitro. Biomaterials* 1999; **20**:701-709.

15. Schulz-Torres D, Freyman TM, Yannas IV, Spector M. Tendon cell contraction of collagen-GAG matrices *in vitro*: effect of cross-linking. *Biomaterials* 2000; **21**:1607-1619.

16. Delvoye P, Wiliquet P, Leveque J-L, Nusgens BV, Lapiere CM. Measurement of mechanical forces generated by skin fibroblasts embedded in a three-dimensional collagen gel. *J Invest Dermatol* 1991; **97**:898-902.

17. Kolodney MS, Wysolmerski RB. Isometric contraction by fibroblasts and endothelial cells in tissue culture: a quantitative study. *J Cell Biol* 1992; **117**:73-82.

18. Eastwood M, McGrouther DA, Brown RA. A culture force monitor for measurement of contraction forces generated in human dermal fibroblast cultures: evidence for cell-matrix mechanical signalling. *Biochim Biophys Acta* 1994; **1201**:186-192.

19. Chapuis J-F, Lucarz-Bietry A, Agache P, Humbert P. A mechanical study of tense collagen lattices. *Eur J Dermatol* 1996; **6**:56-60.

20. Jenkins G, Redwood KL, Meadows L, Green MR. Effect of gel re-organization and tensional force on alpha2beta1 integrin levels in dermal fibroblasts. *FEBS* 1999; **263**:93-103.

21. Lee CR, Breinan HA, Nehrer S, Spector M. Articular cartilage chondrocytes in type I and type II collagen-GAG matrices exhibit contractile behavior in vitro. *Tissue Engineering* 2000; **6**:555-565.

22. Klein CE, Dressel D, Steinmayer T, Mauch C, Eckes B, Kreig T, Bankert RB, Weber L. Integrin alpha2beta1 is upregulated in fibroblasts and highly aggressive melanoma cells in three-dimensional collagen lattices and mediates the reorganization of collagen I fibrils. *J Cell Biol* 1991; **115**:1427-1436.

23. Schiro JA, Chan BMC, Roswit WT, Kassner PD, Pentland AP, Hemler ME, Eisen AZ, Kupper TS. Integrin alpha2beta1 (VLA-2) mediates reorganization and contraction of collagen matrices by human cells. *Cell* 1991; **67**:403-410.

24. Guidry C, Grinnell F. Studies on the mechanism of hydrated collagen gel reorganization by human skin fibroblasts. *J of Cell Science* 1985; **79**:67-81.

25. Steinberg BM, Smith K, Colozzo M, Pollack R. Establishment and transformation diminish the ability of fibroblasts to contract native collagen gel. *J Cell Biol* 1980; **87**:304-308.

26. Fukamizu H, Grinnell F. Spatial organization of extracellular matrix fibroblast activity: Effects of serum, transforming growth factor b, and fibronectin. *Exp Cell Res* 1990; **190**:276-282.

27. Clark RAF, Folkvord JM, Hart CE, Murray MJ, McPherson JM. Platelet isoforms of platelet-derived growth factor stimulate fibroblasts to contract collagen matrices. *J of Clinical Investigations* 1989; **84**:1036-1040.

28. Dubertret L, Brunner-Ferber F, Misiti J, Thomas KA, Dubertret M-L. Activities of human acidic fibroblast growth factor in an in vitro dermal equivalent model. *J Invest Dermatol* 1991; **97**:793-798.

29. Gillery P, Serpier H, Polette M, *et al.* Gamma-interferon inhibits extracellular matrix synthesis and remodeling in collagen lattice cultures of normal and scleroderma skin fibroblasts. *Eur J of Cell Biol* 1992; **57**:244-253.

30. Lucarz-Bietry A, Chapuis J-F, Agache P, Humbert P. A histological and ultrastructural comparative study of retracted and tense collagen lattices. *Eur J Dermatol* 1995; **5**:524-530.

31. Arora PD, Narani N, McCulloch CAG. The compliance of collagen gels regulates transforming growth factor-β induction of α-smooth muscle actin in fibroblasts. *Am J Pathol* 1999; **154**:871-882.

32. Grinnell F, Ho C-H, Lin Y-C, Skuta G. Differences in the regulation of fibroblast contraction of floating versus stressed collagen matrices. *J of Biol Chem* 1999; **274**:918-923.

33. Harris. Silicone rubber substrata: a new wrinkle in the study of cell locomotion. *Science* 1980; **208**:177-179.

34. Roy P, Petroll WM, Cavanagh HD, Chuong CJ, Jester JV. An *in vitro* force measurement assay to study the early mechanical interaction between corneal fibroblasts and collagen matrix. *Exp Cell Res* 1997; **232**:106-117.

35. Lee J, Leonard M, Oliver T, Ishihara A, Jacobson K. Traction forces generated by locomoting keratocytes. *J Cell Biol* 1994; **127**:1957-1964.

36. Oliver T, Dembo M, Jacobson K. Traction forces in locomoting cells. *Cell Motility and the Cytoskeleton* 1995; **31**:225-240.

37. Roy P, Petroll WM, Chuong CJ, Cavanagh HD, Jester JV. Effect of cell migration on the maintenance of tension on a collagen matrix. *Ann Biomed Eng* 1999; **27**:721-730.

38. Pelham RJJ, Wang Y-L. Cell locomotion and focal adhesions are regulated by substrate flexibility. *Proc Nat Acad Sci, USA* 1997; **94**:13661-13665.

39. Prajapati RT, Eastwood M, Brown RA. Duration and orientation of mechanical loads determine fibroblast cyto-mechanical activation: Monitored by protease release. *Wound Repair and Regeneration* 2000; 8:238-246.

40. Prajapati RT, Chavally-Mis B, Herbage D, Eastwood M, Brown RA. Mechanical loading regulates protease production by fibroblasts in three-dimensional collagen substrates. *Wound Repair and Regeneration* 2000; 8:226-237.

41. Brown RA, Prajapati R, McGrouther DA, Yannas IV, Eastwood M. Tensional homeostasis in dermal fibroblasts: mechanical responses to mechanical loading in three-dimensional substrates. *J Cell Physiol* 1998; **175**:323-332.

42. Brown RA, Talas G, Porter RA, McGrouther DA, Eastwood M. Balanced mechanical forces and microtubule contribution to fibroblast contraction. *J Cell Physiol* 1996; **169**:439-447.

43. Eastwood M, Porter R, Khan U, McGrouther DA, Brown RA. Quantitative analysis of collagen gel contractile forces generated by dermal fibroblasts and the relationship to cell morphology. *J Cell Physiol* 1996; **166**:33-42.

44. Leavitt J, Gunning P, Kedes L, Jariwalla R. Smooth muscle alpha-actin is a transformation-sensitive marker for mouse NIH 3T3 and rat-2 cells. *Nature* 1985; **316**:840-842.

45. Okomoto-Inoue M, Taniguchi S, Sadano H, Kawano T, Kimura G, Gabbiani G, Baba T. Alteration in expression of smooth muscle alpha-actin associated with transformation of rat 3Y1 cells. *J of Cell Science* 1990; **96**:631-637.

46. Gibson LJ, Ashby MF. *Cellular Solids: Structure and properties.* In: Clarke DR, Suresh S, Ward IM, editors. Cambridge Solid State Science Series. Cambridge: Cambridge University Press; 1997.

47. Yannas IV. Collagen and gelatin in the solid state. *J Macromol Sci Revs Macromo Chem* 1972; **C7**:49-104.

48. Galbraith CG, Sheetz MP. A micromachined device provides a new bend on fibroblast traction forces. *Proc Nat Acad of Sci, USA* 1997; **94**:9114-9118.

49. Dembo M, Wang Y-L. Stresses at the cell-to-substrate interface during locomotion of fibroblasts. *Biophys J* 1999; **76**:2307-2316.

50. Freyman TM, Yannas I, Yokoo R, Gibson L. Fibroblast contraction of a collagen-GAG matrix. *Biomaterials* (in press).

51. Yannas IV. Biologically-active analogs of the extra-cellular-matrix-artificial skin and nerves. *Angew Chem Int Edit* 1990; **29**:20-35.

52. Harris AK, Stopak D, Wild P. Fibroblast traction as a mechanism for collagen morphogenesis. *Nature* 1981; **290**:249-251.

53. Munevar S, Wang Y, Dembo M. Imaging traction forces generated by migrating fibroblasts. *Biophys J* 2001; **80**:1131.

54. Maroudas N. Chemical and mechanical requirements for fibroblast adhesion. *Science* 1973; **244**:353-354.

55. Ingber DE, Folkman J. Tension and compression as basic determinants of cell form and function: Utilization of a cellular tensegrity mechanism. In: Stein WD, Bronner F, ed. *Cell Shape.* San Diego: Academic Press, Inc., 1989. p. 3-25.

56. Oster G. Cell motility and tissue morphogenesis. In: Stein WD, Bronner F, ed. *Cell Shape.* San Diego: Academic Press, Inc., 1989. p. 33-58.

57. Abercrombie M, Heaysman JEM, Pegrum SM. The locomotion of fibroblasts in culture. *Exp Cell Res* 1970; **59**:393-398.

58. Ronnov-Jessen L, Petersen OW. A function for filamentous α-smooth muscle actin: retardation of motility in fibroblasts. *J Cell Biol* 1996; **134**:67-80.

59. Middleton CA, Sharp JA. *Cell locomotion in vitro.* Los Angeles: University of California Press; 1984.

60. Stoflet ES, Schmidt LJ, Elder PK, Korf DN, Foster DN, Strauch AR, Getz MJ. Activation of a muscle-specific actin gene promoter in serum-stimulated fibroblasts. *Molecular Cell Biology* 1992; **3**:1073-1083.

61. Desmouliere A, Rubbia-Brandt L, Abdiu A, Walz T, Macieira-Coelho A, Gabbiani G. α-Smooth muscle actin is expressed in a subpopulation of cultured and cloned fibroblasts and is modulated by γ-interferon. *Exp Cell Res* 1992; **201**:64-73.

62. Couchman JR, Blencowe S. Adhesion and cell surface relationships during fibroblast and epithelial migration in vitro. In: Haemmerli G, Strauli P, ed. *Motility of vertebrate cells in culture and in the organism.* Basel: Karger, 1984. p. 23-38.

63. Rudolph R, Berg J, Ehrlich H. Wound contraction and scar contracture. In: Cohen IK, Diegelmann RF, Lindblad WJ, ed. *Wound healing: Biochemical and clinical aspects.* Philadelphia: W.B. Saunders, 1992. p. 114.

64. Eastwood M, McGrouther DA, Brown RA. Fibroblast repsonses to mechanical forces. *Proc Instn Mech Engrs Part H* 1998; **212**:85-92.

65. Chicurel ME, Chen CS, Ingber DE. Cellular control lies in the balance of forces. *Curr Opin Cell Biol* 1998; **10**:232-239.

66. Choquet D, Felsenfeld DP, Sheetz MP. Extracellular matrix rigidity causes strengthening of integrin-cytoskeletal linkages. *Cell* 1997; **88**:39-48.

67. Smilenov LB, Mikhailov A, Pelham RJ, Marcantonio EE, Gundersen GG. Focal adhesion motility revealed in stationary fibroblasts. *Science* 1999; **286**:1172-1174.

Appendix A. Collagen-Glycosaminoglycan Matrix Production

(adapted from Spilker 2000)

1. Turn on cooling system for blender (Granco overhead blender, Granco Co., Kansas City, MO) and allow to cool to 4°C (Brinkman cooler model RC-2T, Brinkman Co., Westbury, NY).

2. Prepare 0.05 M acetic acid (HOAc) solution: add 17.4 ml HOAc (glacial acetic acid, Mallinckrodt Chemical Co., Paris, KY). (This solution has a shelf life of ~ 1 wk.)

3. Blend 3.6 g of dry microfibrillar bovine tendon collagen (Integra Lifesciences, Plainsboro, NJ) with 600 ml of 0.05 M HOAc on HIGH speed setting for 90 minutes at 4°C. At this point, turn the freeze drier (Genesis 25LE, Virtis) on and then turn on the condenser.

4. Dissolve 0.32 g chondroitin-6-sulfate (C-4384, Sigma Chemical Co., St. Louis, MO) in 120 ml HOAc.

5. Calibrate peristaltic pump (Manostat Cassette Pump, Cat. #. 75-500-0.00, Manostat, New York, NY) to 40 ml/5 min.

6. Add 120 ml of chondroitin-6-sulfate solution dropwise to the blending (HIGH) collagen dispersion over 15 m using the peristaltic pump (ensure blender is at 4°C). At this point, turn on the FREEZE button on the freeze drier. Make sure the HEAT button is off. The shelf temperature should reach -43°C in about 90 m.

7. Blend 90 additional minutes on HIGH speed at 4°C.

8. Degas in a vacuum flask for 15 m or until bubbles are no longer present. (Can be stored at 4°C in a capped bottle for up to about 4 months, re-blend 15 m on LOW speed, 4°C, and degas before using if stored for more than four weeks.)

9. Transfer degassed slurry to a stainless steel tray (0.57 ml/mm^2). Make sure that no air bubbles form while transferring the slurry. Bubbles can be removed with a clean pipet.

10. Gently slide the tray into the freeze drier and close the door.

11. Wait ~1 h or until slurry is completely frozen.

12. Make sure the condenser drain plug is closed and the CHAMBER RELEASE switch is off and then turn on the VACUUM switch. Press on the freeze drying chamber door to ensure it is sealed.

13. After the pressure is below 200 mTorr (~1 h) set the shelf temperature to 0°C and turn on the HEAT switch.

14. Wait overnight for complete sublimation of the ice crystals.

15. Turn the shelf temperature up to 20°C and wait ~1 h.

16. Turn off the VACUUM switch and turn the CHAMBER RELEASE switch on. After the chamber returns to atmospheric pressure open the door and remove the steel tray.

17. Carefully place the matrix sheets into labeled aluminum foil packets leaving one end open.

18. Place packets into a vacuum oven (105°C) and pull a vacuum of < 50 Torr. Hold at this pressure for 24 h. After the chamber returns to atmospheric pressure remove the packets and quickly seal them. The matrices are treated as sterile from this point forward. Store matrix sheets in sealed packets in a dessicator until needed.

Appendix B. Cell Culture Protocols

Equipment:

Sterile hood
Disposable sterile plastic pipets
Water bath (37°C)
Cell culture incubator (37°C and 5% CO_2) (Ultima, Revco, Asheville, NC)
Pipetmen (10, 200 µl)
Tissue culture flasks (Falcon T-75, Beckton-Dickinson, Franklin Lakes, NJ)
Pipetaid
50 ml centrifuge tubes
Centrifuge (Labofuge 400, Heraeus,)
Cryovials
Hemacytometer (Bright-Line, Hausser Scientific, Horsham, PA)

Solutions

Complete Culture Medium:
- 500 ml Dulbecco's Modified Eagle Medium (DMEM) (10316-024, Gibco, Grand Island, NY)
- 50 ml Fetal bovine serum (SH30084.03 Certified Australian, Hyclone, Logan, UT)
- 5 ml Penicillin & Streptomycin (15140-122, Gibco)
- 5 ml Fungizone® (15295-017, Gibco)
- 5 ml L-Glutamine (25030-081, Gibco)

Trypsin-EDTA (25300-062, Gibco)
Dulbecco's Phosphate Buffered Saline (DPBS) (14190-144, Gibco)
Cell Freezing Medium (11101-011, Gibco)
Dispase Solution [2.0 U/ml]
- 100 ml DPBS
- 260 mg Dispase (17105-041, Gibco)

Trypan Blue (15250-061, Gibco)

Procedures:

Heat Inactivation of FBS

1. Thaw frozen FBS (agitated 37°C water bath or overnight at 4°C ; follow manufacturers instructions if different)

2. Heat inactivate by heating to 56°C for 30 minutes in a water bath. Place a thermometer in a similar bottle filled with water in the water bath to determine when the FBS has reached 56°C.

3. Aliquot heat inactivated FBS (50 ml) and store at -20°C.

Medium Mixing

1. Remove 65 ml from DMEM bottle.

2. Add FBS (50 ml), penicillin/streptomycin (5 ml), fungizone (5 ml), and L-glutamine (5 ml).

3. Resulting medium will be: 10% FBS, 2% penicillin/streptomycin, 1% Fungizone®, and 1% L-glutamine.

Cell Passaging

Culture medium must be changed every 3 days. Fibroblasts should be passaged (split) 1-5 after reaching ~90% confluence. A T-75 culture flask at 90% confluence will contain 3 to 5 million cells. Perform procedure under sterile conditions and warm all solutions to 37°C before use.

1. Remove DMEM from culture flasks.

2. Rinse flasks by adding 5 ml DPBS (wait ~30 s).

3. Remove DPBS and add 4 ml trypsin-EDTA.

4. Place flasks in incubator for 5 m to allow for cell detachment.

5. Remove flask from incubator and gently bump the bottom with hand. If cells do not release, place flask back into the incubator for up to 2 additional minutes.

6. Transfer cell suspension from flasks to 50 ml centrifuge tube.

7. Centrifuge at 900 RPM for 5 minutes

8. Add 17 ml DMEM to each new flask

9. Remove supernatant (be careful not to disturb cell pellet at the bottom of tube) and resuspend fibroblasts in fresh DMEM

10. Evenly Distribute fibroblast suspension to new flasks (1-5)

Cell Freezing

Fibroblasts can be stored in liquid N_2 vapor for extended periods of time. Perform procedure under sterile conditions and warm all solutions to 37°C before use.

1. Produce a cell suspension from cells at ~90% confluence using the procedure outlined in the "Cell Passaging Procedure".

2. Count cells using "Cell Counting Procedure"

3. Resuspend cells in cell freezing medium at a density of ~ 1 million cells/ml.

4. Distribute 1 ml to each cryovial. Ensure that cryovials are sealed.

5. Place cryovials into a styrofoam container with walls ~15 mm thick and pack container with cotton gauze. Seal with tape and place in the vapor phase of liquid N_2 dewar.

6. Wait 4 h for cell suspension to freeze and then transfer cryovials to a plastic box in the dewar racks.

Cell Counting Procedure

1. Remove 100 µl from cell suspension while maintaining sterile conditions.

2. Mix 100 µl of cell suspension with 100 µl of Trypan blue.

3. Place cover slip on hemacytometer and pipet 10 µl mixture into notch.

4. Count the number of cells in enough squares to yield more than 100 cells. Before counting, determine a standard for cells touching which edges should be included. For example, cells touching the upper and left edges are counted; those touching the lower and right edges are not counted. This procedure ensures that cells on the border between squares are not double counted.

5. Determine the total volume from which the 100 µl cell suspension sample was taken. Using the following formula determine the number of cells:

$$\#Cells = \frac{\#counted}{squares\ counted} \cdot Dilution(2) \cdot 10{,}000 \cdot Volume(ml)$$

Obtaining Fibroblasts from a Rabbit Dermis Explant

Equipment:

hair clippers
razor
shaving cream
cooler (with ice)
3 scalpels (with blades) (sterile)
surgical scissors (sterile)
2 forceps (sterile)
cotton gauze
sterile table covering
sterile gloves
water bath
incubator
T-75 tissue culture flasks

Solutions:

pentobarbital (Nembutal Sodium Solution), 50 mg/ml
sterile PBS (2% penicillin/streptomycin, 1% Fungizone®)
iodine sponge
70% ethanol
DMEM
Dispase solution

Explant Procedure:

1. Sacrifice rabbit by overdose of pentobarbital (consult animal care staff for current procedure) and place rabbit on sterile table covering.

2. Shear an area on the dorsum of the rabbit with the hair clippers.

3. Use shaving cream and razor to shave the exposed skin until smooth.

4. Clean the shaved portion of the skin vigorously with the iodine sponge to disinfect the area. Then use the cotton gauze and ethanol to clean off the iodine and disinfect the area further. Assemble forceps, scalpel, scissors, and scalpel blades on sterile field. Using the scalpel or scissors, remove a section(s) of skin of the desired size (~1 cm^2).

5. Using the forceps, rinse the section of skin in chilled, sterile PBS and then place the section into a separate container with chilled, sterile PBS for transport back to the lab. An extra container of chilled, sterile PBS may be necessary for an additional rinse to remove blood.

6. Place dispase solution, sterile PBS, forceps, scalpels and blades (2), T-75 flasks and a petri dish into a sterile hood.

7. Rinse the sample one additional time in the PBS and transfer the section of skin to the dispase solution. Incubate at 37°C for at least 30 m.

8. Following incubation in the dispase, gently pull off the epidermis using the forceps. Finally, scrape the top surface of the remaining dermis with a scalpel blade.

9. Place the remaining dermis into the petri dish and cut into ~1 mm^3 pieces using crossed scalpels. Transfer these pieces into the culture flask using a pipette pre-wet with culture medium. Initially only fill the flask with 4 ml of culture medium so that the pieces do not float. After a day or two the pieces will adhere to the bottom of the flask and the total volume of medium can be increased to 17 ml.

10. Monitor the migration of cells out of the explant using an inverted microscope. Culture medium should be replaced at least every third day. Once a sufficient number of cells have migrated onto the culture flask, remove the pieces of dermis and passage the cells.

Appendix C. Mechanical Testing of Collagen-GAG Matrix

C.1 Tension Testing Protocol

Sample Preparation

1. Using a template (85 x 25 mm) cut the collagen-GAG matrix sheet on a teflon sheet using a razor blade. Only push straight down on the blade, do not slice or saw at the matrix.

2. Measure the width and thickness of each sample three times using a micrometer. Average these three measurements together and record.

3. Using a piece of nylon suture thread and fabric paint (Decart, Inc., Morrisville, VT) mark parallel lines, 15 mm apart, perpendicular to the length of the sample on either side of the midline.

4. Allow the paint to dry overnight.

5. Re-hydrate samples in 0.05M acetic acid at 4°C for 24 h.

6. Rinse acetic acid out of samples with phosphate buffered saline (PBS). Repeat 3 times.

7. Store in PBS at 4°C until ready to test.

Mechanical Testing

1. Turn on the mechanical tester (Instron model 4201, Canton, MA). Requires a 15 m warm-up period.

2. Fill acrylic tray with PBS and hook-up temperature controlled pump (Model 1104, VWR Scientific, New Brunswick, NJ).

3. After PBS reaches 37°C, place a matrix sample into the acrylic tray.

4. Calibrate the mechancial tester by pressing the 'Load Cal' button. Attach the nylon line to the load cell and zero the load cell by pressing 'Load Bal' button.

5. Carefully clamp either end of the sample and slowly move the crosshead up until the load barely begins to register. Lower the crosshead until the load zeros. If the load does not return exactly to zero, reset the zero point with the 'Load Bal' button.

6. On the mechanical tester set the following: load range = 5%; crosshead speed = 1 mm/min.; set gage length using the 'G.L. Reset' button.

7. Turn on the PC, start LabView and execute the file Mod_4201.vi. Be sure that the gage length reads zero before executing the program or the load data will have a false starting point.

8. Turn on the second PC attached to the video camera, the time/date generator and the VCR.

9. Adjust the video camera (TM-1001-02 Pulnix America Inc., Sunnyvale, CA) so that the paint lines are in focus and will remain in the field of view during the test. Set the time and date on the time/date generator.

10. Press record on the VCR and start the crosshead motion by pressing the UP arrow.

11. Immediately following the movement of the crosshead, the LabView program will begin acquiring data and the time/date generator will stamp the starting time on the screen.

12. Wait until either the sample begins to tear, or the crosshead has moved 20 mm.

Optical Strain Measurement

1. Turn on the VCR and PC with HLImage++ software. Connect the video monitor connector on the back of the VCR to BNC connector #0 on the PC.

2. Advance the video tape to the frame where the time/date stamp initiated.

3. Start the HLImage++ software and input the correct camera settings.

4. Press Save Images to Disk and Play on the VCR simultaneously to gather 30 images at 1 minute intervals.

5. Open each image in the sequence in order with Scion Image. Make these images into a stack ('Stacks' menu; 'Windows to Stack'). Save stack under an appropriate file name.

6. Determine the following positions by noting the x or y coordinates of the cursor (in Pixels): *top of matrix in last image; bottom of matrix in last image; left of matrix; right* of matrix; minimum width between the lines. Also, using the 'Options' menu; 'Threshold', determine the best level of thresholding to contrast between the lines and the matrix.

7. Load and execute the macro "Mod Interactive Strain"

8. Enter the values determined in step 6 when prompted by the macro.

9. The macro will return a table of values which correspond to the average distance between the lines in each image. Save this table as a text file.

10. Cycle through each image in the stack and determine the time the image was acquired after the time stamp began.

11. The values for distance between the lines can be correlated with the load values recorded by LabView by comparing the time each image was acquired with the load data acquisition rate.

Optical Strain Measurement Macro Code

The following macro was used to measure the distance between the fabric paint lines on samples during tension tests. Subsequent images are converted into a stack. The user must input the region of interest on the stack of images, the minimum width between the lines, and the proper threshold value to get the highest quality images. The macro will prompt the user for these values when the macro is executed. The region of interest is defined by the left, right, upper and lower most portion of the image where the black lines are observed. The macro then converts each image into a binary file and measures the distance between the lines at intervals of 20 pixels on each image. These distances are then averaged for each image and a table of distances for each image are returned.

The macro identifies the lines as a change from black to white. Since the lines have a finite width, the macro identifies both edges of the line and uses the middle of the line to perform the measurement. Any break in the line which would cause the program to return a distance which is too large is corrected for by comparing values with the minimum width entered by the user.

```
MACRO 'Interactive Strain Stack'

var
        RSwitch1, RSwitch2, LSwitch1, LSwitch2, matrixbottom, minwidth, matrixleft,
        matrixright, width, height, left1, left2, right1, right2, i, j , k, n, m, matrixtop, wid,
        thresh :integer;
        left, right, check, Total : real;
begin
          matrixtop := GetNumber('Top of Last Matrix', 50, 0);
          matrixbottom := GetNumber('Bottom Last Matrix', 350, 0);
          matrixleft := GetNumber('Left of Matrix',50, 0);
          matrixright := GetNumber('Right of Matrix', 500, 0);
          minwidth := GetNumber('Minimum Width', 100, 0);
          thresh := GetNumber('Thresh. Value', 85, 0);
        GetPicSize(width,height);
          SetOptions('User1;User2');
        SetUser1Label('Distance');
        SetUser2Label('AvgStrain');
          wid := matrixright - matrixleft;
        k := 1;
        if nSlices = 0 then
                begin
                        PutMessage('This Window is Not a Stack');
                        exit;
                end; { Test for Stack }
        For n := 1 to nSlices do
                        begin
                        SelectSlice(n);
                        j := matrixtop;
                SetCounter(k);
                rUser1[rCount] := 0;
                k := k + 1;
```

```
        m := 0;
        Total := 0;
            SetThreshold(thresh);
            MakeBinary;
            Invert;
While j < matrixbottom do
        begin
                GetRow(matrixleft, j, wid);  {Stores pixel values for this line in the
                linebuffer}
                RSwitch1 := 0;
                RSwitch2 := 0;
                LSwitch1 := 0;
                LSwitch2 := 0;
                left1 :=0; left2 :=0; right1 :=0; right2 :=0;
                For i := 1 to wid do
                begin                          { 0 = white; 255 = black}
                        If LineBuffer[i] = 255 then If LSwitch1 = 0 then
                                begin
                                        left1 := i;
                                        LSwitch1 := 1;
                                end;
                        If LineBuffer[i] = 0 then If LSwitch1 = 1 then If LSwitch2 =
                        0 then
                begin
                        left2 := i;
                        LSwitch2 := 1;
                end;
                If LineBuffer[i] = 255 then If RSwitch1 = 0 then If LSwitch2 = 1
                then
                begin
                        right1 := i;
                        RSwitch1 := 1;
                end;
                If LineBuffer[i] = 0 then If RSwitch1 = 1 then If RSwitch2 = 0 then
                begin
                        right2 := i;
                        RSwitch2 := 1;
                end;
        end;  {IF to gather line positions}
        left := (left1 + left2)/2;
        right := (right1 + right2)/2;
        SetCounter(k);
        check := right - left;
        If check > minwidth then
                begin
                    rUser1[rCount] := right - left;
                    m := m + 1;
                Total := Total + rUser1[rCount];
```

```
                    k := k + 1;
                  end;
              j := j + 20;
        end;  { While Loop j }
        rUser2[n] := Total / m;
end;  { Select Slice For Loop }
        UpdateResults;
        ShowResults;
end;
```

Labview code for Mod_4201.vi

This program allows the user to acquire load data from the Instron mechanical tester and synchronize the video recording of images for the optical strain measurement. Once the program is executed, it does not save any load data until the voltage from the "Position" output from the Instron is different from zero. This output is set to zero when the 'G.L. Reset' button on the mechanical tester is pressed. Once the voltage is greater than zero, the program changes the potential on Analog Output Channel # 0 to 5 V causing the time/date generator to start. The program simultaneously begins to acquire and save load data to the specified file. Following the test, the voltage on Output Channel # 0 is reset to 0 V.

A second LabView program, Mod_Digital4201.vi, allows the user to save images for the optical strain measurement directly on the computer, eliminating the need for the VCR. This program triggers in the same way once the Position output from the mechanical tester is > 0 V, but it then outputs a digital pulse on Digital Output Channel # 0. This digital pulse triggers the HL++ Image program to acquire images at the rate set on its control panel. For this purpose, Digital Output Channel # 0 should be wired to the input wire # 5 on the PC with the HL++ Image software. This method was not used to gather data reported in this thesis.

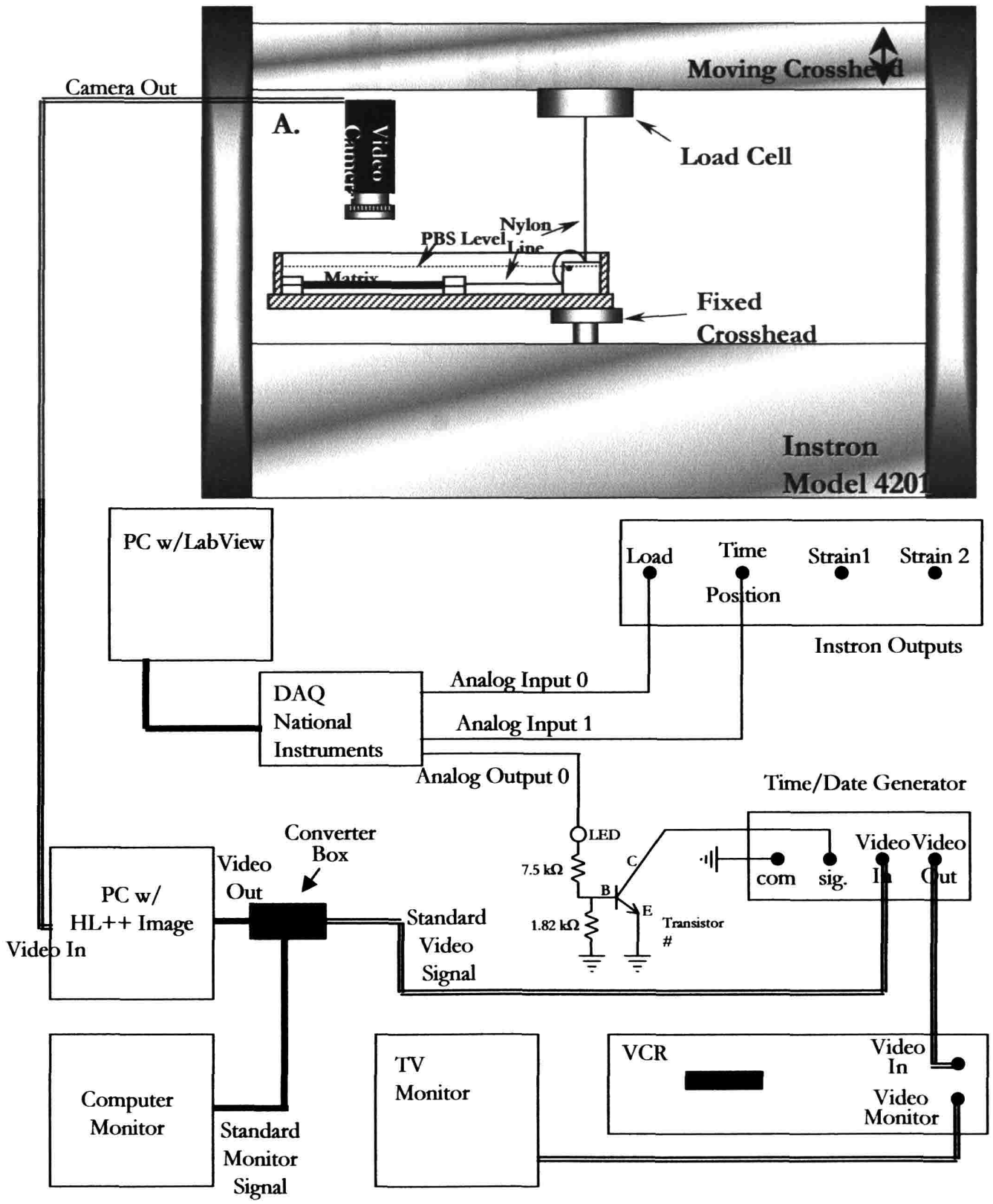
Camera Out
A.
Video Camera
Moving Crosshead
Load Cell
Nylon Line
PBS Level
Matrix
Fixed Crosshead
Instron Model 4201
PC w/LabView
Load
Time
Position
Strain1
Strain 2
Instron Outputs
DAQ National Instruments
Analog Input 0
Analog Input 1
Analog Output 0
Time/Date Generator
LED
7.5 kΩ
C
B
E
1.82 kΩ
Transistor #
com
sig.
Video In
Video Out
Converter Box
PC w/ HL++ Image
Video In
Video Out
Standard Video Signal
Computer Monitor
Standard Monitor Signal
TV Monitor
VCR
Video In
Video Monitor
22 gage wire
BNC cable

Front Panel

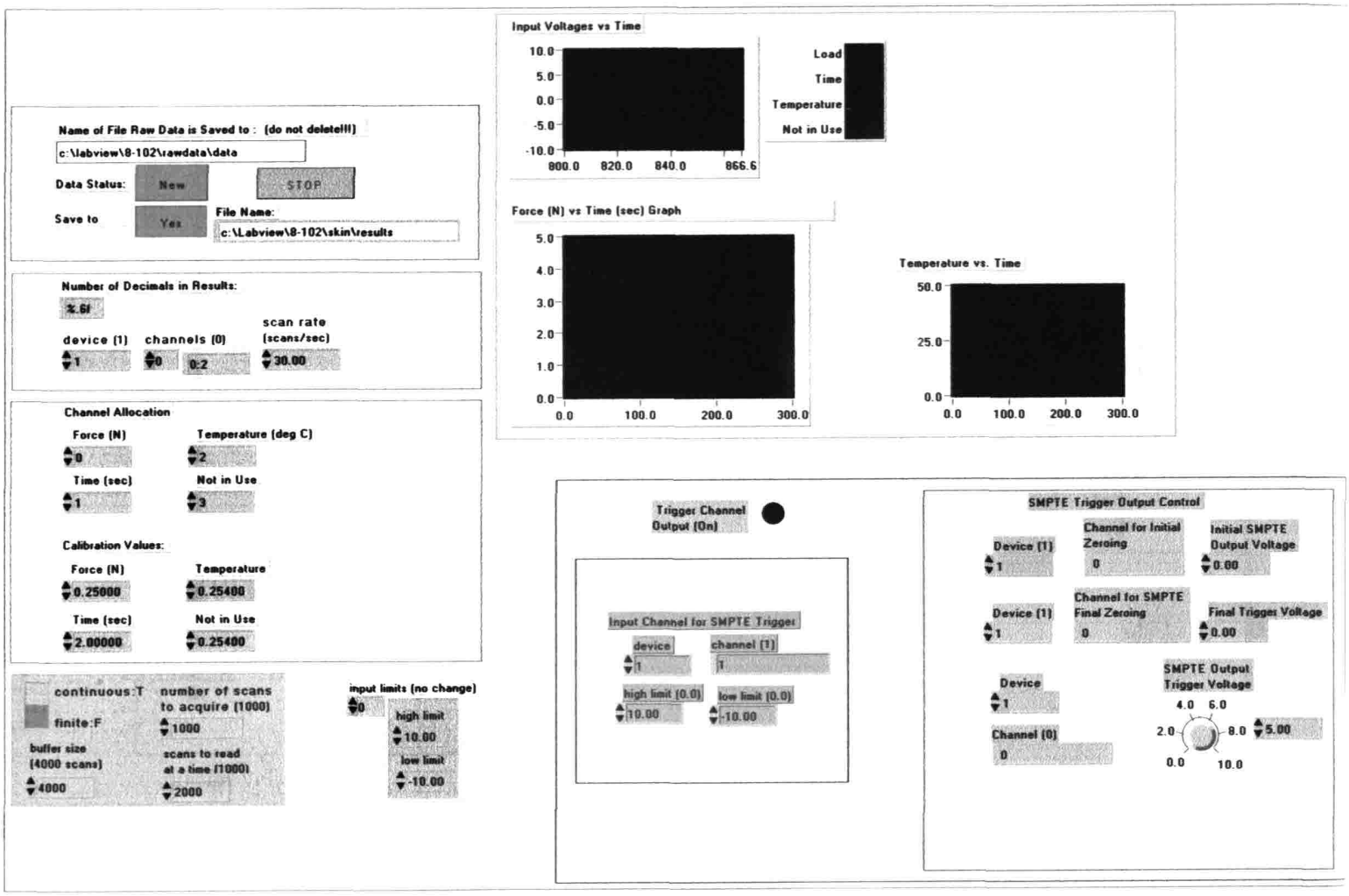
Input Voltages vs Time
10.0
5.0
0.0
-5.0
-10.0
800.0
820.0
840.0
866.6
Load
Time
Temperature
Not in Use
Force (N) vs Time (sec) Graph
5.0
4.0
3.0
2.0
1.0
0.0
0.0
100.0
200.0
300.0
Temperature vs. Time
50.0
25.0
0.0
0.0
100.0
200.0
300.0
Name of File Raw Data is Saved to : (do not delete!!!)
c:\labview\8-102\rawdata\data
Data Status:
New
STOP
Save to
Yes
File Name:
c:\Labview\8-102\skin\results
Number of Decimals in Results:
%.6f
device (1)
1
channels (0)
0
0:2
scan rate (scans/sec)
30.00
Channel Allocation
Force (N)
0
Temperature (deg C)
2
Time (sec)
1
Not in Use
3
Calibration Values:
Force (N)
0.25000
Temperature
0.25400
Time (sec)
2.00000
Not in Use
0.25400
continuous:T
finite:F
buffer size (4000 scans)
4000
number of scans to acquire (1000)
1000
scans to read at a time (1000)
2000
input limits (no change)
0
high limit
10.00
low limit
-10.00
Trigger Channel Output (On)
Input Channel for SMPTE Trigger
device
1
channel (1)
1
high limit (0.0)
10.00
low limit (0.0)
-10.00
SMPTE Trigger Output Control
Device (1)
1
Channel for Initial Zeroing
0
Initial SMPTE Output Voltage
0.00
Device (1)
1
Channel for SMPTE Final Zeroing
0
Final Trigger Voltage
0.00
Device
1
Channel (0)
0
SMPTE Output Trigger Voltage
4.0
6.0
2.0
8.0
0.0
10.0
5.00

Block Diagram

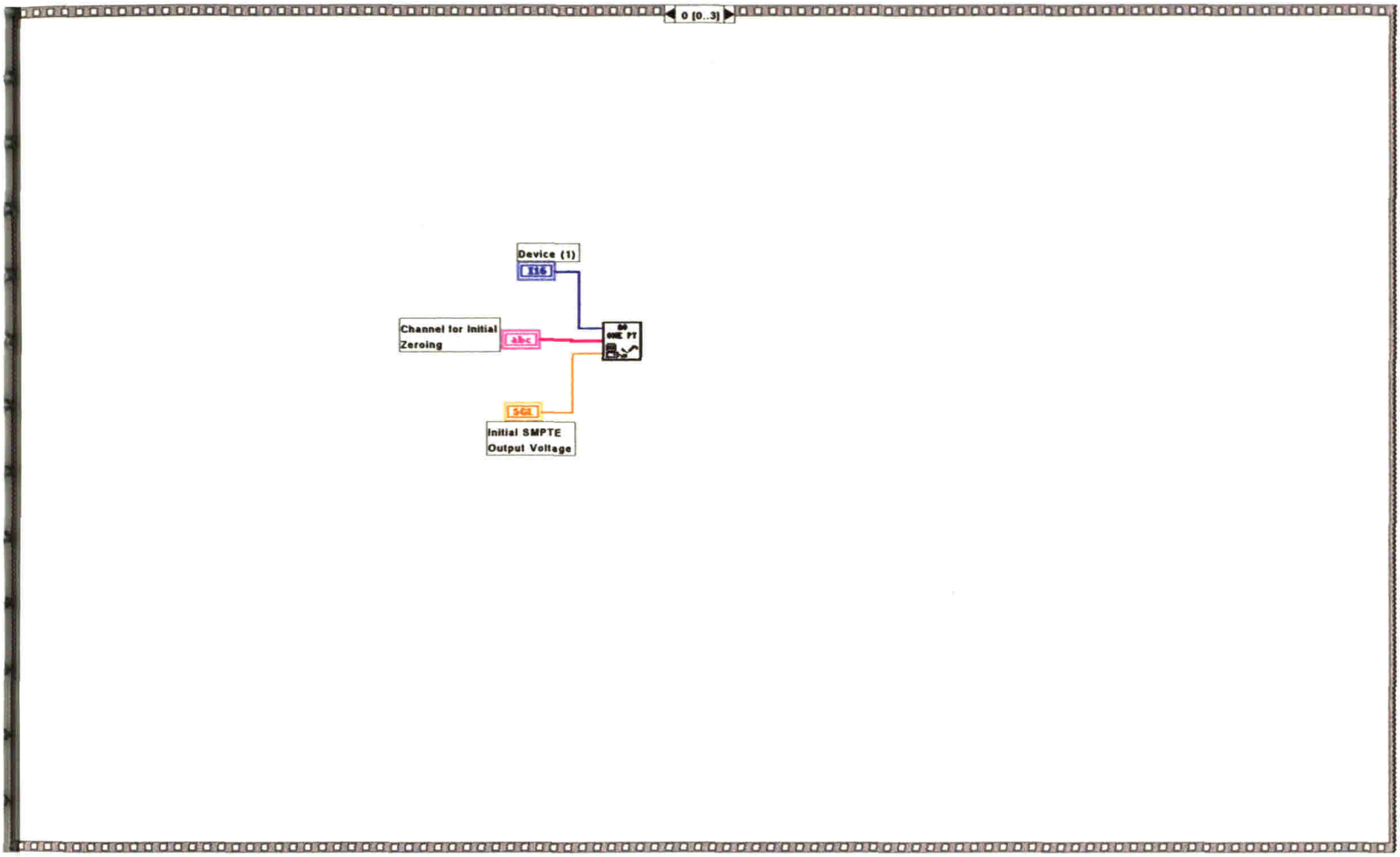

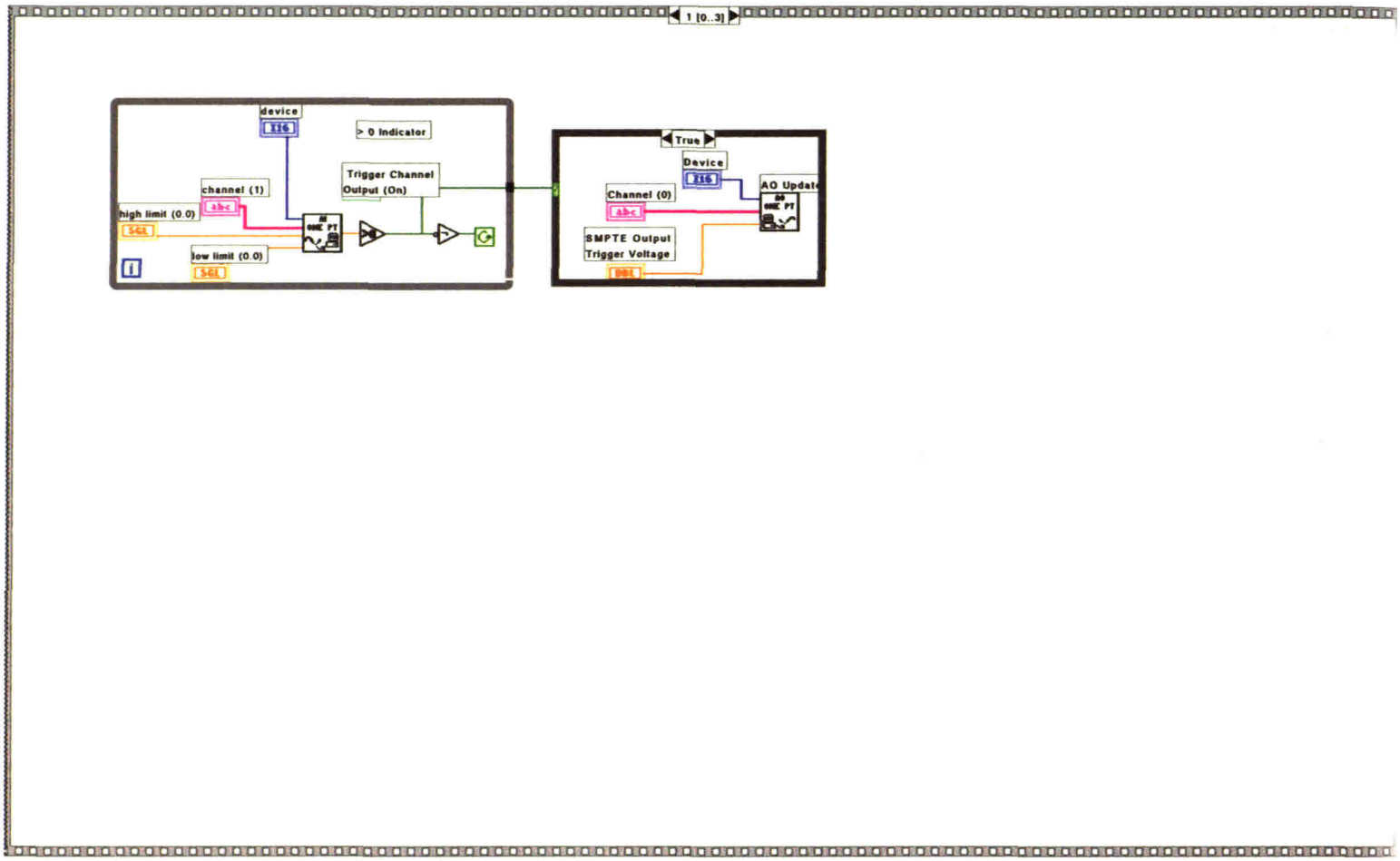
1 [0..3]
device
I16
> 0 Indicator
Trigger Channel
Output (On)
channel (1)
abc
high limit (0.0)
SGL
low limit (0.0)
SGL
i
True
Device
I16
Channel (0)
abc
SMPTE Output
Trigger Voltage
DBL
AO Update
DAQmx PT

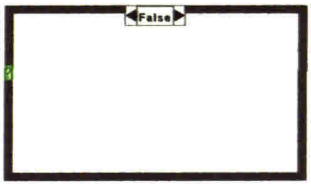
False

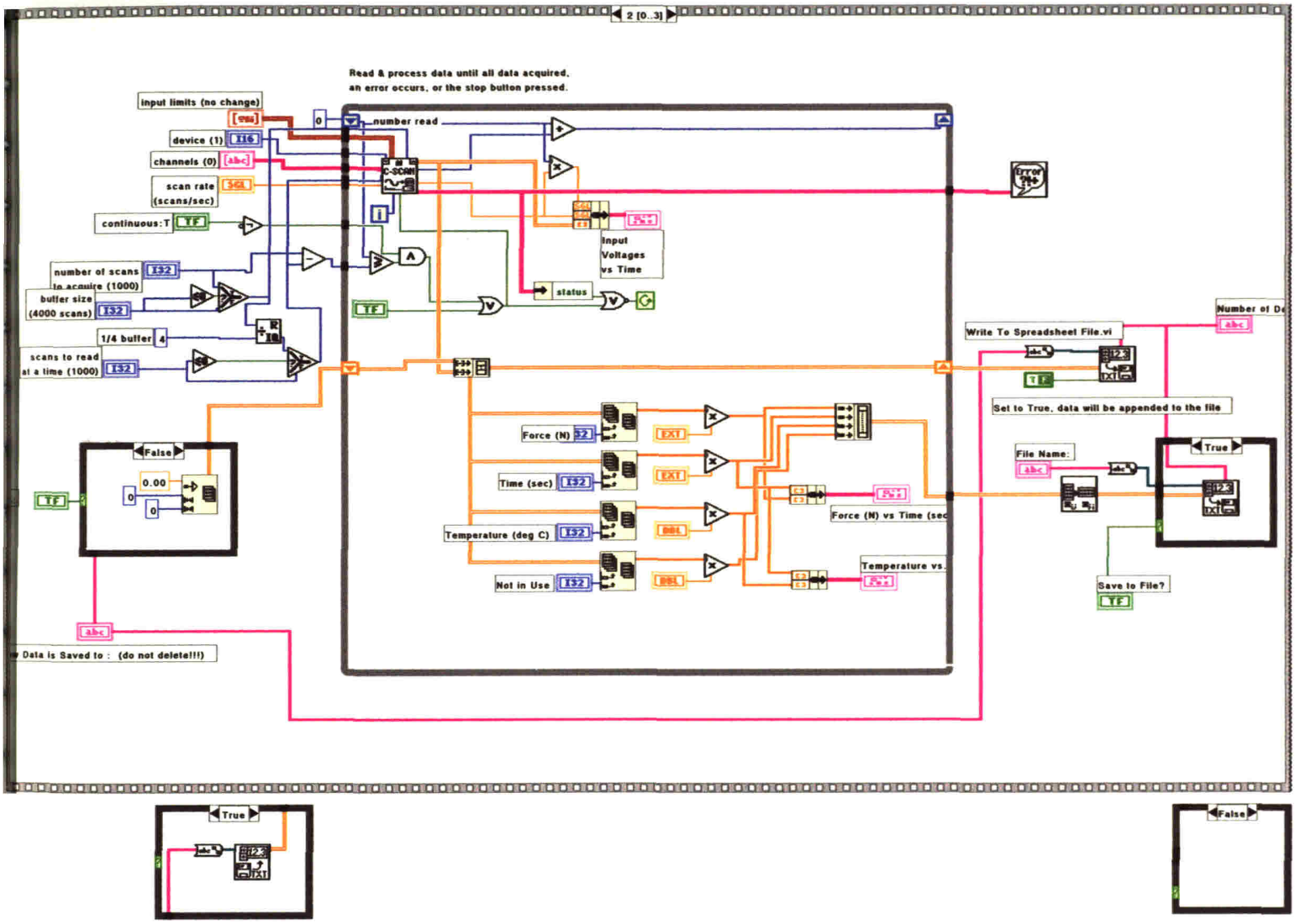
2 [0..3]
Read & process data until all data acquired,
an error occurs, or the stop button pressed.
input limits (no change)
device (1)
channels (0)
scan rate (scans/sec)
continuous:T
number of scans to acquire (1000)
buffer size (4000 scans)
1/4 buffer
scans to read at a time (1000)
number read
C-SCAN
Input Voltages vs Time
status
Force (N)
Time (sec)
Temperature (deg C)
Not in Use
Force (N) vs Time (sec
Temperature vs.
Write To Spreadsheet File.vi
Set to True, data will be appended to the file
File Name:
Save to File?
Number of D
False
0.00
Data is Saved to : (do not delete!!!)
True
True
False

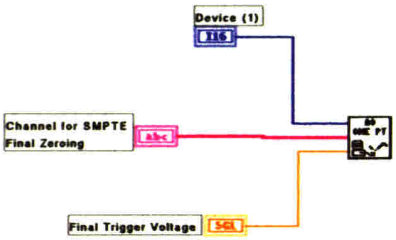
3 [0..3]
Device (1)
Channel for SMPTE Final Zeroing
Final Trigger Voltage

Front Panel

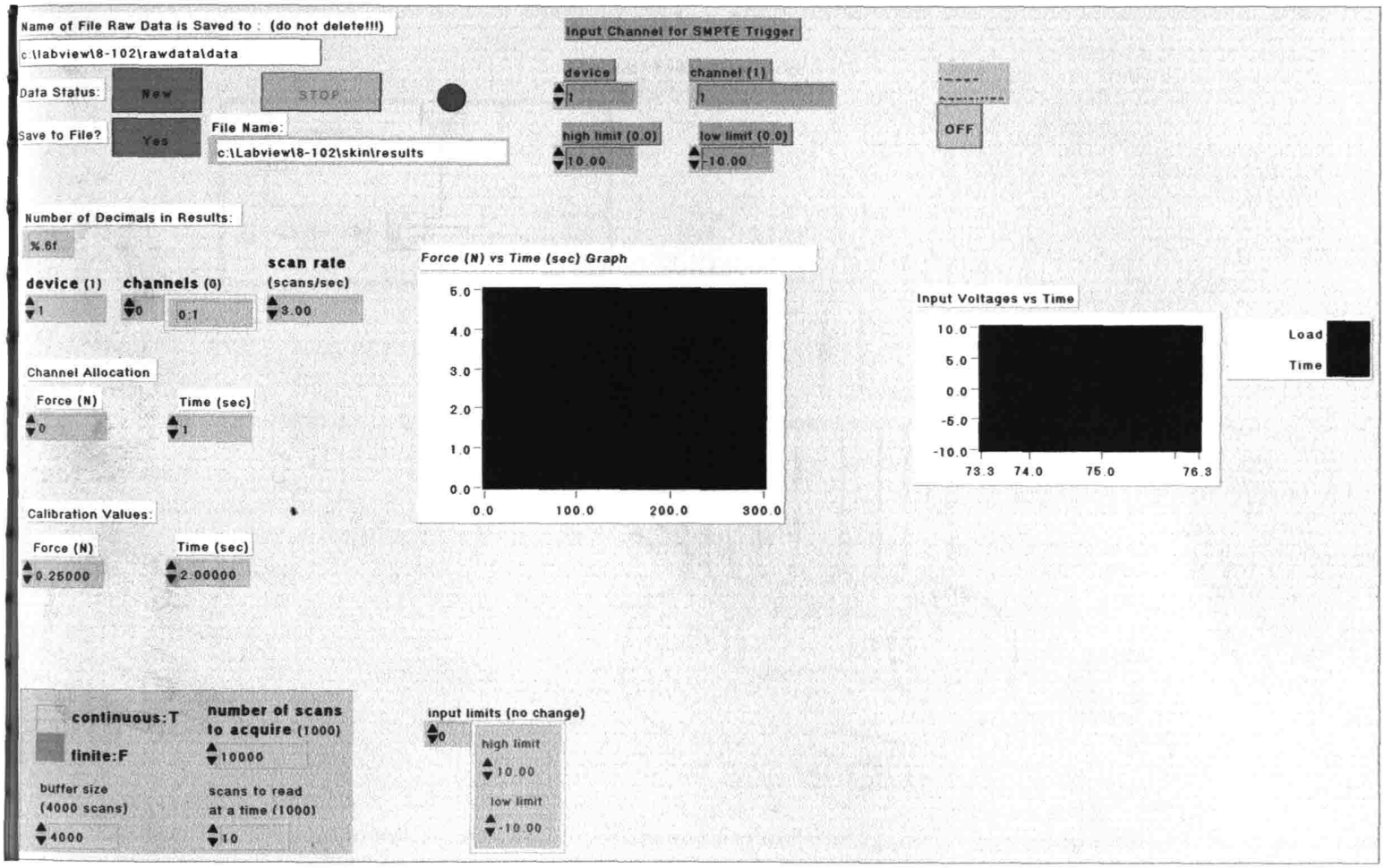
Name of File Raw Data is Saved to : (do not delete!!!)
c:\labview\8-102\rawdata\data
Data Status:
New
STOP
Save to File?
Yes
File Name:
c:\Labview\8-102\skin\results
Input Channel for SMPTE Trigger
device
channel (1)
high limit (0.0)
low limit (0.0)
10.00
-10.00
OFF
Number of Decimals in Results:
%.6f
device (1)
channels (0)
0:1
scan rate (scans/sec)
3.00
Channel Allocation
Force (N)
Time (sec)
Force (N) vs Time (sec) Graph
5.0
4.0
3.0
2.0
1.0
0.0
0.0
100.0
200.0
300.0
Input Voltages vs Time
10.0
5.0
0.0
-5.0
-10.0
73.3
74.0
75.0
76.3
Load
Time
Calibration Values:
Force (N)
0.25000
Time (sec)
2.00000
continuous:T
finite:F
number of scans to acquire (1000)
10000
buffer size (4000 scans)
4000
scans to read at a time (1000)
10
input limits (no change)
high limit
10.00
low limit
-10.00

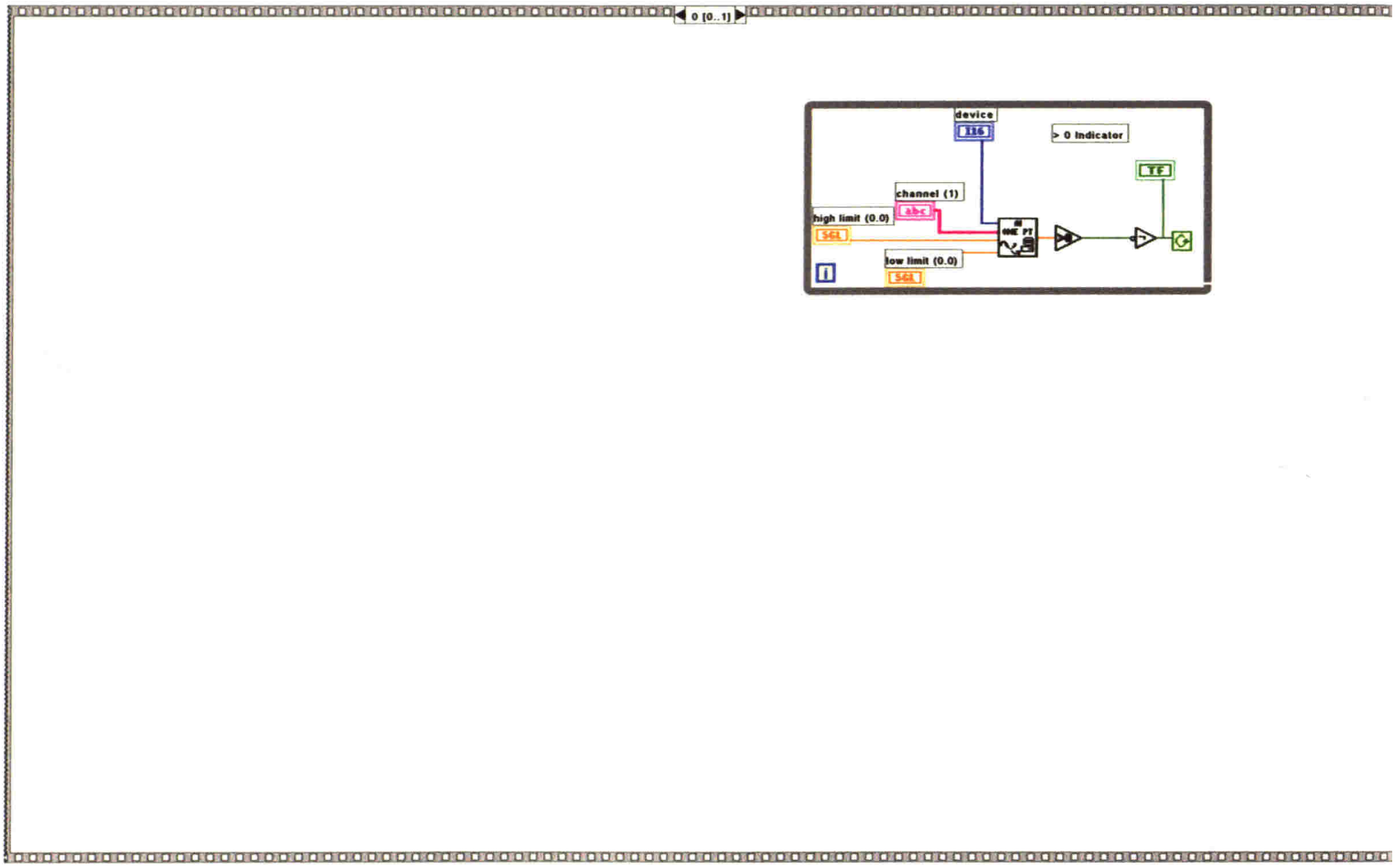
0 [0..1]
device
I16
> 0 Indicator
TF
channel (1)
high limit (0.0)
SGL
low limit (0.0)
SGL
i

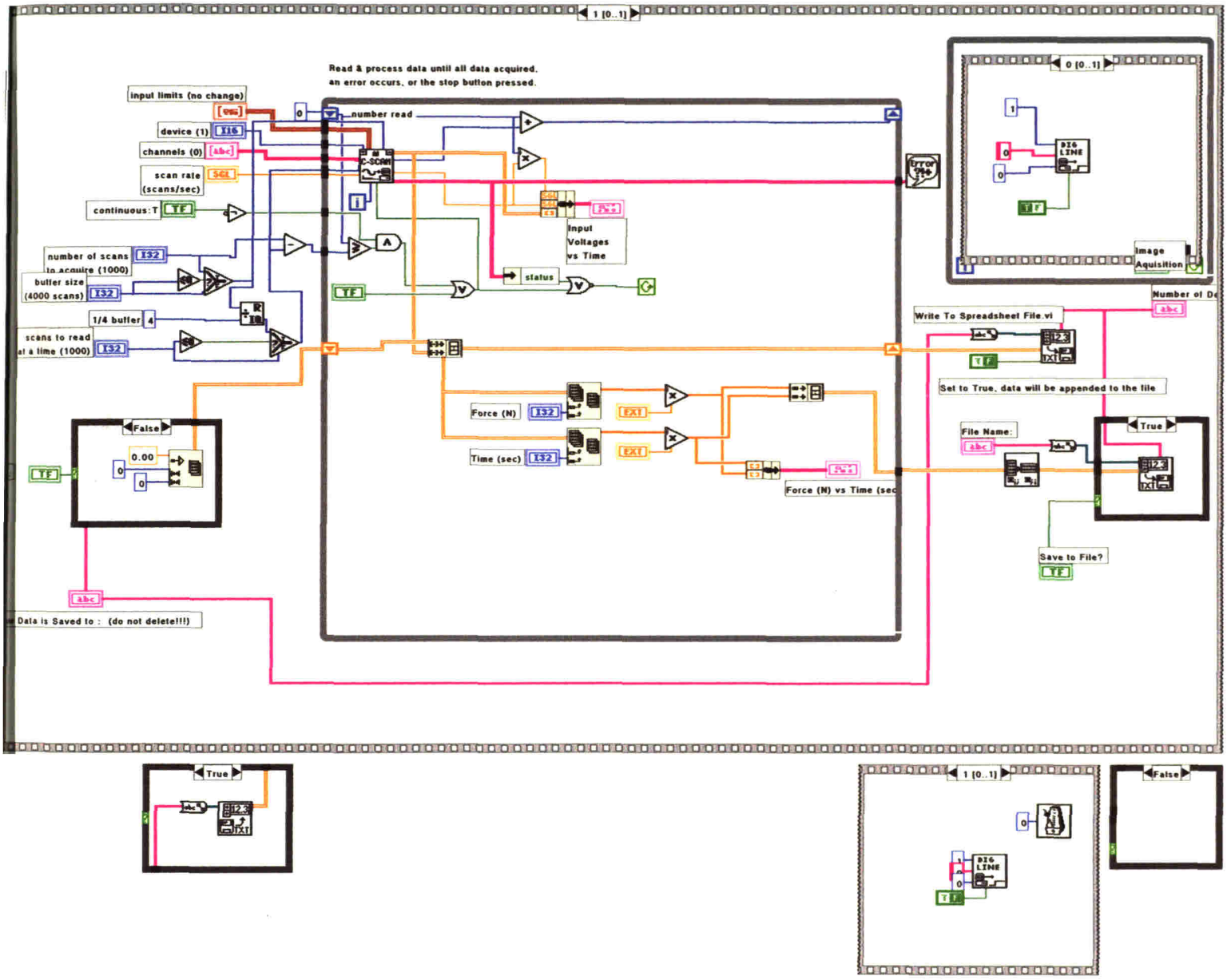
Read & process data until all data acquired,
an error occurs, or the stop button pressed.
input limits (no change)
device (1)
channels (0)
scan rate (scans/sec)
continuous:T
number of scans to acquire (1000)
buffer size (4000 scans)
1/4 buffer
scans to read at a time (1000)
number read
C-Series
Input Voltages vs Time
status
Force (N)
Time (sec)
Force (N) vs Time (sec
Error
0 [0..1]
DIG LINE
Image Aquisition
Number of D
Write To Spreadsheet File.vi
Set to True, data will be appended to the file
File Name:
True
False
Save to File?
Data is Saved to : (do not delete!!!)
1 [0..1]

C.2 Compression Testing Protocol

Sample Preparation

1. Using a micrometer set to 13 mm cut out strips of matrix using a razor blade. Always cut the matrix by pushing straight down, do not slice or saw the matrix.

2. Once the sample is cut, check to make sure the edges are parallel. If not, discard and cut another piece.

3. Set the micrometer to 5 mm and cut pieces off of the 13 mm wide strip. Use the micrometer to check the dimensions and whether the edges are parallel. Measure the thickness of each sample. If sample dimensions are not 13 x 5 mm with parallel edges discard.

4. Place samples on PBS. After a few minutes the samples will be pulled into the PBS and will be fully hydrated. Do not force the samples under the surface of the PBS. This will result in trapped air bubbles.

Mechanical Testing

1. Turn on the PC and proximity sensor power supply. Load the LabView program CompressionTest2.vi.

2. Setup the CFM as shown in Fig. (2.5).

3. Execute the LabView program and press the green button labeled 'Initial Point' so that the voltage for a free beam is acquired.

4. Position the beam just above the bottom of the petri dish and place the sample between the adjustable horizontal stage and the beam end.

5. Adjust the level of PBS such that the matrix sample is just barely floating over the bottom of the petri dish.

6. Advance the adjustable horizontal stage so that the matrix sample is touching the beam evenly across the entire 13 mm edge.

7. Press the green button labeled 'Second Point' to acquire another data point.

8. Advance the stage in increments of 0.2 mm and acquire additional data points by pressing the appropriate button on the LabView program after each stage advance.

Labview code for CompressionTest2.vi

This program allows the user to data points for the purpose of testing the compressive stiffness of the collagen-GAG matrix. Upon execution, the program waits to gather data until the user clicks on the green 'Go' buttons, sequentially. After clicking on each button the program waits the amount of time specified in the 'Time to Wait for Visco Response' text box and then gathers data at a rate of 1 per second for the amount of time specified in the text box labeled 'Time to Gather Data' and averages those data to produce one data point. The average voltage is displayed in the red text box to the right of each button. These average values are saved along with the displacement values set in the boxes on the left-hand side of the screen to the data file specified.

Connector Pane

CompressionTest2.vi

Front Panel

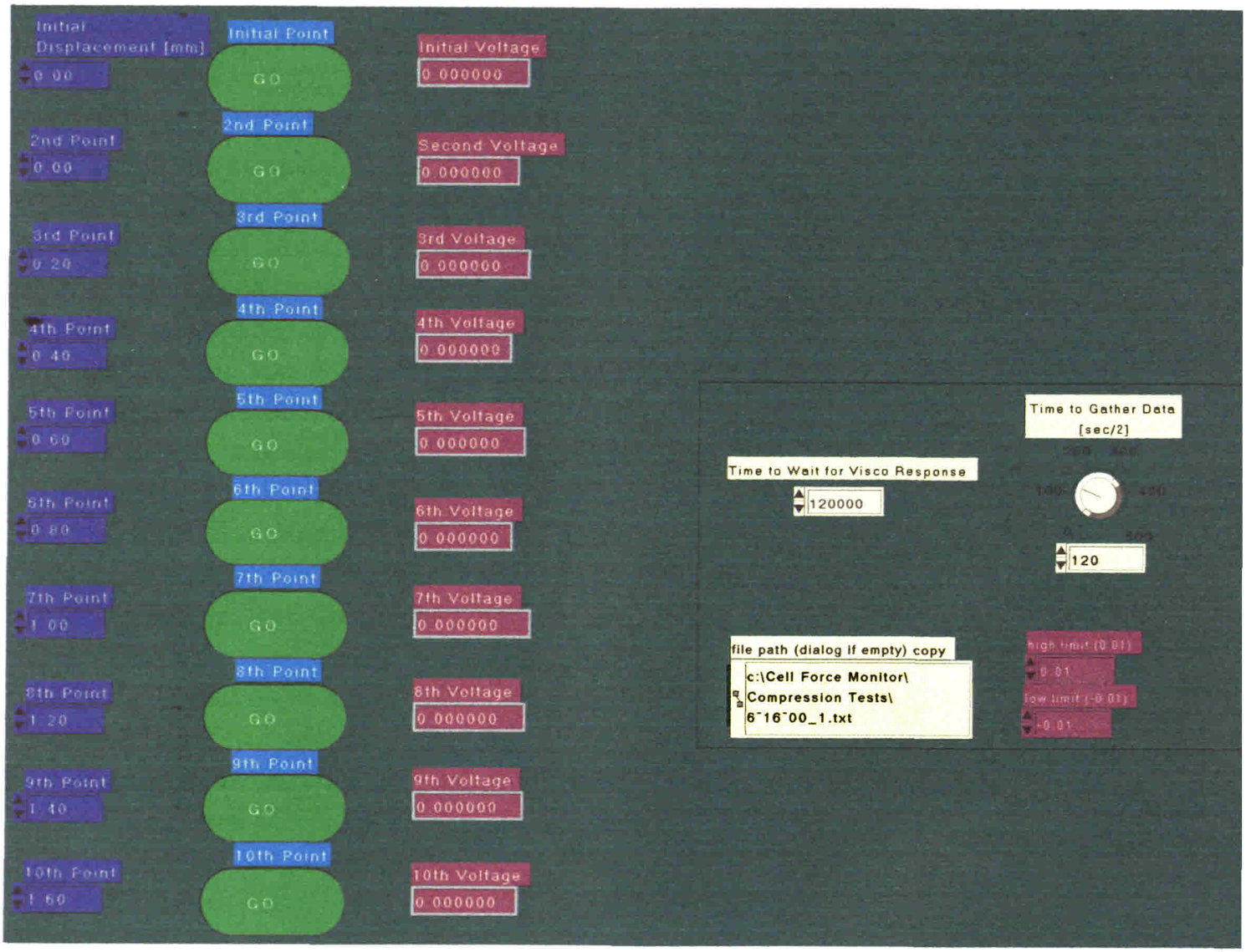

Block Diagram

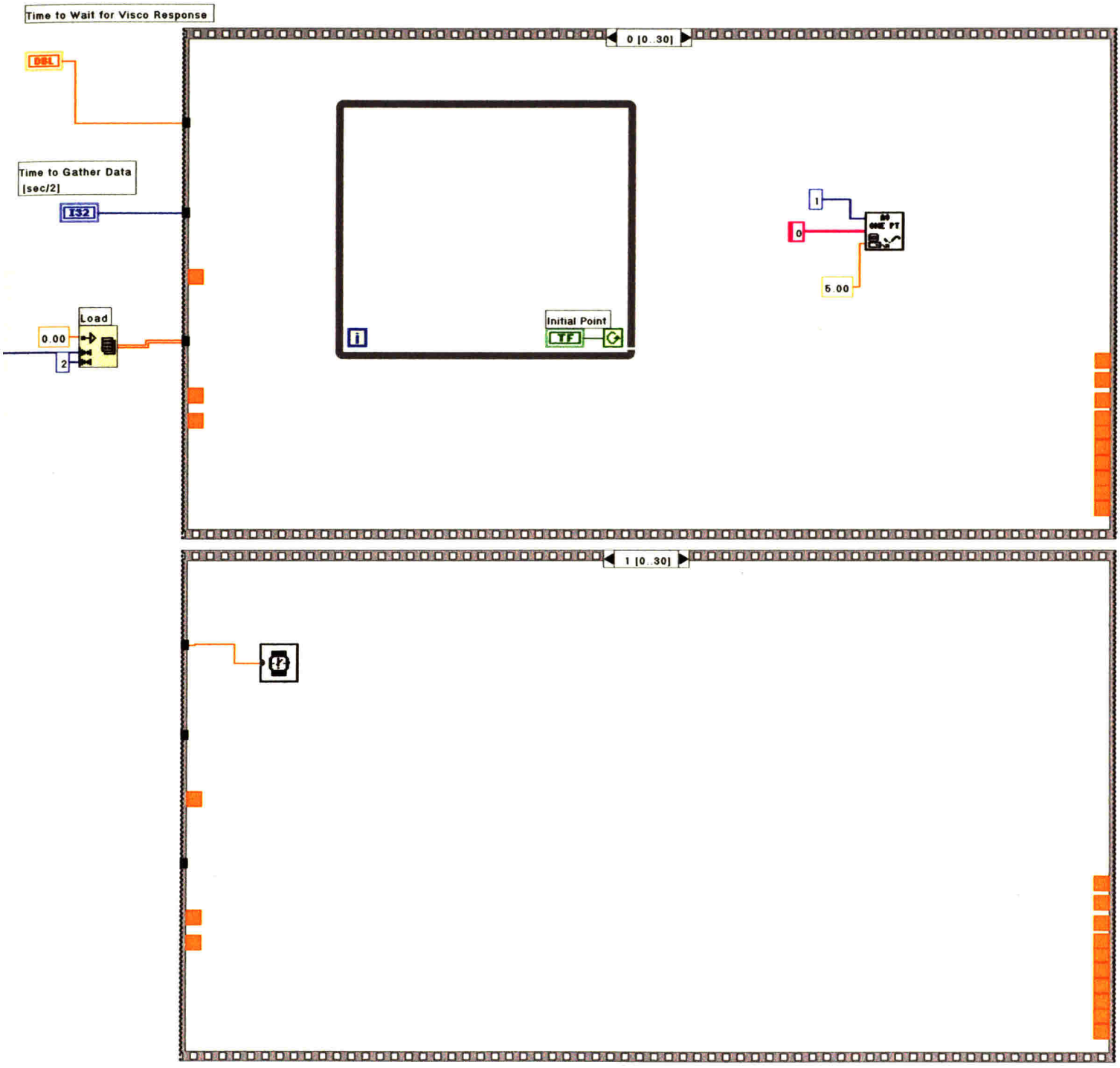

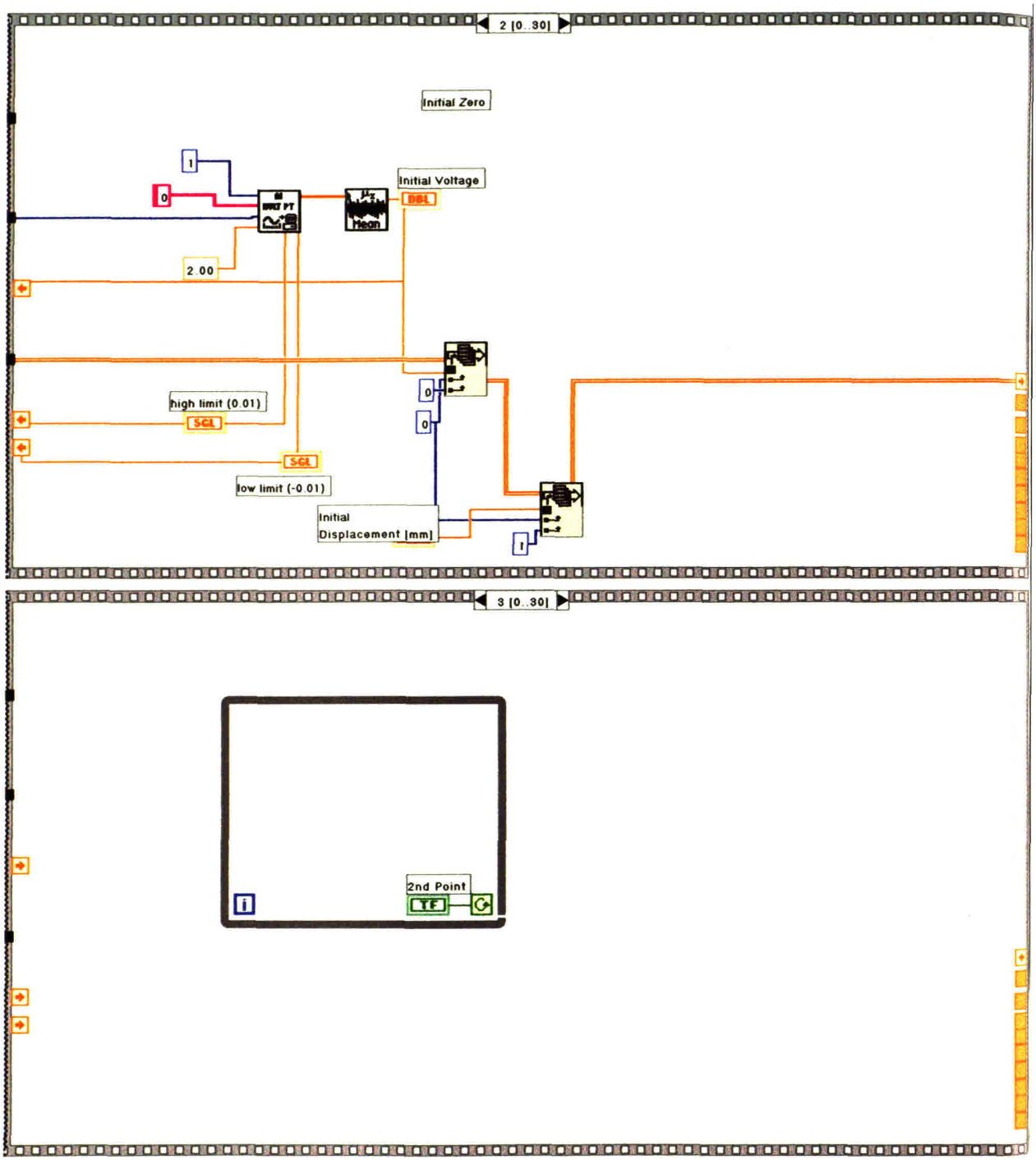
2 [0..30]
Initial Zero
1
0
Initial Voltage
DBL
2.00
high limit (0.01)
SGL
SGL
low limit (-0.01)
0
0
Initial
Displacement [mm]
1
3 [0..30]
i
2nd Point
TF

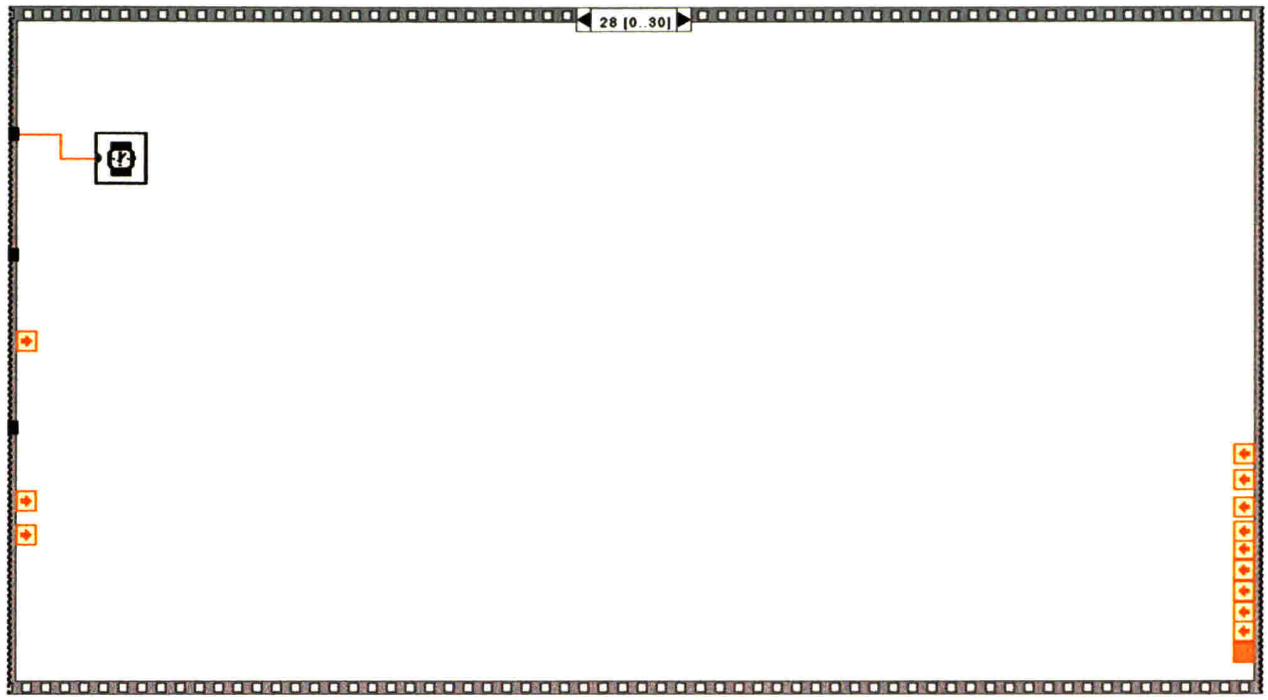
28 [0..30]

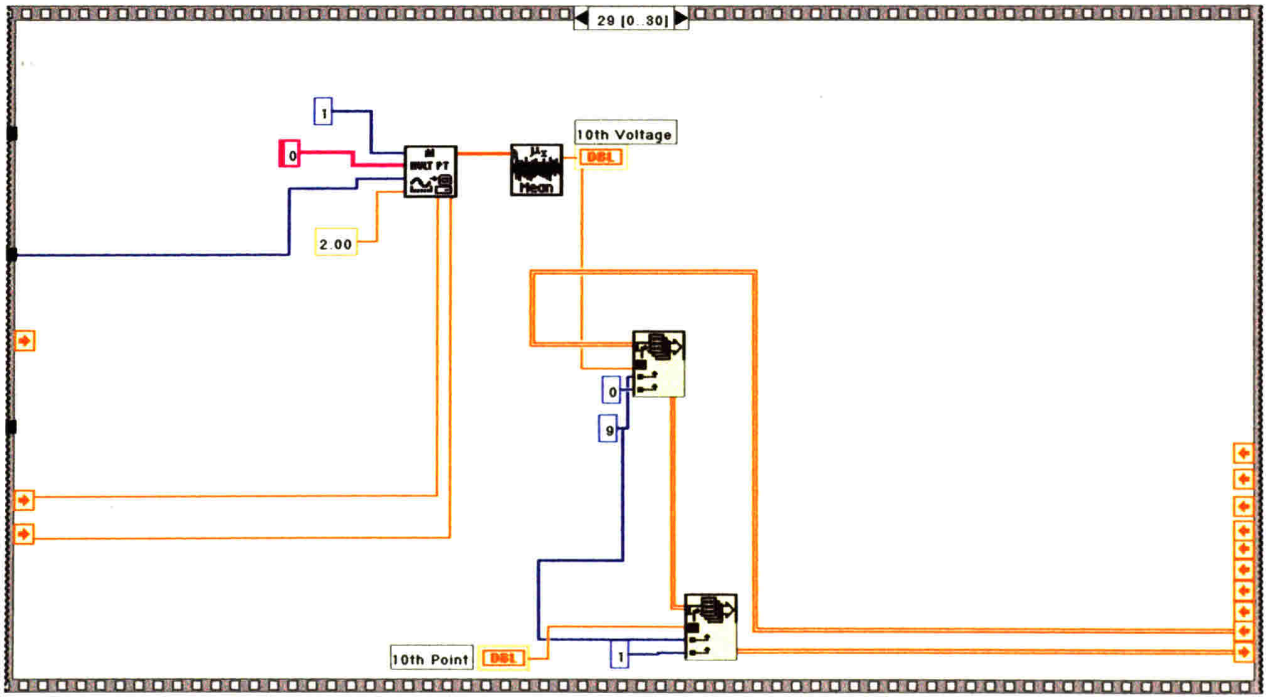
29 [0..30]
1
0
2.00
10th Voltage
DBL
0
9
10th Point
DBL
1


30 [0..30]
Initial Voltage
file path (dialog if empty) copy
%.7f

Appendix D. Pore Diameter Determination

D.1 Type-I Collagen Immunohistochemical Staining Protocol

Solutions:
Phosphate Buffered Saline 10 mM (P-3813, Sigma Chemical Co., St. Louis, MO)

TRIZMA Base (pH ~ 9.0) (SigmaUltra T-6791, Sigma)
100 mM concentration TRIZMA Base, 1.21 g
dH_2O, 100 ml

Goat Serum (G-9023, Sigma)
Freeze in 100 µl aliquots.
1:10 concentration goat serum, 100 µl
PBS, 900 µl

Primary Antibody Monoclonal Anti-Collagen Type-I (C-2456, Sigma)
Freeze in 10 µl aliquots.
1:200 concentration Primary antibody, 10 µl
PBS, 2 ml

Secondary Antibody Anti-Mouse IgG (whole molecule) FITC conjugate (F-9006, Sigma)
Freeze in 10 µl aliquots.
1:50 concentration Secondary antibody, 10 µl
PBS, 490 µl

Staining Procedure:
1. Cut out samples of the collagen-GAG matrix (~ 1 mm x 1 mm) using a razor blade.

2. Rehydrate matrix samples in siliconized microcentrifuge tubes (0.5 ml) for 1 m in 70% EtOH. Rinse for 1 m in PBS (x2).

3. Soak in PBS for at least 5 m.

4. Soak in 200 µl of goat serum for 30 m. Shake tubes at 0, 15, and 28 m.

5. Place samples in primary antibody for 30 m. Shake tubes at 0, 15, and 28 m.

6. Rinse samples in PBS 5 m. Shake at 0 and 5 m.

7. Place in secondary antibody for 30 m. Shake tubes at 0, 15, and 28 m.

8. Rinse in PBS for 5 m (x2)

9. Rinse in TRIZMA base solution for 5 m (x2). Store at 4°C in TRIZMA solution.

D.2 Image Capture and Analysis Protocol

Equipment:
confocal fluorescent microscope (Whitehead Institute Microscopy Facility)
3 mm thick microscope slide with well (Erie, Cat. #48327-000, VWR, Bridgeport, NJ)
transfer pipette
stained matrix samples

Solutions:
TRIZMA Base (pH ~ 9.0) (SigmaUltra T-6791, Sigma)
100 mM concentration TRIZMA Base, 1.21 g
dH_2O, 100 ml

1. Fill the well of extra thick microscope slide with well with TRIZMA buffer.

2. Place immunostained matrix sample into the well. Add buffer so that the sample is floating/supported by the liquid.

3. Set the confocal fluorescent microscope to image FITC stained samples. (Proper filter and laser settings).

4. Acquire images according to the current protocol available for the microscope (Whitehead facility)

5. Open images with Scion Image (BIORAD macro may be necessary depending on the version of Scion Image, available from www.nih.gov)

6. Select 'Options'; 'Threshold'; Slide red region on LUT to optimize the selection of matrix struts without selecting pore space.

7. Select 'Process'; 'Binary'; 'Make Binary'; The pixels will then be assigned to black or white.

8. Edit the image using the paintbrush tool. Make sure to only edit using pure black or white. Corrections should be made so that pores and pore walls are at least 2 pixels wide. Any speckled areas inside pores or pore walls should be corrected as well.

9. Using the circular selection tool, select a circular region including as many pores as possible.

10. Load Linear Intercept Macros

11. Execute the 'Linear Intercept' macro; this macro will produce a table of linear intercept values, in pixels, for each theta value. If intercept values in metric units are preferred, calibrate Scion Image by measuring a known distance in an image taken under the same

conditions. Select 'Analyze'; 'Set Scale'; and enter the appropriate conversion from pixels to metric units, before executing the macro.

12. Click on the Measurements window and save under an appropriate file name.

13. Execute the 'Plot Intercepts' macro to show the best fit ellipse and the constants C0, C1, and C2 which define the ellipse (see macro below for equation).

14. The major and minor axes can be determine for each image using either the table of measurements, or the constants.

D.3 Linear Intercept Macro Code

```
macro 'Linear Intercept'   (Adapted from Simone)
{This macro measures the linear intercept distance over a given ROI
at intervals of angle "ThetaStep"}
var
 left,top,width,height,MinDim,nx,ny,i,j,k:integer;
                ThetaStep,NSteps,PI,x1,x2,y1,y2,dy,dx:real;
 Theta,valx,valy,plength,scale,AspectRatio:real;
  IntLength,LineSum,dummy:real;
 Intercepts:integer;
  switch,indicator:boolean;
  unit:string;
begin
  SetOptions('User1;User2');
  GetRoi(left,top,width,height);
  if width=0 then begin
    PutMessage('Selection required.');
    exit;
  end;
  if width<height  then MinDim:=width
    else MinDim:=height;
  PI:=3.141592654;
  GetScale(scale,unit,AspectRatio);
  NSteps:=18;{GetNumber('Enter # steps between 0 and 90 deg.',3,0);}
  ThetaStep:=PI/(2*NSteps);

{block out next line when doing cumulative measurements}

  SetCounter(2*NSteps);
  SetUser1Label('Theta(rad)');
  SetUser2Label('Lx10^3');
  for j:=0 to 2*NSteps-1 do begin
    LineSum:=0;
    Intercepts:=0;
    x1:=left;
    y1:=top;
    Theta:=j*ThetaStep;
   nx:=10*sin(Theta)*width/height;
   ny:=10*abs(cos(Theta));
    for i:=0 to nx do begin
     if Theta=0 then begin
              x1:=left;
              x2:=x1+width;
     end  else begin
              x1:=left+(width*i/(nx+1))+width/(2*(nx+1));
              x2:=x1+(height*cos(Theta)/sin(Theta));
```

```
          end;
    y2:=top+height;
    if x2>=left+width then begin
       x2:=left+width;
       y2:=y1+(x2-x1)*sin(Theta)/cos(Theta);
    end  else if x2<left then begin
                    x2:=left;
                   if Theta>PI/2 then   y2:=y1+(x2-x1)*sin(Theta)/cos(Theta);
                  end;
     {plength is the length of the line to be drawn in pixels}
     plength:=sqrt(sqr(x2-x1)+sqr((y2-y1)/AspectRatio));
     valx:=x1;
     valy:=y1;
    dx:=(x2-x1)/plength;
    dy:=(y2-y1)/plength;
    switch:=true;
    if plength>=MinDim then begin
    LineSum:=LineSum+(plength/scale);
     for k:=0 to plength do begin
         if GetPixel(x1+k*dx,y1+k*dy)>0
             then indicator:=true
             else indicator:=false;
         if (switch=true) and (indicator=true) then begin
            Intercepts:=Intercepts+1;
            switch:=false;
         end;
         if  (indicator=false) then switch:=true;
       end;
   end;
 end;
for i:=1 to ny do begin
    if Theta<=PI/2 then begin
            x1:=left;
            x2:=left+width
      end  else begin
            x1:=left+width;
            x2:=left;
      end;
    y1:=top+height*i/(ny+1);
    y2:=y1+(width*sin(Theta)/abs(cos(Theta)));
     if y2>top+height then begin
       y2:=top+height;
       x2:=x1+((y2-y1)*cos(Theta)/sin(Theta));
     end;
     {plength is the length of the line to be drawn in pixels}
      plength:=sqrt(sqr(x2-x1)+sqr((y2-y1)/AspectRatio));
    valx:=x1;
     valy:=y1;
```

```
      dx:=(x2-x1)/plength;
      dy:=(y2-y1)/plength;
      switch:=true;
      if plength>=MinDim then begin
      LineSum:=LineSum+(plength/scale);
      for k:=0 to plength do begin
           if GetPixel(x1+k*dx,y1+k*dy)>0
              then indicator:=true
              else indicator:=false;
           if (switch=true) and (indicator=true) then begin
              Intercepts:=Intercepts+1;
              switch:=false;
           end;
           if  (indicator=false) then switch:=true;
        end;
     end;
    end;{i}
   IntLength:=LineSum/Intercepts;
  dummy:=rUser2[j+1];
   rUser1[j+1]:=180*Theta/PI;

{to do cumulative measurements, type in 'dummy+ before Intlength in the next line}

   rUser2[j+1]:=IntLength*1000;
  end; {j}
  ShowResults;
end;

Macro 'Plot Intercepts'
{This macro plots the linear intercept distance as a function of angle
in cylindrical coordinates
It then finds the best-fit ellipse to a set of linear intercept distance vs. angle data
using multiple linear regression of the equation Y=C0+C1*X+C2*Z, where
Y=1/L^2 ,  where L is one half  the linear intercept distance at Theta
X=cosine(2*Theta),    Z=sine(2*Theta)
C0=(Mii+Mjj)/2 , C1=(Mii-Mjj)/2 , C2=Mij.
The objective is to solve for M11, Mjj, and Mij
The best-fit ellipse it then plotted on top of the linear intercept measurements}

var
  left,top,width,height,X0,Y0,X1,Y1,i,n:integer;
  pscale,aspectRatio,dx1,dx2,dy1,dy2,maxdim:real;
  unit:string;
 sumX,sumY,sumZ,sumXZ,sumXY,sumYZ,sumZsqr,sumXsqr:real;
 C0,C1,C2,Mii,Mjj,Mij,Y,X,Z,PI,Theta1,Theta2,L1,L2:real;

begin
 PI:=3.141592654;
```

```
SaveState;
 SetForegroundColor(255);
 SetBackgroundColor(0);
 width:=400;
 height:=400;
 maxdim:=0;
 for i:=1 to rCount do begin
   if rUser2[i]>maxdim then maxdim:=rUser2[i];
 end;
 pscale:=.8*(width+height)/(2*maxdim);
 SetNewSize(width,height);
 MakeNewWindow('Linear Intercepts vs. Theta');
 SetLineWidth(1);
 X0:=(width/2);
 Y0:=(height/2);
 MakeLineROI(0,Y0,width,Y0);
 Fill;
 MakeLineROI(X0,0,X0,height);
 Fill;
  for i:=1 to rCount do begin
   dx1:=pscale*0.5*rUser2[i]*cos(rUser1[i]*PI/180);
   dy1:=pscale*0.5*rUser2[i]*sin(rUser1[i]*PI/180);
   if i<rCount then begin
     dx2:=pscale*0.5*rUser2[i+1]*cos(rUser1[i+1]*PI/180);
     dy2:=pscale*0.5*rUser2[i+1]*sin(rUser1[i+1]*PI/180);
   end else begin
     dx2:=-pscale*0.5*rUser2[1]*cos(rUser1[1]*PI/180);
     dy2:=-pscale*0.5*rUser2[1]*sin(rUser1[1]*PI/180);
   end;
   MoveTo(X0+dx1,Y0+dy1);
   LineTo(X0+dx2,Y0+dy2);
   MoveTo(X0-dx1,Y0-dy1);
   LineTo(X0-dx2,Y0-dy2);
 end;
 n:=rCount;
 sumX:=0;
 sumY:=0;
 sumZ:=0;
 sumXY:=0;
 sumYZ:=0;
 sumXZ:=0;
 sumZsqr:=0;
 sumXsqr:=0;
 for i:=1 to n do begin
   Y:=1/(sqr(rUser2[i]/2));
   X:=cos(2*PI*rUser1[i]/180);
   Z:=sin(2*PI*rUser1[i]/180);
   sumX:=sumX+X;
```

```
    sumY:=sumY+Y;
    sumZ:=sumZ+Z;
    sumXY:=sumXY+(X*Y);
    sumYZ:=sumYZ+(Y*Z);
    sumXZ:=sumXZ+(X*Z);
    sumZsqr:=sumZsqr+sqr(Z);
    sumXsqr:=sumXsqr+sqr(X);
  end;
  C1:=((sumXY*sumZsqr)-(sumXZ*sumYZ))/((sumXsqr*sumZsqr)-sqr(sumXZ));
  C2:=((sumYZ*sumXsqr)-(sumXY*sumXZ))/((sumXsqr*sumZsqr)-sqr(sumXZ));
  C0:=(sumY/n)-C1*(sumX/n)-C2*(sumZ/n);
NewTextWindow('Results');
writeln('C0 = ',C0);
writeln('C1 = ',C1);
writeln('C2 = ',C2);

  for i:=1 to rCount do begin
    Theta1:=rUser1[i]*PI/180;
    if i<rCount then Theta2:=rUser1[i+1]*PI/180
     else Theta2:=rUser1[1]*PI/180;
    L1:=1/sqrt(C0+C1*cos(2*Theta1)+C2*sin(2*Theta1));
    L2:=1/sqrt(C0+C1*cos(2*Theta2)+C2*sin(2*Theta2));
    dx1:=pscale*L1*cos(Theta1);
    dy1:=pscale*L1*sin(Theta1);
    if i<rCount then begin
      dx2:=pscale*L2*cos(Theta2);
      dy2:=pscale*L2*sin(Theta2);
     end else begin
      dx2:=-pscale*L2*cos(Theta2);
      dy2:=-pscale*L2*sin(Theta2);
    end;
    MoveTo(X0+dx1,Y0+dy1);
    LineTo(X0+dx2,Y0+dy2);
    MoveTo(X0-dx1,Y0-dy1);
    LineTo(X0-dx2,Y0-dy2);
  end;
end;
```

Appendix E. Cell Force Monitor

E.1 Construction

Below are the equipment and schematics necessary to build the most recent version of the cell force monitor.

Equipment:

Kaman Instrumentation, Colorado Springs, CO
- KD-2300 1SU Proximity Sensor
- P-3450 6-Channel Power Supply

Edmund Scientific, Barrington, NJ (Cat. # N011A)
- L53-830 12"x12" Bench Plate
- L36-494 1.5" Stainless Steel Mounting Posts
- L53-026 Rotary Mount Assembly
- L38-971 Side Drive Mini 1.25" Square Translation Stage
- L03-650 Adjustable Height Rack and Pinion Post

Goodfellow, Berwyn, PA
- CU070360 98%Cu-2%Be Foil 0.15 mm Thick
- ET303250 UHMW Polyethylene Sheet 5 mm Thick

National Instruments, Austin, TX
- AT-MIO-16XE-50 Multifunction Data Acquisition Card
- SH6868-EP Shielded Cable, 1 m
- SC-2043 SG Strain Gage Accessory

McMaster-Carr Supply, New Brunswick, NJ
- 95868A110 Nylon SHC Screws #4-40, ½" length
- GE 6700 Non-Corrosive Silicone (for silicone well)

Roboz Surgical Instruments, Rockville, MD
- Schwartz Clip (strong angle)

Schematics:

Schematics and mechanical drawings of the CFM components follow.

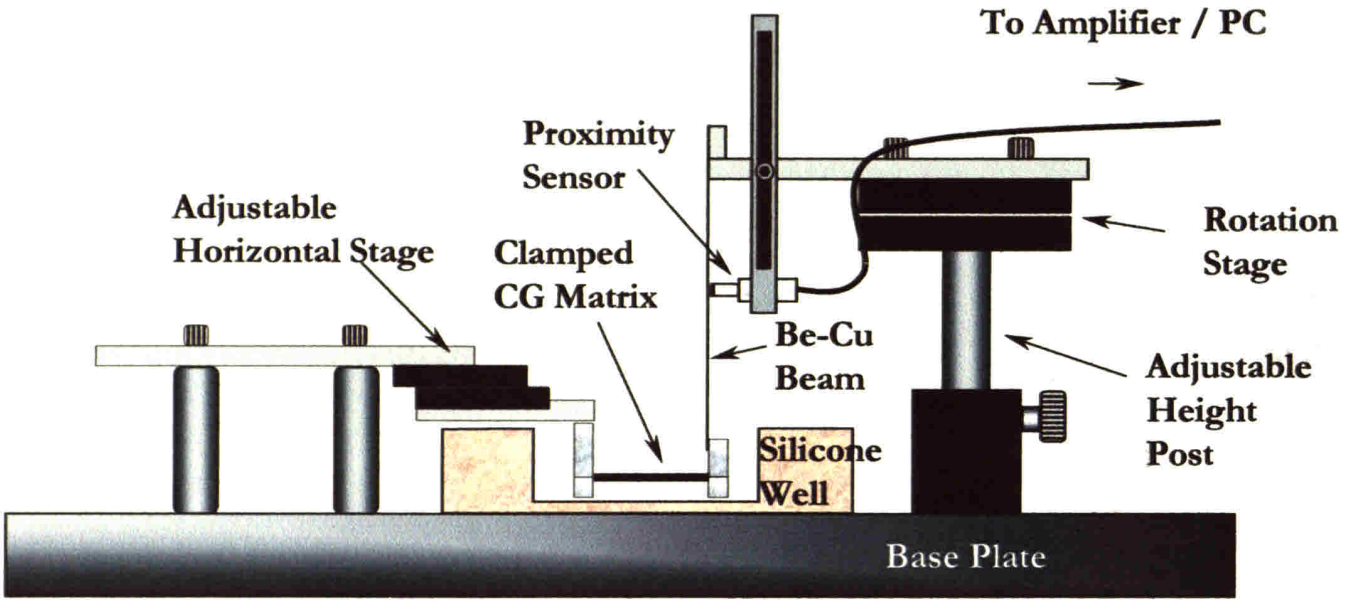

Figure. E.1.1 Schematic of the cell force monitor (CFM) showing the assembly of the equipment described above. Mechanical drawings for the aluminum support pieces are shown in the following figures.

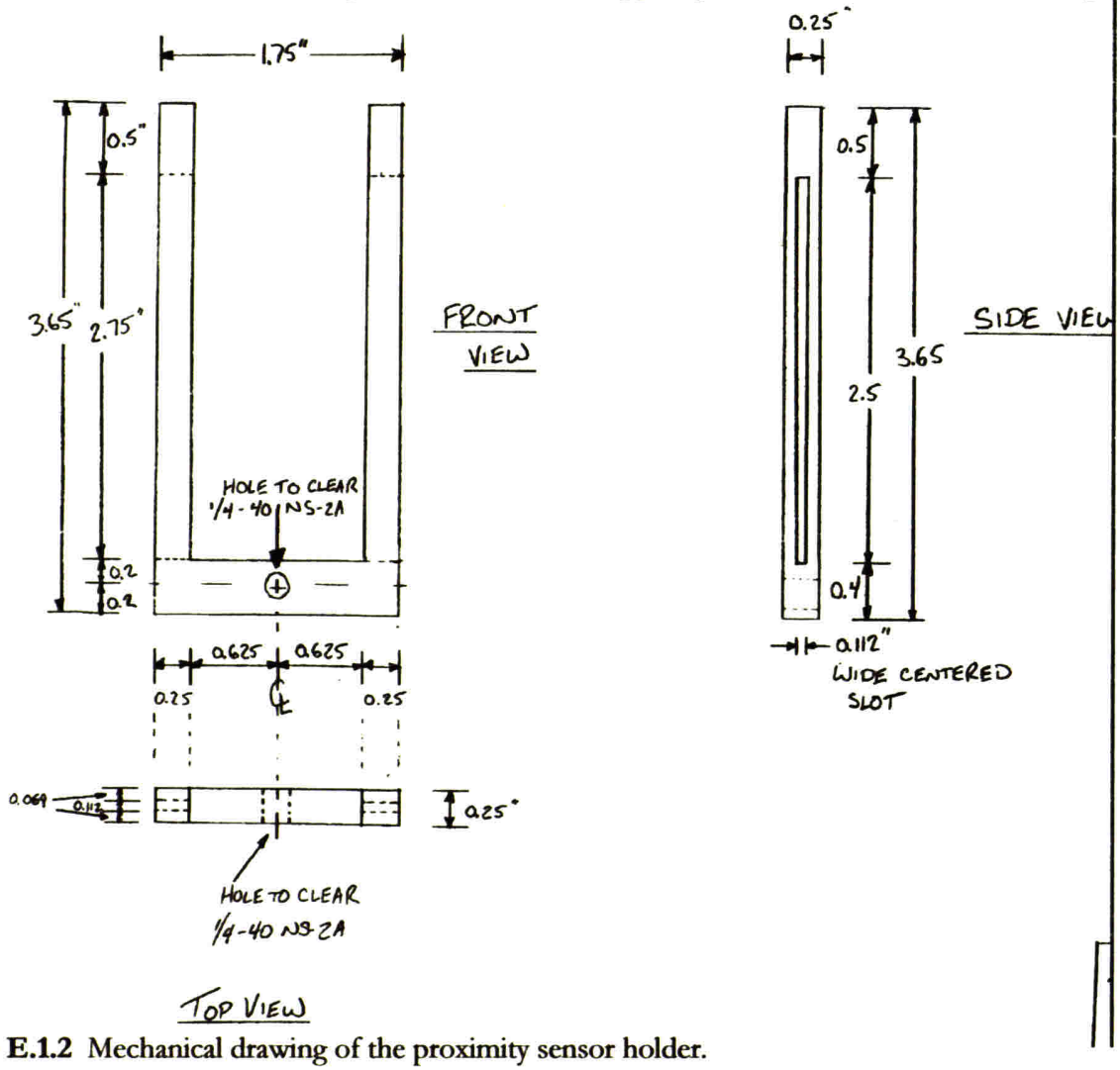

Figure E.1.2 Mechanical drawing of the proximity sensor holder.

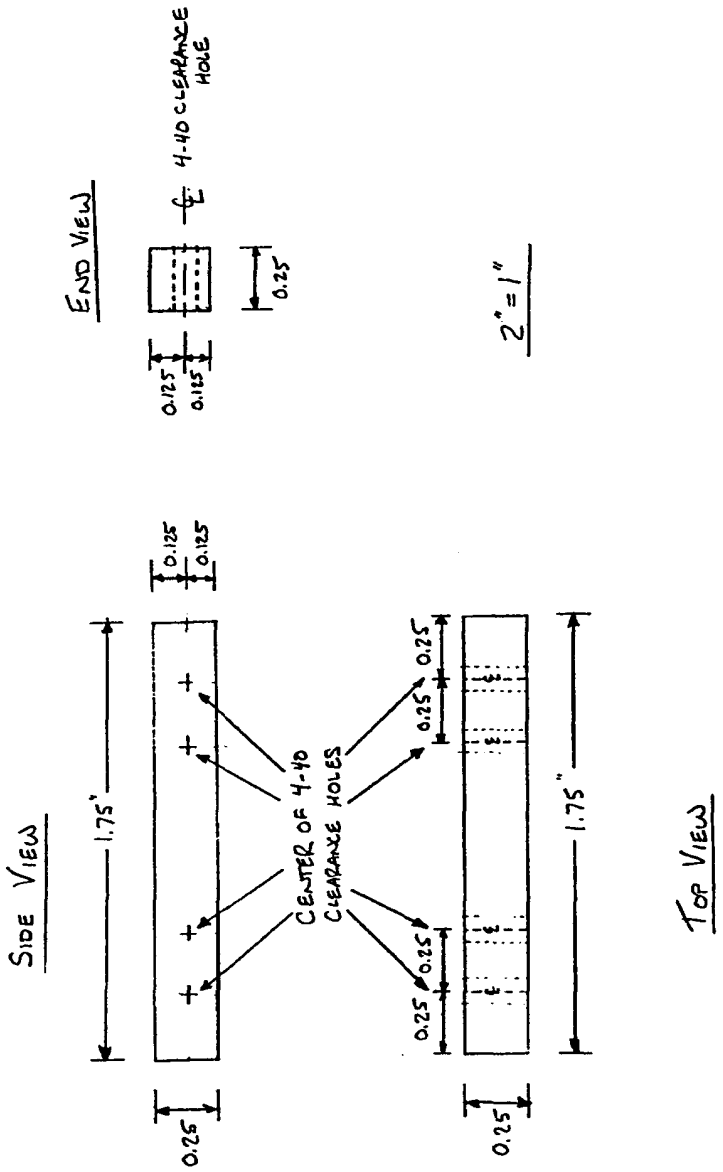

Figure E.1.3 Mechanical drawing. This piece attaches to the end of the piece shown in Fig. E.1.4 to hold the Be-Cu beam.

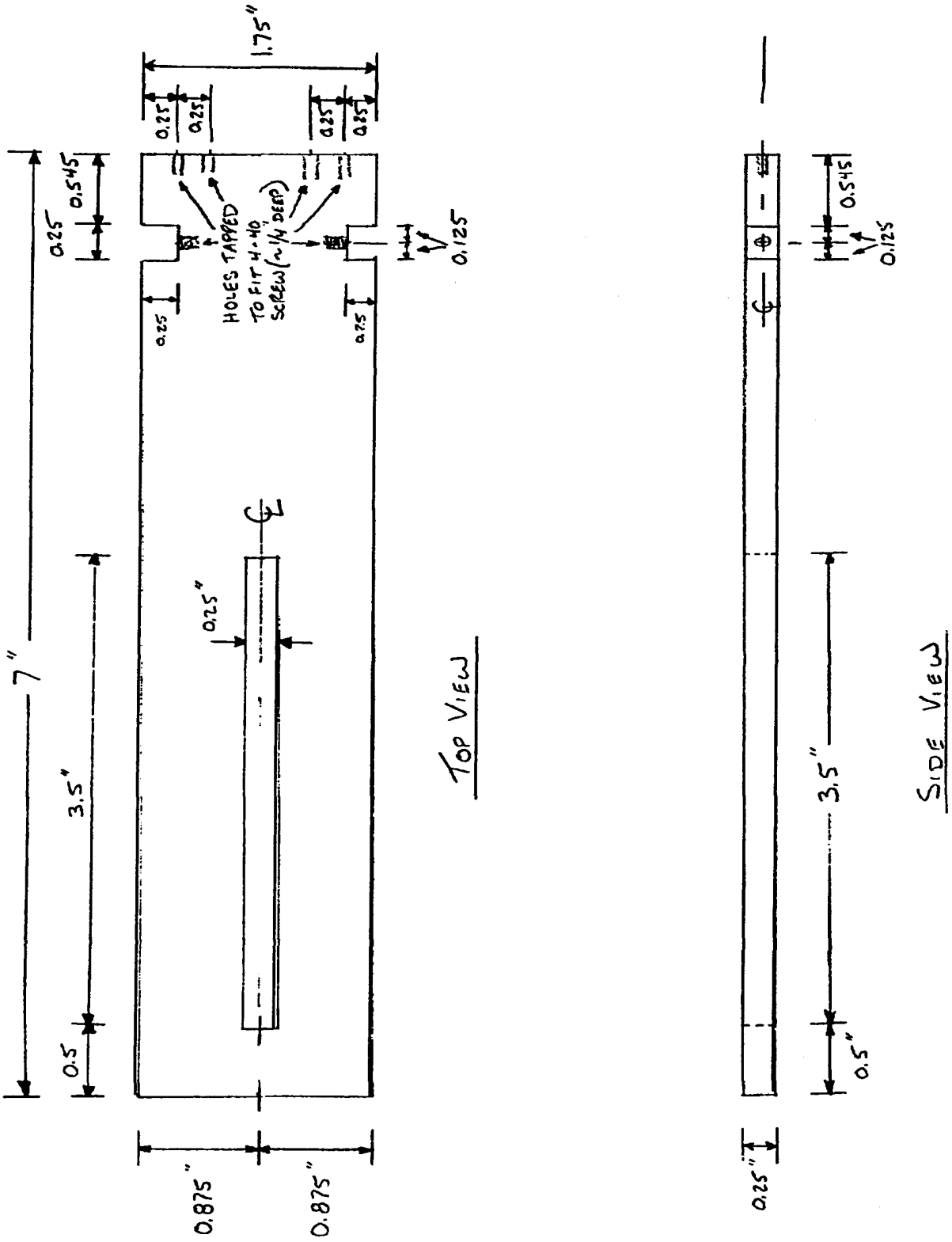

Figure E.1.4. Mechanical drawing. Horizontal support attaching the proximity sensor mount to the rotation stage.

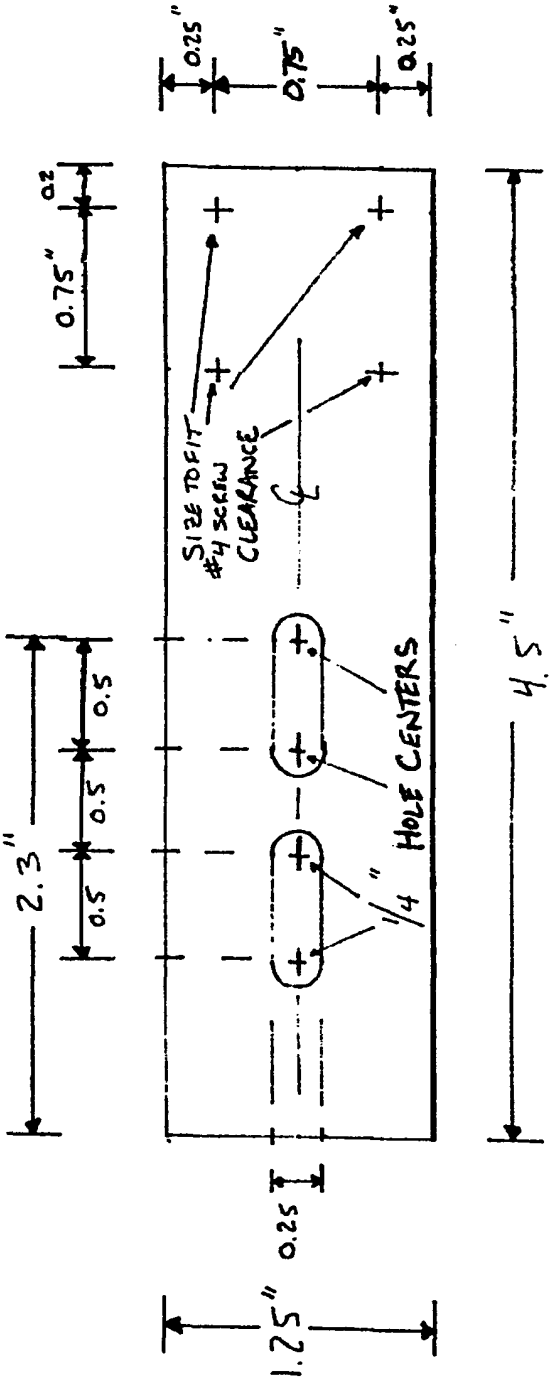

Figure E.1.5. Mechanical drawing of aluminum support which attaches the horizontal stage to the steel posts.

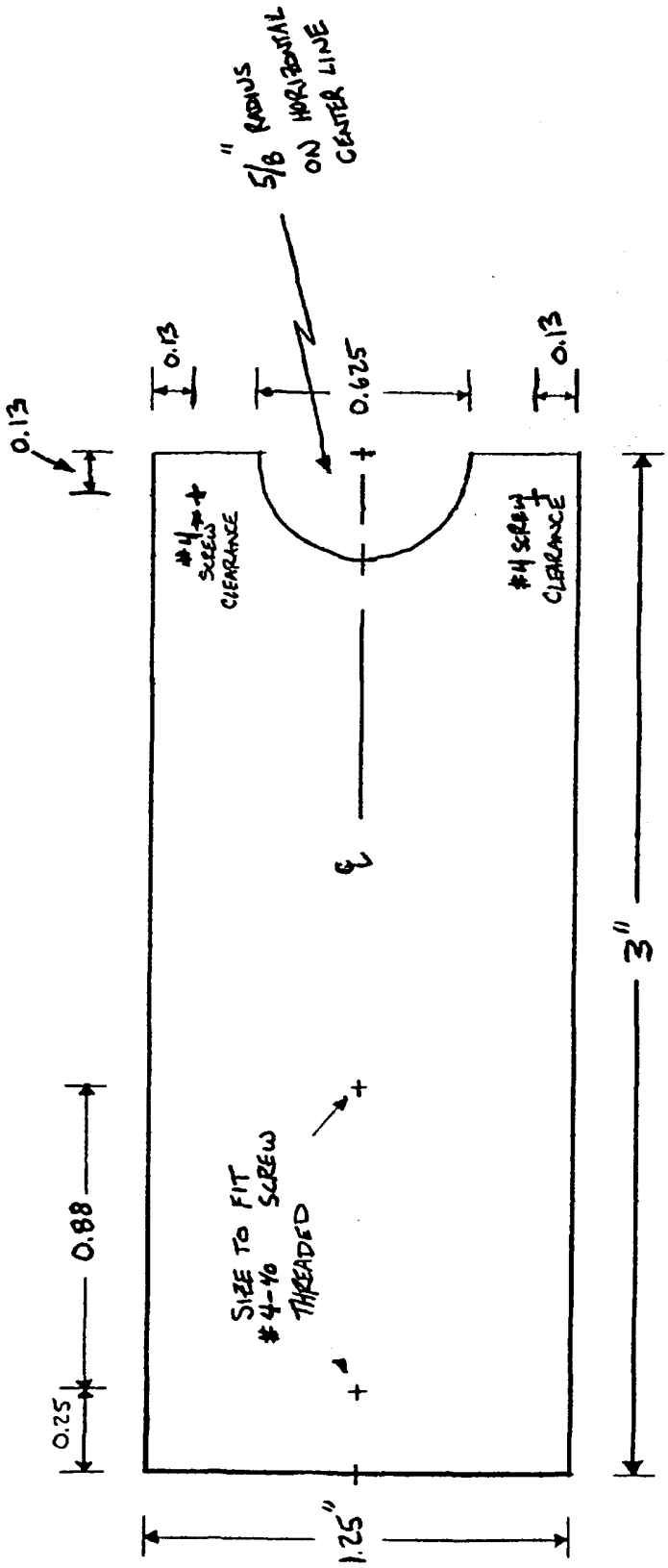

Figure E.1.6. Mechanical drawing of aluminum support which connects the horizontal stage to the fixed clamp.

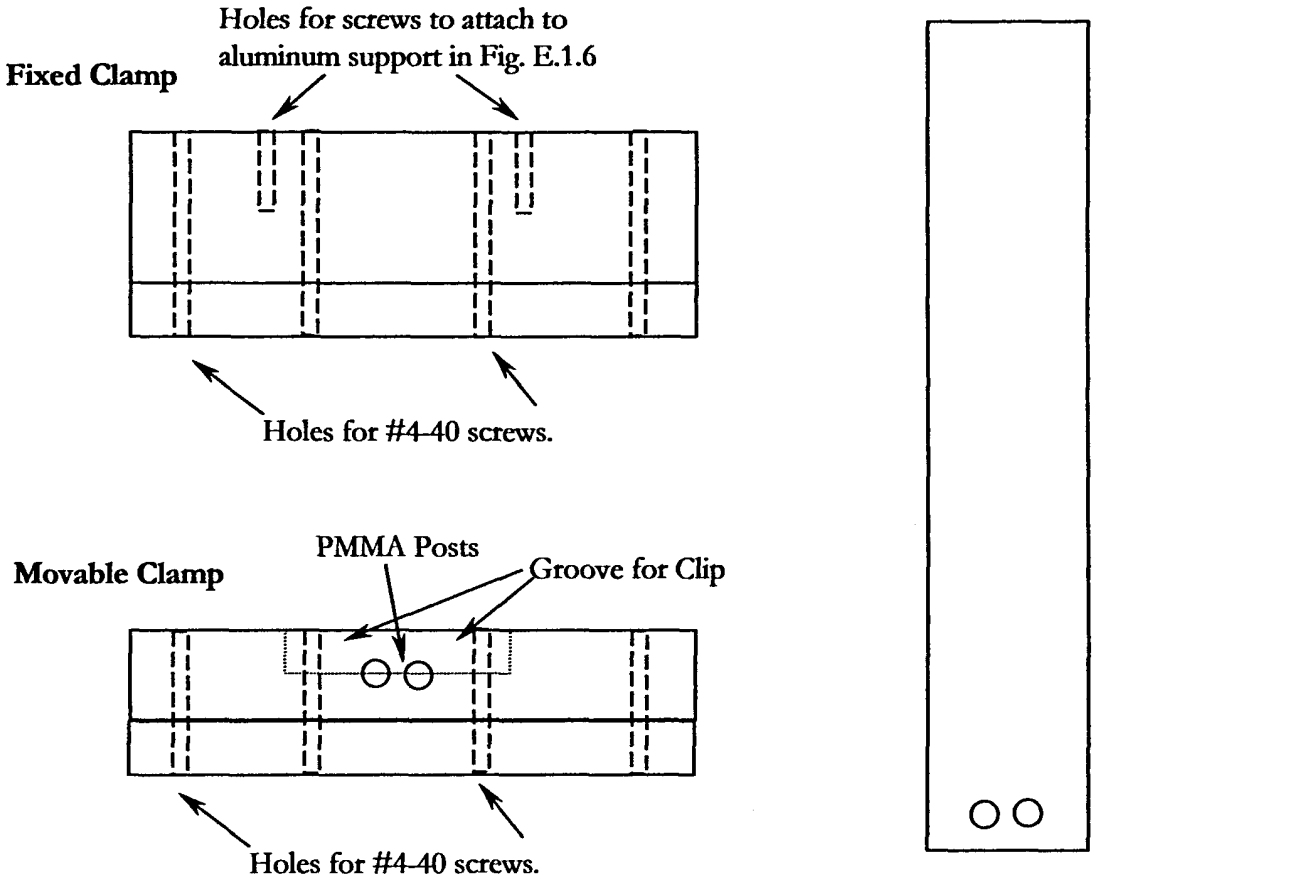

Figure E.1.7. Schematic of UHMW polyethylene clamps. Dimensions of clamps may change depending on the size of the matrix sample or the beam. The lower piece of each clamp is 5 mm high and 5 mm deep. The upper portion of the fixed and moveable clamps is 5mm deep and 13 mm and 8 mm high, respectively. The clamp is positioned on the beam by sliding the PMMA posts into the holes in the beam end. The clamp is fastened to the beam by placing the clip over the beam and in the clamp's groove.

E.2 Calibration Protocol

Displacement:

1. Firmly attach metal L to horizontal adjustable stage so that as the stage is retracted it will displace the beam end. Ensure that the metal L contacts the beam exactly at its end and does not move with applied force.

2. Adjust horizontal stage so the beam is hanging freely.

3. Start LabView, load Calibration2000.vi, set appropriate file name, and execute.

4. Click the "Initial Zero" button to acquire the voltage for a freely hanging beam. This value will not be used for calibration purposes, but establishes the baseline. The voltages to the right of the "Initial zero" button will change once the data has been acquired.

5. Adjust the horizontal stage so that the metal L is just contacting the beam end. Acquire the next data point by clicking the 'First Point' button.

6. For the remaining data points retract the horizontal stage appropriate amounts for calibration of the CFMs. A typical value is 0.3 mm per point. These values will depend on the maximum displacement expected during the cell contraction experiments.

7. Repeat the calibration procedure three times.

8. Using MS Excel or another spreadsheet program, determine the slope [mm/V] of the displacement calibration curve for each CFM for each calibration run. Determine the average slope and standard error in the slope for of each beam.

Force:

1. Using stainless steel posts, position the CFM on the edge of the base plate so that the beams are oriented horizontally and deflection upon the addition of weight to the beam end is in the same direction as the cell contraction experiments.

2. Start LabView, load Calibration2000.vi, set appropriate file name, and execute.

3. Click on the "Initial Zero" button to acquire the voltage for a freely hanging beam. This value will not be used for calibration purposes, but establishes a baseline. The voltages to the right of the "Initial zero" button will change once the data has been acquired.

4. Carefully apply known masses over the desired range and acquire data points as described above. Typical mass values for calibration are 10, 20, 100, 300, and 500 mg. These values will depend on the maximum force expected during the cell contraction experiments.

E.3 Contraction Experiment Setup Protocol

The following protocol is that used for the experiments in Chapter 6. Cell numbers and seeding techniques can be tailored to fit experimental parameters. (Matrix sample dimensions of 50 mm x 28 mm used for this example). See the next section for the variations used for the experiments in Chapter 4.

Equipment:

UHMW polyethylene clamps
#4-40 nylon screws
forceps
hex driver
razor blade
Teflon® sheet
Teflon® template (50 x 28 mm)
collagen-GAG matrix
CFM
silicone dishes
pipetman (10, 200, 1000 µl) (sterile)
pipet tips (10, 200, 1000 µl) (sterile)
disposable, plastic pipettes (sterile)
surgical clips (Roboz Surgical Instruments)
50 ml centrifuge tubes

Solutions:

complete DMEM w/ 10% FBS
Dulbecco's Phosphate Buffered Saline
Trypsin/EDTA

Setup Procedure:

1) Spray down hood, clamps, screws, forceps, hex driver, matrix, teflon sheets, razor blade, clips and screws for CFM, silicone dishes, pipetman, and two 1,000 µl pipette tips.

2) Cut out 3 matrix samples and fix in clamps using the template, Teflon® sheet, and razor blade. Pan side of matrix should face up when attached to the CFM. The pan side is identified by a smoother appearance. Be sure to use matching clamp top and bottoms. Pair clamps A&B, C&D, E&F. Letters on clamps should face the matrix sample. Position matrix between the clamp pieces, squeeze clamp pieces together, and hold firmly. Carefully pierce the matrix through the holes in the clamp and fasten with screws. Place clamped matrix samples into 50 ml centrifuge tubes.

3) Produce a cell suspension of the desired cell concentration using the protocols in Appendix B. For this experiment the cells were seeded at a concentration of ~2 million per ml. A total of 4 million cells were seeded onto each of three matrix samples.

4) Add 10 ml DMEM to the clamped matrix samples while waiting for the trypsin to release the cells. Lay tube on its side so the clamped matrix sample is only touching the DMEM along one edge. This allows the DMEM to rehydrate the matrix without trapping air bubbles.

5) After the matrix has rehydrated fully (~10 m) place on the Nutator in the incubator until the cell suspension is prepared.

6) Following full preparation of the cell suspension add the desired number of cells (~4

million in 2 ml DMEM) to each matrix sample. Place the centrifuge tubes back onto the Nutator for 10 m to facilitate cell attachment.

7) Place the CFM in the sterile hood and execute the LabView program CFM2000.vi. This will acquire the free beam voltages so that the cell seeded matrices can be zeroed.

8) Place clamped, seeded samples in the silicone wells so the clamps are as they would be in the CFM.

9) Fill the silicone well with 28 ml of warmed DMEM. Line up the silicone dish so the moving clamp is not touching the sides. Tap beam with your finger to see if the clamp moves freely. If not, check to see if the clamp is hitting the sides. If it is not hitting the sides, raise the beam up until the clamp moves freely.

10) Using the micrometers adjust the samples to get the zeroed voltage for each beam.

11) Place CFM into incubator and press the 'Finished Calibrating' button.

E.4 Variation on Cell Seeding of Collagen-GAG Matrix Samples

Pipet Seeding (Chapter 4)

1. Begin as described in the Contraction Experiment Setup Protocol. Execute the LabView program so that the voltage for the beam hanging freely is acquired.

2. Attach clamped, dry matrix samples to the CFM. Set the rotation stage and the adjustable vertical post so that the matrix sample is in one horizontal plane and the clamps are parallel.

3. Rehydrate the matrix sample by pipetting 1 ml of DMEM with 10% FBS onto the top surface. Then place the entire CFM into the incubator for 30 m to allow to sample to hydrate fully.

4. Remove the CFM from the incubator. Place a piece of filter paper (S&S #595, Dassel, Germany) on top of the matrix sample for 30 s to remove excess medium.

5. Evenly distribute 830 μl of the cell suspension on top of the matrix sample using a pipet. Place the CFM into the incubator for 10 m to allow the cells to attach.

6. Follow steps 9 to 11 from E.4.

E.5 Non-linear Regression Analysis of CFM Data

To get curve fit parameters for contraction over time data with MATLAB software.

1. Save data in text file format (tab delimited) so that the first column contains the values of time and subsequent columns contain values of force at that time. To save computation time, the data can be abridged so that only every ~10^{th} data point is used for the analysis.

2. Log on to the Athena network. Copy the text data file to the working directory.

3. Start MATLAB.

4. Copy the function edecay.m to the directory or create this function using the text editor supplied with MATLAB.

5. Type 'Load *Datafilename*.txt'

6. Type 'x=*Datafilename*(:,1);' where 1 indicates the column of values to be used for the x axis.

7. Type 'y=*Datafilename*(:,2);' where 2 indicates the column of values to be used for the y axis.

8. Type 'beta = [Fa τ]' where Fa and τ are guesses for the value of these two fitting parameters. These values just need to be estimates and the software should quickly close on the appropriate values regardless of the quality of the estimate.

9. Type 'betafit = nlinfit(x,y,'edecay',beta)'. This step will have MATLAB determine the actual values of Fa (b1) and τ (b2) which fit the exponential equation using the data in x and y.

MATLAB Code for edecay.m:

```
function y = edecay(beta,x)
%EDECAY function to curve fit a decaying exponential
% y = edecay(beta,x) gives the predicted values of time constant
% and asymptotic value as a function of
% the vector of parameters, beta, and the matrix of data, x.
% beta must have elements and x must have 1 column.
% The equation is of the form
% y = b1*(1-exp(-x/b2))
b1=beta(1);
b2=beta(2);
y = b1*(1-exp(-x/b2))
```

E.6 Annotated Labview Code

Calibration:

This LabView program acquires voltages from the CFMs so that each of three CFMs can be calibrated for load and displacement with five known values simultaneously. Upon execution of the program, the user must prepare the CFM(s) as desired and click on the green buttons on the left-hand side of the front panel to acquire data points. Following each click of a button the program acquires data within the range ±1 V (to change set "high limit" and "low limit") at a rate of 2 scans/sec (to change set "scan rate") and averages these data over 60 s (to change set "number of samples") for each data point for each CFM. Following acquisition of the 5th data point, data are automatically saved to the file name specified.

Contraction Experiments:

This LabView program acquires voltages from the CFMs, following an initial zeroing step, over a pre-set period of time and rate. Voltage data are saved to the file name specified as the data are acquired. Upon execution, the program waits for 60 s (to change set "Time to Wait") for the electronics to equilibrate. After this time, the voltage of each CFMs will be displayed in the white rectangles on the far right-hand side of the front panel. These values are updated once per second. The voltage acquired initially for the beam is displayed in the white rectangles in the left-hand column. This procedure allows the user to adjust the horizontal stage so that the continuously updated voltage is equivalent to the initial voltage displayed in the left-hand column of white rectangles. Following zeroing, the button "Finished Calibrating" should be clicked and the acquisition of data for the contractile experiment will begin. These data will be acquired at a rate of 1 per sec (to change set "scan rate") and averaged over 100s (to change set "number of scans to read") to yield each saved data point. This process will proceed until the time reaches the value set by the "Time of Test" dial. The program will not stop until the green "Go" button in the lower left-hand corner is clicked. Note: only click this button once, it will take at least the time required to acquire two more data points (200 s) to stop the program.

Connector Pane

Calibration2000.vi

Front Panel

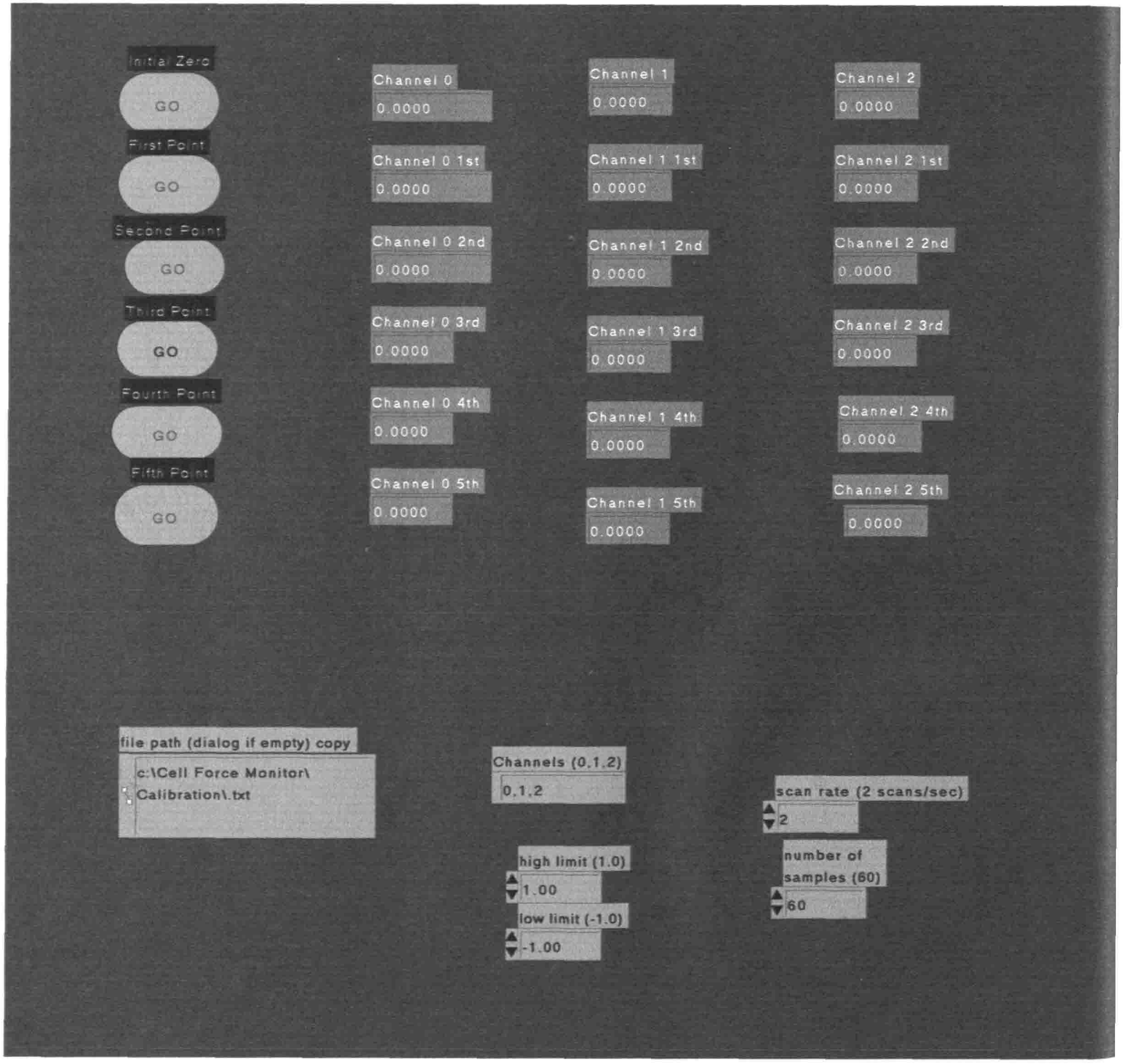

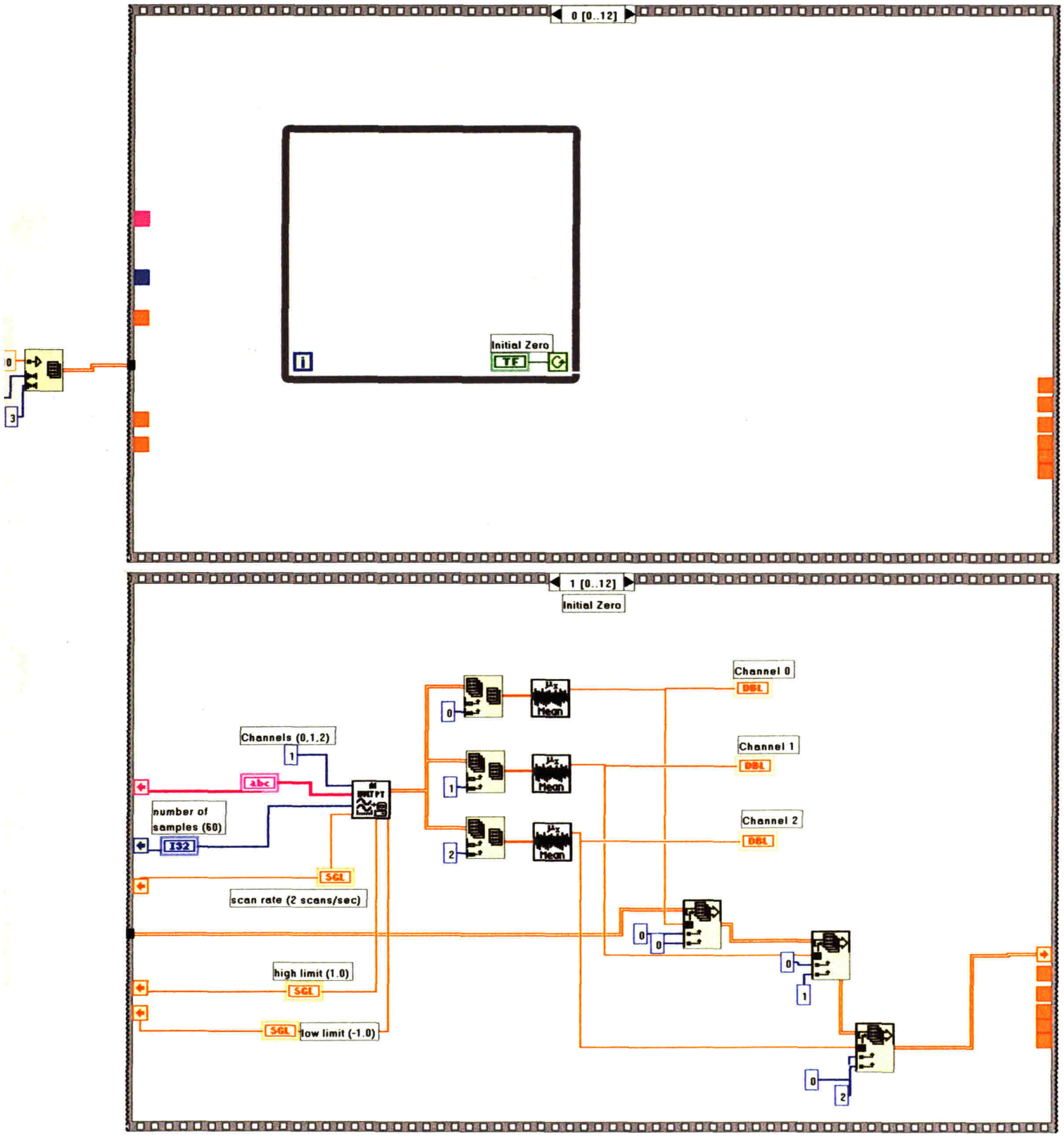
0 [0..12]
Initial Zero
TF
1 [0..12]
Initial Zero
Channels (0,1,2)
abc
number of samples (60)
I32
SGL
scan rate (2 scans/sec)
high limit (1.0)
SGL
SGL
low limit (-1.0)
Mean
Channel 0
DBL
Channel 1
DBL
Channel 2
DBL

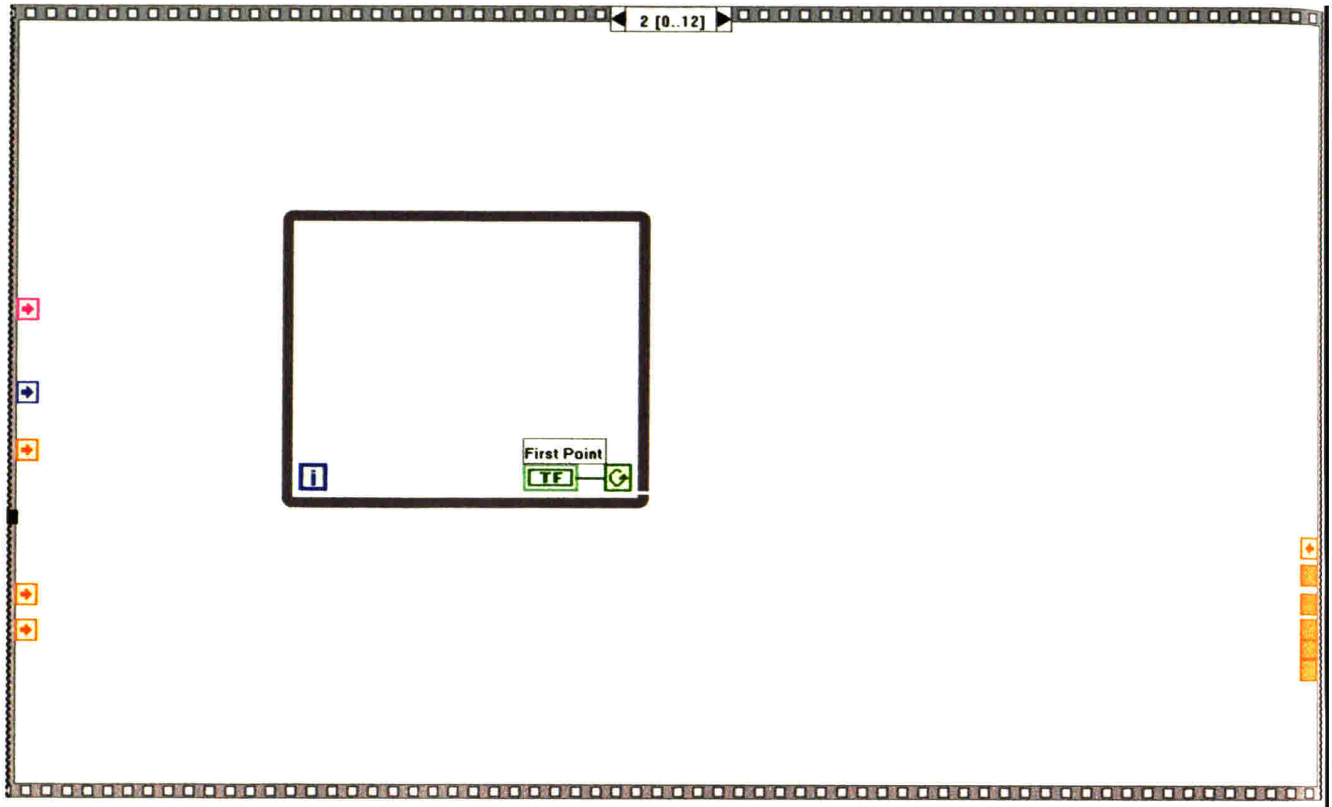
2 [0..12]
First Point
TF

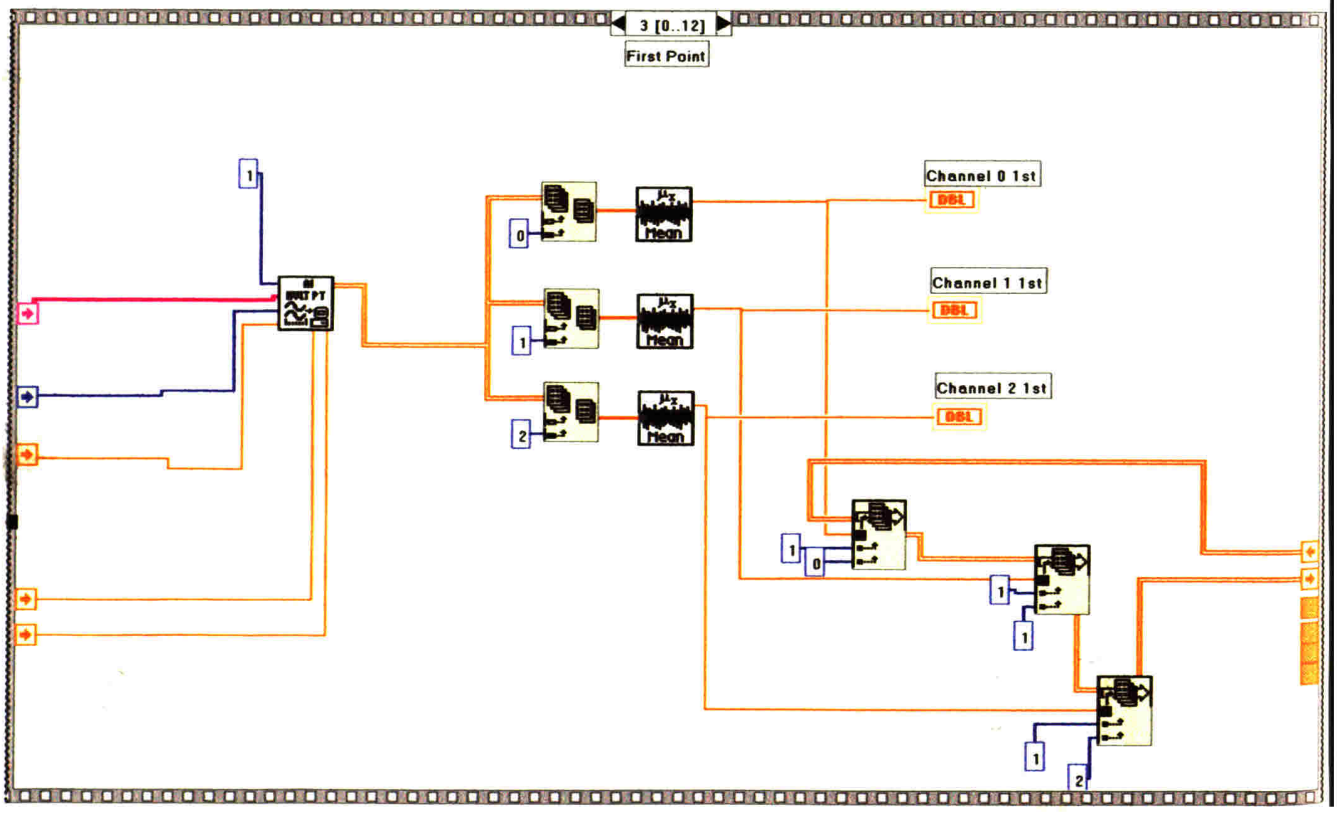
3 [0..12]
First Point
Channel 0 1st
DBL
Channel 1 1st
DBL
Channel 2 1st
DBL
Mean
Mean
Mean

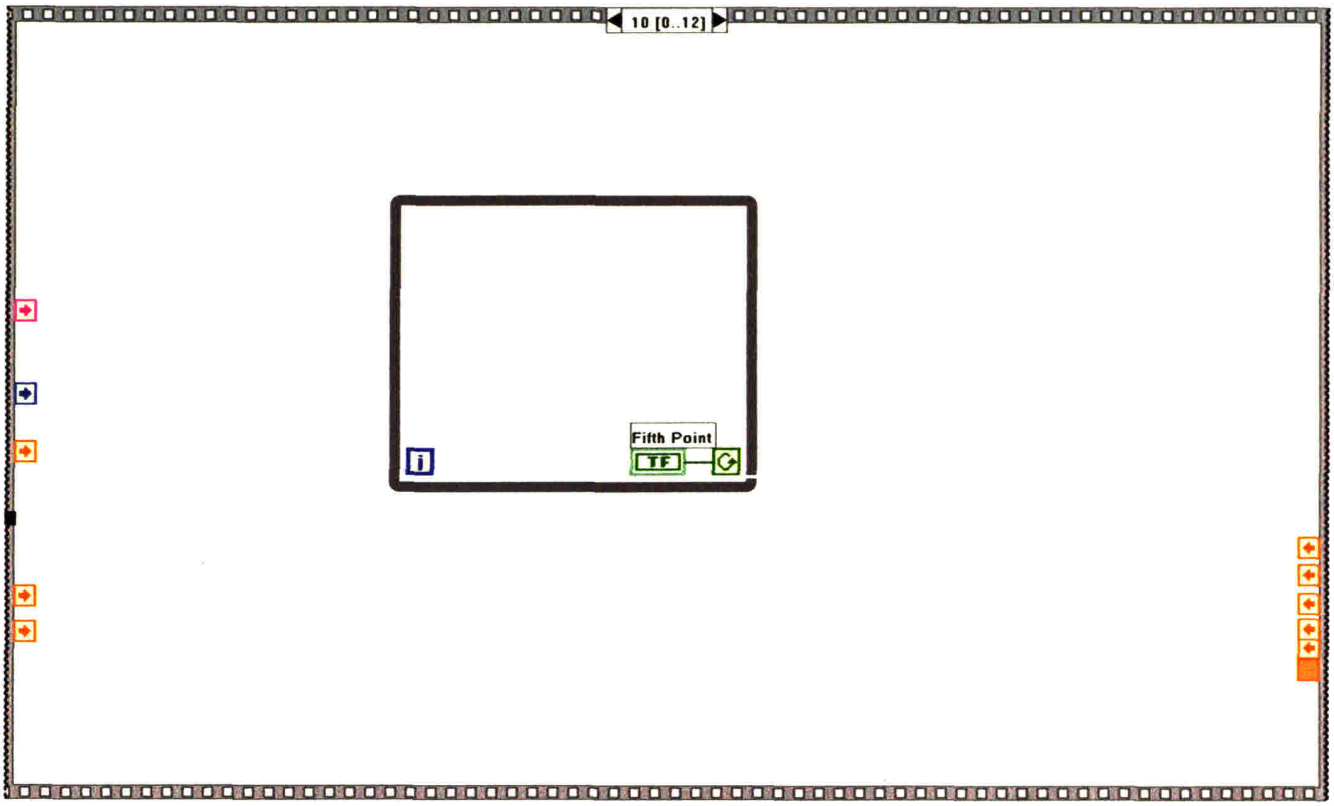
10 [0..12]
Fifth Point
TF
i

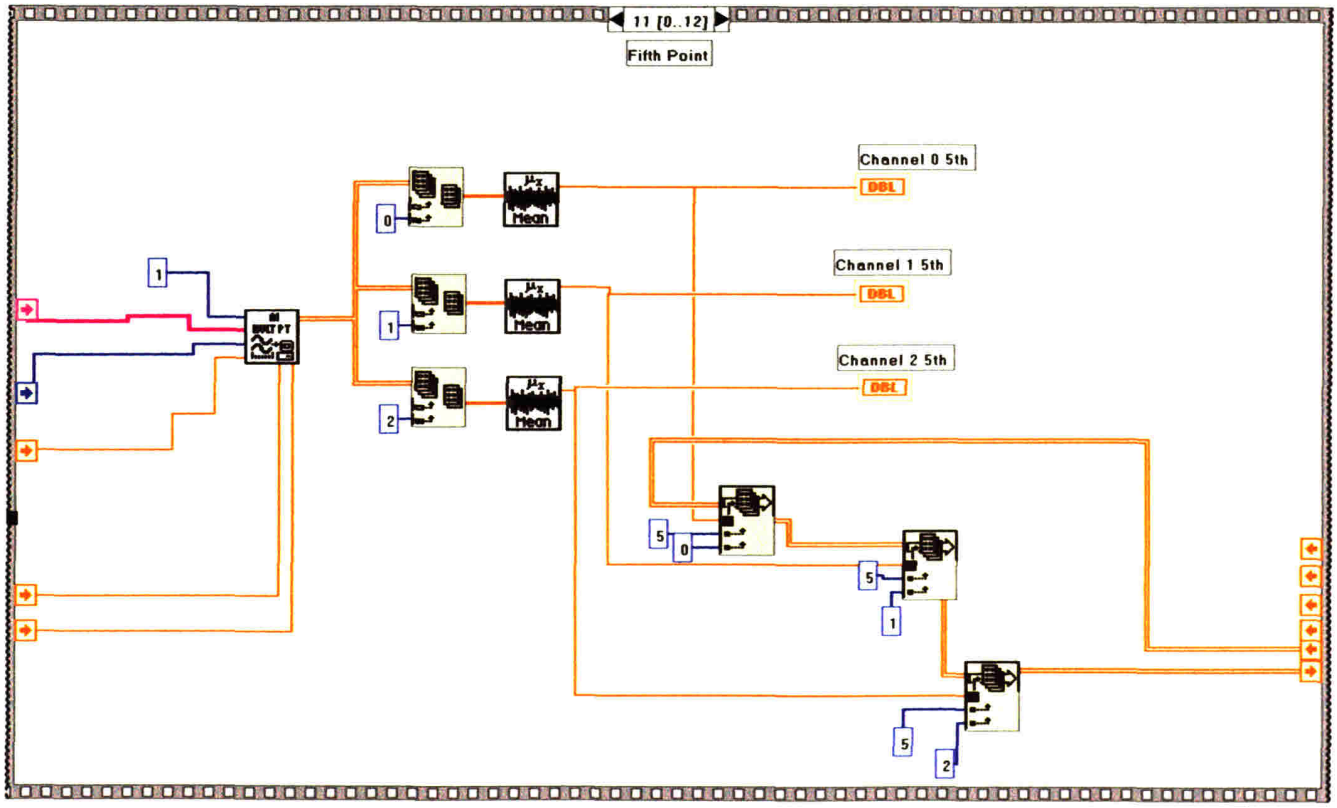
11 [0..12]
Fifth Point
Channel 0 5th
DBL
Channel 1 5th
DBL
Channel 2 5th
DBL
Mean
Mean
Mean
0
1
2
1
5
0
5
1
5
2

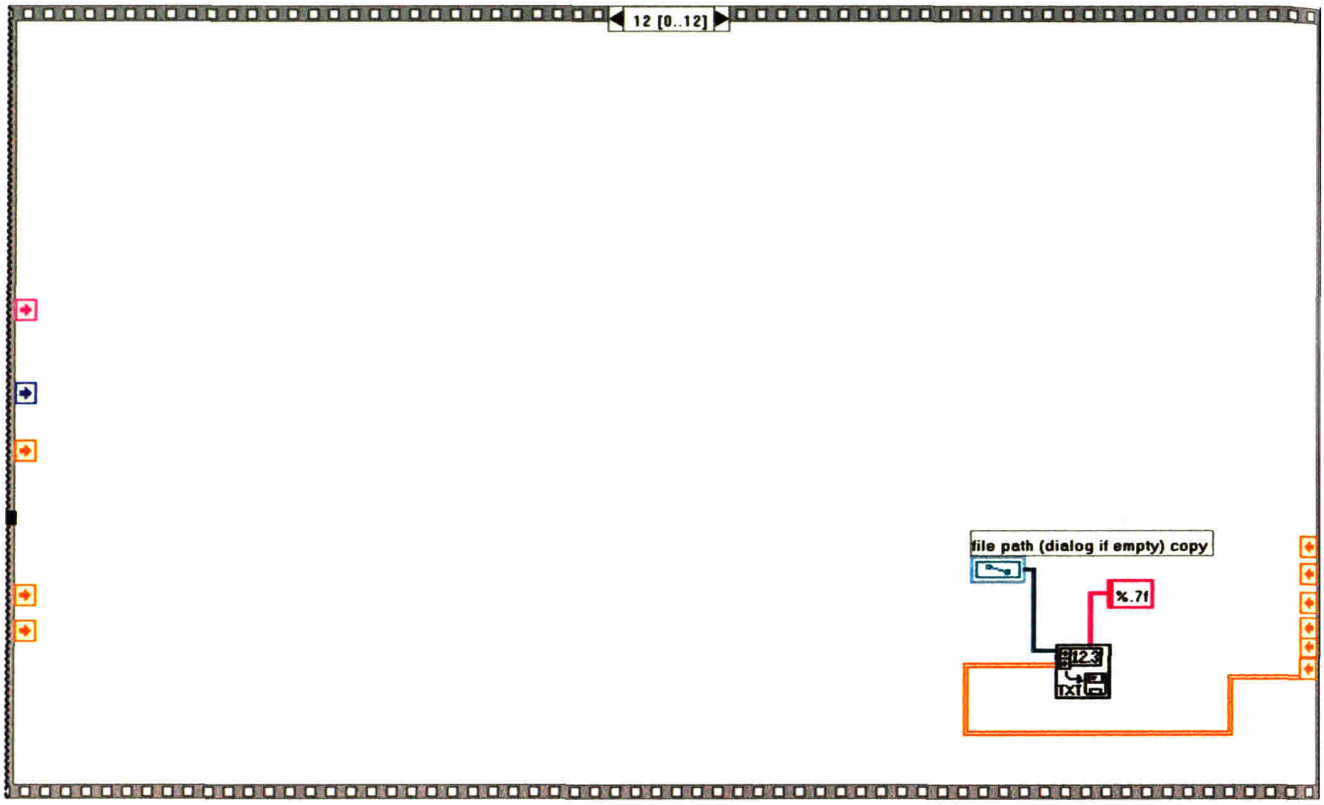
12 [0..12]
file path (dialog if empty) copy
%.7f
txt

Connector Pane

CFM2000.vi

Front Panel

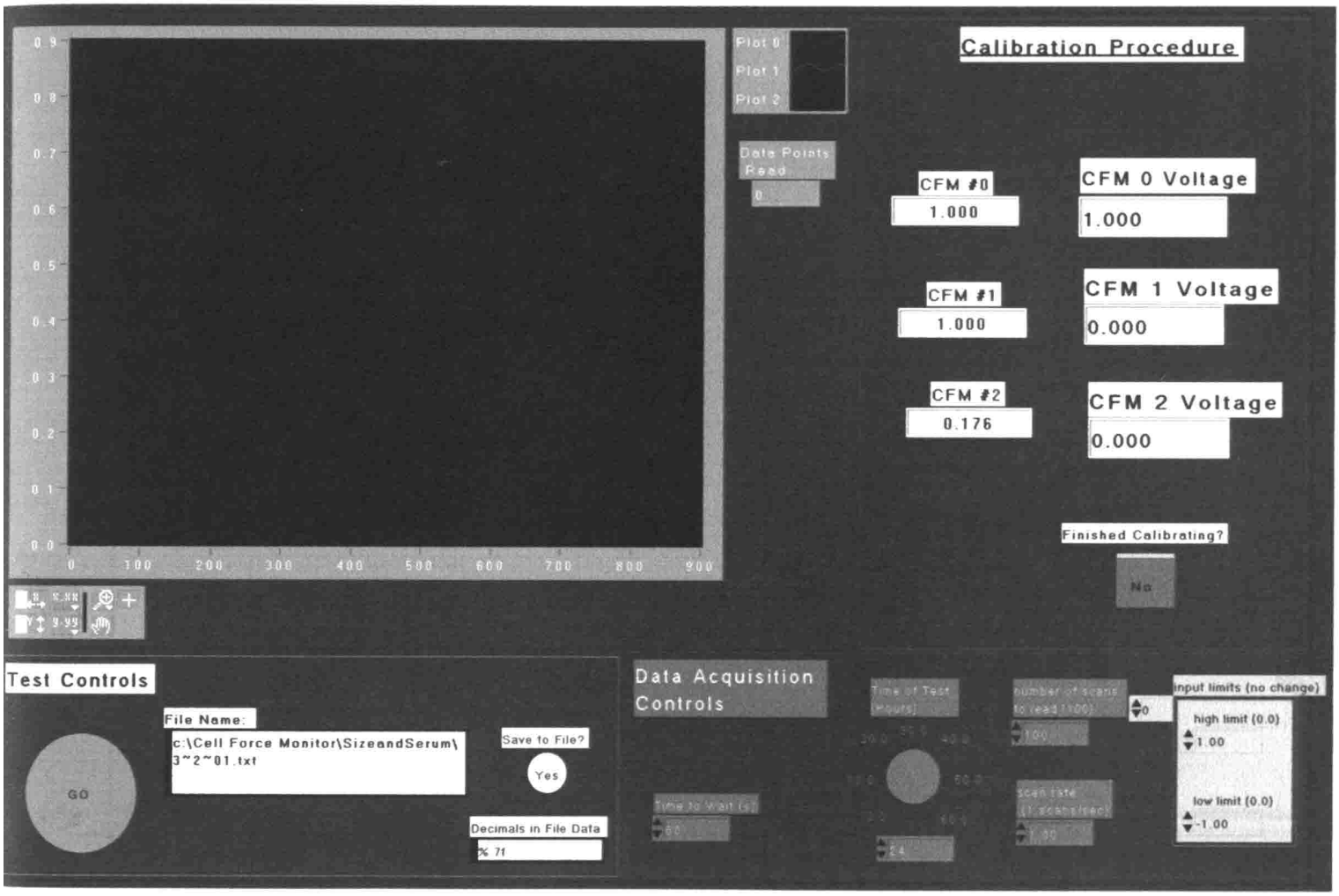

Block Diagram

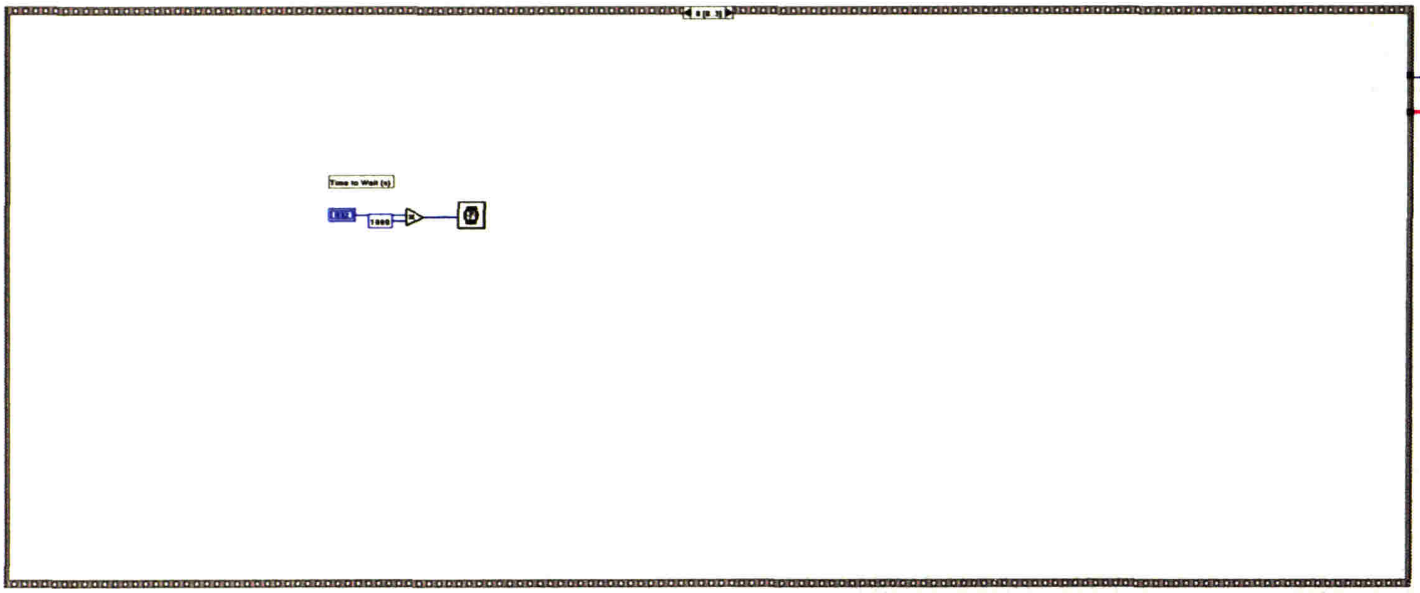

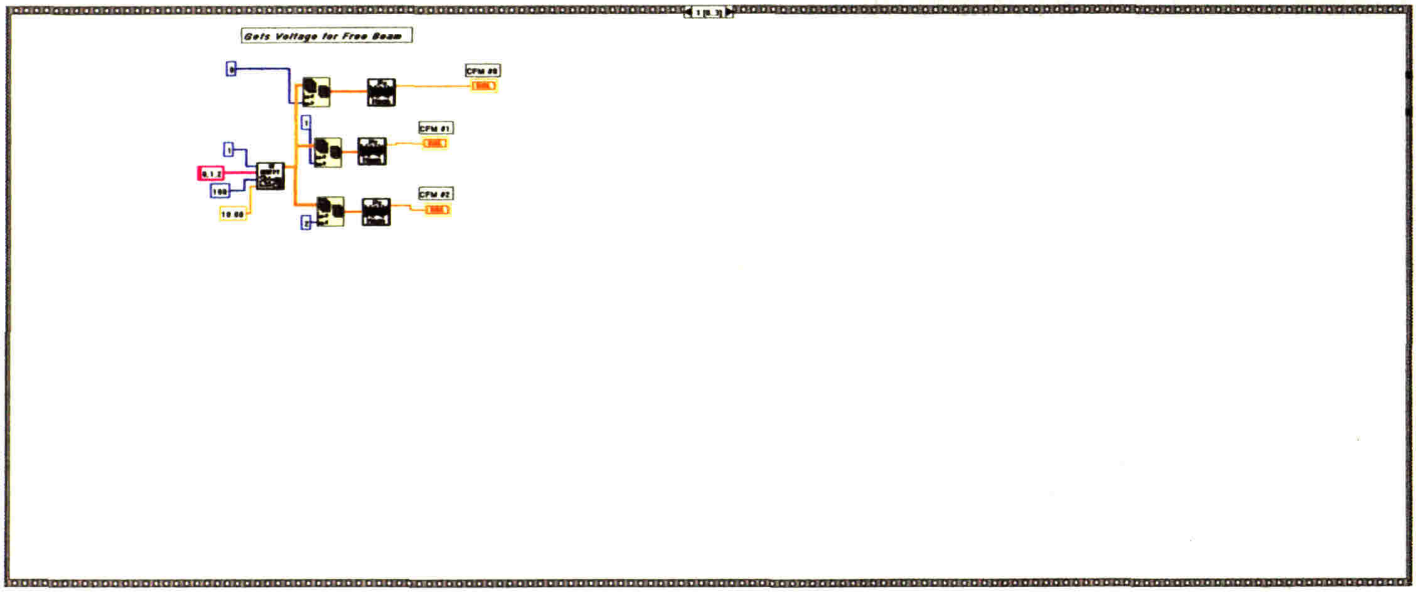

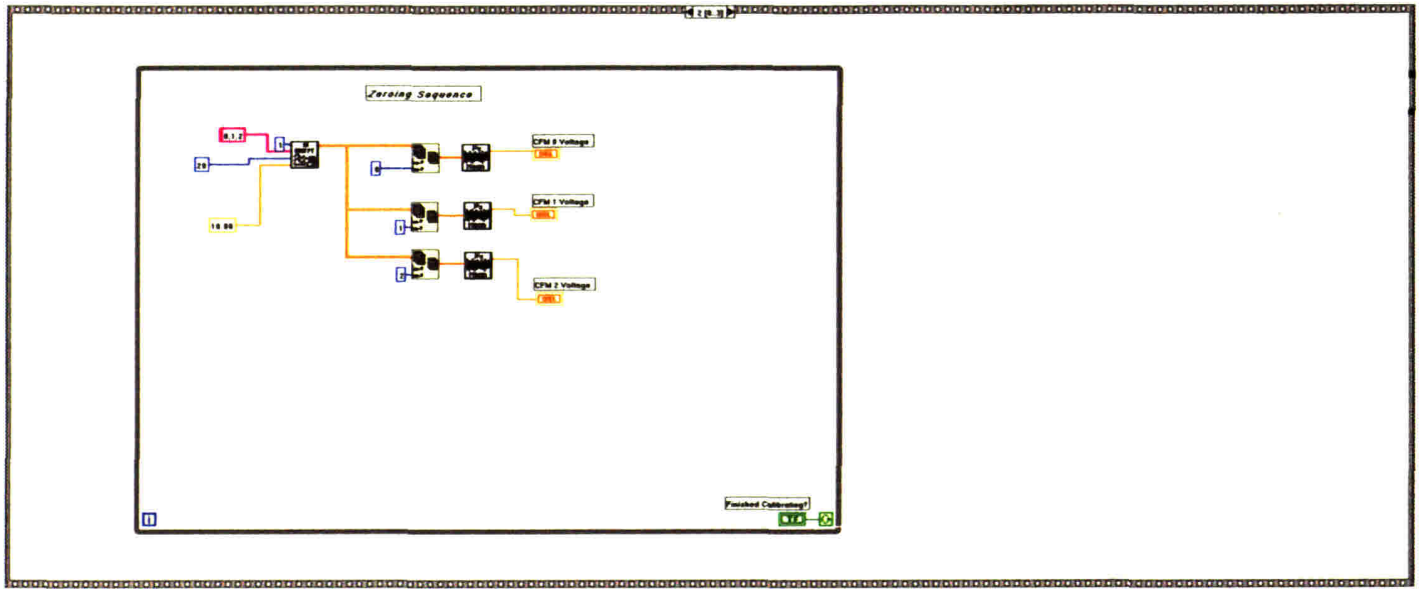

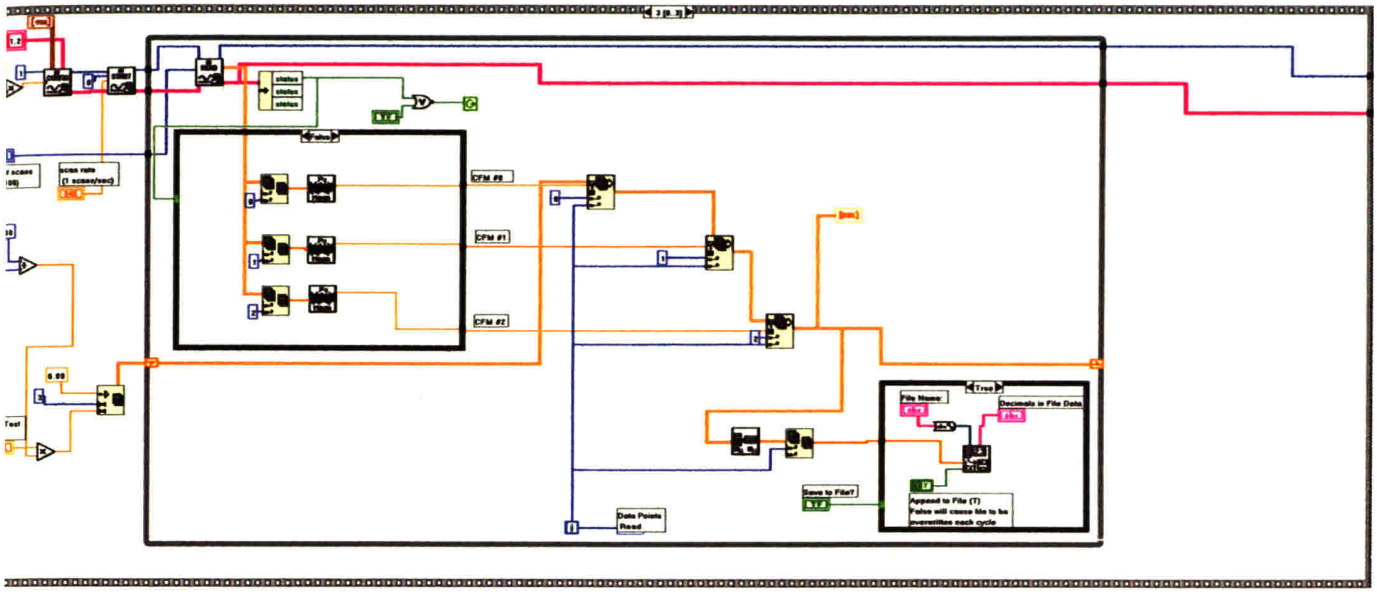
CFM #0
CFM #1
CFM #2
Data Points Read
Save to File?
File Name:
Decimals in File Data
Append to File (T)
False will cause file to be overwritten each cycle

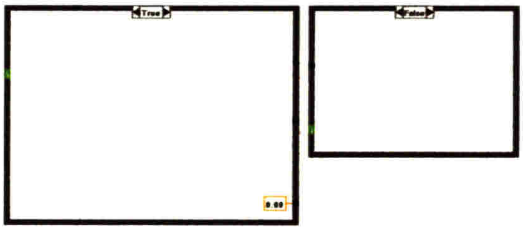
True
False

Appendix F. Free-Floating Matrix Contraction

Protocol for seeding and measuring the contraction of free-floating, fibroblast-seeded, matrix disks. This is a general procedure and the number of samples and cell densities will vary depending on the required experimental parameters. All steps should be performed following cell-culture sterile protocol.

Equipment:

12-well tissue culture plates
forceps
collagen-GAG matrix sheet
9.0 mm diameter trephine (Katena Products Inc., Cat. # K20-2062, Denville, NJ)
Teflon® sheet
sheet with printed disks (0.5 mm)
50 ml centrifuge tubes
disposable, plastic pipettes
Nutator

Solutions:

2% agarose solution (FMC BioProducts, SeaPlaque agarose Cat. # 50100, Rockland, ME)
DMEM with 10% FBS (see Appendix B)
2.0 U/ml dispase solution (Gibco)
10% Neutral Buffered Formalin (see Appendix G.2)

Protocol:

1. Autoclave the agarose solution. This will both melt and sterilize the solution.

2. Pipette enough melted agarose solution into each well of a 12-well plate to cover the bottom. Place the cover on the plate and refrigerate until agarose solidifies.

3. Using the trephine cut out matrix disks on the Teflon sheet. Be careful not to tear the matrix while cutting.

4. Rehydrate matrix disks by placing them into DMEM in a 50 ml centrifuge tube.

5. Make a cell suspension following the protocol for cell passaging in Appendix B.

6. Add the cell suspension to the tube with rehydrated matrix disks. Place the 50 ml centrifuge tube onto the Nutator in the incubator. Wait 10 m.

7. Remove 12-well plates with solidified agarose from the refrigerator and add 1 ml of DMEM to each well. Carefully place one cell-seeded matrix disk into each well. Cover 12-well plate and place into the incubator. Wait overnight.

8. Add an additional 0.5 ml of DMEM to each well. (Change the medium (1.5 ml) every other day through the course of the experiment.) Measure the diameter of each matrix sample by comparing the disk size to printed circles of known diameter (0.5 mm increments). If the disk appears elliptical estimate the major and minor axis dimensions.

9. Repeat disk diameter measurements on days 3, 5, 7, 9, 11, 13, and 15.

10. On pre-selected days (1, 5, and 15) sacrifice 4 matrix samples from each group for cell number determination (n=3) and histological analysis (n=1). Place one sample in 10% neutral buffered formalin and follow GMA embedding protocol. Rinse the other 3 samples in 37°C DPBS and digest in a solution of 2.0 U/ml dispase. Determine the cell number in each of these samples using the cell counting procedure outlined in Appendix B.

Appendix G. Histology

G.1 *Paraffin Embedding Protocol*

Protocol for embedding formalin-fixed, cell-seeded, collagen-GAG matrix samples in paraffin. Alternately the Tissue-Tek embedding machine at Prof. Spector's lab can be used on program 4 following the first step.

Equipment:
Razor Blade
Forceps
Tissue-Tek Embedding Cassettes (Tissue Tek 4170, Sakura Finetek, Torrance, CA)
Steel Embedding Molds 30 x 24 x 5 mm (Tissue Tek 4164, Miles Scientific, Naperville, IL)
Pencil

Solutions:
Paraplast Plus Paraffin (5159-464, VWR Scientific, Boston, MA)

Embedding Protocol:
1. Cut fixed matrix with a razor blade so that it is at least 2 mm smaller than the embedding mold dimensions. Place samples into embedding cassettes and label cassette with pencil.

2. Dehydrate samples in graded ethanols (5 m each): dH_2O, 50%, 70%, 80%, 95%, 95%, *100%, 100%, 100%*

3. Clear with xylenes 2 times each for 5 m.

4. Infiltrate in paraffin bath 2 times for 30 m each.

5. Embed in paraffin.

6. Cool and store in refrigerator.

G.2 Glycomethacrylate Embedding Protocol

Protocol for embedding formalin-fixed, cell-seeded, collagen-GAG matrix samples in glycomethacrylate.

Equipment:
Plastic Embedding Mold (16643A, Polysciences, Warrington, PA)
Forceps
Aluminum Block Holders (Energy Beam Sciences, Agawam, MA)
Plastic Transfer Pipets
Fume Hood

Solutions (from Polysciences):
10% Neutral Buffered Formalin:
- 900 ml dH_2O
- 100 ml 38% Formaldehyde
- 4.0 g Monobasic Sodium Phosphate NaH_2PO_4
- 8.95 g Dibasic Sodium Phosphate Na_2HPO_4

JB-4 A Embedding Solution: 100ml JB-4 A solution + 0.9g JB-4 A Catalyst

Embedding Protocol:
1. Fix samples in 10% neutral buffered formalin for 24-48 hrs at room temperature

2. Dehydrate samples in graded ethanols as follows (5 m each): dH_2O, 50%, 70%, 80%, 95%, 95%, 100%, 100%, 100%

3. Cut samples into pieces for cross-section and planar section. Do not exceed ~ 3mm for any one dimension.

4. Infiltrate samples with catalyzed JB-4 A solution at 4°C for 24 h. Replace with fresh JB-4 A and place under vacuum for several hours. Hold at 4°C for an additional 24 h. If air bubbles are present, repeat vacuum treatment.

5. Mix 25ml JB-4 A with 1ml JB-4 B and pipet ~4 ml into each well of the plastic molds.

6. Place each sample into a well. The JB-4 mixture will polymerize quickly after ~25 m so after this time make sure the samples are in the proper orientation. Mixture will become progressively more brown as polymerization proceeds.

7. After the JB-4 mixture becomes viscous enough that the samples do not float, place one aluminum stub onto each well and place the plastic mold tray in a refrigerator (4°C) and wait overnight.

8. Remove embedded samples from mold and store at 4°C.

G.3 Hematoxylin and Eosin Staining Protocol

Protocol for staining formalin-fixed, cell-seed, collagen-GAG matrix samples which been GMA embedded and sectioned at 5 μm thickness. Cell nuclei will stain a dark red-brown, cytoplasm a salmon pink, and the matrix a lighter shade of salmon pink. Over staining with Eosin will result in high background staining. Eosin is water soluble so background will rinse out in tap water.

Solutions:

Eosin Y (Sigma-Aldrich, St. Louis, MO)

Weak Ammonium Hydroxide Water
- Tap water, 200 ml
- *Ammonium hydroxide*, 2-4 drops

Acid-Alcohol
- 70% EtOH, 200 ml
- Hydrochloric Acid, 1 ml

Harris's Hematoxylin (HHS-16, Sigma)

Cytoseal 60 Mounting Medium (8310-16, Stephens Scientific)

Staining Procedure:

1. Place slides to be stained in staining rack and place in Harris's Hematoxylin for 90 m.
2. Rinse in running tap water for 2 m.
3. "Blue" with weak ammonium hydroxide water for 2 m.
4. Rinse in running tap water for 2 m.
5. Differentiate in acid-alcohol for 2 m.
6. Rinse in running tap water for 5 m.
7. Counterstain with Eosin for 3 m.
8. Rinse in running tap water 3 m. Check that the matrix and cytoplasm are stained and the background staining is not too strong. If matrix or cytoplasm are not stained repeat step 7 and rinse again for a shorter period of time. If the background is too strong rinse, continue to rinse, checking at 1 m intervals, until an acceptable level is reached.
9. Air dry and then mount with mounting medium.

G.4 α-Smooth Muscle Actin Staining Protocol

Protocol for staining formalin-fixed, cell-seeded, collagen-GAG matrix samples. Paraffin embedded, sectioned at 10 μm thickness.

Solutions: (stains ~ 25 slides)
Phosphate Buffered Saline (P-3813, Sigma Chemical Co., St. Louis, MO)
Mix 1 Sigma Phosphate Buffered Saline (PBS) packet in 1 L distilled water (dH_2O)

Trypsin (T-7409, Sigma)
Store trypsin powder in refrigerator.
0.1% Solution: Trypsin, 0.01 g
PBS, 10 ml

Hydrogen Peroxide, 30%
Store stock solution in refrigerator.
3% Solution: 30% Hydrogen Peroxide, 1 ml
dH_2O, 9 ml

Goat Serum (G-9023, Sigma)
Freeze in 1 ml aliquots.
20% Solution: Goat Serum, 2 ml
PBS, 8 ml

Primary Antibody, Anti α-Smooth Muscle Actin (A-2547, Sigma)
Freeze in 25 μl aliquots.
1:400 concentration: Primary antibody, 25 μl
PBS, 10 ml

Mouse Serum (for negative control) (M-5905, Sigma)
Freeze in 20 μl aliquots.
1:200 concentration: Mouse serum, 20 μl
PBS, 10 ml

Secondary Antibody, Goat Anti-Mouse IgG (B-0529, Sigma)
Freeze in 33 μl aliquots.
1:300 concentration: Secondary antibody, 33 μl
PBS, 10 ml

ExtrAvidin Peroxidase Reagent (E-2886, Sigma)
Store in 100 μl aliquots in the refigerator - DO NOT FREEZE!
1:50 concentration: ExtrAvidin Peroxidase, 200 μl
PBS, 10 ml

AEC Staining Kit (Zymed)
Mix up 8 ml according to the package instructions.

Mayer's Hematoxylin Solution (MHS-16, Sigma)

Glycerol Gelatin (GG-1, Sigma)

Staining Procedure

1. Put slides in dipping rack. Hang rack from the side of a 2 L beaker with enough xylene to cover the slides. Add stir bar and stir gently for 1 h.

2. While slides are deparaffinizing, remove antibodies from the freezer:
   25 µl Primary Antibody
   33 µl Secondary Antibody
   20 µl Mouse Serum
   2 ml Goat Serum

   Also, remove trypsin from the refrigerator and allow to come to room temperature before opening to avoid adding moisture to the desiccated compound.

3. Mix up PBS in glass beaker with stir bar. Add 1 packet of PBS to 1 L of dH_2O. Stir for several minutes to mix.

4. Mix up trypsin with PBS to make 10 ml.

5. After 1 h of xylene, remove the slides and deparaffinize as follows:

100% EtOH	2 m
100% EtOH	2 m
95% EtOH	2 m
80% EtOH	2 m
70% EtOH	2 m
dH_2O	2 m
PBS	2 m
PBS	2 m

6. Gently dry slides, but not sections with Kimwipes. Circle sections to be stained with PAP pen. Add trypsin solution to circled sections. Do not let sections dry out between steps!!!

7. Incubate in trypsin solution (0.1%) for 1 h at room temperature. Tip trypsin off slides into waste container.

8. PBS wash x 2, 2 m each.

9. Dry slides but not sections.

10. Incubate in hydrogen peroxide (3%) for 10 m.

11. Repeat steps 8 & 9.

12. Incubate with excess goat serum (20%) for 10 m.

13. Tip off excess serum, do NOT wash slides.

14. Incubate with primary antibody or mouse serum (negative control) for 2 hours at room temperature.

15. Tip off excess antibody. Be careful not to contaminate your negative control with the primary antibody. To avoid contamination in the rinse bath, use a transfer pipette to gently rinse sections individually before washing.

16. Repeat steps 8 & 9.

17. Incubate with the secondary antibody for 1 h at room temperature.

18. Repeat steps 8 & 9.

19. Incubate with ExtrAvidin Peroxidase for 20 m at room temperature.

20. Begin warming glycerol gelatin.

21. Repeat steps 8 & 9.

22. Rinse slides in dH_2O. While slides are in the dH_2O, mix up AEC according to instructions on the staining kit.

23. Dry slides and begin incubating in AEC solution. Begin timing after the first slide started. Watch how long it takes to dry the slides and apply the AEC solution. Try to keep that pace when you stop the development so that all slides stain similarly.

24. Incubate in AEC solution for 15 m.

25. Stop development by tipping AEC off slides into an appropriate waste container (AEC is a carcinogen!) and place the slides in a slide holder in dH_2O. Rinse in dH_2O x2, 2 m each. Check slides for development. If some slides are not developed enough, repeat the AEC step for 2-5 m as needed.

26. Mayer's hematoxylin solution for 15 m.

27. Running water bath for 15 m to develop the hematoxylin.

28. Coverslip with warmed glycerol gelatin. If the gelatin hardens too early, place slides on 40°C surface (like water bath edge) or in 57°C oven for a few minutes to re-melt the gelatin.

G.5 Image Capture and Analysis Protocol (aspect ratio)

Equipment:
Stained microscope slides
Compound microscope (Labophot, Nikon) with 10 and 20x objectives
Digital camera fitted to microscope (DEI-750, Optronics Engineering)
PC with image capture software (Snappy Video Snapshot, Play Inc., Rancho Cordova, CA) and image analysis software (Scion Image; www.nih.gov)
TV Monitor (Panasonic AG-DS555, Rockville, MD)

Procedure:
Turn On/Setup System:
1. Power-up microscope, computer, black camera box and TV monitor.

2. Place slide on microscope and focus on specimen using 10x objective

3. While looking into microscope turn wheel by light until only a small dot of light is visible.

4. Using condenser height adjustment knob bring dot of light into sharp focus (octagonal).

5. Turn wheel by light so that almost the entire field of view is light. Use silver knobs to center the light.

6. Turn wheel by light so that light covers entire field of view.

7. Switch to 20x objective.

Image Acquisition:
1. Start 'Snappy' program.

2. Under 'Setup' select: Live Camera, Highest quality, Color, Use Current Window, 640 x 480, and Connected to TV

3. Using image controls on camera keyboard, focus on microscope, microscope light intensity, and wheel on condensor under microscope stage obtain the best possible image.

4. Randomly select regions of the section which contain some cells, but do not contain large clumps of cells.

5. Fine tune image controls to get an image that clearly defines cell edges and also allows for cell nucleus identification. Note: cell nuclei will become difficult to see if contrast is too high.

6. White balance the image

7. Click on 'Snap' to acquire image

8. If image is satisfactory save to file.

Measurement of Cell Elongation:

1. Start Scion Image

2. Open image file

3. Select 'Options'; 'Density Slice'; Slide red region on LUT so that only a sliver on the very bottom appears

4. Double-click on paint brush tool. Select 2 pixels for size.

5. Click on red sliver on LUT so that brush icon turns red

6. Outline all cells that: are in contact with matrix, and have a visible nucleus

7. Save file in TIFF format

8. Select 'Analyze'; 'Options'; Check Perimeter/Length, Ellipse Major and Minor Axis, and Angle;

9. Select 'Analyze'; 'Analyze Particles'; 'Outline Particles'

10. If all particles were analyzed properly Select 'Analyze'; 'Show Results' then 'Edit' ; 'Copy Measurements' and Paste in Excel Spreadsheet

11. Finally save image file again

Appendix H. Live Cell Imaging

Equipment:

thick microscope slide w/ well (see D.2)
22 mm diameter cover slip
forceps
15 ml centrifuge tube
collagen-GAG matrix sheet
new razor blade
temperature controlled slide holder (Biostage 600SM, 20/20 Technologies, Wilmington, NC)
light microscope fitted with digital camera
VCR
PC with image capture card
{see G.5 for model and manufacturer}

Solutions:

DMEM with 25 mM HEPES (GIBCO Cat. # 12320-032, Grand Island, NY)

Imaging Procedure:

1. Produce a very thin piece of the collagen-GAG matrix using the razor blade. This can be accomplished by using a gentle slicing motion along the planar surface of the matrix.

2. Produce a cell suspension of ~1 million cells in 5 ml using the protocol described in Cell Passaging (App. B). Place the thin matrix piece into this suspension (15 ml centrifuge tube). Place the tube on the Nutator in the incubator for 10 m to facilitate cell attachment.

3. Using a 1 ml pipette place a few drops of the warmed DMEM into the microscope slide well. Using the forceps, transfer the matrix sample into the well.

4. Spread the matrix sample out with the forceps so that at least one edge of the matrix will be pinched by the cover slip. Carefully place the cover slip on top of the well to avoid trapping a significant amount of air. It is nearly impossible to trap no air.

5. Finally, use a Kimwipe to remove excess medium by blotting the edge of the cover slip. This will result in a tight seal over the well.

6. Place the slide on the microscope fitted with the temperature controlled stage (37°C). Connect the digital camera output to the VCR input and connect the VCR output to the TV input.

7. Adjust the microscope so that a cell which is attached to a strut is clearly visible. Keep the light source as low as possible to avoid overheating the cell. Adjust the camera settings (brightness, sharpness, *etc.*) to obtain the best quality image. Press 'Record' on the VCR.

8. Check the image every 5 - 10 m to ensure the cell is still in focus and in the field of view. The timing will depend on the number of active cells in the region of interest.

9. Following the experiment, images can be gathered from the video tape by connecting the output of the VCR to the input for an image capture card in a PC. Generally, the tape will need to be reviewed several times before image capture to determine which images will convey the actions of the cell.